SISSA   **ISAS**

SCUOLA INTERNAZIONALE SUPERIORE DI STUDI AVANZATI
INTERNATIONAL SCHOOL FOR ADVANCED STUDIES

Interplay between Generation Mechanisms and Detection of SuperSymmetric Dark Matter in the LHC Era

Thesis submitted for the degree of
Doctor Philosophiæ

PhDThesis of:
Giorgio Arcadi

Supervisor:
Prof. Piero Ullio

defended on September 19th 2012

Related to this thesis are the following papers:

1. G. Arcadi and P. Ullio, `Accurate estimate of the relic density and kinetic decoupling in non-thermal dark matter models`, **Phys.Rev. D84 (2011) 043520**, arXiv:1104.3591.

2. G. Arcadi, L. Di Luzio and M. Nardecchia, `Gravitino Dark Matter in Tree Level Gauge Mediation with and without R-parity`, **JHEP 1112 (2011) 040**, arXIv: 1110.2759.

3. G. Arcadi, R. Catena and P. Ullio, `Interplay between Direct Detection and Collider for Neutralino Dark Matter`, in preparation.

During my PhD I have produced an additional paper, not included in this thesis:
G. Arcadi, L. Di Luzio and M. Nardecchia, `Minimal Flavour Violation and Neutrino Masses without R-parity`, **JHEP 1205 (2012) 048** , arXiv: 1111.3941.

Acknowledgments

My first thank goes to my supervisor prof. Piero Ullio for all the support and the good advices during my PhD. A special mention is also deserved by Marco Nardecchia and Luca di Luzio for being first good friend and then good collaborators. I also warmly thank my other collaborator Riccardo Catena for the useful discussions and support. I also thank all the people with whom I have interacted during the preparation of my papers, in particular Alberto Tonero, Umberto de Sanctis and Michele Pinamonti who gave me valuable advices while I was learning to use the package Madgraph.

I also thank all my friends and colleagues at SISSA with a special mention to Maurizio Monaco and Alessandro Lovato who have been my flatmates and are sharing with me the experience of research since the University. I also thank my officemates Aurora Meroni, Hani Santosa and Maryam Tavakoli, who made more enjoyable the long working days, and Alberto Tonero for our tennis matches. A special thanks also goes to Nicola Bassan, Alessandro Renzi, Ambra Nanni, Antonella Garzilli, Eolo di Casola, Barbara de Marco, Rossella Aversa, Barbara de Marco, Irene Amado and Daniel Arean Fraga.

My warmest thank goes to my family, for the support which have been never missing during my studies.

Contents

Abstract:

The object of this thesis is the study of several, possibly complementary, aspects of generation mechanism and detection of the two dark matter (DM) candidates provided by the Minimal Supersymmetric extension of the Standard Model (MSSM), i.e. the gravitino and the neutralino.

We have first of all focused on the generation mechanism of neutralino dark matter, examining the possible consequences of relaxing some of the hypothesis on which the typically adopted thermal WIMP paradigm relies.

We have, indeed, considered non-thermal dark matter production scenarios motivated, in the context of Supersymmetric theories, in supergravity and superstring frameworks. These classes of theories often feature the presence of long-lived states capable of dominating the energy budget of the Universe at early stages before possibly decaying into dark matter particles.

Non thermal production have been studied in a systematic way by mean of a numerical code developed for this purpose. In particular the impact in selecting a preferred mass scale for the Dark matter and, consequently, the impact on the interpretation of new physics discovered or excluded at LHC have been discussed.

The second aspect of neutralino dark matter generation which has been investigated is the assumption of kinetic equilibrium during the whole phase of dark matter generation and the validity of the factorization usually implemented to rewrite the system of coupled Boltzmann equation for each coannihilating species as a single equation for the sum of all the number densities. To this purpose has been developed and numerically implemented a formalism for the computation of the kinetic decoupling temperature in the case of coannhilating particles. This formalism has been applied to a definite scenario referred as G2-MSSM.

The next topic discussed in this thesis, remaining in the context of neutralino DM, is the capability of current and next generation direct detection experiments of probing the MSSM parameter space. Focusing on some definite setups, satisfying the cosmological bounds on the DM relic density and the current particle physics constraints, the possibility for them of producing direct detection signals has been inspected through Montecarlo Simulations. The final purpose of this analysis is to show as indications about the DM properties, as provided by an experimental detection, can influence some features of the underlying Supersymmetric model which can be probed in the next future by LHC.

We have finally moved the focus to the other dark matter candidate within the MSSM, i.e. the gravitino. Remarkably it is a viable dark matter candidate also in presence of R-parity violation. Gravitino dark matter have been studied in the context of a class of Supersymmetric models referred as Tree-Level Gauge Mediation (TGM). These models provide rather definite predictions for the mass of the dark matter being it related to the mechanism of mediation of SUSY breaking. In particular has been investigated a realization of TGM predicting a gravitino mass in the range 10-100 GeV. Cosmological bounds have been investigated both in presence

and in absence of R-parity. The model results disfavored in case the R-parity holds, being in severe tension with Big Bang Nucleosynthesis; on the contrary is naturally feasible in presence of a small amount of R-parity violation.

Introduction

The identification of the dark matter (DM) component of the Universe is one of the most pressing issues in Science today. DM constitutes most the matter component of the Universe and contributes by an amount of around 23 percent to its current energy budget. The DM abundance in the present Universe is typically expressed through the quantity $\Omega_{\mathrm{DM}}h^2$ with $\Omega_{\mathrm{DM}} = \frac{\rho^0_{\mathrm{DM}}}{\rho^0_c}$ with ρ^0_{DM} and ρ^0_c being, respectively, the today's values of DM energy density and of the so-called critical density, namely the energy density for a flat Universe, and h the value of the current Hubble expansion rate in units of 100 km Mpc^{-1} s^{-1}. The precise value of Ω is currently determined by the combination of the data coming from the Wilkinson Microwave Anisotropy Probe (WMAP) experiment [Komatsu 2011] as well as from the measurement of Baryon Acoustic Oscillation in the distribution of galaxies performed by the Sloan Digital Sky Survey [Percival 2010] and the measurement of the Hubble constant performed by the Hubble space telescope [Riess 2009] :

$$\Omega_{\mathrm{DM}}h^2 = 0.1123 \pm 0.0035 \tag{1.1}$$

On the other hand observations have not provided yet a clear indication neither about the particle nature nor the relevant features, such as mass and interactions, of the DM. As a consequence there is a huge variety of viable DM candidates including particles with a mass (close to) the Planck scale that are only gravitationally interacting, see e.g. [Chung 1998], as well as ultra-light scalar particles possibly forming a condensate, see e.g. [Hu 2000]. In this context a possible rationale is provided once the Dark Matter generation mechanism is considered.

The most popular scenarios rely on Early Universe generated cold (i.e. the fact the DM is non relativistic at the time of the onset of structure formation) stable thermal relics; dark matter is assumed to be a particle state with sizable couplings with SM states but possessing, at the same time, a conserved quantum number, thus related to a suitable symmetry, which enforces its stability. The first property instead ensures that DM particles are thermalized in the early stages of the cosmological history.

Among these scenarios, the dominant paradigm conjectures the existence Weakly Interacting Massive Particles (WIMP) . It relies on a very general and elegant argument: the time evolution of the stable massive species is determined by the interplay of pair production form and annihilation into SM particles. The final relic abundance is set when the annihilation rate is no more efficient with respect to the expansion rate of the Universe (pair production stops at earlier times when the thermal bath

temperature becomes lower than around the DM mass). The thermal relic abundance of the DM scales with the inverse of its pair annihilation rate, matching the cosmologically measured DM density when the annihilation cross section is about $3 \cdot 10^{-26} \text{ cm}^3 \text{ s}^{-1}$, a natural value for weak-force type couplings. This is the well celebrated WIMP miracle, allowing to embed a DM candidate in most of the proposed extensions to the standard model (SM) of particle physics.

Although extremely attractive, the WIMP scenario in the MSSM faces several shortcomings. One of the purposes of this thesis is to discuss some aspects of WIMP phenomenology, reconsidering in particular some of the main assumptions at the base of the standard thermal WIMP paradigm. First of all we have relaxed the assumption of DM as a thermal relic, reconsidering non-thermal WIMP production scenarios, featuring the existence of long lived massive states, which do not thermalize with the primordial heat bath and dominate the Early Universe's history, producing dark matter at decay. Non thermal production mechanisms have been treated in a systematic way by developing a numerical code for accurate computations of the dark matter relic density in this kind of scenarios. Among the various scenarios emerged from our numerical study the most interesting is the one already depicted in the pioneering work [Moroi 2000]. Here the relic abundance of the non-thermally produced DM retains the scaling with inverse of the pair annihilation cross section and is well approximated by the the result for thermal relic WIMPs scaled up by the ratio $T_{\text{t.f.o.}}/T_{\text{RH}}$ where $T_{\text{t.f.o.}}$ is the so called freeze-out temperature defined in the thermal scenario while T_{RH}, lower with respect to the former, is related to the timescale of ending of the decay process of the heavy states source of non thermal dark matter. Remarkably, this scenario requires sensitively higher values of the DM pair annihilation cross section with respect to the thermal WIMP paradigm.

DM particles with large pair annihilation cross section are receiving growing interest triggered by the fact that cross sections larger than the standard face-value for WIMP DM are needed to provide a DM positron source accounting for the rise in the positron fraction in the local cosmic-rays measured by the PAMELA detector [Adriani 2009]. The picture of non-thermal generation of DM has however a much broader phenomenological impact, e.g., shifting significantly the mass scale for which a DM particle embedded in a SM extension is cosmologically relevant or excluded.

The second aspect, relying on WIMP generation mechanism, which have been questioned in this thesis is the hypothesis that kinetic equilibrium, (namely the fact that the DM posses interactions, not responsible of changes in its number density, with the SM states which ensure its coupling with the thermal bath), holds along the whole phase of dark matter generation. This hypothesis is particularly relevant in the case of coannihilations. Coannihilations occur when there are additional states, close in mass with the DM and sharing with it the quantum number which guarantees its stability. The particles participate in interactions with the thermal bath particles changing this quantum number and can thus influence the final DM relic density. If kinetic equilibrium holds, the set of coannihilating particles can be

treated as a unique particle species parametrizing all the annihilation by an effective thermally averaged cross section. In this thesis we will show in a specific example how to describe a system of coannihilating particles when the hypothesis of kinetic equilibrium is not imposed accounting as well the presence of non-thermal DM production. As a byproduct we have also developed a formalism for the first time the formalism to compute the DM kinetic decoupling temperature for a system undergoing a low-temperature of reheating and for which kinetic equilibrium is maintained in a chain of coupled processes rather than by the elastic scattering of a single DM particle on thermal bath particles. This is an important result since thermal kinetic decoupling, namely when DM scattering goes out of equilibrium (as opposed to the thermal chemical decoupling which refers to the departure from equilibrium of the pair annihilation processes) determines the small-scale cutoff in the spectrum of matter density fluctuations, see, e.g.,[Profumo 2006, Bringmann 2007].

All these aspects regarding the WIMP DM generation mechanisms will be investigated in the context of a definite class of models, namely the R-parity preserving Supersymmetric (SUSY) extensions of the standard model, in particular their minimal realization, the so-called Minimal Supersymmetric Standard Model (MSSM) , featuring as DM WIMP candidate, the lightest neutralino [1].

Interestingly, in this class of models, the existence of a DM candidate and of the symmetry enforcing its stability, the so-called R-parity, are not properties introduced ad-hoc to address the DM problem, but rather a byproduct of other features in the theory [2].

Current experimental facilities have reached the necessary sensitivity to probe the typical scale of SUSY Wimp interactions. The various employed search strategies can be classified into three main categories. The first kind, dubbed as Indirect Detection (ID), relies on the idea of measuring the primary and secondary products of DM self annihilations. At the moment several experiments are active on this kind of searches, relevant examples are the Fermi Large Area Telescope (LAT) [Atwood 2009] and the Pamela satellite [Adriani 2009] detecting, respectively, γ-rays and electrons/positrons, as well as the ICECUBE [Ahrens 2003] experiment, looking for neutrinos, which is expected to release data in the next future. The Pamela experiment was the first to provide a potential signal of detection manifesting into an excess of positrons with respect to the expected sources. On the other hand the dark matter interpretation is not the only one possible but it is challenged by explanations of the reported excess invoking local astrophysical sources. On general grounds ID strategies are affected by large contamination of the signals by not fully understood backgrounds. The attention on ID have anyway boosted after the recent claim [Weniger 2012] of a detection signal in γ-rays which is currently under investigation from the Fermi collaboration.

The second dark matter search strategy is instead referred as Direct Detection

---

[1] Within the MSSM there is another particle, namely the so-called sneutrino, possessing the features of WIMP. As clarified in the following, however, it is already experimentally excluded.

[2] We just mention that this feature appears also in several other BSM framework, such as, for example, a heavy photon in T-parity conserving versions of Little Higgs models [Birkedal 2006]

(DD) and aims to detect signals of interactions among the local DM population of our galaxy within a laboratory detector. More precisely DD experiments aim to measure the energy deposited by the DM particles through scattering processes with the nuclei of a targed detector. In the recent year several experiments have reached the necessary sensitivity to probe the interaction cross section typical of WIMP DM. Among these, there have presented result compatible with a detection. The first is DAMA/LIBRA [Bernabei 2008] which has detected an annual modulation in the total event rate which is the effect expected from WIMPs scatterings because of the orbit of the Earth around the Sun. A second detection signal, pointing towards a light DM candidate (mass of the order of few 10-20 GeV), has been provided by the COGENT [Aalseth 2011] collaboration which has, in addition, confirmed the annual modulation, although with lower statistical significance. An excess of events with respect to the expected background, as well pointing towards light DM, have been finally detected by the CRESST experiment [Angloher 2012]. All these results are however contrasted by the outcome of experiments like CDMS [Ahmed 2010] and especially XENON100 [2012] which have not found any evidence of DM signals and have thus produced exclusion plots in the plane WIMP mass versus scattering cross section which seem to exclude, especially in the case of Xenon, the regions of parameter space preferred by DAMA, COGENT and CRESST. These contrasted outcomes likely rely on the different assumptions adopted by the various collaborations in the data analysis. Indeed, also depending on the detection technique, these kind of experiments are affected by issues regarding the understanding of the target material, like the precise determination of the nuclear form factor or the so-called channeling effect, and the detector performance, like the determination of the energy thresholds or the background/signal contamination. There are, in addition, several uncertainties originated by the still not precise knowledge of some DM properties, like its local density, which influence the determination of the signal.

The most powerful probe of Beyond the Standard Model (BSM) physics and, consequently DM phenomenology, is at the moment the Large Hadron Collider (LHC) [Roszkowski 2010, Bertone 2010], aiming to directly produce Supersymmetric particles, including the dark matter. On the other hand we remark that LHC cannot really detect possibly produced dark matter particles whose presence is instead signaled by missing energy. In Supersymmetric frameworks [3] DM particle are unlikely directly pair produced by proton collisions but are rather the endpoint of even complex decay chains started by the production of states carrying QCD quantum numbers. SUSY DM detection hence relies on the searches of events in which a sizable amount of missing energy is accompanied by a large variety of final states, typically multiple jets and possibly leptons. From the detection of this final product, together with the measure of the missing energy, it is possible to reconstruct the original decay chain possibly inferring quantities like the DM mass and the ones (or the relative mass splitting) of the decaying Supersymmetric particles.

---

[3] The issue of not direct DM detection at collider is proper of any particle physics framework, not only SUSY.

From the discussion above it is evident that no one of these different search strategies can provide alone a complete picture of the dark matter individual properties. This task can be instead accomplished by combing the possible information coming from the different dark matter searches, i.e ID, DD and collider, in order to compensate their respective shortcomings. In Supersymmetric setups the complementarity among the DM search strategy is further enforced by the fact that the interaction cross sections relevant for detection as well as the pair annihilation cross section, governing the DM relic density, often share the dependence on some parameters and can be even related by crossing symmetries [4].

In this thesis we will discuss an example of combination of two dark matter experimental searches, i.e. collider and Direct Detection. More precisely we will examine whether a future DD experiment can probe some definite MSSM setups. To this purpose we will study, through Montecarlo techniques, properly accounting for the astrophysical uncertainties, the capability of the DD experiments of reconstructing, from an hypothetical signal, the DM mass and scattering cross-section in the considered setups. We will then show that the information obtained in this way, once combined with the requirement of the a correct neutralino relic density as well as with other particle physics bounds, can be translated into peculiar collider signatures, potentially probed in the very next future, which will be studied through dedicated simulations.

In the last part of this thesis we will definitely relax the WIMP paradigm by considering the other dark matter candidate present in the MSSM: the gravitino. This particle is often referred as a Super-Weakly interacting particle (superWIMP) in view of its only gravitational-strength interactions, which cannot maintain it in thermal equilibrium in the Early Universe. Its production mechanism relies instead on high-energy particle collisions occurring in the very early stages of the cosmological history, soon after the inflationary phase (see e. g. [Rychkov 2007] for an extensive treatment). Additionally, gravitino dark matter may be produced, in R-parity conserving realizations of the MSSM, through the decays of the other Supersymmetric particles. Given the extreme weakness of the interactions of the gravitino the unique relevant decays are the ones of the Next-to-lightest SUSY particle (NLSP) which is then metastable.

Gravitino phenomenology is actually very model dependent being, in particular, sensitive to the gravitino mass. For this reason we will focus on particular class of SUSY models, dubbed as as Tree-Level Gauge Mediation (TGM) which offers rather definite predictions regarding this parameters. TGM have been also the playground for discussing dark matter phenomenology in the case that the hypotheses regarding its stability are partially relaxed. We will consider, in fact, the case of a small violation of the R-parity, i.e. the symmetry guaranteeing the stability of SUSY dark matter within the MSSM. Despite this violation does not alter the viability of the dark matter, candidate since its lifetime remains much greater the age of the universe, it has anyway important implications; among these it opens the possibility of

---

[4]This features is not only proper of SUSY but can be encountered in other particle frameworks.

indirect DM detection through the products of the small amount of decays occurring at present times.

We also remind that R-parity is not an ad-hoc introduced DM feature but is an intrinsic property of SUSY framework. As we will show, an even small violation, has then profound implications in many sectors of the theory.

The thesis is organized as follows. In the next Chapter we will provide a general review of the thermal and non-thermal production mechanisms of WIMP dark matter. We will then specialize the discussion of this mechanism to the R-parity conserving realizations of the MSSM with neutralino DM. In chapter 3 we will then present an accurate numerical scheme for the computation of the DM relic density in several scenarios of non-thermal production also when the hypothesis of kinetic equilibrium is relaxed. Chapter 4 will be instead devoted to the combined study of DD and collider signals depicted above. The last chapter, before summarizing our conclusions, will be focused on the gravitino cosmology, discussed in the context of two realizations, respectively with and without R-parity conservation, of the TGM scenario.

Theoretical framework

Contents

2.1   WIMP Dark Matter production

2.1.1   Thermal production

The thermal WIMP scenario can be described, on general grounds, by mean of a particle physics framework embedding, besides the SM states, a set $\{\chi_a\}$ of BSM states. The WIMP DM is the lightest state of this set $\{\chi_a\}$ of particles which are assumed to share a conserved quantum number and to have sizable couplings with SM particles; the first property ensures that DM, as the lightest of them, is stable, while the second guarantees thermalization at sufficiently large temperatures. The conserved quantum number allows for inelastic scattering processes making the $\{\chi_a\}$ indistinguishable in the thermal bath at high temperatures.

In order to play the role of DM candidate we have also to require that χ_0 has zero electric and color charges.

To trace the number density of the χ_a states, especially when two or more of these are nearly degenerate in mass (in this case the standard paradigm is to refer them as coannihilating particles), one should refer to a system of coupled Boltzmann equations. For a state χ_a the corresponding Boltzmann equation is given by:

$$\left(\partial_t - H\mathbf{p}\cdot\nabla_{\mathbf{p}}\right)f_{\chi_a}(p,t) = \frac{1}{E}\,\hat{\mathbf{C}}_{\chi_a}[f_{\chi_a},f_{\chi_b},\cdots] \tag{2.1}$$

where $f(p,t)$ is proportional to (see eq. (2.2) below) the phase-space distribution function of the given state and $\hat{\mathbf{C}}$ is the collisional operator embedding all the interactions involving χ_a.

The changes in number density are due to pair production from and annihilation into SM particles; at the same time the relative number densiities of the states $\{\chi_a\}$ are redistributed by inelastic scattering of a given χ_a into a different χ_b state; the decays of χ_c into lighter χ_d particles and and of these to the lightest stable species.

The number density of each state is given by integrating over the three momentum the corresponding distribution function:

$$n_{\chi_a} \equiv \int \frac{d^3p}{(2\pi)^3} g_{\chi_a} f_{\chi_a}(p,t) \tag{2.2}$$

where g_{χ_a} represents the number of internal degrees of freedom of the particle state χ_a. The processes accounting for changes in the number density can be schematized as follows:

$$
\begin{aligned}
&\chi_a \chi_b \leftrightarrow X \\
&\chi_a X_i \leftrightarrow \chi_b X_j, \quad \forall a \neq b \\
&\chi_a \to \chi_b + Y, \quad \forall a > b \\
&\chi_b \to \chi_a + X, \quad \forall b > a
\end{aligned}
\tag{2.3}
$$

These represent, respectively, annihilation processes into SM states with rate :

$$\sigma_{\chi_a \chi_b} \equiv \sum_X \sigma\left(\chi_a \chi_b \to X\right), \tag{2.4}$$

inelastic scatterings off of thermal bath states,

$$\sigma_{\chi_a \chi_b} \equiv \sigma\left(\chi_a f_{X_i} \to \chi_b f_{X_j}\right) \tag{2.5}$$

and decays of χ_a states with Γ_{χ_a,χ_b} representing the inclusive decay rate:

$$\Gamma_{\chi_a \chi_b} \equiv \sum_X \Gamma\left(\chi_a \to \chi_b + X\right) \tag{2.6}$$

Actually the collisional operator $\hat{\mathbf{C}}$ also includes the contribution of elastic scatterings of the χ_a states over the SM particles of the thermal bath.The corresponding operators get however erased when eq. (2.1) is integrated according to (2.2) since they are not responsible of changes in the DM number density.

The Boltzmann equation for the number density of one member of the particle set embedding the DM is then given by. [Griest 1991, Edsjo 1997]:

$$
\begin{aligned}
\frac{dn_{\chi_a}}{dt} + 3H n_{\chi_a} = &-\sum_b \langle \sigma_{\chi_a \chi_b} v_{ab} \rangle \left(n_{\chi_a} n_{\chi_b} - n_{\chi_a}^{\text{eq}} n_{\chi_b}^{\text{eq}} \right) \\
&- \sum_{b,i,j} \langle \sigma'_{\chi_a \chi_b} v_{ab} \rangle n_{\chi_a} n_{f_{X_i}}^{\text{eq}} - \langle \sigma'_{\chi_b \chi_a} v_{ba} \rangle n_{\chi_b} n_{f_{X_j}}^{\text{eq}} \\
&- \sum_{b<a} \Gamma_{\chi_a \chi_b} n_{\chi_a} + \sum_{b>a} \Gamma_{\chi_b \chi_a} n_{\chi_b}
\end{aligned}
\tag{2.7}
$$

where the additional term to the derivative on the left hand side represents the dilution due to the expansion of the Universe, with H being the Hubble parameter. In writing (2.7) we have introduced the thermally averaged cross sections generally defined as:

$$\langle \sigma_{\chi_a \chi_b} v_{ab} \rangle \equiv \frac{1}{n_{\chi_a}^{\text{eq}} n_{\chi_b}^{\text{eq}}} \int d^3 p_{\chi_a} d^3 p_{\chi_b} \frac{g_{\chi_a} g_{\chi_b}}{(2\pi)^6} f_{\chi_a}^{\text{eq}} f_{\chi_b}^{\text{eq}} \sigma_{\chi_a \chi_b} v_{ab} \tag{2.8}$$

with v_{ab} defined as:

$$v_{ab} = \frac{\sqrt{(p_a \cdot p_b)^2 - m_a^2 m_b^2}}{E_a E_b} \tag{2.9}$$

We have also introduced the quantities n_i^{eq} (where i indicates either a χ_a or a SM state) representing the number density obtained from the integral (2.2) assuming for the species i a thermal equilibrium phase space density.

The evolution of the set χ_a can be then studied by solving a system of equations of the form (2.7). However this is usually not done since it is a system of coupled stiff equations which one needs to solve numerically; moreover it is usually not necessary to do it, since one is interested only in the number density of the lightest state after all heavy states have decayed into the stable one. Rather than tracing the number density n_{χ_a} of the individual state χ_a, one usually solves a single equation written for the sum of all the number densities, $n_\chi = \sum_a n_{\chi_a}$, i.e. [Griest 1991, Edsjo 1997]:

$$\frac{dn_\chi}{dt} = -3H n_\chi - \langle \sigma v \rangle \left[n_\chi^2 - \left(n_\chi^{\text{eq}} \right)^2 \right] \tag{2.10}$$

In this equation n_χ^{eq} stands for the sum of thermal equilibrium number densities, and the term proportional its square accounts for the production of particles χ_a in pair annihilations of SM thermal bath particles, while the effective thermally averaged annihilation cross section:

$$\langle \sigma_{\text{eff}} v \rangle = \sum_{a,b} \langle \sigma_{\chi_a \chi_b} v_{ab} \rangle \frac{n_{\chi_a}^{eq}}{n_\chi^{eq}} \frac{n_{\chi_b}^{eq}}{n_\chi^{eq}} \tag{2.11}$$

is written as a weighted sum over the thermally averaged annihilation cross section of any χ_a-χ_b pair into SM particles; remarkably, the processes giving a sizable contribution to this sum are only those for which the mass splitting between a state χ_a and the lightest state χ_0 are comparable to the thermal bath temperature T. Moreover the thermally averaged cross sections are defined in terms of the thermal equilibrium distributions [Gondolo 1991]:

$$\langle \sigma_{\chi_a \chi_b} v_{ab} \rangle \equiv \frac{1}{n_\chi^{2,\text{eq}}} \int d^3 p_{\chi_a} d^3 p_{\chi_b} \frac{g_{\chi_a} g_{\chi_b}}{(2\pi)^6} f_{\chi_a}^{\text{eq}} f_{\chi_b}^{\text{eq}} \sigma_{\chi_a \chi_b} v_{ab} \tag{2.12}$$

There are two main assumptions which allow to implement Eq. (2.11) to trace n_χ. The first is kinetic equilibrium for each species χ_a, namely that the scattering processes on thermal bath particles are efficient and make the phase space densities

for each particle trace the spectral shape of the corresponding thermal equilibrium phase space density, namely $f_{\chi_a}(k_{\chi_a}, t) = C(t) \cdot f_{\chi_a}^{eq}(k_{\chi_a}, t)$ (with the coefficient C depending on time but not on momentum) [1] . This assumption allows to factorize the number density out of each thermally averaged annihilation cross section (which is defined in terms of thermal equilibrium phase space densities). To implement the factorization of the individual terms in the sum of Eq. (2.12) one needs also to assume that $n_{\chi_a}/n_{\chi} \simeq n_{\chi_a}^{eq}/n_{\chi}^{eq}$, a quantity which, in the Maxwell-Boltzmann approximation for the equilibrium phase space densities, as appropriate for non-relativistic particles, is proportional to the number of internal degrees of freedom g_{χ_a} and is exponentially suppressed with the ratio between mass splitting and temperature; this approximation is strictly valid only in case inelastic scatterings of χ_a particles are efficient over the whole time interval in which the pair annihilation term is relevant.

Assuming, according to the standard cosmological history, that the Universe is radiation dominated during the time evolution of the DM number density, i.e.:

$$H^2 = \frac{1}{3M_{Pl}^2}\rho, \quad \rho = \frac{\pi^2}{30}g_{\text{eff}}(T)T^4 \tag{2.13}$$

with M_{Pl} being the reduced Planck mass $M_{Pl} = 2.43 \times 10^{18}\text{GeV}$, T photon temperature, and g_{eff} the effective number of degrees of freedom at the temperature T, and that the entropy density of the Universe s follows the conservation law:

$$\frac{ds}{dt} = -3Hs \tag{2.14}$$

and is related to the heat bath temperature by:

$$s = \frac{2\pi^2}{45}h_{\text{eff}}(T)T^3 \tag{2.15}$$

with h_{eff} representing the effective number of entropy degrees of freedom at the temperature T, eq. (2.11) is customarily reformulated in terms of the comoving abundance $Y_{\chi} = n_{\chi}/s$ (notice also that in this framework the assumptions regarding the annihilation term are well motivated, since the kinetic decoupling and the decoupling of inelastic scatterings usually take place at a much lower temperature than chemical decoupling):

$$x\frac{1}{Y_{\chi}}\frac{dY_{\chi}}{dx} = \left(1 - \frac{x}{3}\frac{1}{h_{\text{eff}}}\frac{dh_{\text{eff}}}{dx}\right)\frac{n_{\chi}\langle\sigma_{\text{eff}}v\rangle}{H}\left(1 - \frac{Y_{\chi}^2}{(Y_{\chi}^{\text{eq}})^2}\right) \tag{2.16}$$

with $x = m_{\chi}/T$ typically replacing the time as independent variable. By including eq. (2.13) and (2.14) in eq. (2.16) we obtain:

$$\frac{dY_{\chi}}{dx} = -\left(\frac{8\pi^2M_P^2}{45}\right)^{1/2}g_{\star}^{1/2}\frac{m_{\chi}}{x^2}\langle\sigma_{\text{eff}}v\rangle\left[(Y_{\chi})^2 - (Y_{\chi}^{\text{eq}})^2\right] \tag{2.17}$$

---

[1]Notice also that thank to this assumption it is possible to write the annihilation term for the single species a in eq. (2.7) as $\langle\sigma_{\chi_a\chi_b}v_{ab}\rangle\left(n_{\chi_a}n_{\chi_b} - n_{\chi_a}^{\text{eq}}n_{\chi_b}^{\text{eq}}\right)$.

with

$$g_{\star}^{1/2} = \frac{h_{\text{eff}}}{\sqrt{g_{\text{eff}}}} \left(1 - \frac{x}{3} \frac{1}{h_{\text{eff}}} \frac{dh_{\text{eff}}}{dx} \right) \tag{2.18}$$

This equation can be numerically solved imposing as initial condition, $Y_{\chi} = Y_{\chi}^{\text{eq}}$ at $x < 1$. The dark matter abundance reaches its final value when the annihilation rate drops below the value of the Hubble expansion rate. This is immediately evident from eq. (2.16) being its right hand side proportional to the ratio Γ_{ann}/H with $\Gamma_{\text{ann}} = n_{\chi}^{\text{eq}} \langle \sigma_{\text{eff}} v \rangle$ and thus becoming negligible when this ratio becomes lower than one. The temperature at which $\Gamma_{\text{ann}} = H$ is referred as freeze-out temperature $T_{\text{s.f.o}}$ and results approximatively equal to $m_{\chi_0}/20$.

The final dark matter relic density is given by:

$$\Omega_{\text{DM}} h^2 = m_{\chi} \frac{s(T_0)}{\rho_c h^{-2}} Y_{\chi}(T_0) \tag{2.19}$$

where $Y_{\chi}(T_0)$ represents the solution of eq.(2.17). Assuming that at freeze-out the Universe is still in a radiation dominated phase, with effective number of relativistic degrees of freedom as inferred from the SM particle spectrum, and no entropy injection intervening after $T_{t.f.o.}$ we can simply approximate:

$$Y_{\chi}(T_0) = Y_{\chi}(T_{\text{s.f.o}}) = Y_{\chi}^{\text{eq}}(T_{\text{s.f.o.}}) = \frac{H \, s}{\langle \sigma_{\text{eff}} v \rangle} |_{T_{\text{s.f.o.}} \approx m_{\chi_0}/20} \tag{2.20}$$

from we which we obtain:

$$\Omega_{DM} h^2 \simeq \frac{3 \times 10^{-27} \text{cm}^3 \text{s}^{-1}}{\langle \sigma_{\text{eff}} v \rangle}. \tag{2.21}$$

Remarkably the numerical solution shows the Ω is very sensitive to the thermally averaged annihilation cross section while the dependence on the DM mass. It is also evident the only dependence of the relic density on the particle physics framework resides the annihilation cross section. The cosmological value of the relic density is achieved for a cross section of the order of $3 \times 10^{-26} \text{cm}^3 \text{s}^{-1}$, a typically predicted value by Electroweak Interaction. This is the well celebrated ' Wimp Miracle'.

2.2 Non-thermal production

Although extremely successful and attractive we notice that the Wimp Miracle relies on some important assumptions, namely radiation domination and no entropy injection during the DM generation phase and even after its freeze-out, which are based on the extrapolation, not yet experimentally confirmed, of the properties of Universe from the earliest epoch at which the standard model for cosmology is well-tested, the onset of the synthesis of light elements (Big Bang Nucleosynthesis, BBN) at a temperature T_{BBN} of about 1 MeV, to the much earlier epoch of WIMP thermal freeze-out. In addition, no extra source of DM particles on top of the thermal component.

There are particle physics models in which all these hypothesis are actually strongly violated. In this thesis we will focus on theories containing heavy states that are very weakly (e.g., gravitationally) coupled to ordinary matter, such as the gravitino or moduli fields in SUSY setups (see also [Jeannerot 1999] for alternative setups). These states do not thermalize in the early Universe, they may dominate the Universe energy density, they are long-lived and potentially a copious source of entropy and DM particles at decay. The so-called cosmological gravitino or moduli problem refers to the very severe observational limits one encounters when these phenomena intervene during or after the BBN; on the other hand they can be perfectly consistent with available data if the lifetime of these fields is shorter than the age of the Universe at the onset of BBN, about 1 s, or, equivalently, if the Universe is reheated to a temperature $T_{\rm RH}$ larger than T_{BBN}, where the reheating temperature $T_{\rm RH}$ is defined as the temperature at which the Universe starts evolving in according to a radiation dominated phase after the field decays.

In order to take into account these more general scenarios we enlarge our particle physics framework with a new set of states $\{X_i\}$, from now on referred as cosmological moduli. As already mentioned these states are very weakly interacting, out of thermal equilibrium in the early Universe and long-lived; we assume they can condensate, potentially dominate the Universe energy density at an intermediate stage in its evolution, and late decay producing both SM particles, with a sharp increase in the entropy density, and χ_a fields. Moreover the framework may contain also additional long-lived states, say ψ_i, out of thermal equilibrium but with a sub-dominant contribution to the energy density, possibly sharing the quantum number protecting the stability of χ_0; these particles may also be produced in the decay of the X_i states.

The impact on cosmology of moduli fields can be sketched through the following schematic picture. Consider for simplicity the case of a single modulus X which decays when it dominates the Universe energy density; focussing on Planck suppressed interactions, its decay width can be written in the form:

$$\Gamma_X = D_X \frac{m_X^3}{M_{Pl}^2}, \tag{2.22}$$

with D_X some coefficient depending on the specific model, m_X the field mass. Assuming instantaneous conversion of the energy density (i.e. istantaneous reheating) into radiation, one usually defines the reheating temperature $T_{\rm RH}$ through the expression:

$$\Gamma_X \equiv \sqrt{\frac{\pi^2 g_{\rm eff}(T_{\rm RH})}{90}} \frac{T_{\rm RH}^2}{M_{Pl}}, \tag{2.23}$$

where $g_{\rm eff}(T_{\rm RH})$ is the effective number of relativistic degrees of freedom at $T_{\rm RH}$. Inverting this expression, one finds approximately that the onset of the standard radiation dominated phase happens at the temperature:

$$\frac{T_{\rm RH}}{1\,{\rm MeV}} \simeq 0.62 D_X^{1/2} \left[\frac{10.75}{g_{\rm eff}(T_{\rm RH})}\right]^{1/4} \left(\frac{m_X}{10\,{\rm TeV}}\right)^{3/2}. \tag{2.24}$$

To avoid spoiling predictions of the standard BBN, one needs to require $T_{\mathrm{RH}} \gtrsim 4$ MeV [Kawasaki 2000], which, for D_X of order one, translates into a lower limit on the mass of the cosmological modulus of about 30 TeV.

At this level of approximation the evolution of the system would be fully specified by the X decay width (or T_{RH}) and the amount of energy density converted into dark matter particles (which, in the treatment above, was implicitly assumed to be tiny compared to amount going into radiation). Having instead in mind to be able to treat a system in which, for the full set of X_i fields, spectra, lifetimes and branching ratios in the decay are calculable in the given particle scenario, we will not refer to instantaneous reheating, but rather follow more explicitly the evolution of the moduli. In principle this could be done by studying a full set of coupled equations of motion, having specified the potentials for each field [Dine 1996]. The result would be that, at early times, each field stays frozen in a time dependent minimum; when t^{-1} becomes of the order of the X_i mass, the equation of motion takes the form of the one for a damped harmonic oscillator. The oscillations satisfy a pressureless equation of state and hence the scalar field behaves like a condensate evolving as a matter fluid; provided that enough energy is initially stored in X_i, the Universe enters a phase of matter domination lasting until the field decays, with the transition that needs to be treated as a continuos process. In practice, even for models for which the physics related to the X_i fields is given in some detail, it is difficult to describe potentials and their temperature evolutions beyond the toy model level; for our purposes it will be sufficient to follow the evolution of the system starting from the phase of coherent oscillations. Each state X_i is then traced through an equation for its energy density:

$$\frac{d\rho_{X_i}}{dt} + 3H\rho_{X_i} = -\Gamma_{X_i}\rho_{X_i} \,, \tag{2.25}$$

and in case of several moduli present at the same time, the single equations are included in the system at the time $t = 3/2H = m_{X_i}$, assuming the energy density stored in the field at this time is equal to $(1/2)m_{X_i}^2 M_{Pl}^2$[Giudice 2001, Dine 1996, Acharya 2008a]; we will comment later on the fact that the final density of dark matter is not sensitive to these assumptions.

The decay of the X_i particles produces SM particles, χ_a states cascading to the DM particle, and, eventually, the long-lived ψ_i fields, in turn decaying into radiation and, possibly, DM particles. From the first principle of thermodynamics, one can write an equation for the total energy density and pressure associated to SM, χ_a and ψ_j states, respectively, ρ and p, in an implicit form:

$$\frac{d\rho}{dt} + 3H(\rho + p) = \sum_i \Gamma_{X_i}\rho_{X_i} \,. \tag{2.26}$$

This equation is treatable once separating ρ and p in components. Starting with the ψ_j particles, one can safely assume that they are produced in given number at decays, get diluted and redshifted by the Universe expansion without interacting with other species and decay themselves (an eventual term associated to the production via

inelastic scattering off SM or χ_a particles is not introduced since such term becomes relevant only at large temperatures, while we will only consider here the case of moderate to low $T_{\rm RH}$; also, we are not considering the possibility of a ψ_j particle decaying into a lighter ψ_k state, since we will not encounter a case of this kind in explicit models and it would just complicate the notation). The Boltzmann equation for the ψ_j number density is:

$$\frac{dn_{\psi_j}}{dt} + 3H n_{\psi_j} = \sum_i \frac{B_{\psi_j,X_i}}{m_{X_i}} \Gamma_{X_i} \rho_{X_i} - \Gamma_{\psi_j} n_{\psi_j} \,, \qquad (2.27)$$

where B_{ψ_j,X_i} is the mean number of particles ψ_j generated in the decay of the field X_i, i.e. it is the product of the branching ratio of decay into ψ_j times the mean multiplicity. The dark matter number density is traced by eq.(2.10) with the addition of source terms related to the decay of the X_i and ψ_j fields:

$$\frac{dn_\chi}{dt} + 3\,H\,n_\chi = -\langle\sigma_{\rm eff} v\rangle \left[n_\chi^2 - (n_\chi^{eq})^2 \right] + \sum_i \frac{B_{X_i}}{m_{X_i}} \Gamma_{X_i} \rho_{X_i} + \sum_j B_{\psi_j} \Gamma_{\psi_j} n_{\psi_j} \quad (2.28)$$

where $B_{X_i} \equiv \sum_a B_{\chi_a,X_i}$ and $B_{\psi_j} \equiv \sum_a B_{\chi_a,\psi_j}$ have been defined in analogy to B_{ψ_j,X_i}. Notice that the DM number density is still described by a single equation describing the sum of the number densities of the states $\{\chi_a\}$, in agreement with the hypothesis of kinetic equilibrium. This issue will be illustrated in detail in the next chapter, focusing on a specific particle physics scenario, and the problem of kinetic decoupling in models with non-thermal generation of DM particles will be addressed as well.

We keep track of the SM states only through their contribution to the radiation energy density and pressure which, using Eq. (2.26) and subtracting the contribution from ψ_j and χ_a fields, obey the equation:

$$\begin{aligned}
\frac{d\rho_R}{dt} + 3H(\rho_R + p_R) \;\simeq\; & \sum_i \left(1 - \frac{\sum_j B_{\psi_j,X_i} \langle E_{\psi_j,X_i}\rangle + B_{X_i} m_\chi}{m_{X_i}} \right) \Gamma_{X_i} \rho_{X_i} \\
& + \sum_j \left(\langle E_{\psi_j}\rangle - m_\chi B_{\psi_j} \right) \Gamma_{\psi_j} n_{\psi_j} \\
& + m_\chi \langle\sigma_{\rm eff} v\rangle \left[n_\chi^2 - (n_\chi^{eq})^2 \right] \,.
\end{aligned} \qquad (2.29)$$

In this equation $\langle E_{\psi_j,X_i}\rangle$ is the mean energy of the particle ψ_j at injection from the decay of the modulus X_i:

$$\langle E_{\psi_j,X_i}\rangle \equiv \int dE' \, \frac{d\mathcal{N}_{\psi_j,X_i}}{dE'} \, E' \qquad (2.30)$$

with $d\mathcal{N}_{\psi_j,X_i}/dE'$ the energy spectrum from the decay normalized to 1; $\langle E_{\psi_j}\rangle$ is

instead the mean energy for ψ_j particles:

$$
\begin{aligned}
\langle E_{\psi_j} \rangle(t)\, n_{\psi_j}(t) \;\;\equiv\;\; & \int_0^t dt' \sum_i \frac{B_{\psi_j, X_i}}{m_{X_i}} \Gamma_{X_i} \rho_{X_i}(t') \\
& \int dE' \frac{d\mathcal{N}_{\psi_j, X_i}}{dE'} \left[m_{\psi_j}^2 + \frac{a^2(t')}{a^2(t)} (E'^2 - m_{\psi_j}^2) \right]^{1/2} \cdot \quad (2.31) \\
& \cdot \frac{a^3(t')}{a^3(t)} \exp\left[-\Gamma_{\psi_j}(t - t') \right] \ .
\end{aligned}
$$

Finally, in Eq. (2.29) we have assumed that the mean energy of the χ_a states is equal to the mass m_χ of the lightest state χ_0, neglecting, at this level, thermal corrections and mass splittings between the coannihilating states, as well as the pressure term associated to χ_a.

Eqs. (2.25), (2.27), (2.28) and (2.29) define a system of coupled equations, closed by Friedmann equation giving H. The next chapter will be devoted to its accurate numerical solution, with and without the assumption of kinetic equilibrium during DM production, together with applications to some particle physics frameworks, mainly SUSY models. Here will just depict the main trends of non-thermal production of dark matter, at the level of approximate analytical formulae, in the very simplified scenario in which only one dark matter particle χ and a decaying modulus field X are present in addition to standard model states (see [Moroi 2000] and also e.g., [Pallis 2004, Gelmini 2006b] for a more detailed discussion).

In this simplified picture the system of coupled equations reduces to three equations only: the first for the decaying modulus, the second for number density of particle χ, sourced from the decay and depleted by pair annihilations, and the last for the temperature.

First of all, if the modulus decay induces a large increase in the entropy density and this happens at a later stage with respect to the chemical decoupling for χ, the thermal relic density of χ is greatly diluted and can be neglected, with the only relevant χ source being the particles produced in the decay itself. The entropy injection is a continuos process making the reheating phase last for an extended period during which one can show that the temperature evolves as $T \propto a^{-3/8}$ and the universe expansion rate as $H \propto T^4$ [Giudice 2001, Gelmini 2006b]. A standard approximation is however to treat the decay of the field and the thermalization of the products as instantaneous processes, and define the reheating temperature T_{RH} according to Eq. (2.23); depending on whether at T_{RH} the dark matter pair annihilation rate $\Gamma = n_\chi \langle \sigma v \rangle$ is larger or smaller than the expansion rate H, there are two distinct regimes determining the relic density for χ [Moroi 2000, Gelmini 2007]. If Γ is much larger than H, pair annihilations are very efficient and instantaneously decrease the number density of χ to the critical density level corresponding to $\Gamma(T_{RH}) \simeq H(T_{RH})$ when the annihilations stop; such critical density is then simply equal to:

$$
n_\chi^c \simeq \frac{H}{\langle \sigma v \rangle} \ . \tag{2.32}
$$

Assuming that there are no further entropy injections after T_{RH} we can again normalize the number density introducing the quantity Y_χ such that the relic density can be estimated as:

$$\Omega_\chi^{NT} = \frac{m_\chi s(T_0)}{\rho_c(T_0)} Y_\chi(T_0) = \frac{m_\chi s(T_0)}{\rho_c(T_0)} Y_\chi(T_{\mathrm{RH}}) \propto \frac{m_\chi}{\langle \sigma v \rangle T_{\mathrm{RH}}}, \qquad (2.33)$$

where $\rho_c(T_0)$ and $s(T_0)$ refer to the Universe critical density and entropy density at present. Remarkably we have applied the same rule of thumb as eq. (2.20), valid in the thermal scenario, with the only difference of replacing $T_{\mathrm{s.f.o.}}$ with T_{RH}. Thanks to this we can relate Ω_χ^{NT} with Ω_χ^T and the WIMP pair annihilation cross section through the following approximated expression:

$$\Omega_\chi^{NT} h^2 \simeq \frac{T_{t.f.o.}}{T_{\mathrm{RH}}} \, \Omega_\chi^T h^2 \simeq \frac{m_\chi/20}{T_{\mathrm{RH}}} \cdot \frac{3 \cdot 10^{-26}\ \mathrm{cm}^3\,\mathrm{s}^{-1}}{\langle \sigma v \rangle}. \qquad (2.34)$$

A particle χ whose thermal relic density is small compared to the DM density because the annihilation rate is too large, may become a viable dark matter candidate for an appropriate value of T_{RH}. This simple rescaling holds whenever the particles χ are copiously produced in the modulus decay and if the pair annihilation rate is sufficiently large; in the following, we refer this scenario as 'reannihilation regime'. If instead $n_\chi(T_{\mathrm{RH}})$ is lower than $n_\chi^c(T_{\mathrm{RH}})$, the particles produced in the decay do not interact further and their number density per comoving volume is frozen, being:

$$Y_\chi(T_{\mathrm{RH}}) = \frac{n_\chi(T_{\mathrm{RH}})}{s(T_{\mathrm{RH}})} \simeq \frac{B_X}{m_X} \frac{\rho_X(T_{\mathrm{RH}})}{s(T_{\mathrm{RH}})} \simeq \frac{3}{4} \frac{B_X}{m_X} T_{\mathrm{RH}} \qquad (2.35)$$

and hence giving a non-thermal relic density which is about (see also, e.g., [Gelmini 2006b]):

$$\Omega_\chi^{NT} h^2 \simeq 0.2 \cdot 10^4 \, B_X \frac{10\,\mathrm{TeV}}{m_X} \frac{T_{\mathrm{RH}}}{1\,\mathrm{MeV}} \frac{m_\chi}{100\,\mathrm{GeV}} \qquad (2.36)$$

Notice that, in this case, the final dark matter density depends on the physics of moduli not only through its proportionality to the reheating temperature but also through the ratio between the average number of particles χ produced per decay and the modulus mass B_X/m_X. This non-thermal scaling applies to the cases in which either the pair annihilation rate is small or the average number of particles χ produced per decay B_X is small.[2]

2.3 Kinetic equilibrium and decoupling

The standard computation of the DM relic abundance relies on an additional assumption besides the one already discussed when comparing with non-thermal production scenario, i.e. the dark matter is in thermal kinetic equilibrium with the SM

---

[2]Ref. [Gelmini 2006b] classifies two extra scenarios, already studied, e.g., in Ref. [Giudice 2001], corresponding to the case in which the main source of χ particles is pair production from SM background states; these applies essentially only in the limit of $B_X \to 0$ which we are not going to discuss, although the method outlined here would be suitable for them as well.

states of the thermal bath. The standard freeze-out paradigm, indeed, only refers to the chemical decoupling of the DM states, namely the fact that annihilations are no more compensated by their inverse processes and, consequently, the dark matter abundance decreases until it remains fixed when annihilation themselves become no more effective at a temperature of around $\frac{1}{20}$ the DM mass. However dark matter also interacts by mean of elastic or inelastic scattering processes with SM states. These kind of processes keep the DM in the so called thermal equilibrium [Boehm 2001, Green 2005], i.e. the DM is part of the heat bath implying that its distribution function still traces the thermal one and, consequently, its temperature, defined (see expression below) from the second moment of the distribution function, coincides with the one of the thermal bath. In most of scenarios kinetic equilibrium is expected to hold much longer with respect to chemical one as consequence of the fact the scattering rate over SM states, $\sigma \, v' n_{\text{rad}}^{\text{eq}}$, is much larger of the DM pair annihilation rate $\sigma \, v n_\chi^{\text{eq}}$. This is due to the dependece of the scattering rate on the number density of SM states, dominated by the relativistic contribution scaling as T^3, resulting much greater than the one of the DM states $n_\chi^{\text{eq}} \sim T^{3/2} \exp\left(-\frac{m_\chi}{T}\right)$ while the two cross section are usually related by crossing symmetries, thus resulting comparable. As already mentioned, this framework allows, in the standard WIMP scenario the single equation description for the DM also in the case it is part of a larger set of particles.

The departure from the thermal equilibrium occurs when scattering processes becomes ineffective respect to the Hubble expansion rate and is identified by a characteristic temperature referred as kinetic decoupling temperature T_{kd}. This temperature has a deep observational relevance since the physics processes involved in dark matter interactions at the time of kinetic decoupling influence density perturbations on very small scales and hence the properties of the first generations of structures to form. More precisely matter density perturbations at very small scales are smoothed-out by free streaming of DM particles after kinetic decoupling [Green 2004, Green 2005] and an analogous effect is triggered by viscosity effects in DM-radiation interaction when DM is still coupled to the thermal bath [Hofmann 2001] . The combination of this two effects result in a fundamental small scale cut-off in the power spectrum of DM density perturbations which determine the mass scale of the first gravitationally bound structures [Loeb 2005]. The current dark matter distribution is influenced, at small scales, by these protohalos, provided that they are able to survive up to present times (see e.g. [Diemand 2005, Rubino-Martin 2006, Green 2007, Goerdt 2007, Berezinsky 2008]) and can be probed by current dark matter detection experiments [Bringmann 2009].

Compared to the chemical decoupling temperature an estimate of T_{kd} is more difficult to achieve and an accurate determination requires an ad hoc formalism. In particular it results that departure from thermal equilibrium starts when the scattering rate is still greater than the Hubble expansion rate [Bringmann 2007]. Indeed, for weakly interacting particles, the maintenance of thermal equilibrium requires a high number of collision; for this reason, in order to estimate T_{kd}, one should compare the so-called relaxation time τ_r, defined as the typical time scale needed

to restore thermal equilibrium after a perturbation, rather than the scattering rate associated to the last scattering time.

The relaxation time can be approximatively computed in the following way: during each scattering process, the relativistic SM states transfer to a non relativistic DM particle a momentum Δp of the order of the temperature of the heat bath. The numerous collisions induce a random walk over the momentum space [Bringmann 2007], thus, assuming Δp constant during the relaxation process, the total variation of the DM momentum after N collisions is given by $\Delta p N^{1/2}$. The relaxation time can be determined as $\tau_r \approx N_c/\Gamma_{\rm sc}$ with $\Gamma_{\rm sc}$ being the scattering rate while N_c represents the number of collisions needed by thermal equilibrium to hold. This number can be computed by imposing that the total momentum variation of the DM is equal to the typical momentum of a thermally distributed WIMP, i.e. $(m_\chi T)^{1/2}$. Substituting the result one finally gets:

$$\tau_r = \frac{T}{m_\chi} \frac{1}{\Gamma_{\rm sc}} \tag{2.37}$$

The kinetic decoupling temperature can be derived from the relation $\tau_r^{-1}(T_{\rm kd}) = H(T_{\rm kd})$. Given that T/M_χ is lower (or much lower) than 1 the value obtained for the temperature results sensitively greater than the value at which the scattering rate matches the expansion rate.

A proper treatment of the decoupling process, possibly leading to a more accurate determination of the decoupling temperature, requires the solution of the Boltzmann equation governing the dynamics of the DM phase space distribution. This is a rather troublesome task since processes with very different time scales are involved in the kinetic decoupling; on one side there is the propagation of the non-relativistic dark matter (slow process) while on the other there is the relativistic propagation of the SM states (fast processes). A rather elegant solution to this issue is obtained by defining a kinetic temperature parameter T_χ for the WIMP defined from the second momentum of the distribution function:

$$T_\chi = \frac{2}{3} \left\langle \frac{p^2}{2m_\chi} \right\rangle, \quad \left\langle \frac{p^2}{2m_\chi} \right\rangle \equiv \frac{1}{2m_\chi n_\chi} \int \frac{d^3p}{(2\pi)^3} p^2 f_\chi(p) \tag{2.38}$$

This temperature results equal to the one of the heat bath as long the phase space distribution f_χ traces the thermal equilibrium one $f_\chi^{\rm eq}(T, m_\chi)$ while represents the characteristic temperature associated with the DM distribution function after kinetic decoupling. Performing the integral of the second momentum of the distribution function one can derive, from eq. (2.1), a Boltzmann equation describing the time evolution of the kinetic temperature T_χ. Furthermore, around kinetic decoupling, the dark matter mass results much larger then all the other scales involved in the equation. This allows to expand the original collisional operator in powers of p^2/m_χ^2, decoupling the two categories of processes involved in kinetic decoupling, and allowing for a rather simple expression for the equation for T_χ [Bringmann 2007]:

$$(\partial_t + 5H) T_\chi = 2m_\chi c(T) (T - T_\chi) \tag{2.39}$$

with the parameter $c(T)$ encoding all the informations about the interactions relevant for equilibrium. The expression for $c(T)$ is model dependent and can be obtained from a suitable expansion of the collision operator of the original Boltzmann equations. In appendix B we will derive it in two examples referring, respectively, to elastic and inelastic scattering cases. Analogously to the equation for the DM number density we can be introduce a variable redefinition in order to cut away the term accounting for Hubble expansion. Choosing again $x = m_\chi/T$ as independent variable we can define the new variable y [Bringmann 2009]:

$$y \equiv m_\chi g_{\text{eff}}^{-1/2} \frac{T_\chi}{T^2} \tag{2.40}$$

which brings (2.39) to:

$$\frac{dy}{dx} = 2 \frac{m_\chi c(T)}{H \tilde{g}^{-1/2}} \left(1 - \frac{T_\chi}{T}\right) \tag{2.41}$$

where $\tilde{g}^{-1/2} \equiv g_{\text{eff}}^{1/2} / \left(1 + \frac{1}{4} \frac{g'_{\text{eff}}}{g_{\text{eff}}} T\right)$ (with the $'$ referring to derivative with respect to x). This expression makes rather clear the trends of the solution. At high temperature the scattering rate is expected to be larger than H, the term in front of the right-hand side is much greater than 1 and T_χ coincides with T. On the contrary a low temperatures the right-hand side goes to zero than $y \equiv g_{\text{eff}}^{-1/2} \frac{T_\chi}{T^2} \to$ constant implying that $T_\chi \propto m_\chi g_{\text{eff}} T^2/m_\chi \propto a^{-2}$. The numerical solution of eq.(2.39) (see also next chapter) shows that there is a rather sharp transition between these two asymptotic regimes such that the kinetic decoupling can be numerically determined by their matching.

2.4 WIMP dark matter in the MSSM

In the previous section we have discussed WIMP dark matter generation from general perspective. Now we will focus on a specific particle physics framework, i.e. $N = 1$ Supersymmetric theories, more specifically their minimal realization, the so called Minimal SuperSymmetric Standard Model, MSSM (for a review see, for example, [Martin 1997]). Supersymmetry is one of the most appealing and investigated BSM theoretical frameworks. In this thesis we will consider SUSY models in view of their capability of providing viable dark matter candidates; we also briefly review other theoretical motivations for the introduction of Supersymmetry.

For example SUSY seems a natural ingredient of Grand Unification Theories (GUT) since, by introducing new states, it improves the unification of the gauge couplings with respect to the case of the presence of only SM states; furthermore it is very naturally linked with gravity theories, in particular many SUSY models can be seen as low energy limit of string theories.

The main theoretical argument in favor of SUSY is, however, probably the solution of the so-called hierarchy problem, i.e. the issue of canceling the quadratic divergencies of the radiative corrections to the higgs boson mass. Interestingly this motivation implies that the superpartners should lie close to the EW scale; the exact

requirement on the mass scale depends on the amount of fine-tuning regarded as tolerable (this issue it is also known as naturalness problem). On the other hand, the recent discovery of a higgs boson candidate with mass of around 126 GeV, combined with the negative outcome of searches of superpartner production seem to disfavor the naturalness argument, despite some way-outs are still feasible (see for example [Strumia 2011, Papucci 2011, Baer 2012a] for recent discussions).

As already mentioned the focus of this thesis will be the properties of DM candidates in the MSSM, hence, apart of few exceptions, we will pursue a phenomenological approach without theoretical prejudices.

In the next subsection we provide a brief recap of the MSSM, mainly in order to fix the notation, then in the following one we will concentrate on the dark matter candidates.

2.4.1   Definition of MSSM

According to Supersymmetry, standard model fermions are embedded into larger multiplets called chiral mutliplets each one containing also a bosonic state (sfermion) representing the superpartner of the corresponding standard model state and sharing with it the same quantum numbers under the SM symmetry group. Standard model gauge bosons are as well part of multiplets, referred as gauge multiplets, containing a fermionic superpartner (gaugino). The main interactions, allowed by the SM gauge symmetry group as well as by baryon and lepton number conservation, are described by the so called superpotential (for simplicity gauge and generation indices will be omitted):

$$W = Y_e h_d l e^c + Y_d h_d q d^c + Y_u h_u q u^c + \mu h_u h_d \tag{2.42}$$

where q, l, e^c, d^c and u^c represents the chiral multiplets associated to the $SU(2)_L$ doublets and singlets while $Y_{e,u,d}$ are the SM Yukawa matrices. h_u and h_d represent a pair of higgs doublets; contrary to the SM, at least two higgs doublets are needed because the superpotential is required to be holomorfic. They must also have opposite hypercharge in order to avoid the triangle anomaly. Experimental evidences require that supersymmetry is not exact at the EW scale. For this reason, in addition to the terms coming from the superpotential, the MSSM lagrangian allow a set of terms, explicitly violating supersymmetry without reintroducing quadratic divergencies, (and thus referred as soft SUSY breaking terms), accounting for the still undiscovered mechanism of breaking of this symmetry:

$$
\begin{aligned}
\mathcal{L}_{\text{soft}} = {} & \frac{1}{2}M_1 \tilde{B}\tilde{B} + \frac{1}{2}M_2 \tilde{W}\tilde{W} + \frac{1}{2}M_3 \tilde{g}\tilde{g} + h.c. \\
& + \sum_{\tilde{f}=q,l,u^c,d^c,e^c} \mathbf{m}_{\tilde{f}}^2 \tilde{f}\tilde{f}^* + m_{h_u}^2 h_u h_u^* + m_{h_d}^2 h_d h_d^* \\
& + \left(\mathbf{A}_e h_d \tilde{l}^* \tilde{e}^c + \mathbf{A}_d h_d \tilde{q}^* \tilde{d}^c + \mathbf{A}_u h_u \tilde{q}^* \tilde{u}^c + h.c. \right) \\
& + \left(B \tilde{h}_u \tilde{h}_d + h.c. \right)
\end{aligned}
\tag{2.43}
$$

where $\tilde{f}$ ($\tilde{f} = \tilde{q}, \tilde{l}, \tilde{u}^c, \tilde{d}^c, \tilde{e}^c$)) are the scalar components of the chiral multiplets while $\tilde{B}$, $\tilde{W}$, $\tilde{g}$, $\tilde{h}_u$ and $\tilde{h}_d$ are the superpartners of the gauge and higgs bosons, called, respectively, Bino, Wino, gluino and Higgsinos. The superpotential (2.42) contains the minimal set of interactions required by the Standard Model. However other terms can be included without conflicting with Supersymmetry. The most general MSSM superpotential contains the following additional terms:

$$\tilde{W} = \mu_i\, \ell_i h_u + \lambda_{ijk}\, \ell_i \ell_j e_k^c + \lambda'_{ijk}\, d_i^c \ell_j q_k + \lambda''_{ijk}\, d_i^c d_j^c u_k^c \,, \qquad (2.44)$$

where we have again omitted, for simplicity, $SU(2)$ indices. The first three terms of (2.44) violate lepton number while the last one violates baryon number. The new interactions introduced by these operators are responsible of several exotic phenomena whose non observation constrain somehow the couplings μ_i, λ, λ' and λ''. In particular the strongest bounds comes from proton decay, which is induced by any combination of a lepton and a baryon violating coupling. The rates obtained largely exceed the experimental bounds unless the couplings involved in the considered processes are extremely suppressed (for detailed list of bounds see, for example [Smirnov 1996b, Fileviez Perez 2005]).

The customary solution to avoid dangerous sources of lepton and baryon number violation is the introduction of a discrete symmetry, called R-parity defined as:

$$R = (-1)^{3B+L+2s} \qquad (2.45)$$

with B, L and s representing, respectively, baryon number, lepton number and spin. SM states and the corresponding superpartners are differntly charged with respect to this new symmetry, having, respectively, charge $+1$ and -1. As a consequence the superpotential (2.44) is now forbidden restoring lepton and baryon number conservation analogously to the SM. Corollaries of R-parity conservation are that collider processes must produce supersymmetric particles in pairs and, moreover, heavier supersymmetric particles can decay only into lighter supersymmetric ones. The most important corollary is, however, the fact that the lightest superpartner (LSP) must be stable, thus being a potentially candidate for dark matter. Remarkably, in SUSY theories, DM stability is not enforced by an ad hoc introduced property but it is rather a by product of general features of the theory. From now on we will mostly restrict to R-parity preserving realizations of the MSSM. On the other hand, models with viable dark matter phenomenology, exist also in the case that R-parity is only quasi-exact (in agreement with bounds from lepton and baryon number violating processes). These will be the object of study of the last part of this thesis.

As already mentioned the definition of the MSSM implies the request of minimal field content. Apart from superparnters, theoretical consistency requires only the enlargement of the higgs sector with respect to the Standard Model. On the other hand it is customary to consider, in addition, a gravity multilplet containing the spin-2 graviton and its spin-3/2 fermionic superpartner, the gravitino. In particular the latter is a state with great phenomenological relevance. Its mass depends on the mechanism of SUSY breaking and can be greater or of the same order the mass of the other superpartners, as well as much lighter, being in this case the DM candidate.

A part from the gravitino the MSSM spectrum is derived from (2.42) and (2.43) in the following way.

The superpartners of the quarks and of the leptons are eigenstates of 6×6 matrices (ad exception of sneutrinos for which the matrix is only 3×3) of the form:

$$M_{\tilde{u}}^2 = \begin{pmatrix} \mathbf{m}_{\tilde{q}}^2 + \mathbf{m}_u^2 + \Delta_{\tilde{u}_L} & v\left(\mathbf{A}_u^\dagger \sin\beta - \mu Y_u \cos\beta\right) \\ v\left(\mathbf{A}_u \sin\beta - \mu^* Y_u \cos\beta\right) & \mathbf{m}_{\tilde{u}^c}^2 + \mathbf{m}_u^2 + \Delta_{\tilde{u}_R} \end{pmatrix}$$

$$M_{\tilde{d}}^2 = \begin{pmatrix} \mathbf{m}_{\tilde{d}}^2 + \mathbf{m}_d^2 + \Delta_{\tilde{d}_L} & v\left(\mathbf{A}_d^\dagger \cos\beta - \mu Y_u \sin\beta\right) \\ v\left(\mathbf{A}_u \cos\beta - \mu^* Y_d \sin\beta\right) & \mathbf{m}_{\tilde{d}^c}^2 + \mathbf{m}_d^2 + \Delta_{\tilde{d}_R} \end{pmatrix}$$

$$M_{\tilde{l}}^2 = \begin{pmatrix} \mathbf{m}_{\tilde{l}}^2 + \mathbf{m}_l^2 + \Delta_{\tilde{l}_L} & v\left(\mathbf{A}_e^\dagger \cos\beta - \mu Y_e \sin\beta\right) \\ v\left(\mathbf{A}_e \cos\beta - \mu^* Y_e \sin\beta\right) & \mathbf{m}_{\tilde{e}^c}^2 + \mathbf{m}_l^2 + \Delta_{\tilde{l}_R} \end{pmatrix}$$

$$M_{\tilde{\nu}}^2 = \mathbf{m}_{\tilde{\nu}}^2 + \mathbf{m}_\nu^2 + \Delta_{\tilde{\nu}_L} \tag{2.46}$$

where:

$$\Delta_{\tilde{f}_L} = m_Z^2 \cos 2\beta (T_{3f} - Q_f \sin^2\theta_W)$$

$$\Delta_{\tilde{f}_R} = m_Z^2 \cos 2\beta Q_f \sin^2\theta_W$$

$$\mathbf{m}_u = diag(m_u, m_c, m_t), \quad \mathbf{m}_d = diag(m_d, m_s, m_b)$$

$$\mathbf{m}_l = diag(m_e, m_u, m_\tau), \quad \mathbf{m}_\nu = diag(m_{\nu_e}, m_{\nu_\mu}, m_{\nu_\tau})$$

$$v = \sqrt{\frac{v_u + v_d}{2}}$$

$$\tan\beta = \frac{v_u}{v_d} \tag{2.47}$$

with v_u and v_d being the v.e.v's of the higgs fields. If all the entries of the matrices above where of the same order their off-diagonal elements would originate at the tree-level FCNC processes at excessively large rates. In order to put these effects under control is to assume the matrices $\mathbf{m}_{\tilde{q}}$ and $\mathbf{A}_f$ diagonal in the flavor space so that the matrices (2.46) can at most induced between states $\tilde{f}_L$ and $\tilde{f}_R$.

The two complex higgs doublets originate 5 higgs bosons., two neutral CP-even labeled as h and H, one neutral CP-odd A, and two charged states $H^\pm$. Their masses are, at the tree level [Martin 1997]:

$$m_A^2 = 2|\mu|^2 + m_{h_d}^2 + m_{h_u}^2$$

$$m_{h,H}^2 = \frac{1}{2}\left(m_A^2 - m_Z^2 \mp \sqrt{(m_A^2 - m_Z^2)^2 + 4m_Z^2 m_A^2 \sin^2 2\beta}\right)$$

$$m_{H^\pm}^2 = m_A^2 + m_W^2 \tag{2.48}$$

Interestingly from (2.48) it is evident that, while the masses of H, A and $H^\pm$, can assume any value, the mass of the h state is bounded, a tree level, by:

$$m_h \leq m_Z |\cos 2\beta| \tag{2.49}$$

LEP constraints on the higgs mass imply that sizable loop corrections to (2.49) are needed in order to properly determine the higgs mass. Once all the relevant corrections are included the mass of the h is still bounded from above also for SUSY masses much above the TeV scale, more precisely (for a review of the MSSM higgs sector see e.g. [Djouadi 2008]):

$$m_h \lesssim 135 \text{GeV} \tag{2.50}$$

The superpartners $\tilde{B}$ and $\tilde{W}$ of the neutral $SU(2) \times U(1)$ gauge bosons mix with the two higgsinos $\tilde{h}_u$ and $\tilde{h}_d$ according to the following mass matrix (it is written in the basis $\left(\tilde{B}, \tilde{W}, \tilde{h}_u, \tilde{h}_d \right)$):

$$M_N = \begin{pmatrix} M_1 & 0 & -\cos\beta \sin\theta_W M_Z & \sin\beta \sin\theta_W M_Z \\ 0 & M_2 & \cos\beta \cos\theta_W M_Z & -\sin\beta \cos\theta_W M_Z \\ -\cos\beta \sin\theta_W M_Z & -\sin\beta \cos\theta_W M_Z & 0 & -\mu \\ \sin\beta \sin\theta_W M_Z & -\sin\beta \cos\theta_W M_Z & -\mu & 0 \end{pmatrix} \tag{2.51}$$

The physical mass states are four Maiorana fermions, named neutralinos, obtained by the diagonalization of this matrix:

$$\chi_i^0 = N_{i1}\tilde{B} + N_{i2}\tilde{W} + N_{i3}\tilde{h}_u + N_{i4}\tilde{h}_d \tag{2.52}$$

where N_{ij} are the elements of the mixing matrix. Depending on the size of this elements, which are in turn a function of M_1, M_2, μ and $\tan\beta$, a neutralino can be bino-like, wino-like, higgsino-like or a mixed state.

An analogous mixing also occur among charged gauginos and higgsinos. In this case one has a 2×2 mass matrix:

$$M_C = \begin{pmatrix} M_2 & \sqrt{2}\sin\beta m_W \\ \sqrt{2}\cos\beta m_W & \mu \end{pmatrix} \tag{2.53}$$

whose eigenstates are two dirac fermions called charginos. As before a chargino is gaugino or higgsino-like depending on M_2, μ and $\tan\beta$.

The lagrangian (2.43), and thus the entries of the previous matrices, depends on the mechanism of SUSY-breaking and hence on the UV completion of the theory under consideration. One can pursue, anyway, a pure phenomenological approach regarding all the parameters of the lagrangian as free; however the most general MSSM lagrangian posseses more than one hundred parameters making a full analysis extremely challenging. For this reason it is customary to do some assumptions aimed to restrict the number of free parameters. We have already cited, ad example, the assumption of taking diagonal sfermion mass matrices guaranteeing the absence of tree-level FCNC. As an example we mention the most popular realization of the MSSM, i.e. the so called Constrained MSSM (CMSSM), which is determined by only five parameters: a common value m_0 for all the soft scalar mass parameters, assumed in addition to be diagonal in the flavor space, a common mass for the gauginos $M_{1/2} = M_1 = M_2 = M_3$, a parameter A_0 relating the A terms to the

SM Yukawas, i.e. $\mathbf{A}_f = A_0 Y_f$, $\tan\beta$ defined as the ratio of the two higgs $v.e.v.$'s, $\tan\beta = v_u/v_d$, and the sign of the μ parameter. This five parameters are defined at some high scale, typically the GUT or the Planck scale, and the full SUSY spectrum is obtained by solving the suitable Renormalization Group equations (RGE).

2.4.2   Neutralino as DM candidate

In this section we will describe the WIMP dark matter candidates in the R-parity preserving MSSM in view of the general discussion of section (2.1). Having, in particular, in mind the classification given in that section, we can identify the set of superpartners with the states $\{\chi_a\}$ with the LSP as dark matter candidate. An exception, however is constituted by the gravitino. This particle interacts only through gravity, hence too weakly for thermalizing in the early Universe. For the moment we assume that the gravitino is not the LSP classifying it a $\psi-$type state. The case in which the gravitino is the DM candidate presents a sensitively different phenomenology with respect to WIMP DM and will deserve a dedicated discussion. MSSM has two electromagnetically neutral states which can be the LSP and hence the dark matter candidates, the lightest sneutrino and the lightest neutralino. The former is one of the scalar superpartners of the SM neutrinos. However it has already been ruled out as a dark matter candidate because of its coherent interactions with heavy nuclei are too large. Indeed direct detection experiments exclude a stable sneutrino with mass between few GeV and several TeV [Falk 1994]. Lighter sneutrinos are instead excluded by LEP measurments of Z invisible width [2003].

The only WIMP DM candidate is then the lightest neutralino whose relic density can be computed through the techniques introduced in section (2.1). Here we will provide a recap of the thermal scenario while in the next chapter we will discuss non-thermal production according our numerical treatment of Boltzmann equations. As already mentioned, in the standard scenario one has to solve eq.(2.10) with n being the sum of the number densities of all the supersymmetric particles. Despite its elegance, the standard WIMP paradigm suffers several shortcomings in the MSSM. Indeed the pair annihilation cross section very hardly matches the cosmologically favored value. On the contrary in most of the MSSM parameter space the neutralinos results either largely overabundant or underabundant. The occurrence of one of these two cases depends on the intrinsic composition of the neutralino since this determines the relevant processes contributing to the pair annihilation cross section (in the following chapters we will also see that the neutralino composition largely impacts the direct detection cross section).

In the most popular scenarios, including the CMSSM, the lightest neutraino is bino-like. In such a case the main annihilation channel is into a fermion pair occurring through t-channel sfermion exchange. The cross section can be expanded as:

$$\langle \sigma v \rangle = a + b v^2 \tag{2.54}$$

where [Olive 1989]:

$$a = \left(1 - \frac{m_f^2}{m_\chi^2}\right)^{1/2} \frac{g_1^4}{128\pi} \left(Y_{\mathrm{Lf}}^2 + Y_{\mathrm{Rf}}^2\right)^2 \frac{m_f^2}{\Delta_f^2} \qquad (2.55)$$

$$b = \left(1 - \frac{m_f^2}{m_\chi^2}\right)^{1/2} \frac{g_1^4}{128\pi} \left[2Y_{\mathrm{Lf}}^2 Y_{\mathrm{Rf}}^2 \left(-3\frac{m_f^2}{\Delta_f^2} - \frac{6m_\chi^2 m_f^2}{m_f^2}\Delta_f^3 + \frac{10m_\chi^4 m_f^2 - 10m_\chi^4 m_f^2}{m_f^2}\Delta_f^4 \right) \right.$$
$$\left. + \left(Y_{\mathrm{Lf}}^4 + Y_{\mathrm{Rf}}^4\right)\left(\frac{4m_\chi^2 - m_f^2}{\Delta_f^2} + \frac{-8m_\chi^4 + 2m_\chi^2 m_f^4}{\Delta_f^3} + \frac{8m_\chi^6 - 6m_\chi^4 m_f^2 - 2m_\chi^2 m_f^4}{\Delta_f^4} \right) \right]$$
$$+ \left(-3 + \frac{3m_f^2}{4\left(m_\chi^2 - m_f^2\right)} \right) a \qquad (2.56)$$

where

$$\Delta_f = m_{\tilde{f}}^2 + m_\chi^2 - m_f^2 \qquad (2.57)$$

and

$$Y = 2\left(Q_f - T_{3f}\right) \qquad (2.58)$$

with the index f running over all the quarks and leptons. As evident from the expression above the s-wave contribution to the annihilation cross section results suppressed by a factor of the order $m_f^2/m_{\tilde{f}}^2$. This is originate by the so-called chirality flip occurring when two Maiorana fermions annihilate in s-wave into two Dirac fermions. The cross section is then dominated by the p-wave term which is, however, suppressed as well because the LSP are non relativistic at low temperatures. Simplifying the expressions above in the limit of massless final state fermions (always valid ad exception of the top quark) we get:

$$a = 0, \quad b = \sum_f \frac{g^4 t_W^4 (T_f - Q_f)^4 r(1+r)}{2\pi m_{\tilde{f}}^2 (1+r)^4} \quad r = \frac{m_\chi^2}{m_{\tilde{f}}^2} \qquad (2.59)$$

from which is evident the rapid decrease of the annihilation cross section with the the sfermion mass scale. The value of the cross section compatible with cosmology is achieved for values of at least one sfermion mass of around 100-200 GeV. This value is close to the LEP bound for non SM charged particles and is largely excluded by LHC data for what regards squark masses (see for example [ATL 2012e] for the latest results).

A part from regions at very low slepton masses bino, overproduction can be avoided in case of s-channel resonances of annihilation process mediated by Z and higgs bosons, occurring when the dark matter mass is around one half the mass of one of these particles. Another possibility is the occurrence of coannihilations with particles possibly having stronger interactions with SM states with respect to the LSP, among the initial states. Both the solution proposed, however, require a

sizable amount of fine-tuning, moreover they require connection between in principle uncorrelated MSSM parameters.

The scenario is rather different in the case of wino or higgsino dark matter. In this case, in fact, a very efficient s-wave annihilation channel into a pair of charged W bosons is allowed. The annihilation cross section for a wino LSP (the higgsino one is very similar) is given by:

$$\langle \sigma v \rangle = \frac{1}{m_{\chi_1^0}^2} \frac{g^4}{2\pi} \frac{(1 - x_W)^{3/2}}{(2 - x_W)^2} \tag{2.60}$$

where $x_W = m_W^2/m_{\chi_1^0}^2$. For DM masses of the order of few hundreds of GeV this cross section is several orders of magnitude greater with respect to the bino case. Moreover for DM masses above the TeV, the cross section is increased by the so called Sommerfeld enhancement [Hryczuk 2011]. Once also this effect is taken into account the correct DM relic density is achieved for DM of the order 1.4 TeV in the case of higgsino and 2.7 TeV in the case of Wino. Apparently the wino/higgsino scenario is a very straightforward realization of the WIMP miracle paradigm; on the other hand this framework is not much appealing since the high value of masses required for the LSP, and the consequent shift toward the multi-TeV range of the whole MSSM spectrum, results in contrast with naturalness. Moreover this kind of scenarios would have poor prospects of detection of Supersymmetry at LHC.

Until now has been only considered the case of neutralino DM as a pure state, bino, wino or higgsino. The previous discussion instead evidences as mixed-dark matter states can be a favorable cosmological scenario. Indeed in this case both (2.59) and (2.60), weighted by the elements of the mixing matrix N, contribute to the relic density. The most popular and easily realized case is the bino-higgsino mixture; on the other hand this scenario is constrained by direct detection experiments since the scattering cross section of dark matter with nucleons increases with its higgsino component (see chapter .. for more details). On the contrary the mixed bino-wino case is more complex to realize because of the larger amount of fine tuning required for achieving the correct relic density. (For a more extensive discussion of mixed-state neutralino dark matter see e.g. [Arkani-Hamed 2006]). In any case it is again necessary to relate parameters expected to be independent.

This issue is solved in a very elegant way in case of non-thermal production. As already sketched in eq 2.34 and confirmed by our numerical treatment (see next chapter) an efficient production of dark-matter leads to an increase of the relic density of strongly annihilating particles. Wino and higgsino dark matter with masses of the order of few hundreds of GeV can match the cosmological relic density for moderately low values of the reheating temperature, opening the possibility for SUSY spectra detectable at LHC. In the case of bino dark matter, we can instead anticipate that the most relevant effect is the dilution due to the entropy injection associated to the decay of the cosmological moduli. At moderate/low reheating temperatures the bino abundance is then strongly reduced and can achieve the correct value provided that non-thermal production is not too much efficient.

We conclude by briefly referring to kinetic decoupling for neutralino dark matter, restricting to the standard paradigm. Possible deviations, as well as the accurate treatment of as specific case, will be instead arguments of the next chapter.

In case that the dark matter is dominated by the bino component, kinetic equilibrium depends on elastic scattering processes with relativistic SM states whose rates are related, by crossing symmetry, to the pair annihilation cross section. Given then the dependence on the sfermion mass scale the temperature of kinetic decoupling turns to be model dependent, varying in the range between few MeV and few GeV [Profumo 2006, Bringmann 2007]. On the contrary, when the DM posseses a sizable higgsino or wino component also inelastic scattering processes, made possible by the presence of a chargino almost degenerate with the DM, in addition to the above mentioned processes. Particularly interesting is the case, which will be discussed in more detail in the next chapter, of a pure Wino dark matter being, in this case, the mass splitting of around 160 MeV. Indeed, almost irrespectively of the model, a Wino dark matter has unsuppressed, either elastic of inelastic, interactions with the heat bath fixing its kinetic decoupling temperature to the order of few MeV [Hisano 2001].

Non-thermal neutralino Dark Matter

Contents

This chapter is devoted to a detailed examination of the issue of non-thermal generation of DM. In the following will be presented a full numerical solution of the relevant set of equations, including the equation of motion for the heavy fields and the system of coupled Boltzmann equations, implemented by a numerical code, interfaced to an appropriately modified version of the public available DarkSUSY package [Gondolo 2004], which allows, for any definite particle physics scenario, a very accurate computation of the relic abundance of the DM particle. This numerical procedure avoids to introduce approximations such as instantaneous reheating and production of DM particles, or others.

In the following we will provide several examples of its application in a sample of progressively refined particle physics scenarios. First of all we will consider a model independent framework in which DM particles are schematically defined through the values of the mass and a temperature-independent pair annihilation cross section. The main numerical trends of the numerical solution of the Boltzmann equations, already sketched in section 2.1, will be rediscussed in a systematic way; moreover the non-thermal production scenario will be investigated in view of the anomalies in cosmic rays reported by Pamela and Fermi experiments.

We will then focus on non-thermal production of neutralino DM in the MSSM. Our first aim will be to discuss the impact of non-thermal production in selecting the preferred mass scale and intrinsic composition of the neutralino compared to the standard thermal scenario. To this purpose we will restrict, in particular, to the the framework usually dubbed "Split Supersymmetry" [Arkani-Hamed 2005b, Giudice 2004], in which, since the sfermion sector is not playing any relevant role, the parameter space is sharply reduced compared to a general MSSM but it is still enough general.

We will finally examine in detail a specific class of models, referred as G2-MSSM [Acharya 2007], which provide rather precise predictions for the spectrum of low energy SUSY particles as well as of the gravitino and the moduli fields. Such definite framework has been also a good playground for testing the validity of some of the approximations that are usually given for granted in the solution of the Boltzmann equation for DM. Indeed the neutralino LSP is nearly degenerate in mass with a chargino. According the general discussion of the previous chapter dark matter is actually described by a system of two coannihilating particles whose evolution can be encoded in a single equation, under the assumption of kinetic equilibrium. This approach, however, may not be valid in low reheating temperature scenarios. In order to account for this case our numerical code implements the solution of the general system of coupled Boltzmann equations for the single particle species as well as a formalism for determining the kinetic decoupling temperature of the DM.

3.1   The general framework for non-thermal dark matter production

The relic density of dark matter can be evaluated by evolving Eqs. (2.25), (2.27), (2.28) and (2.29), together with the Friedman equation giving H, from an initial time, which we assume to be the time when the heaviest modulus starts its coherent oscillations, up to the stage when the DM comoving number density becomes constant. Following a similar procedure as the one depicted in section 2.1 we have reformulated the system of equation in order to implement the numerical solution. The choice of independent and dependent variables, however, differs from the thermal scenario.

Indeed the entropy density of the primordial thermal bath is not expected to be conserved along the whole phase of dark matter generation and the radiation temperature itself, as will be clarified in a while, has a different behaviour with respect to the scale factor at different stages of the evolution of the DM density. For this reason, in the choice of the independent variable, we have replaced the time t with the rescaled scale factor $A \equiv a/a_I$, with a_I an arbitrary parameter with dimension of the inverse of an energy. The temperature, instead, have been chosen as dependent variable encoding the evolution of the radiation energy density, expressing ρ_R and p_R in terms of the entropy density through the standard definitions:

$$s(T) = \frac{\rho_R(T) + p_R(T)}{T} \equiv \frac{2\pi^2}{45} h_{\text{eff}}(T) T^3 \qquad \text{and}$$
$$\rho_R(T) \equiv \frac{\pi^2}{30} g_{\text{eff}}(T) T^4 = \frac{3}{4} \frac{g_{\text{eff}}(T)}{h_{\text{eff}}(T)} T s(T)\,, \tag{3.1}$$

Finally, following [Giudice 2001], the fields χ_i, X_i and ψ_i are described by the following dimensionless quantities:

$$\xi_{X_i} \equiv \frac{\rho_{X_i} a^3}{\Lambda}\,, \qquad N_{\psi_j} \equiv n_{\psi_j} a^3 \qquad \text{and} \qquad N_\chi \equiv n_\chi a^3\,, \tag{3.2}$$

with Λ an arbitrary energy scale. The values of a_I and Λ are chosen in order to guarantee the best numerical stability to the solution, a sample guess being, respectively, T_{RH}^{-1} and T_{RH}, with the approximate reheating scale as given through Eq. (2.23). After this change of variables the system becomes:

$$
\begin{aligned}
\frac{d\xi_{X_i}}{dA} &= -\frac{A^{1/2}a_I^{3/2}}{\mathcal{H}}\Gamma_{X_i}\xi_{X_i} \\
\frac{dN_{\psi_j}}{dA} &= \frac{A^{1/2}a_I^{3/2}}{\mathcal{H}}\left(\Lambda\sum_i \frac{B_{\psi_j,X_i}}{m_{X_i}}\Gamma_{X_i}\xi_{X_i} - \Gamma_{\psi_j}N_{\psi_j}\right) \\
\frac{dN_\chi}{dA} &= -\frac{\langle\sigma_{\mathrm{eff}}v\rangle}{A^{5/2}a_I^{3/2}\mathcal{H}}\left[N_\chi^2 - (N_\chi^{eq})^2\right] + \frac{A^{1/2}a_I^{3/2}}{\mathcal{H}}\left(\Lambda\sum_i \frac{B_{X_i}}{m_{X_i}}\Gamma_{X_i}\xi_{X_i} + \sum_j B_{\psi_j}\Gamma_{\psi_j}N_{\psi_j}\right) \\
\frac{dT}{dA} &= \left(1 + \frac{T}{4g_{\mathrm{eff}}}\frac{dg_{\mathrm{eff}}}{dT}\right)^{-1}\left\{-\frac{h_{\mathrm{eff}}}{g_{\mathrm{eff}}}\frac{T}{A} + \frac{h_{\mathrm{eff}}}{3g_{\mathrm{eff}}s(T)}\frac{1}{A^{5/2}a_I^{3/2}\mathcal{H}}\left[\sum_j\left(\langle E_{\psi_j}\rangle - m_\chi B_{\psi_j}\right)\Gamma_{\psi_j}N_{\psi_j}\right.\right. \\
&\left.\left. + \Lambda\sum_i\left(1 - \frac{\sum_j B_{\psi_j,X_i}\langle E_{\psi_j,X_i}\rangle + B_{X_i}m_\chi}{m_{X_i}}\right)\Gamma_{X_i}\xi_{X_i} + \frac{m_\chi\langle\sigma_{\mathrm{eff}}v\rangle}{A^3 a_I^3}\left[N_\chi^2 - (N_\chi^{eq})^2\right]\right]\right\}
\end{aligned}
\tag{3.3}
$$

where $\mathcal{H}$ is defined from the Universe expansion rate, as:

$$
\mathcal{H} \equiv (a_I A)^{3/2}H = \left(\frac{\Lambda\sum_i\xi_{X_i} + \rho_R(T)A^3 a_I^3 + m_\chi N_\chi + \sum_j\langle E_{\psi_j}\rangle N_{\psi_j}}{3M_{PL}^2}\right)^{1/2}. \tag{3.4}
$$

In order to examine the general features of the numerical solution of this system we discuss first a minimal framework with a single cosmological modulus X decaying into the DM particle χ. Rather than detailing a specific particle physics scenario, in this first example we define χ only through its mass and pair annihilation rate into SM particles, whose thermal average is assumed not to depend on temperature, as appropriate for S-wave annihilations. We also avoid dealing with eventual other states charged under the quantum number protecting the stability of χ, assuming that they have a sizable mass splitting with respect to χ, and hence have very short lifetimes and do not enter in the Boltzmann equation for χ. In this simplified scenario the equation (2.28) for the dark matter density reduces to the one of the thermal paradigm plus a single source term accounting for the decay of the field X:

$$
\frac{dn_\chi}{dt} = -3Hn_\chi - \langle\sigma v\rangle\left(n_\chi^2 - (n^{\mathrm{eq}})_{\chi,eq}^2\right) + \frac{B_X}{m_X}\Gamma_X\rho_X \tag{3.5}
$$

As already outlined, the relevant parameters for the relic density calculation are the particle mass and pair annihilation cross section, as well as those setting the efficiency in producing dark matter particles and the energy density of the field at decay; regarding the latter we will treat as free parameters B_X and the mass of the modulus m_X, which in turns sets the decay width Γ_X, according expression (2.22), and hence the reheating temperature (we start with the assumption of gravitational interactions in the decay, and comment shortly on how to interpret results in case
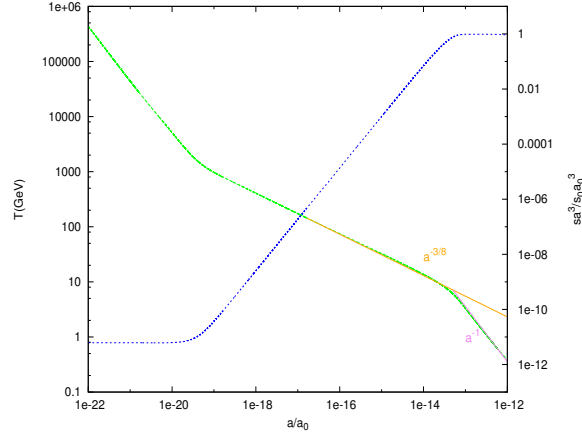
Figure 3.1: Behaviour of the temperature (green curve) and entropy density(blue curve) with the scale factor. The scale factor is normalized to its current value a_0 which has been put to one.

of a more general expressions for Γ_X). Since we are tracing the full evolution of the field X, we are not in the limit of instantaneous reheating and do not implement the definition of reheating temperature as quoted in Eq. (2.23); the $T_{\rm RH}$ we refer to when illustrating results is extrapolated from the numerical solution, matching the $T \propto a^{-3/8}$ scaling obtained in the phase when the X decays act as a large source of entropy to the $T \sim a^{-1}$ scaling in the subsequent radiation dominated regime (this prescription of matching asymptotic solutions is not totally rigorous since we should also take into account eventual changes in the number of relativistic degrees of freedom contributing to the entropy density; in practice, however, since the transition between the two regimes is always rather sharp (see also fig (3.1)), the $T_{\rm RH}$ found in this way is always very accurate in parametrizing the total entropy injection from the X decay; note also that $T_{\rm RH}$ is not used in any step of the numerical computation).

In Fig. 3.2 we consider a sample DM particle with heavy mass, $m_\chi = 1$ TeV, and large pair annihilation cross section, $\langle \sigma v \rangle = 5 \cdot 10^{-24} {\rm cm^3 s^{-1}}$; the ratio Y_χ of the DM number density to the entropy density is plotted as a function of T (note that, since we want to compare directly $T_{\rm RH}$ with T, rather than showing Y_χ versus the inverse of temperature as usually done, we plot it versus T and use a logarithmic scale which decreases from left to right). In the left panel we have fixed B_X to a sample value representative of the case when the branching ratio of the decay into χ is unsuppressed, and vary m_X to select a few values of the reheating temperature; in the right panel, vice versa, we fix m_X and vary B_X. The system of equations is solved assuming the initial energy density in the modulus is equal to $1/2 \, m_X^2 M_{Pl}^2$ and that the radiation energy density is at the same level [Acharya 2008b, Dine 1996]. When $T_{\rm RH}$ is larger than the thermal freeze-out temperature $T_{t.f.o.}$ for this model (the
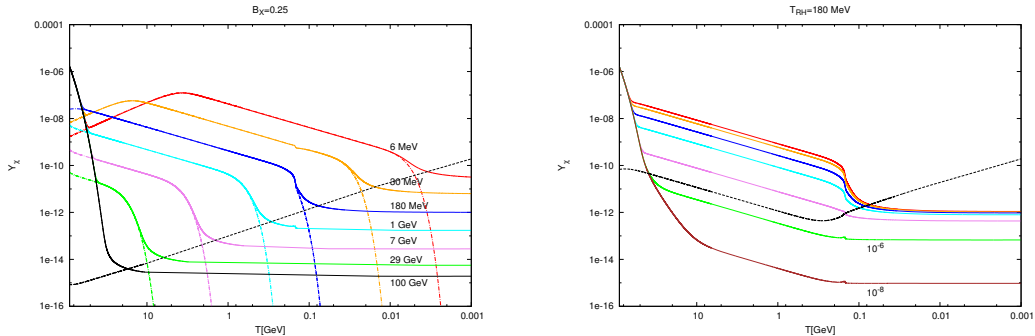
Figure 3.2: The number density of the DM particles normalized the entropy density as a function of temperature, for few values of the reheating temperature and B_X fixed to 0.25 (left panel), and for a sample $T_{\rm RH}$ while varying B_X (right panel). In the left panel we also plot with dashed-dotted lines the quasi-equilibrium density $Y_\chi^{QSE}(T)$ for each $T_{\rm RH}$, and with a dashed line the critical density $Y_\chi^c(T)$ for the case $T_{\rm RH} = 100$ GeV in which reheating takes place before thermal freeze out. In the right panel the dashed line shows $Y_\chi^c(T)$ for $T_{\rm RH} = 180$ MeV. Results refer to a DM particle with mass and pair annihilation cross section being, respectively, 1 TeV and $5 \cdot 10^{-24}$ cm^3 s^{-1}.

case for $T_{\rm RH} = 100$ GeV in the plot), the temperature evolution of Y_χ is obviously the same as in a standard thermal WIMP framework: Y_χ follows first the thermal equilibrium distribution along its Maxwell-Boltzmann tail, in a phase in which the main source of DM particles is pair production by SM background particles and this is balanced by DM pair annihilations, and then at $T_{t.f.o.}$, when n_χ^{eq} becomes smaller than n_χ^c and pair annihilations become inefficient, Y_χ settles on a constant value. When $T_{\rm RH}$ is reduced two effects intervene: first of all, the thermal freeze out temperature tends to increase since the modulus contribution to the Universe energy density increases H and hence n_χ^c; at the same time, the dominant source of DM particles becomes the modulus decays rather than SM pair creation. If χ number density from the decay exceeds n_χ^c, this source term is balanced by DM pair annihilations and n_χ tracks the quasi-static equilibrium (QSE) density, as defined, e.g., in Ref [Cheung 2011]:

$$n_\chi^{QSE} \equiv \left(\frac{B_X \Gamma_X \rho_X}{m_X \langle \sigma_{\rm eff} v \rangle} \right)^{1/2} . \tag{3.6}$$

For our sample DM model, this is the behavior we find in all cases with large B_X and $T_{\rm RH} < T_{t.f.o.}$: starting at high T, Y_χ follows first Y_χ^{eq}, then it becomes equal to Y_χ^{QSE} up to about $T_{\rm RH}$ when the modulus DM source drops exponentially, Y_χ^{QSE} crosses Y_χ^c and hence Y_χ gets frozen. Regarding the temperature scalings in the plot, in the phase when the modulus dominates the energy density and is the main entropy source, we see that both Y_χ^{QSE} and Y_χ^c are proportional to T, except for a short low temperature phase in the examples for $T_{\rm RH} = 30$ and 6 MeV during which the entropy injected but the modulus decay is still negligible compared to
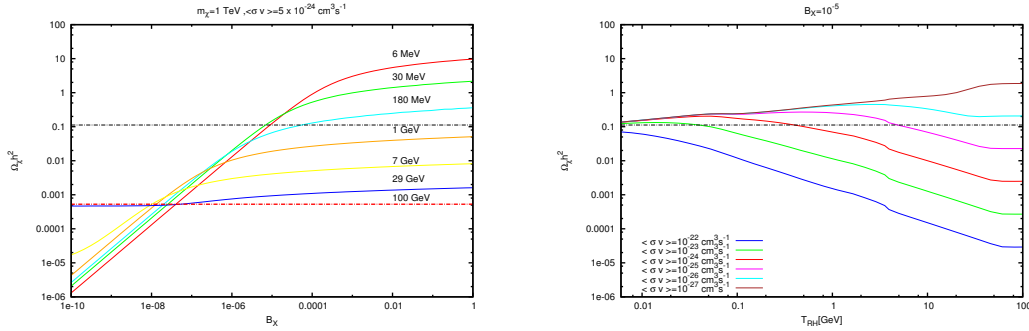
Figure 3.3: Left panel: scaling of the relic density with the parameter B_X for the same sample DM model selected for Fig 3.2 and for a few values of T_{RH}. Right panel: relic density versus T_{RH}, having fixed $B_X = 10^{-5}$ and rescaling the value of $\langle \sigma v \rangle$. The black horizontal lines represent the cosmological DM density as extrapolated by the WMAP 7-year data [Komatsu 2011].

the initial entropy and hence $a \propto T^{-1}$, making Y_χ^{QSE} and Y_χ^c rise as $T^{-3/2}$. For small B_X, Y_χ^{QSE} becomes smaller than Y_χ^c, DM annihilations are inefficient and n_χ simply scales as $B_X \Gamma_X \rho_X / m_X \cdot t$, up to the reheating temperature when the modulus source drops and Y_χ becomes constant; for what concerns the behavior in temperature, once again, in the phase in which the decay injects DM particles, the scaling just given translates into $Y_\chi \propto T$, while for very small B_X one can also see a transient in which the amount of DM produced in the decay is small compared to the thermal component and Y_χ simply reflects the entropy increase, decreasing faster than T.

In Fig. 3.3 we plot the relic densities for the χ state. In the left panel we refer to the same model introduced for Fig. 3.2, select a few values for the reheating temperature and display results as a function of B_X; as expected from the discussion above, one can see that Ω_χ becomes essentially independent of B_X in the limit of large B_X, while it scales linearly with B_X when the modulus source function is too small to make n_χ exceed n_χ^c. Also visible at large B_X is the scaling of the relic density with the inverse of T_{RH}, as expected from the analytical estimate in Eq. (2.34). When B_X is small Ω_χ is expected to scale with T_{RH}/m_X. In our approach T_{RH} and m_X are correlated; from the instantaneous approximation, Eq. (2.23), one expects $m_X \propto T_{\text{RH}}^{2/3}$ giving $\Omega_\chi \propto T_{\text{RH}}^{1/3}$, which is approximately the scaling seen in the plot for very small B_X. The dependence on the reheating temperature is shown more explicitly in the right panel of Fig. 3.3, where, having fixed B_X to an intermediate value, we let the annihilation cross section vary of a few orders orders of magnitude around the value chosen for the plot on the left hand side; the relic density scales with the inverse of $\langle \sigma v \rangle$ whenever reannihilation takes place, while evidently the solution does not depend on $\langle \sigma v \rangle$ in case annihilation processes are inefficient.

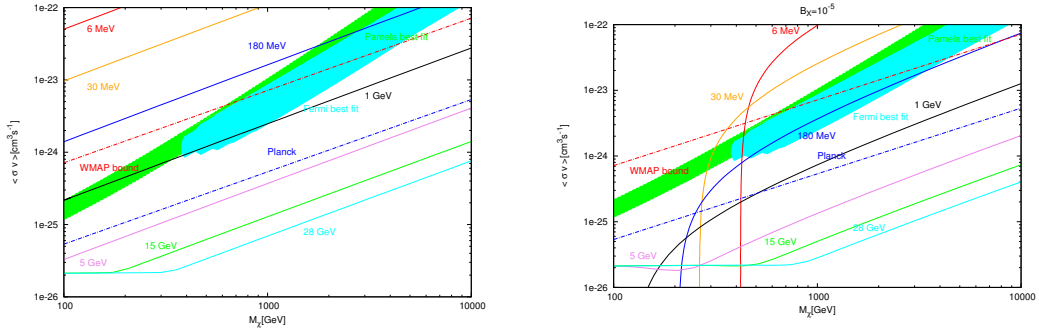In most scenarios containing cosmological moduli it is hard to tune the model in

Figure 3.4: Values of m_X and $\langle \sigma v \rangle$ for which the relic density of the χ particles matches the cosmological DM density, for a few values of T_{RH} and two representative cases for B_X. Also shown are the region in this plane compatible with the Pamela and Fermi electron/positron excesses in case of leptophilic DM [Grasso 2009], and the WMAP limit and Planck projected sensitivity [Galli 2009, Iocco 2010] stemming from the impact of residual DM annihilations on reionization.

such a way that very tiny B_X are obtained, hence the framework we are discussing becomes interesting mainly when χ is associated to a large annihilation cross section, preventing the overproduction of DM with respect to the experimental bound. DM models with a $\langle \sigma v \rangle$ which is two or three orders of magnitudes larger than in the standard thermal relic scenario would be very interesting also from the point of view of indirect DM detection and have been invoked to address the excess in the lepton cosmic ray flux by Pamela and Fermi, see e.g. [Dutta 2009]. In Fig. 3.4, choosing a few sample values of T_{RH} and two representative cases for B_X, we scan the parameter space ($\langle \sigma v \rangle - m_\chi$) searching for configurations in which the χ relic density matches the central value for the cosmological DM density as estimated from the WMAP 7-year data, namely $\Omega_\chi h^2 = 0.1123 \pm 0.0035$ [Komatsu 2011]. A curve corresponding to a given T_{RH} becomes horizontal when T_{RH} becomes larger than $T_{s.f.o.}$, i.e. we recover the standard thermal result of the relic density being independent of mass for S-wave annihilations; on the other hand it becomes vertical when annihilations become inefficient and hence Ω_χ stops depending on $\langle \sigma v \rangle$. In general going from large to small B_X, keeping T_{RH} fixed, shifts the results to smaller $\langle \sigma v \rangle$ and larger m_χ. In the same plot, supposing we are now referring to a leptophilic DM candidate, namely annihilating democratically into the three lepton species [Grasso 2009], we have superimposed the region in the parameter space which have been found to be compatible with the Pamela and Fermi electron and positron data, as derived, e.g., in Ref. [Grasso 2009]; the comparison is meant to be qualitative since we are not considering here a detailed particle physics scenario, it shows however what are the main trends that should be fullfilled to find an agreement. Also shown is the bounds on leptophilic models following from WMAP CMB data [Galli 2009, Iocco 2010]: the limit stems from the impact of residual (namely much later than thermal decoupling) pair annihilations on reionization, and will be soon improved by the Planck experiment in case of no signal.
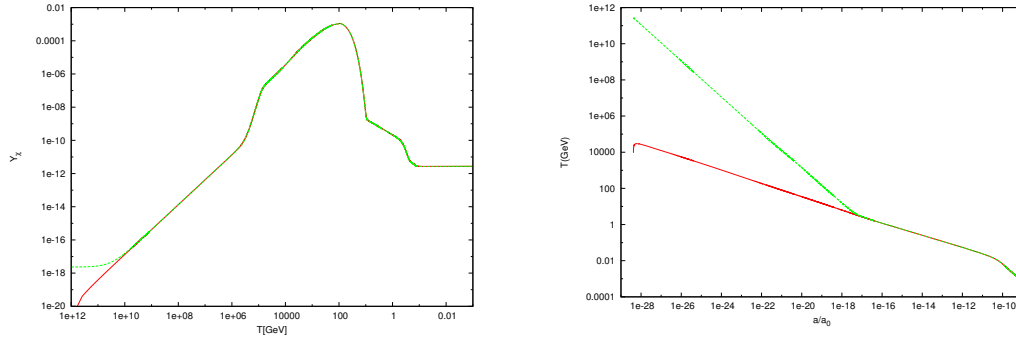
Figure 3.5: Left panel: comoving number density of the dark matter for two choices of initial conditions. The red curve represent the our customary choice for the initial conditions while in the green curve the initial density of the dark matter is the equilibrium value at the initial temperature. Right panel: comiving number density of dark matter for two choices of the initial temperature. As before the red curve represents the standard choices of the initial conditions. In the other curve instead the initial value of the radiation energy density is negligible compared the energy density of the cosmological modulus.

In all the examples displayed a specific set of initial conditions has been implemented to solve the system of equation. Indeed the choice of the initial conditions has a negligible impact on the on the final comoving density of DM particles. In fig. (3.5) we show one of DM models discussed before for different choices of the initial dark matter energy density and temperature (regarded as measure of the radiation energy density). As we notice final resutl is definitely insensitive to different choices of initial conditions. Particularly interesting is the case, depicted in the second panel of the figure, in which the initial radiation energy density is negligible with respect to the energy density of the modulus. In this case there is a sharp increase of temperature up to a maximal value [Giudice 2001], greater than the reheating temperature, after which evolves as $a^{-3/8}$ as already described. Regarding instead the initial energy density it does not impact the DM relic density provided that the physical mechanism determining it starts becoming efficient at temperatures lower than the temperature at which the scaling $T \sim a^{-3/8}$ begins. More precisely: as long as the DM pair annihilation rate is large enough to guarantee, even in the non-standard cosmological scenarios considered here, chemical equilibrium at $T \gtrsim m_\chi$; the final relic density is then determined by the physics taking place between the thermal freeze-out temperature and the reheating temperature. In fig.(3.11) we consider a dark matter model with a very low reheating temperature, around 6 MeV, and for which the scaling $T \sim a^{-3/8}$ begins after the standard freeze-out temperature, varying of several order of magnitudes the initial energy density of the heavy decaying field. If the $T \sim a^{-3/8}$ scaling starts sufficiently earlier than $T_{\rm RH}$, the entropy production guarantees the suppression of the DM thermal component and, at the same time, variations in the entropy release with the field energy density are compensated by a different efficiency in the non thermal production, leaving then
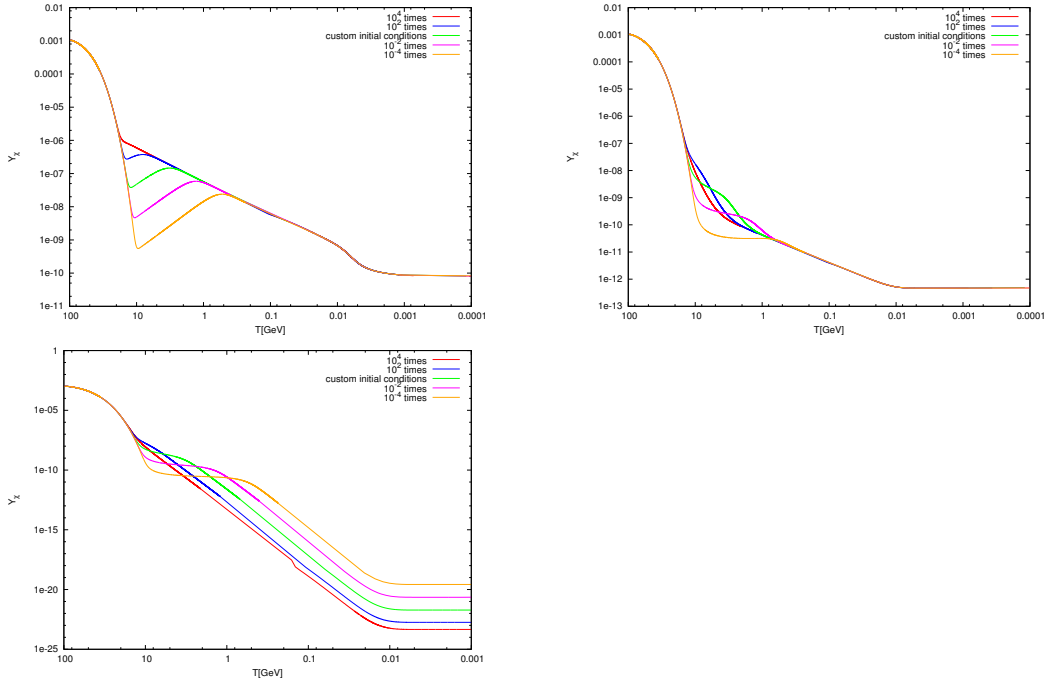
Figure 3.6: Dark matter comoving number density for several values of the initial energy density, reported in the plots. The three plots are associated to three different values of B_X, respectively 0.25, 10^{-5} and 0.

the final result unchanged. If, on the contrary, the DM thermal relic component is not totally diluted either the production rate is not efficient enough (see the last panel of fig.(3.11)), the $T \sim a^{-3/8}$ phase needs to start before the thermal freeze-out temperature, otherwise the variation of dilution due to entropy release stemming from the initial conditions has a direct impact on the relic density as well.

The last issue we wish to discuss in this section is an implicit dependence on the modulus mass m_X we have ignored so far: as mentioned above we have been varying m_X to retrieve different values of $T_{\rm RH}$ as extrapolated from the numerical solution of the system of coupled equations; the underlying assumption here is that we computed the modulus decay assuming gravitational coupling and a two body final state. Having in mind more general scenarios like those, e.g., in Ref. [Nakamura 2006, Dine 2006, Kohri 2004, Moroi 2000, Endo 2006, Moroi 1995], we may consider replacing:

$$\Gamma_X = \frac{1}{4\pi} \frac{m_X^3}{M_{Pl}^2} \quad \rightarrow \quad \Gamma_X = \frac{m_X^3}{\Lambda_{eff}^2} \,, \tag{3.7}$$

where now Λ_{eff} encodes both the coupling of the effective operator responsible for the decay and the kinematical factors. From the approximation of instantaneous reheating one sees that, to keep $T_{\rm RH}$ fixed after this replacement, one needs simply

to approximately shift:

$$m_X \quad \to \quad m_X \cdot \left(\frac{\Lambda_{eff}^2}{4\pi M_{Pl}^2} \right)^{1/3} . \tag{3.8}$$

The modulus mass however appears explicitly also in Eq. (2.28) when, in the DM source function from modulus decays, one converts from the modulus energy density to its number density. To compensate for this and use results displayed in this and the next Sections, one then should also shift the values reference values for B_X as:

$$B_X \quad \to \quad B_X \cdot \left(\frac{\Lambda_{eff}^2}{4\pi M_{Pl}^2} \right)^{1/3} . \tag{3.9}$$

3.2   Non- thermal production of neutralino DM

In this section, while still referring to the schematic picture with a single cosmological modulus X parametrized through its decay width Γ_X and the DM yield B_X, we introduce an explicit particle physics scenario for the $\{\chi_a\}$ fields, considering SUSY theories. These theories offer several scenarios in which non-thermal DM production can arise. First of all, it is quite common to find field configurations for which the scalar potential is flat; these configurations are referred as 'flat directions' and can be described by a chiral superfield. For our purposes, only the scalar component of these multiplets is relevant; playing the role of the cosmological modulus. SUSY breaking can lift the flat directions inducing a mass term for the moduli in the scalar potential. Another possibility is the Polonyi field [Coughlan 1983, Dine 1984, Ellis 1986] which is introduced in many SUSY breaking schemes. Finally supergravity can be seen as a low energy limit of string theory, in which scalar fields can appear in the compactification of extra dimensions.

As a comment we mention that non thermal dark matter production scenarios arise most naturally in supergravity/superstrings theories while scenarios like gauge mediated supersymmetry breaking are more troublesome since the moduli tend to be light and decay after the onset of BBN, see, e.g. [Lyth 1996, Asaka 1998, Acharya 2009b, Acharya 2010b]; to solve this problem, one needs to invoke a mechanism of dilution of the moduli number density, making these models not viable for non-thermal DM production.

As already mentioned, non thermal production will be embedded in minimal realization of SUSY theories, the MSSM, with the stable LSP, and hence dark matter candidate, assumed to be the neutralino. In this section we will pursue a systematic study of the impact of non-thermal effects in its phenomenology, especially regarding the DM mass scale. These effects result very sensitive to the neutralino composition which we remind is parametrized through the elements of the mixing matrix N, as function of the SUSY parameters M_1, M_2, μ and $\tan\beta$.

In order to make more clear the results, we firstly discuss two specific examples. In fig. (3.7) we depicted a generic MSSM model with a WINO LSP of mass of
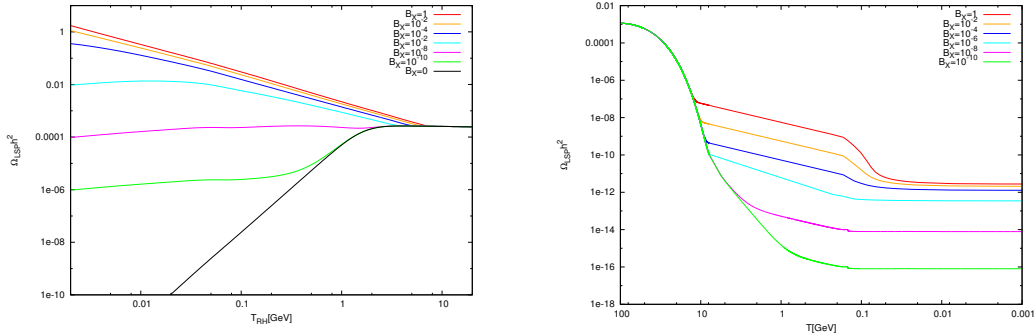
Figure 3.7: Left panel: Dark matter relic density as function of the reheating temperature for a 200 GeV Wino for the values of B_X reported in the plot. Right panel: DM abundance of the same model as the previous panel for a reheating temperature of around and for the values of B_X reported.

around 200 GeV. Its efficient S-wave annihilation, provided an non negligible value of B_X, make the reannihilation regime to occur down to low values of the reheating temperature with the relic density which is a decreasing function of this temperature. Remarkably non-thermal production makes the relic density to match the cosmological value at a much lower value of the DM mass compared to the one, of around 2.7 TeV, selected by thermal production.

In fig.(3.8) instead we consider the case of a bino LSP, also of mass around 200 GeV. Bino annihilation cross section is dominated by SM fermion final states and is much lower compared the Wino case, being it helicity suppressed, making the thermal relic density typically exceed the cosmological value, given the current accelerator bounds on supersymmetric particles. This P-wave suppressed annihilation cross section is typically not able to compensate non-thermal production, thus the relic density increases with the reheating temperature until matches the thermal prediction when this temperature tends to $T_{\text{s.f.o.}}$. As evident from the plot, a low enough reheating temperature allows to dilute the thermally overproduced bino dark matter. The cosmological limit is not again exceeded provided that, depending on the reheating temperature, the branching fraction of decay of the heavy field into dark matter is suppressed.

We are now ready to discuss non thermal production of neutralino through a more systematic approach. Since we will be mainly interested in discussing the shift on the mass scale for neutralino DM due to non-thermal effects, we refer here to a supersymmetric framework maximizing the dichotomy between underproduced and overproduced thermal states, the so-called "Split Supersymmetry" scenario [Arkani-Hamed 2005b, Giudice 2004]. This indicates a generic supersymmetric extension to the SM in which fermionic superpartners have a low mass spectrum (say at the TeV scale or lower), while scalar superpartners are heavy, with a mass scale which can in principle range from hundreds of TeV up to the GUT or the Planck scale [Arkani-Hamed 2005b], a feature which can occur in a wide class of theories, see, e.g. [Arkani-Hamed 2005a, Antoniadis 2005, Kors 2005]. Leaving out
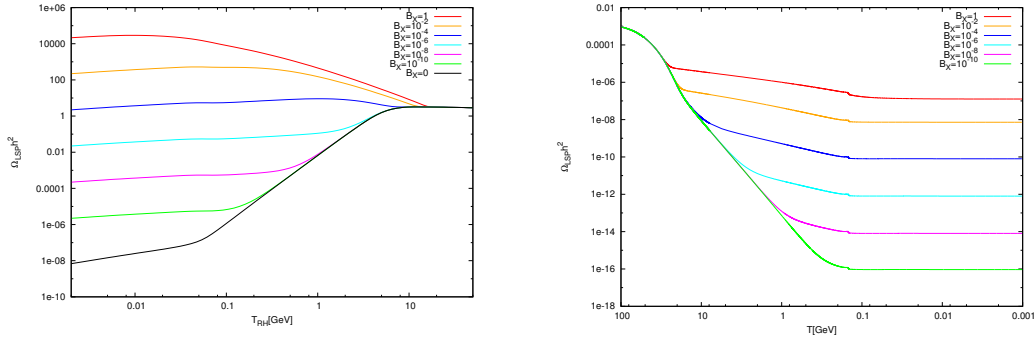
Figure 3.8: Left panel:Dark matter relic density as function of the reheating temperature for a 200 GeV Bino for the values of B_X reported in the plot. Right panel: DM abundance of the same model as the previous panel for a reheating temperature of around 100 MeV.

of the discussion also gravitinos which are assumed to be heavy and not produced in the modulus decay, the system $\{\chi_a\}$ reduces to neutralinos and charginos, whose annihilation and coannihilation effects we treat interfacing the model the DarkSUSY package [Gondolo 2004]. Finally for what regards the Higgs sector, the scenario has only one light state SM-like Higgs; the value of its mass, as well as $\tan\beta$ have no sizable impact on the overall picture, hence we keep them fixed to sample values, respectively, 114.4 GeV [1] and 10.

In Fig. 3.9 we scan the parameter space M_1, M_2 and μ searching for models whose relic abundance matches the central value from the 7-year WMAP estimate of the DM density in the Universe. There are three pairs of plot in which we vary two of these parameters, fixing the third to a heavy scale; in each pair, one plot is for a large B_X, while the other is for a small but not negligible B_X. As in the previous Section, we vary m_X to change the reheating temperature scale, assuming a two-body gravitational decay for the modulus. The thick black solid line corresponds, in each plot, to a reheating temperature exceeding the thermal freeze-out temperature for all models along the curve, namely it gives the models matching the cosmological DM density we would also obtain in the standard picture without non-thermal DM sources: In the M_1-μ plane this happens, starting at small neutralino masses, close to the diagonal $M_1 = \mu$ since it requires a tuning of the right amount of Higgsino and Bino component in the LSP, suppressing the large Higgsino annihilation cross section with the Bino one, which in Split SUSY is extremely small. Would we have allowed for lighter sfermions and other light Higgs states, this curve would have moved only slightly further away for the diagonal,

---

[1]Here for simplicity we have just left the higgs mass to the minimal value allowed by LEP. As already stated the results of this section are unchanged once the recent determination of the higgs mass is taken into account. We just comment that Split Supersymmetry has actually a deep impact in the mass of the higgs m_h because of the large radiative corrections induced by the heavy sfermions which can even made its value to exceed the experimental range [Arbey 2012a]. In this thesis we are regarding split SUSY just as a useful playground for investigating non-thermal neutralino production hence neglecting this kind of issue.
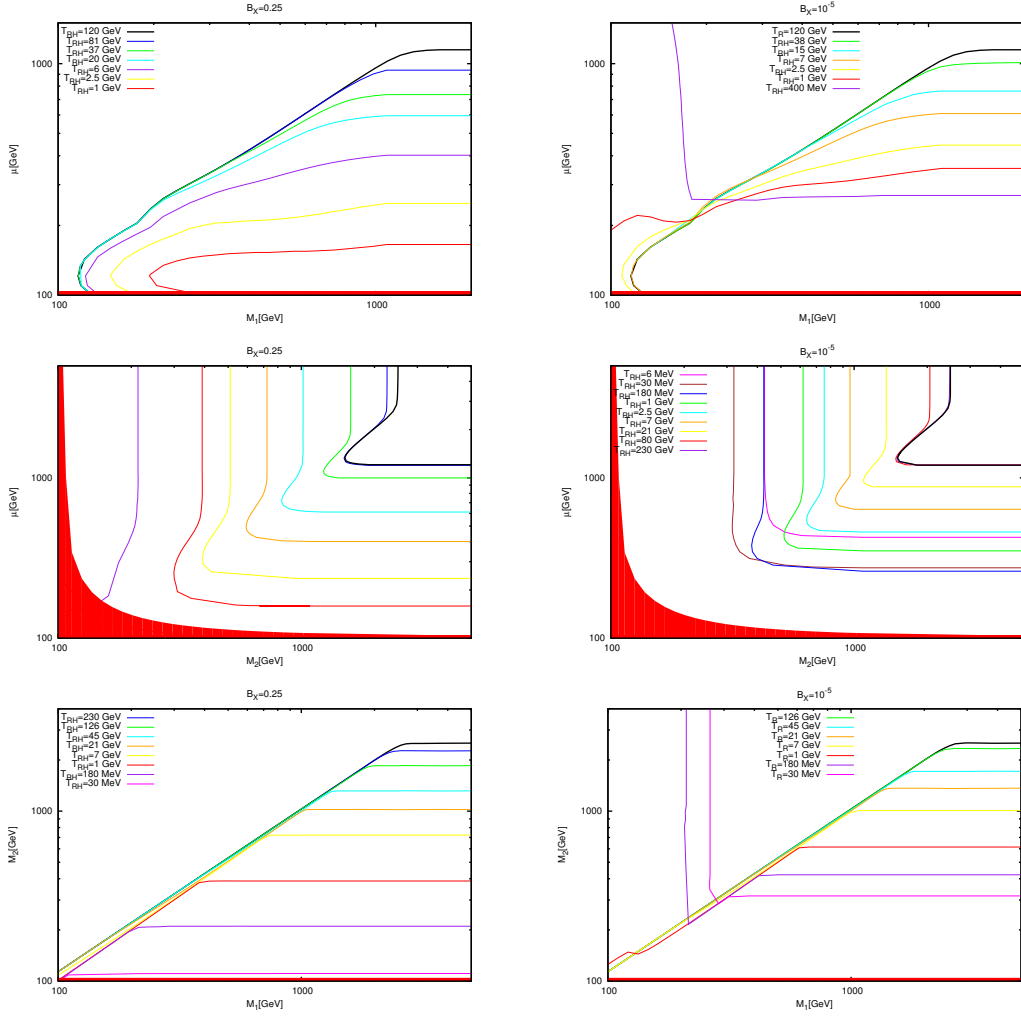
Figure 3.9: Models with relic density equal to the central value from the 7-year WMAP data analysis, i.e. $\Omega_\chi h^2 = 0.1123$, in two-dimensional slices of the M_1, M_2, μ parameter space, corresponding to the limit in which the third parameter is heavy (set to 10 TeV in the numerical computation), for a few values of T_{RH} as indicated in the plots, and two values of B_X, namely 0.25 for left panels and 10^{-5} for right panels. The filled areas correspond to regions violating the LEP lower bound on the chargino mass.

except when sfermion coannihilations or S-channel resonant annihilations on a Higgs take over in setting the effective thermally averaged annihilation cross section, as happens, e.g., in portions of the mSUGRA parameter space, see, e.g. [Edsjo 2003] – we will not discuss these exceptions here. As already mentioned, at about 1.1 TeV a pure Higgsino saturates the thermal relic density bound. Turning to the M_2-μ plot, Winos have an even larger annihilation cross section than Higgsinos and the thermal relic density curve just goes from a pure Higgsino to a heavier pure Wino through a transient with large Higgsino-Wino mixing. Finally the behavior in the M_1-M_2 plane is more peculiar since from the structure of the neutralino mass matrix, Bino and Wino do not mix and, below the mass scale for a pure Wino thermal relic candidate, the tuning here is between the mass spitting between the Bino LSP and the second lightest neutralino and the lightest chargino, which are Wino-like and and whose coannihilations in the early Universe set the thermal relic abundance of a Bino LSP (there are chargino and neutralino coannihilations even for pure Winos and Higgsinos, but with less dramatic effects). Turning on the non-thermal component from the modulus decays, when B_X is large, essentially one just sees in the plots the scaling sketched in Eq. (2.34), with Higgsinos and Winos saturating the WMAP preferred value for Ω_χ with a progressively larger $\langle \sigma v \rangle$ as T_{RH} decreases, and hence for a progressively smaller LSP mass, covering the whole parameter space for Higgsinos lighter than 1.1 TeV and Winos lighter than 2.4 TeV (as the Higgsino mass approaches the W boson threshold the cross section stops increasing; this explains the shape of isolevel curves in that region). A detection at an accelerator of such LSP configurations, hopefully combined with a DM detection signal, would indeed be an indication of a non-standard cosmological phase at DM generation, with non-thermal production as primary scenario (there would also be further possibilities, such as, e.g., the increase of the Universe expansion rate at freeze-out induced by a quintessence component [Salati 2003, Profumo 2003] or a modification of the gravity theory [Catena 2004]). When B_X is small, there is a smooth transition from the regions where the scaling in Eq. (2.34) applies to those where annihilations stop playing a role and Eq. (2.36) applies instead; the latter makes even pure Binos, which, we underline again, in our sample MSSM setup have extremely small annihilation cross sections, become cosmologically viable, another configuration which, if singled out at accelerator and/or DM searches, would point to a non-standard early Universe cosmological history (in plots the filled region stands for the region in which the LEP bound on the chargino mass $m_{\chi^+} > 103.5$ GeV is violated; Tevatron and the recent LHC constraints are not shown since we have made just schematic assumptions on sfermions and not discussed at all gluinos, the particles most critical for a early discovery at a hadron collider).

We conclude this analysis of the MSSM with some important comment regarding the gravitino. In this and in the previous section is considered the presence of only one modulus field decaying either into radiation or into Dark Matter. In generic supergravity/superstrings theories it is found that cosmological moduli have unsuppressed, at least order percent, branching ratios of decay into gravitinos [Nakamura 2006, Endo 2006]. Gravitinos are not in thermal equilibrium and may
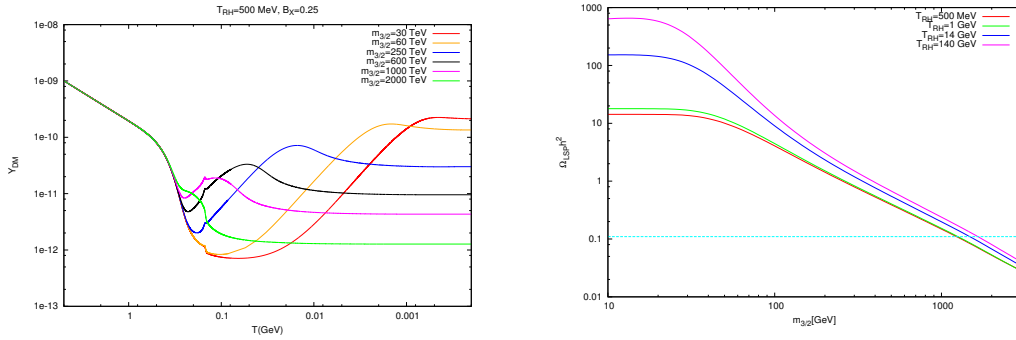
Figure 3.10: Left panel: Dark matter yield for a Wino LSP non thermally produced both by modulus and gravitino decay, for the values of the gravitino mass reported in the plot. Right panel: Relic density varying the gravitino mass of the Wino LSP for several values of the reheating temperature.

be long lived enough to affect BBN with their decay. Furthermore, assuming the dark matter stability protected, as usual, by R-parity, each gravitino should decay at least into one DM particle. Non thermal DM production from gravitino decay is usually much more efficient than the one from moduli decay since it occurs at a later stage in the history of the Universe. Preserving BBN implies a lower bound on the gravitino mass which, depending on the model, can reach order of 100 TeV; masses of several order larger are required in order to prevent the DM to overclose the Universe.

The scenario of non-thermal production from gravitino decay is illustrated in fig. (3.10). It shares main features with the case of the decay of cosmological moduli. In particular, efficiently annihilating particles like Winos feature a reannihilation regime with the DM abundance scaling with the inverse of a temperature $T_{3/2}$ defined according to (2.24). In this setup, the correct relic density, for a Wino DM, is matched for a value of the gravitino mass of the order of 1000 TeV. In the case of a Bino DM, for which reannihilations do not occur, this lower bound increases of around one order of magnitude.

This last problem can be addressed in several ways. One possible solution, which is for example realized in the G2-MSSM (see also [Kaplan 2006]) which will be discussed in the next section, is to allow the presence of moduli with mass of the order of the gravitino mass, whose decay rate into these particles is then kinematically suppressed. These fields will dominate the energy density of the Universe before gravitino decay diluting their number density in order to avoid overproduction of dark matter.

Despite being cosmologically viable, a 100 TeV or more massive gravitino is rather troublesome for Susy models. In generic Supergravity theories, infact, scalar soft masses get a contribution proportional to gravitino mass and are then expected to be at least of the same order. Such heavy superpartners would disfavor Supersymmetry as a solution to the hierarchy problem. Addressing the hierarchy problem in SUSY models with non-thermal dark matter goes beyond the scopes of this thesis. We just

mention that models with have scalars are still perfectly viable from several points of view: gauginos can be kept close to the electroweak scale, and then appealing dark matter candidates are still available, and the correct gauge coupling unification is not spoiled. Furthermore heavy scalars help to relax some unpleasant aspects of Supersymmetry like flavour violation. We finally remark that it is nevertheless possible to find setups in which scalars can be rather light also in presence of heavy gravitinos; explicit examples can be found in [Randall 1999, Acharya 2010a].

3.3   Non-thermal DM production in the G2-MSSM

As an example of framework in which we can make definite predictions for the spectra of both the set of particles $\{\chi_a\}$ and the cosmological moduli, we discuss the case of the G2-MSSM [Acharya 2007, Acharya 2008a]. Within a specific class of string M-theories, in this scenario the compactification of extradimensions gives rise to a $N = 1$ supergravity in which SUSY breaking, due to the dynamics of a hidden sector, is trasmitted to the visible sector by a combination of gravity (dominant contribution) and anomaly mediation. We briefly summarize here the main features of the spectrum, following Ref. [Acharya 2008a]: In the G2-MSSM the visible sector can be described by a GUT theory broken into the MSSM at the unification scale $M_{\rm unif}$, at about 10^{16} GeV, coinciding with the compactification scale. The RGEs boundary conditions are mainly functions of the gravitino mass $m_{3/2}$, which can be estimated from the UV theory parameters to lie in the range between ten and several hundred TeVs. The gauginos are expected to be the lightest SUSY particles; at $M_{\rm unif}$ the gaugino masses are generated from a universal loop-suppressed gravity mediation contribution combined with a non-universal anomaly mediation term. The ratio of the gaugino masses to the gravitino mass depends almost linearly on the quantity δ that parametrizes a threshold correction to the unified gauge coupling; in the following, δ will be kept as a free parameter. The value of the masses at the electroweak scale is computed following the RGE evolution, including threshold corrections, such as the very large correction coming from higgs-higgsino loops, which is proportional to μ [Pierce 1997]; whether the lightest neutralino is the Bino or the Wino depends on the sign and magnitude of this latter correction. For $\mu > 0$ and for δ in the range $-10 \leq \delta \leq 0$ the lightest neutralino is a pure Wino, with mass in the range between about 100 and few hundred GeV (even the gluino is fairly light, $m_{\tilde{g}} < 1$ TeV, a feature implying a rather rich phenomenology at LHC [Feng 1999, Acharya 2009a, Feldman 2010] and making the model testable in the near future). Concerning the other states in the MSSM spectrum, the Higgsino mass parameter μ and soft SUSY breaking term B are generated by a Giudice-Masiero mechanism and are heavy, of the order of $m_{3/2}$. Sfermions are also heavy with a flavor universal contribution to their soft masses at $M_{\rm unif}$ being about $m_{3/2}$; RGEs affect mostly the third generation of squarks with the stops and the left handed sbottom becoming the lightest sfermions at the Electroweak scale (the left-handed stop mass becomes about $0.25 \cdot m_{3/2}$, the right handed stop and the left

handed sbottom masses about $0.5 \cdot m_{3/2}$). In the Higgs sector $\tan\beta$ is fixed by μ and B through the electroweak symmetry breaking condition and takes a value of order one; the light CP even Higgs is Standard Model like, while all the other Higgs bosons are heavy, again at about the $m_{3/2}$ scale. In summary, the features relevant to discuss non-thermal DM production in this model are: The pure Wino LSP as DM candidate, as enforced by the proper choice of δ (we will restrict to values $\delta < -3$ since they are theoretically favored [Acharya 2008a]) and required to provide an annihilation cross section sufficiently large for the model to fit into the scenario in which the branching ratio for the decay of the moduli into the LSP is unsuppressed; A charged Wino as next to lightest SUSY particle, with a tiny mass splitting with respect to the LSP, about 200 MeV, due to the one-loop electroweak corrections to the neutralino and chargino masses [Feng 1999]; The possibility for the moduli to decay into gluinos and third-generation squarks. While other SUSY particles do not play a role in our analysis, the relevant part of the spectrum will be computed here implementing the appropriate one-loop RGE running.

For what regards the moduli fields, as already mentioned, in a string framework like the G2-MSSM, they arise in the effective supergravity theory after the compactification of the extra-dimensions. The theory predicts the presence of a large number of moduli fields with mass of order or heavier than the gravitino mass. In our numerical computation of the DM relic density, we follow the scenario outlined in Ref. [Acharya 2008b]: The modulus sector is composed by $N+1$ fields with $N = \mathcal{O}(50 - 100)$ including:

- 1 heavy modulus X_N with $m_{X_N} = 600\, m_{3/2}$;

- 1 meson field Φ with $m_\Phi = 1.96\, m_{3/2}$;

- N-1 light moduli X_i with $m_{X_i} = 1.96\, m_{3/2}$.

Their decay rates can be written in the form given in Eq. (2.22), i.e. they are proportional to the mass of the modulus to the third power and inversely proportional to the square of the reduced Planck mass. The constant in front can be computed esplicitly [Acharya 2008b] in the model; we keep D_{X_N} for the heavy modulus and D_Φ for the meson fixed to the benchmark values of, respectively, 2 and 710, while D_{X_i}, which is one the quantities the LSP relic density is mostly sensitive to, will be treated as a free parameter allowed to vary in the range between 4 and 16 (preferred range in the scenario considered here [Acharya 2008b]). With this choice, the lifetimes for the three type of states is split to about: 10^{-10} s for X_N, 10^{-5} s for Φ and $10^{-3} - 10^{-2}$ s for the light moduli. The branching ratios into SUSY particles of the decays are also calculable in this theory, with the main channel being into squark pairs, mostly the lightest stop, which in turn cascade down to the LSP and the chargino; in general, the branching ratio of decay of the light moduli into Susy particles is 25% with on average two DM particles produced at the end of the decay chain, giving $B_{X_i} \sim 0.5$. Gravitinos are produced in the heavy modulus decay, while gravitino pair production in the decay of the meson and the light moduli is

kinematically forbidden for the given values of m_ϕ and m_{X_i}, a choice quite natural for the G2-MSSM but still not totally general [Acharya 2007]. We will comment further on this point below. Gravitinos are also long lived:

$$\Gamma_{3/2} = \frac{1}{288\pi} \frac{m_{3/2}^3}{M_{Pl}^2} \tag{3.10}$$

producing one SUSY particle per decay, cascading again into one DM particle.

The system in Eq. (3.3) is solved numerically for this G2-MSSM setup, with the set of moduli just outlined and having chosen $N = 99$ and including the gravitino as ψ field. The quantities which are kept as free parameters in our analysis are the gravitino mass, the parameter δ (allowing to shift the ratio between LSP and gravitino mass) and D_{X_i}. Except for gravitinos, all other decay products are, for the moment, treated as particles in kinetic equilibrium. The system is evolved starting with the oscillations of the heavy modulus, when its initial energy density $1/2\, m_{X_N}^2\, M_{Pl}^2$ is equal to the radiation energy density, while the other moduli are included in the system at the beginning of their oscillations. For what regards the generation of DM, the relevant production phase is only the one from the decays of the light moduli, since the thermal DM component, as well as those from the decay of the heavy modulus and the meson, get diluted in the entropy injection phases. The dependence of DM comoving number density Y_χ on temperature in this scenario is perfectly specular to those shown in Fig. 3.2 for models whose number density follows first a phase of the quasi-static equilibrium and then reannihilation. Gravitinos play a marginal role: produced in the heavy modulus decay, they get diluted and decay at a late stage (possibly after the end of the reannihilation phase for χ) when $Y_{3/2}$ is tipically 3 to 4 orders of magnitude smaller than the final Y_χ, hence not contributing significantly to the DM relic density.

In left panel of Fig. 3.11 we plot the neutralino relic density versus $m_{3/2}$, for a few values of D_{X_i} and a sample value for δ, showing also on the upper horizontal scale the corresponding value of the Wino LSP mass for such given δ. Given that the reannihilation regime applies, from Eq. (2.34) we expect Ω_χ to be proportional to m_χ and inversely proportional to $\langle\sigma v\rangle$ and $T_{\rm RH}$, with the latter in turn approximately proportional to $D_{X_i}^{1/2}\,(m_{3/2})^{3/2}$, see Eq. (2.24) where the scaling in the modulus masses has been replaced by the scaling in terms of the gravitino mass. In the limit in which the Wino pair annihilation cross section just scales with the inverse of the square of the Wino mass, one would find:

$$\Omega_\chi h^2 \propto \frac{[F(\delta)]^3\,(m_{3/2})^{3/2}}{D_{X_i}^{1/2}} \tag{3.11}$$

where the function $F(\delta)$ parametrizes the quasi-linear relation between m_χ and $m_{3/2}$. In the plot, the result of the full numerical solution roughly confirms these approximate scalings, except for small m_χ for which $\langle\sigma v\rangle$ is not inversely proportional to m_χ^2. To match the experimental value the DM abundance, lighter $m_{3/2}$ and larger D_{X_i} are favored. In the right panel of Fig. 3.11 we consider the plane
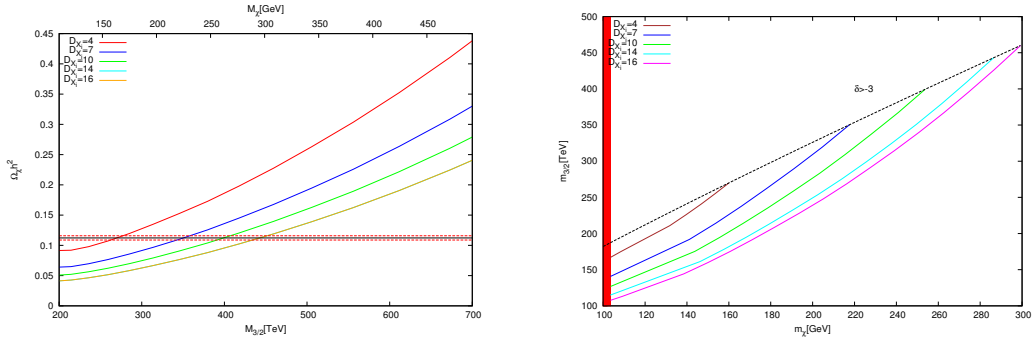
Figure 3.11: *Left panel*: Wino relic density versus the gravitino mass $m_{3/2}$ for a few sample values of D_{X_i} and $\delta = -3$; the upper horizontal scale shows the corresponding value of for m_χ for this specific value of δ. The band gives the $1 - \sigma$ determination of the DM relic density from the 7-year WMAP dataset. *Right panel*: models with relic density equal to the central value from the WMAP data, in the plane m_χ versus $m_{3/2}$, obtained by varying δ in the range $-10 < \delta < -3$ and few sample values of D_{X_i}. The filled area marks the region violating the LEP lower limit on the chargino mass; the region of the plane above the dashed line would correspond to models with $\delta > -3$.

m_χ versus $m_{3/2}$ and, varying δ and for a few values of D_{X_i}, we plot models that have $\Omega_\chi h^2$ equal to the mean value from the WMAP data; the plot illustrates the fact that, even in a model as constrained as the G2-MSSM, there is still a rather large sensitivity to the parameters setting the theory at high energy. A relic density compatible with cosmological measurements is obtained for LSP lighter than about 300 GeV and for reheating temperatures in the range between about 100 MeV and 1 GeV. The results of our analysis are consistent, as an overall picture, with the results presented in Refs. [Acharya 2008b, Feldman 2010], although there are slight numerical differences when comparing model by model; most likely these differences stem mainly from the determination of the mass spectrum of the G2-MSSM which is probably less accurate with respect to the original references, although the more careful numerical treatment implemented here for the relic density calculation may have some impact as well. As a final remark, we mention that we have also cross-checked the result that, to obtain a relic density compatible with the DM density as measured by WMAP, it is necessary to forbid the decay of the light moduli into gravitinos; in case it is not, in all G2-MSSM setups, gravitino decays become the main dark matter source, at a stage when reannihilations are inefficient, largely overproducing dark matter.

3.4   Kinetic equilibrium and decoupling in the G2-MSSM

Until now, as already emphasized in the previous chapter, the evolution of the DM number density have been traced, both in the thermal and in the non thermal scenario, assuming that kinetic equilibrium between the χ_a states and the thermal

bath particles is maintained at all stages over which the comoving number density changes. This is typically guaranteed by invoking crossing symmetries relating the scattering to the annihilation cross section; however in many explicit models, like the G2-MSSM, the two processes are not related by crossing symmetry and the hyphothesis of thermal equilibrium should be verified case by case with a dedicated study. We focus here on the G2-MSSM (a more general framework with non-thermal Wino DM will be also considered at the end) and discuss the steps which should be followed when relaxing the hypothesis of kinetic equilibrium, introducing a more general set of Boltzmann equations.

The energy spectrum of SUSY particles produced in the decay of moduli is usually very different from the thermal distribution; in particular in the G2-MSSM scenario, light particles are generated in the decay of very heavy fields. The cascade process generally starts with the production a pair of squarks, followed by their decay into gluino and quark, and with the gluino in turn decaying with a three body process into the LSP, the Wino-like chargino or the Bino, with branching ratios depending on parameters in the model. As a last step, the Bino decays as well into the chargino or the LSP, while the chargino, given the small mass splitting with respect to the LSP, has a longer lifetime. The chargino decay occurs either through a two body process in which a pion is produced together with the LSP, or through a three-body in which a neutrino and an electron are produced; the rates of these processes are given by, respectively, [Chen 1996, Chen 1997]:

$$\Gamma_{\chi^{\pm},\mathrm{2b}} = \frac{2f_\pi^2 G_\mathrm{F}^2}{\pi}\Delta m_\chi^2\sqrt{\Delta m_\chi^2 - m_\pi^2} \qquad \mathrm{and} \qquad \Gamma_{\chi^{\pm},\mathrm{3b}} = \frac{2G_\mathrm{F}^2\Delta m_\chi^5}{15\pi^3}\,, \qquad (3.12)$$

where Δm_χ is the chargino-neutralino mass splitting, $f_\pi = 93$ MeV is the pion decay constant and G_F is the Fermi constant. The two-body decay is dominant when kinematically allowed; this is the case in the G2-MSSM, since the minimum mass splitting between charged and neutral Wino, induced but electroweak radiative corrections to the two masses is $\Delta m_\chi \simeq 160$ MeV [Feng 1999] . We have studied the decay chain of the moduli with the package PYTHIA [Sjostrand 2006] for a few sample benchmark models in the G2-MSSM, assuming a stable Wino-like chargino, and found energy distributions for the Wino-like neutralinos and charginos which are typically peaked at $E/m_\chi \sim 10$ and with very broad tails up to the kinematical threshold; among decay products, the number of charginos is typically about 3 times larger than the number of neutralinos.

The injected ultra-relativistic particles lose energy via scattering on thermal bath states. Were these processes inefficient, the non-thermal DM generation would give rise to a model of the Universe with warm or even hot DM, a possibility which has been investigated, e.g., in Refs. [Lin 2001, Hisano 2001, Gelmini 2006a]. As a first rule of thumb, the energy depletion is efficient whenever the relative energy loss rate times the time interval the over which the process is active, which we indicate as $\Delta\tau$, is larger than 1:

$$\left(-\frac{1}{E}\frac{dE}{dt}\right)\cdot\Delta\tau > 1\,. \qquad (3.13)$$

In our case this condition needs to hold from the relativistic regime down to the non-relativistic low-temperature environments induced by the reheating phase. The expression for $-dE/dt$ is in the form:

$$- \frac{dE}{dt} = \int dE' \left(E - E' \right) \frac{d\Gamma}{dE'} \left(E, E' \right) \tag{3.14}$$

where $\Gamma(E)$ the scattering rate for the process under scrutiny, integrated over the phase space distribution functions of the thermal bath particles in the initial state and the phase space of the out-scattered particles. The expressions we will report below are derived in the limit of small momentum transfer between the non-thermally produced states and the thermal bath particles; the latter on average have energies equal to about $3T$. The small momentum transfer approximation holds whenever the non-thermal particles are non-relativistic in the CM frame of the scattering process, namely for [Hisano 2001]:

$$m_\chi^2 \gtrsim 6TE \,. \tag{3.15}$$

Assuming instantaneous production at reheating, this relation can be translated into:

$$T_{RH} \lesssim 1.7 \, \text{GeV} \, \left(\frac{m_\chi}{100 \, \text{GeV}} \right) \left(\frac{10}{E/m_\chi} \right) \,, \tag{3.16}$$

a condition which is satisfied in the region of the G2-MSSM parameter space providing a viable DM candidate.

Charginos lose energy via electromagnetic interactions and their energy loss rate takes the form [Reno 1988, Braaten 1991]:

$$\left(-\frac{dE}{dt} \right)_{\chi^\pm} = \frac{\pi \alpha^2 T^2}{3} \Lambda \tag{3.17}$$

with $\Lambda \sim O(1)$. The elastic scattering of a Wino-like neutralino on a background lepton is very inefficient, since it proceeds via a Z boson or a slepton exchange and the corresponding amplitudes are suppressed, respectively, by the tiny higgsino fraction in the LSP and by the slepton masses, which in the G2-MSSM are very heavy. Whenever kinematically allowed, the dominant effect is the inelastic scattering into the charged Wino, which is mediated by a W boson. There are then two effects making a neutralino produced in the decay of the modulus lose energy, namely the energy loss in the inelastic scattering itself and the fact that the produced chargino will efficiently lose energy. For relativistic neutralinos, the inelastic scattering rate

and the energy loss rate in inelastic scatterings are, respectively, given by:

$$
\begin{aligned}
\Gamma_{\chi^0 \to \chi^\pm} &= \sum_{(a,b)} \frac{2\tilde{g}_{Wab}\, G_{\rm F}^2}{\pi^3} \exp\left(-\frac{m_\chi \Delta m_\chi}{2ET}\right) T^4 \frac{E}{m_\chi} \\
&\qquad \cdot \left(6\frac{ET}{m_\chi} + \Delta m_\chi\right) \tag{3.18} \\
\left(-\frac{dE}{dt}\right)_{\chi^0 \to \chi^\pm} &= \sum_{(a,b)} \frac{16\tilde{g}_{Wab}\, G_{\rm F}^2}{\pi^3} \exp\left(-\frac{m_\chi \Delta m_\chi}{2ET}\right) T^5 \left(\frac{E}{m_\chi}\right)^3 \\
&\qquad \cdot \left(8\frac{ET}{m_\chi} + \Delta m_\chi\right). \tag{3.19}
\end{aligned}
$$

where, considering the generic process in which the heat bath particle a is scattered into the particle b via an interaction vertex with a W boson, we have included in the coefficient $\tilde{g}_{Wab}$ the product of the number of internal degrees for a, that for b, as well as a rescaling factor in case the coupling constant in the vertex is different from the SU(2) gauge coupling g (e.g., for the scattering process $\chi^0 + e^\pm \to \chi^\pm + \nu_e$, $\tilde{g}_{Wab} = 8$); the sum goes over any (a,b) thermal bath particle pairs.

In Fig. 3.12 we consider two of the G2-MSSM singled out in the previous Section as models embedding a viable DM candidate, at the light and heavy ends of the mass range displayed in Fig. 3.11, i.e. two models with Wino masses, respectively, of 103.5 and 300 GeV, obtained for $D_{X_i} = 16$, $\delta = -3.5$ and $\delta = -3$ and gravitino masses of 107 and 460 TeV, and corresponding to scenarios with approximate reheating temperatures of 100 MeV and 900 MeV. For such models we plot ratios of scattering and decay rates Γ, or of relative energy loss rates $-1/E \cdot dE/dt$, to the Universe expansion rate H; in the panels on the right-hand side, results are shown for relativistic particles, $E/m_\chi = 10$, while on the left-hand side the non-relativistic limit is considered, $E/m_\chi = 1.005$. To sketch the efficiency of the chargino energy losses, the appropriate timescale $\Delta\tau$ in Eq. (3.13) is the shortest between the chargino lifetime and the timescale for back-scattering of the chargino into the neutralino, i.e. the rule of thumb condition in Eq. (3.13) holds whenever the curves in plots corresponding to the chargino energy loss lie above the curves for the decay rate and the inelastic scattering rate. More quantitatively, for the two processes, these ratios are:

$$
\begin{aligned}
\left(\frac{\Delta E}{E}\right)_{\chi^\pm, 1-\text{life}} &\approx 1.86 \cdot 10^2 \Lambda \left(1 - \frac{m_\pi^2}{\Delta m_\chi^2}\right)^{-1/2} \left(\frac{T}{1\,\text{MeV}}\right)^2 \left(\frac{160\,\text{MeV}}{\Delta m_\chi}\right)^3 \\
&\qquad \cdot \left(\frac{100\,\text{GeV}}{m_\chi}\right) \tag{3.20} \\
\left(\frac{\Delta E}{E}\right)_{\chi^\pm, 1-\text{scat.}} &\approx 6.77 \cdot 10^{-2} \Lambda \left(\frac{1\,\text{GeV}}{T}\right)^3 \left(\frac{m_\chi}{100\,\text{GeV}}\right) \left(\frac{10}{E/m_\chi}\right)^3, \tag{3.21}
\end{aligned}
$$

with the smallest of these being much larger than one in all cases except for relativistic charginos injected at temperatures of the order of 1 GeV or larger. The
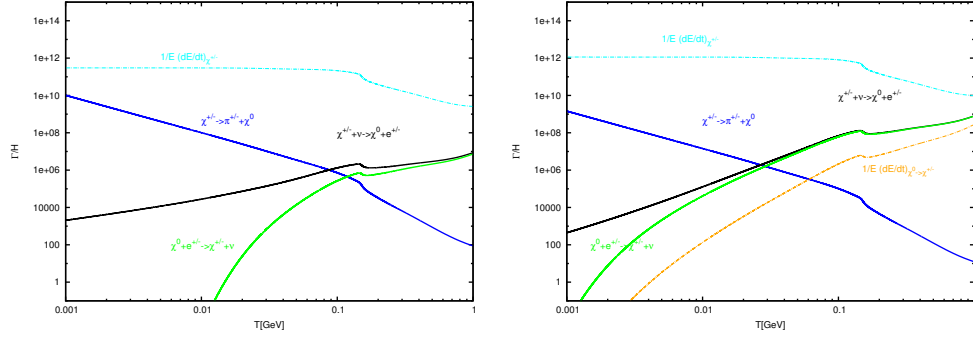
(a) Case 1:$m_\chi = 103.5$ GeV, $T_R = 100$ MeV, $E/m_\chi = 1.005$.

(b) Case 2:$m_\chi = 103.5$ GeV, $T_R = 100$ MeV, $E/m_\chi = 10$.
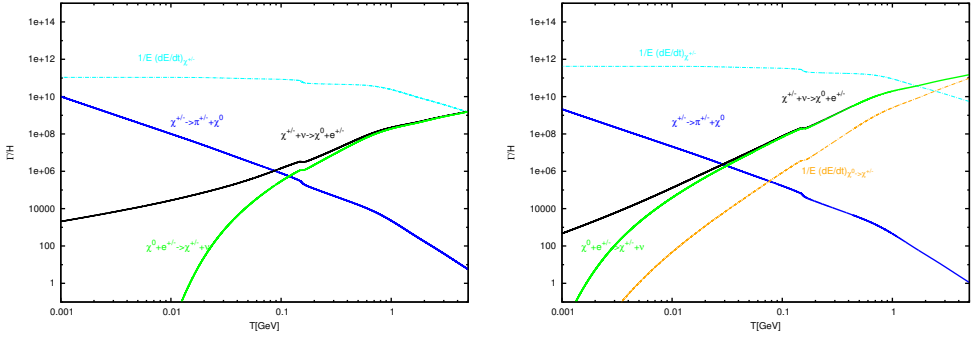
(c) Case 3:$m_\chi = 300$ GeV, $T_R = 900$ MeV, $E/m_\chi = 1.005$.

(d) Case 4:$m_\chi = 300$ GeV, $T_R = 900$ MeV, $E/m_\chi = 10$.

Figure 3.12: Ratios between the effective rate of energy loss rate $-1/E \cdot dE/dt$ (dashed lines), or of the scattering/decay rate Γ (solid lines), to the Universe expansion rate H, for a few processes involving charginos and neutralinos. The upper panels refer to a G2-MSSM DM model with $m_\chi = 103.5$ GeV and $T_{RH} = 100$ MeV, while the lower panels to one with $m_\chi = 300$ GeV and $T_{RH} = 900$ MeV; the plots on the left hand-side refer to non-relativistic particles, $E/m_\chi = 1.005$, while those on the right-hand side correspond to a sample relativistic case, $E/m_\chi = 10$.

latter is however the regime in which inelastic scatterings turning a neutralino into a chargino and viceversa are extremely efficient (as shown in the plots the rate for this process is many orders of magnitude larger than H) and the energy loss rate via this process is also very large (the relevant timescale is now $\sim H^{-1}$). This shows that the relativistic charginos injected at any of the temperatures of interest in our model instantaneously thermalize. For what regards neutralinos, in the relativistic limit, the energy depletion is guaranteed by inelastic scatterings and by chargino energy losses down to background temperatures of about 2 MeV; however when becoming non-relativistic and at low temperatures, the rate for inelastic scatterings becomes smaller than H and the assumption of kinetic equilibrium may not hold any more. To study the evolution of the system at low temperature and model kinetic decoupling, we follow the approach of Bringmann and Hofmann [Bringmann 2007] (see also [Bringmann 2009] and appendix A for a brief review) who have developed a formalism to treat kinetic decoupling starting from the Boltzmann equation for the phase-space distribution function of the WIMP DM candidate; we extend here their treatment to the case of two co-annihilating particles. Let $f_{\chi^0}(p, t)$ and $f_{\chi^\pm}(p, t)$ be the phase space distribution functions for, respectively, the neutral and charged Winos. We have just shown that charginos are kept into kinetic equilibrium at all temperatures of interest for our problem, so we can assume that the shape of the chargino distribution traces the thermal distribution function, namely:

$$f_{\chi^\pm}(p, t) \propto f_{\chi^\pm}^{eq}(p, t). \tag{3.22}$$

On the other hand, the distribution function of the neutralinos could have a shape which is slightly different from the thermal one, since we have shown that energy losses may not be efficient in the non-relativistic regime; this departure is parametrized defining the temperature of neutralinos T_{χ^0} through the second moment of the distribution function:

$$\int \frac{d^3 p}{(2\pi)^3} \, g_{\chi^0} \, p^2 \, f_{\chi^0}(p, t) \equiv 3 m_\chi \, T_{\chi^0}(t) \, n_{\chi^0}(t). \tag{3.23}$$

For neutralinos in kinetic equilibrium, T_{χ^0} coincides with the thermal bath temperature; after kinetic decoupling the neutralino temperature will scale instead as $T_{\chi^0} \propto T^2$.

The two distribution functions obey the system of coupled Boltzmann equations:

$$
\begin{aligned}
(\partial_t - H\mathbf{p} \cdot \nabla_{\mathbf{p}}) \, f_{\chi^0}(p, t) &= \frac{1}{E} \hat{\mathbf{C}}_{\chi^0}[f_{\chi^0}, f_{\chi^\pm}] \\
(\partial_t - H\mathbf{p} \cdot \nabla_{\mathbf{p}}) \, f_{\chi^\pm}(p, t) &= \frac{1}{E} \hat{\mathbf{C}}_{\chi^\pm}[f_{\chi^0}, f_{\chi^\pm}],
\end{aligned}
\tag{3.24}
$$

where $\hat{\mathbf{C}}$ stands for the collisional operator, embedding all interactions involving neutralinos and charginos, namely annihilation and scattering processes, as well as the production of neutralinos and chargino from moduli decays and the neutralino source from chargino decays. Integrating these equation over phase space one obtains

two equations for the time evolution of the neutralino and chargino number densities:

$$
\begin{aligned}
\frac{dn_{\chi^0}}{dt} + 3\,H\,n_{\chi^0} =\ & \left(\widetilde{\Gamma}_{\chi^0\leftrightarrow\chi^\pm} + \Gamma_{\chi^\pm}\right)\left[g_{\chi^0}n_{\chi^\pm} - g_{\chi^\pm}n_{\chi^0}\exp\left(-\frac{\Delta m_\chi}{T}\right)\right] \quad (3.25)\\
& - \langle\sigma v\rangle_{\chi^0\chi^0}\left[n_{\chi^0}^2 - (n_{\chi^0}^{eq})^2\right]\\
& - \langle\sigma v\rangle_{\chi^0\chi^\pm}\left[n_{\chi^0}n_{\chi^\pm} - n_{\chi^0}^{eq}n_{\chi^\pm}^{eq}\right]\\
\frac{dn_{\chi^\pm}}{dt} + 3\,H\,n_{\chi^\pm} =\ & \left(\widetilde{\Gamma}_{\chi^0\leftrightarrow\chi^\pm} + \Gamma_{\chi^\pm}\right)\left[g_{\chi^\pm}n_{\chi^0}\exp\left(-\frac{\Delta m_\chi}{T}\right) - g_{\chi^0}n_{\chi^\pm}\right]\\
& - \langle\sigma v\rangle_{\chi^\pm\chi^\pm}\left[n_{\chi^\pm}^2 - (n_{\chi^\pm}^{eq})^2\right]\\
& - \langle\sigma v\rangle_{\chi^\pm\chi^0}\left[n_{\chi^\pm}n_{\chi^0} - n_{\chi^\pm}^{eq}n_{\chi^0}^{eq}\right] + \sum_i \frac{B_{X_i}}{m_{X_i}}\Gamma_{X_i}\rho_{X_i}\,.
\end{aligned}
$$

In these equations, the first term on the right hand sides accounts for inelastic scatterings of neutralinos into charginos and decays of charginos into neutralinos (as well as the inverse processes); g_{χ^0} and $g_{\chi^\pm}$ are the number of internal degrees of freedom for the neutralino and chargino, while $\Gamma_{\chi^\pm}$ is the chargino decay rate as obtained including the two contributions in Eq. (3.12). For inelastic scatterings we have assumed that: *i)* the diagram with W boson exchange in the t-channel is the dominant one (since those with sfermion exchanged are highly suppressed); *ii)* the momentum transfer in the t-channel is small and the collision term can be computed expanding in its powers, see also [Bringmann 2007, Bringmann 2009]; *iii)* Δm_χ and T are small with respect to m_χ and only the lowest order terms in an expansion in Δm_χ and T give sizable contributions; under these assumptions, we find:

$$
\widetilde{\Gamma}_{\chi^0\leftrightarrow\chi^\pm} = \sum_{(a,b)} \frac{\tilde{g}_{Wab}8G_{\mathrm{F}}^2}{\pi^3}T^3\left(\Delta m_\chi^2 + 6\Delta m_\chi T + 12T^2\right)\,, \qquad (3.26)
$$

(some further details and a sketch of the derivation of this expression is given in Appendix (A)). When including pair annihilation terms in Eq. (3.25) we have taken advantage of the fact that it involves non relativistic particles annihilating mainly via S-wave processes and hence the cross section has a very mild dependence on momentum, allowing then us to write an expression analogue to thermal case also when the neutralino distribution function starts deviating from the kinetic equilibrium value. Furthermore, since the relativistic particles injected from the moduli decays mostly lose energy as charginos, decaying afterwards into neutralinos, we have simplified the treatment including these as a source function of "thermal" charginos only. Obviously, summing the two equations one retrieves Eq. (2.28) with n_χ being the sum of the number density for the two coannihilating species.

Taking the second moment of the first equation in the system in Eq. (3.24), one finds that the neutralino temperature T_{χ^0} obeys the relation:

$$
\frac{dT_{\chi^0}}{dt} + 2HT_{\chi^0} = \left[\left(\widetilde{\Gamma}_{\chi^0\leftrightarrow\chi^\pm} + \Gamma_{\chi^\pm}\right)g_{\chi^0}\frac{n_{\chi^\pm}}{n_{\chi^0}}\right](T - T_{\chi^0}) \qquad (3.27)
$$

(the derivation of this equation is also sketched in the appendix).

The numerical solution of the problem proceeds now analogously to what done so far. After the appropriate change of variables, the system in Eq. (3.25) replaces Eq. (2.28) in the system of Eq. (3.3). The explicit solution for $n_{\chi^0}(t)$ and $n_{\chi^\pm}(t)$ are then implemented in Eq. (3.27) to find $T_{\chi^0}(t)$.

Our first application is to the G2-MSSM models singled out in the previous section as cosmologically favored. As we had guessed in the analysis we performed at the level of energy loss and scattering rates and shown graphically in Fig. 3.12, the departure from kinetic equilibrium tends to be at a temperature sensibly lower than the nominal reheating temperatures for these models (which are of the order of 100 MeV or larger). The numerical solution indeed shows that the ratio $n_{\chi^\pm}/n_{\chi^0}$ tends to follow very closely the ratio of the thermal equilibrium number densities $n^{eq}_{\chi^\pm}/n^{eq}_{\chi^0}$ over the whole phase of DM production in the moduli decays, as well as at later times. The solution of the equation for the neutralino temperature shows that kinetic equilibrium is maintained up to a temperature of the order of 10 MeV, independently of the neutralino mass since, in the non-relativistic limit, the inelastic scattering rate (which together with chargino electromagnetic interactions enforces the equilibrium) depends only on the chargino-neutralino mass splitting which is essentially the same over the whole range of selected models. The transition between $T_{\chi^0} = T$ to the regime $T_{\chi^0} \propto T^2$ takes place on relatively short timescales; since at 10 MeV non-thermal production has become irrelevant, we would have found the very same scaling when computing the kinetic decoupling for a population of thermal particles: the evolution of the number density ratio and of T_{χ^0} for G2-MSSM DM models are those shown as black lines in Fig. 3.13 and labelled, respectively, 'thermal distributions' and 'standard decoupling'.

To illustrate the impact of non-thermal production and non-standard cosmologies on the kinetic decoupling process, we allow then for a slight variant to the underlying particle physics framework, still referring to a pure Wino as DM candidate but assuming now that the reheating temperature can be reduced to values much closer to the bound from BBN than in the G2-MSSM. In Fig. 3.13 one sees a modification with respect to the standard case when the gap between reheating temperature and standard kinetic decoupling temperature is reduced, i.e. for $T_{\rm RH}$ equal to about 20 MeV or lower: The additional DM source makes the ratio $n_{\chi^\pm}/n_{\chi^0}$ differ from the ratio of thermal distributions. The impact on T_{χ^0} is two folded: the chargino decays tend to populate the system with neutralinos that are on average more energetic than for a thermal distribution, delaying the onset of the regime $T_{\chi^0} \propto T^2$ and making the transition into this regime to be less sharp; at the same time, if $T_{\rm RH}$ is so low that reheating increases significantly the expansion rate of the Universe H at the time of kinetic decoupling ($T_{\rm RH} = 8$ and 5 MeV in the plot) the departure from $T_{\chi^0} = T$ tends to be anticipated. This latter feature was already pointed in [Gelmini 2008], showing that the non-thermal production could induce higher kinetic decoupling temperatures compared to the standard case; in case of Wino DM, however, the production and decay or charginos in the moduli decay has always a larger impact. The kinetic decoupling temperature is directly related to

the minimum mass scale for structures in the Universe; we have shown here that even in case of injection of particles with efficient energy losses on the thermal bath, the low-temperature non-thermal production can leave an imprint on structure formation. The development of a precise numerical treatment of the kinetic decoupling is then a valuable tool to test this class of models.

Finally, in the examples considered here, we find a marginal change in the DM relic density when computing it in the case when we trace the the number densities of the individual coannihilating species as opposed to the case when a single equation for the sum of number densities is solved; this is due to the fact that the departure of the ratio $n_{\chi^{\pm}}/n_{\chi^0}$ from the ratio of thermal distributions takes place only when such quantity is very small (moreover, in our examples, the annihilation rates for each of the coannihilation channels are comparable). Considering however models for which crossing symmetry arguments between annihilation and scattering cross sections are even more severely violated, one should find cases in which the standard thermal assumption is invalid at higher temperatures, possibly even close to the chemical freeze out temperature; in those cases there should be a sizable change in the relic abundance as well and the formalism we developed would be suitable for an accurate computation of the relic density for such case.

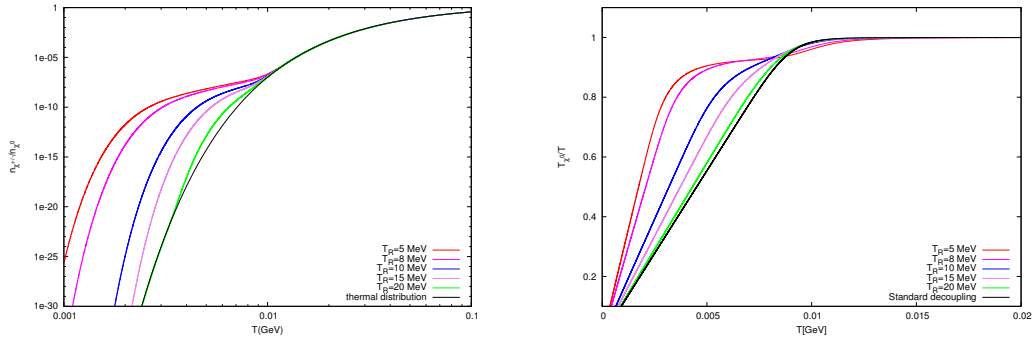Figure 3.13: Left panel: ratio of the chargino number density over the neutralino number density for several values of T_{RH}. Right panel: Ratio $T_{\chi 0}/T$ as function of the temperature of the thermal bath for same values of T_{RH}. Plots are obtained for a Wino with mass equal to 200 GeV, however results depend only on the chargino-neutralino mass splitting which is about 160 MeV in the scenario under consideration.

Dark Matter detection and collider physics

Contents

In the previous chapters we have examined several mechanisms providing the DM a relic abundance compatible with the experimental limit. In particular it results evident that the viability of the DM candidate often imposes specific constraints on some SUSY parameters and can even determine, at least partially, the underlying Supersymmetric spectrum.

In this chapter we will investigate whether an eventual indication of some relevant DM properties, like its mass or the ones responsible for its relic density, can influence the prospects of SUSY detection at LHC.

More specifically we will consider the case of an hypothetical signal from a direct detection (DD) experiment, studying the possibility of translating the provided information about the DM properties into peculiar collider signatures which can be tested by LHC searches in the near future.

DD experiments rely on the idea of measuring the energy deposited by a WIMP particle interacting with the nuclei of a target detector. If a WIMP nucleon scattering is detected it is possible to infer, from the event rate and the spectrum of the measured recoil energies, important properties, in particular the DM mass and

scattering cross section. The latter carries information on the SUSY spectrum and can, in several scenarios, be correlated to the pair annihilation cross section, which influences the DM relic density. This kind of correlations can depict definite scenarios possessing characteristic signatures which can be tested by LHC searches in the near future.

Our study will proceed along the following lines: we have first of all identified some scenarios in which the DD cross-section can be correlated to a specific mechanism accounting for the correct DM relic density. We have then investigated their detection prospects by mean of a bayesian study of a 1-Ton realization of the Xenon experiment. We have finally identified the main collider processes related to these scenarios and performed a dedicated detector simulation, using the setup of the ATLAS experiment, aimed to investigate the current detector constraints and the immediate feature capability of discovery.

4.1   Direct detection of MSSM neutralino

In this section we will briefly review the main aspects relative to the neutralino direct detection evidencing the potential information which can be provided on the underlying particle physics framework. On the other hand, as will be clarified in a while, direct detection is also influenced by some astrophysical properties, like the local dark matter density, which can make more uncertain the capability of current and next future experiments of constraining the MSSM parameter space. Before moving to our main focus we will hence briefly account for these aspects referring to the original literature for the details.

Neutralino dark matter can be directly detected thanks to its couplings with SM quarks (see e.g. [Rosiek 1995] for a collection of the relevant Feynman rules) which allow for elastic scattering with the nuclei in a detector [Jungman 1996, Smith 1990]. In each scattering process is deposited a recoil energy $E_{\mathrm{nr}} = \left(\mu_\chi^2 |v|^2 / M \right) (1 - \cos\theta)$ with $\mu_\chi = m_\chi M / (m_\chi + M)$ being the reduced mass of the DM-nucleus system, $\vec{v}$ the speed of the DM relative to the nucleus, defined as $\vec{v} = \vec{v}_\chi + \vec{v}_E$ where $\vec{v}_E$ and $\vec{v}_\chi$ are, respectively, the Earth velocity in the Galaxy rest frame and the WIMP velocity in the rest frame of the Earth, and θ is the scattering angle in the center of mass frame. The differential recoil rate for a WIMP candidate with elastic scattering cross section σ_{χ_i}, is defined as:

$$\frac{dR_{\mathrm{nr}}}{dE_{\mathrm{nr}}} = \sum_i c_i \frac{\rho_\chi \sigma_{\chi_i} |\ F_i(q_i)\ |^2}{2m_\chi \mu_{i\chi}^2} \int_{v > \sqrt{M_i E / 2\mu_{\chi_i}^2}} \frac{f(v,t)}{v} d^3 v \qquad (4.1)$$

with the sum over i accounts for the presence of several nuclear species in the detector, each with mass fraction c_i. q_i represent the recoil momentum $q_i = \sqrt{2 M_i E_{\mathrm{nr}}}$ of the nucleus i and $F(q_i)$ is a nuclear form factor (normalized in such a way the $F^2(0) = 1$) parametrizing the finite size of the target nucleus itself. The recoil rate depends finally also on the local DM density ρ_χ and on its velocity distribution

$f(v, t)$ which is integrate from the minimal velocity:

$$v_{\min} = \sqrt{\frac{M_i E_{\mathrm{nr}}}{2\mu_\chi^2}} \tag{4.2}$$

for which energy deposition can occur.

Once deposited in a nucleus, the recoil energy can be transferred either to electrons, allowing for the observation of scintillation either ionization, or to the other nuclei, producing phonos, and then inferred form the detection of this kind of effects. Many detection techniques exist, depending on the experimental setup; in all cases however a large variety of effects, ranging from intrinsic fluctuations in the physical/chemical processes determining the production and propagations of the phonons, scintillation or ionization signals, to the technical limitations in the measure of the signals themselves, can cause a mismatch between the measured signal and the effective recoil energy which result in a finite energy resolution. The observed recoil rate is then smaller than the ideal expression (4.1), which is indeed [Akrami 2011]:

$$\frac{dR}{dE} = \int_0^\infty dE_{\mathrm{nr}} \phi(E, E_{\mathrm{nr}}) \frac{dR_{\mathrm{nr}}}{dE_{\mathrm{nr}}}(E_{\mathrm{nr}}, t) \tag{4.3}$$

where $\phi(E, E_{\mathrm{nr}})\Delta E$ is the probability of observing an event with recoil energy E_{nr} with a measured energy in the range $E, E + \Delta E$ (in the limit $\Delta E \to 0$) after accounting for efficiencies (and data cuts) and the finite energy resolution.

The expected number of signal events is obtained by integrating (4.3) over the range of sensitivity of the given detector:

$$\mu_{\mathrm{S}} = M_{\mathrm{det}} T \int_{E_{\min}}^{E_{\max}} dE \frac{dR}{dE}(E) \tag{4.4}$$

Here M_{det} and T represent, respectively, the detector mass and the exposure time. In this definition the time dependence of the differential recoil rate is neglected since it is not relevant for the experimental setup which we are going to simulate [1].

Besides the possible alterations related to the detector performance or the background rejection/contamination already parametrized by the integral (4.3) the signal itself may be intrinsically affected by uncertainties related to the astrophysical quantities contained in the recoil rate. First of all there is an uncertainty in the normalization of the incident DM flux, which scales with the local halo density, often quoted to be unknown within a factor 2 [Caldwell 1981]. Moreover the determination of the DM energy spectrum in the detector frame is affected by uncertainties in determining their velocity distribution in the galactic frame as well as the proper motion of the Sun/Earth system.

The issue reletative the DM local density have been addressed by adopting the very precise determination obtained in [Catena 2010] by mean of a statistical analysis including a large variety of observational constraints. This determination relies partially on the assumption of spherical symmetry for the DM distribution.

---

[1]The time dependence of the recoil rate is instead the main discriminant for the DM detection for several alternative setups like DAMA-LIBRA.

Concerning instead the DM velocity distribution function it is customary to adopt a Maxwell-Boltzmann function with velocity dispersion scaled up of a factor $\sqrt{3/2}$ with respect to the Sun circular velocity (taken at the standard value of 220 km s^{-1}) and truncated to the value assumed for the escape velocity. This results a motivated choice since the Maxwellian distribution is the configuration maximizing the entropy for a self-gravitating collisionless system and is associated to the spherical isothermal sphere density profile, which declines at large radii as r^{-2} and hence supports a flat rotation curve. On the other hand it seems opposed by recent results from N-body simulations like Via Lactea [Diemand 2008] and Aquarius [Springel 2008] which find that DM halos have density profiles declining as r^{-3} at large radii and velocity distributions showing significant departures from the Maxwell-Boltzmann shape. Adopting a distribution function directly read out from the simulations is however troublesome since they treat the galaxy as made of DM only, neglecting the feedback of baryons while, in reality, stellar and gas components dominate the potential well in the inner Galaxy and out to, at least, our Galactocentric distance [Kuijken 1990].

In this thesis we will follow the alternative approach of [Catena 2012] relying on the fact that, assuming that the DM distribution is isotropic, there is a one-to-one correspondence between the spherycally symmetric density profile and the underlying distribution function. The latter is then determined by extending the bayesian approach of [Catena 2010] consistently with the local dark matter density and the available dynamical constraints.

As last topic we will now examine in detail the scattering cross section of a neutralino dark matter. As already mentioned it is determined by the neutralino-quark couplings which can be described, in the non-relativistic limit, by an effective lagrangian made, also taking into account the Majorana nature of the neutralino, by the following two operators [Jungman 1996, Falk 1999] :

$$\mathcal{L} = \alpha_{2q}\bar{\chi}\gamma^{\mu}\gamma^5\chi\bar{q}\gamma_{\mu}\gamma^5 q + \alpha_{3q}\bar{\chi}\chi\bar{q}q \tag{4.5}$$

The just reported axial vector and scalar couplings give rise to two distinguishable components, namely the spin-dependent (SD) and spin independent cross sections. The nuclear form factor can be splitted in an analogous manner in such a way that:

$$\sigma F^2(q) \rightarrow \sigma^{\mathrm{SD}}F_{\mathrm{SD}}^2(q) + \sigma^{\mathrm{SI}}F_{\mathrm{SI}}^2(q) \tag{4.6}$$

The Xenon experiment is sensitive only to the SI cross section; from now on we will then refer only to this component. This can be written as:

$$\sigma^{SI} = \frac{\mu_{\chi i}^2}{\pi}\left[ZG_S^p + (A - Z)G_S^n\right]^2 \tag{4.7}$$

where

$$G_S^N = \sum_{q=u,d,s,c,b,t} \langle N|\bar{q}q|N\rangle \frac{m_p}{m_q}\alpha_{3q}$$

$$\langle N|\bar{q}q|N\rangle = \begin{cases} \frac{m_N}{m_q}f_{Tq}^N & q = u,d,s \\ \frac{2}{27}\frac{m_N}{m_q}f_{TG}^N & G = c,b,t \end{cases}$$

$$f_{TG}^N = 1 - \sum_{q=u,d,s} f_{Tq}^N \tag{4.8}$$

The quantities f_{Tq}^N and f_{TG}^N represent the contribution to the composition of the nucleus N from respectively, light (u,s,d) and heavy (c,b,t) quarks, with the latter arising from gluon anomalous interactions [Shifman 1978, Vainshtein 1980]. The matrix elements for light quarks can be determined from the estimates of the following combinations of matrix elements [Cheng 1989, Gasser 1991, Borasoy 1997, Knecht 1999, Pavan 2002, Sainio 2002]:

$$\Sigma_{\pi N} = \frac{1}{2}(m_u + m_d)\langle p|(\bar{u}u + \bar{d}d)|p\rangle = 64 \pm 8\text{MeV} \tag{4.9}$$

$$\sigma_0 = \frac{1}{2}(m_u + m_d)\langle p|\bar{u}u + \bar{d}d - 2\bar{s}s|p\rangle = 36 \pm 7\text{MeV} \tag{4.10}$$

$$z = \frac{\langle p|\bar{u}u - \bar{s}s|p\rangle}{\langle p|\bar{d}d - \bar{s}s|p\rangle} = 1.49 \tag{4.11}$$

$$\frac{m_u}{m_d} = 0.553 \quad \frac{m_d}{m_s} = 18.9 \tag{4.12}$$

Using these one can write, ad example:

$$f_{Tu}^{(p)} = \frac{2\Sigma_{\pi N}}{m_p\left(1 + \frac{m_d}{m_u}\right)\left(1 + \frac{B_d}{B_u}\right)} = 0.026 \tag{4.13}$$

$$f_{Td}^{(p)} = \frac{2\Sigma_{\pi N}}{m_p\left(1 + \frac{m_u}{m_d}\right)\left(1 + \frac{B_u}{B_d}\right)} = 0.039 \tag{4.14}$$

$$f_{Ts}^{(p)} = \frac{2\left(\frac{m_s}{m_d}\right)\Sigma_{\pi N}y}{m_p\left(1 + \frac{m_d}{m_u}\right)} = 0.36 \tag{4.15}$$

$$f_{TG}^{(p)} = 0.575 \tag{4.16}$$

where

$$\frac{B_d}{B_u} = \frac{2 + (z-1)y}{2z - (z-1)y} = 0.8 \tag{4.17}$$

$$y = 1 - \frac{\sigma_0}{\Sigma_{\pi N}} = 0.4375 \tag{4.18}$$

The dependence on the SUSY spectrum is contained in the effective coupling α_{3q} which can expressed as [Ellis 2005]:

$$
\alpha_{3q} = -\frac{gm_q}{4m_W B}\left[Re\left[\delta_1\left(gN_{12}-g'N_{11}\right)\right]DC\left(-\frac{1}{m_H^2}+\frac{1}{m_h^2}\right)\right.
$$
$$
\left. Re\left[\delta_2\left(gN_{12}-g'N_{11}\right)\right]\left(\frac{D^2}{m_H^2}+\frac{C^2}{m_h^2}\right)\right]
$$
$$
-\frac{1}{2\left(m_{1i}^2-(m_q+m_\chi)^2\right)}Re\left[X_i\,Y_i^*\right]-\frac{1}{2\left(m_{2i}^2-(m_q+m_\chi)^2\right)}Re\left[W_i\,V_i^*\right]\quad(4.19)
$$

where:

$$
X_i \equiv \eta_{11}^\star\frac{gm_qN_{1,5-i}^*}{2m_W B}-\eta_{12}^\star e_ig'N_{11}^\star \tag{4.20}
$$

$$
Y_i \equiv \eta_{11}^\star\left(\frac{y_i}{2}g'N_{11}+gT_{3i}N_{12}\right)+\eta_{12}^\star\frac{gm_qN_{1,5-i}}{2m_W B} \tag{4.21}
$$

$$
W_i \equiv \eta_{21}^\star\frac{gm_qN_{1,5-i}^*}{2m_W B}-\eta_{22}^\star e_ig'N_{11}^\star \tag{4.22}
$$

$$
V_i \equiv \eta_{21}^\star\left(\frac{y_i}{2}g'N_{11}+gT_{3i}N_{12}\right)+\eta_{22}^\star\frac{gm_qN_{1,5-i}}{2m_W B} \tag{4.23}
$$

where y_i and T_{3i} are, respectively, the hypercharge and the isospin and

$$
\delta_1 = N_{13}\left(N_{14}\right)\quad \delta_2 = N_{14}\left(-N_{13}\right)
$$

$$
B = \sin\beta\left(\cos\beta\right)\quad C = \sin\alpha\left(\cos\alpha\right)
$$

$$
D = \cos\alpha\left(-\sin\alpha\right) \tag{4.24}
$$

where the quantities inside the parenthesis refer to down type quarks. m_{1i} and m_{2i} are the 2×2 squark matrices with i=1 for up-type squarks and i=2 for down type ones and m_q are the masses of the corresponding quarks. η_{ij}, finally, are the elements of the matrices which diagonalize the squark mass matrices:

$$
\begin{pmatrix} \tilde{q}_1 \\ \tilde{q}_2 \end{pmatrix} = \eta\begin{pmatrix} \tilde{q}_L \\ \tilde{q}_R \end{pmatrix},\quad diag\left(m_1^2,m_2^2\right)=\eta M_{\tilde{q}}^2\eta^{-1}
$$
$$
\begin{pmatrix} \eta_{11} & \eta_{12} \\ \eta_{21} & \eta_{22} \end{pmatrix} \equiv \begin{pmatrix} \cos\theta_f & \sin\theta_f e^{i\gamma_f} \\ -\sin\theta_f e^{-i\gamma_f} & \cos\theta_f \end{pmatrix} \tag{4.25}
$$

Notice that the last line of expression (4.19) is strictly valid if $m_q^2\gtrsim m_{\tilde{q}}^2-m_\chi^2$, otherwise should be corrected as shown in [Drees 1993b, Drees 1993a].

All the quantities involved in the differential recoil rate are computed through the package DARKSUSY [2].

---

[2]Analogously to what done in [Akrami 2011] we have changed the default values of the hadronic matrix elements contained in DARKSUSY according the more updated values here reported. The same has been done for some parameters related local DM density in order to agree with the results of [Catena 2010, Catena 2012].

4.2 Theoretical framework for direct detection and relic density

From expression (4.19) it is evident that the SI scattering cross section is influenced by two different kinds of contribution. The first one, corresponding to the first two lines of (4.19) is originated by interactions of the neutralino mediated by the CP-even higgs bosons. This contribution typically turn to be the dominant because of the dependence on the light higgs mass m_h. On the other hand this interactions require a non-negligible higgsino component in the dark matter particle, as pointed out by the presence of the matrix elements N_{13} and N_{14}. At the same time the DM higgsino fraction has a potentially deep influence in the dark matter relic density since it weights the impact of the very efficient annihilation processes into W-boson pairs. The scattering cross section is also influenced by interactions involving the squarks. This contribution is typically suppressed by the heaviness of the squark masses which dominates the denominators of the last line of (4.19). This may not be the case, however, when at least one of the squarks is very close in mass to the dark matter particle, in such a way that the difference of the squared masses results comparable with m_h and, at the same time, the higgsino fraction is low or even negligible. Remarkably, in this kind of setup, the lightest squark can influence the relic density through coannihilation effects.

This just sketched cross correlation between DD and relic density will be examined in detail in the next sections. Our analysis, based on multi-parameter scans of the MSSM phase space, will depict some definite scenario, then identified by mean of one or more benchmark points, in which the combined constraints on the dark matter viability can become a guideline in the identification of characteristic SUSY spectra detectable in the near future collider searches. In addition, this scenarios will be required to satisfy a series of constraints coming from flavor physics and current SUSY searches at LHC.

4.2.1 pMSSM setup

For our investigation of the MSSM parameter space we adopt the framework dubbed as pMSSM [Djouadi 1998a] which is defined by the following assumptions [Arbey 2012b]:

- all soft-SUSY breaking parameters are real and there is no new source of CP-violation with respect to the SM;

- the soft mass terms of the sfermions, as well as the A terms, are diagonal in the flavor space implying no new souces of flavor violation, at the Tree-Level, with respect to the SM;

- soft SUSY-breaking masses and trilinear couplings for the first two generations of sfermions are equal at the EW breaking scale;

Given these assumptions the pMSSM described by 22 parameters defined at the EW breaking scale:

- μ, m_A and $\tan\beta$ parameters describing the higgs sector;

- first/second generation sfermion mass parameters $m_{\tilde{q}}$, $m_{\tilde{u}_L}$, $m_{\tilde{d}_L}$, $m_{\tilde{l}}$, $m_{\tilde{e}_R}$;

- first/second generation trilinear terms A_u, A_d and A_e;

- third generation mass parameters $m_{\tilde{q},3_L}$, $m_{\tilde{t}_R}$, $m_{\tilde{b}_R}$, $m_{\tilde{l},3_L}$, $m_{\tilde{\tau}_R}$;

- third generation trilinear couplings A_t, A_b and A_τ;

This parameter definition makes the pMSSM very manageable for phenomenological studies without loss of generality. On the other hand a detailed exploration of the full parameter space results very challenging because of its relatively high dimensionality. Requiring however the presence of correlations among observables, like the ones depicted before, together with the current constraints from collider searches, allows for a sensitive reduction of the number of free-parameters.

We remind, first of all, that relevant portions of the parameter space are already excluded by the current negative results in LHC SUSY searches. This constraints most severely affect the mass of the gluino and of the squarks of the first two generation, ruling out, in some setups, values even up to 1 TeV [Aad 2011b, Chatrchyan 2011] [3] . Restricting, for reasons which will be clarified in the next, to values of the DM mass below 500 GeV, the squarks of the first generations cannot relevantly influence the SI cross section. For this reason we will set their soft mass terms to a unique value m_0, fixed in the multi-TeV range decoupled from the rest of the spectrum, and the relative A-terms to 0. The gluino mass, although does not enter directly into the SI cross section, influences, through radiative corrections, the squark masses. For this reason it will be left to vary over the range reported in the next subsection from a lower value of 600 GeV.

We also observe that eq. (4.19) is not affected anyhow by the slepton sector. For simplicity we will keep fixed the masses of the first two generations at the same value m_0 just reported while the third generation ones will be described by a parameter $m_{03,l}$ left free to vary in order to leave open the possibility of an influence on the relic density. As additional simplifying assumption we will reduce to four the remaining parameters related to third generation sfermions, namely two mass terms $m_{03,R}$ and $m_{03,L}$, respectively for right-handed and left-handed squarks, and two trilinear couplings A_t and $A_b = A_\tau$.

A final restriction is applied to the DM mass. In order to match the current sensitivity of DD experiments and the LHC reach within few years we restrict to DM candidates with mass below 500 GeV. We will further neglect the scenario of

---

[3]Most of the exclusion limits available in the literature rely on oversimplified models or at most on the CMSSM and their translation into a multi-parameter model like the pMSSM is not straightforward. In the scans considered in the next section we will not apply excessively tight constraint determining more accurate limits case by case through our detector simulations.

Wino dark matter since does not show relevant correlations among DD and relic density. We will thus assume the unification relation $M_1 \approx 0.48 M_2$ ad exception of the scenarios of low DM masses, namely below 100 GeV, where the two parameters will be regarded as independent in order to overcome the LEP bound on M_2.

4.2.1.1 pMSSM scans and numerical tools

The first part of our analysis, relying on the search of viable dark matter scenarios, is based on flat scans over the MSSM parameters. Under the hypotheses described above the parameter space is reduced to 10-11 quantities varied over the following ranges:

$$
\begin{aligned}
10 &\leq M_1 \leq 500\,\text{GeV} \\
100 &\leq M_2, \mu \leq 3000\,\text{GeV} \\
600 &\leq M_3 \leq 3000\,\text{GeV} \\
100 &\leq m_{03,L}, m_{03,R}, m_{03,l} \leq 3000\,\text{GeV} \\
90 &\leq m_A \leq 3000\,\text{GeV} \\
3 &\leq \tan\beta \leq 60 \\
-9 &\leq A_t, A_b \leq 9\,\text{TeV}
\end{aligned}
\tag{4.26}
$$

SUSY spectra have been generated by the package SUSPECT [Djouadi 2007] and required to be physical, i.e to satisfy the EW breaking condition, and to have a neutralino as LSP. The following constraints have been then applied to the spectra obtained in this way. First of all we have considered the direct detection and the relic density constraints computing the relevant quantities through the package DARKSUSY. For the direct detection we have used the bounds from the XENON experiment [Aprile 2011, 2012]; regarding the relic density we have instead adopted the cosmological value as an upper bound in order to taken into account possible deviations form the standard cosmological hystory (see previous chapter).

Additional bounds should be applied to the generated models, besides the ones strictly related to the DM phenomenology. A first series of bounds comes from flavor physics, especially from the processes $b \to s\,\gamma$ and $B_s \to \mu^+\mu^-$ computing their branching fractions with the package SuperIso [Mahmoudi 2008, Mahmoudi 2009]. For the former process we have considered, as range of viability the interval $[2.77, 4.37] \times 10^{-4}$, while for the latter we have adopted the recently updated upper limit of 4.5×10^{-9} [Chatrchyan 2012a, Aaij 2012]. We have also taken into account the recent detection of a light boson at LHC as well as the limits on the process $A \to \tau^+\tau^-$ [Aad 2011a, Chatrchyan 2012b]. The last constraints come, finally, from the potential effects of the presence of light supersymmetric particles on the higgs decays, in the form of additional loop contribution as well as the presence of the decay channel into two dark matter particles if kinematically allowed. We have used HDECAY [Djouadi 1998b] to compute the relevant branching fractions.

4.2.2 Relic density constraints

In the particle physics framework just depicted we can classify 4 possible scenarios in which the dark matter relic density does not exceed the cosmological limit:

1. Dark matter annihilations into a fermion pair mediated by a very light sfermion (with mass of the order 100-200 GeV). In light of our assumptions and taking into account the current collider constraints the only candidate is the lightest stau.

2. Enhanced contribution, in the annihilation cross section, from processes mediated by Z and Higgs bosons (see fig. 4.3) in correspondence of resonances. This kind of scenarios will be considered in particular for DM masses lower than 100 GeV. These can anyway occur also higher masses where we can have resonances associated to the CP-odd higgs.

3. Relevant higgsino fraction triggering the additional annihilation channel into a W boson pair, much more efficient than the annihilation into two fermions.

4. Coannihilation with sfermions. In our setup this possibility is restricted to third family sfermions. The main focus will be on case of stop or sbottom coannihilatios since it shows a clear correlation among annihilation and scattering cross section, being these practically related by a crossing symmetry, and, as we will discuss in the following, also with collider production cross section.

We will now describe in more detail the single scenarios, starting from the coannihilation one. Its effectiveness depends on the parameters entering in the following 2×2 mass matrices whose diagonalization determines the physical stop, sbottom and stau states:

$$
\begin{aligned}
m_{\tilde{t}}^2 &= \begin{pmatrix} m_{03,L}^2 + m_t^2 + (T_3 - Q \sin^2 \theta_W) m_Z^2 \cos 2\beta & v(A_t \sin \beta - \mu Y_t \cos \beta) \\ v(A_t \sin \beta - \mu Y_t \cos \beta) & m_{03,R}^2 + m_t^2 + (T_3 - Q \sin^2 \theta_W) m_Z^2 \cos 2\beta \end{pmatrix} \\
m_{\tilde{b}}^2 &= \begin{pmatrix} m_{03,L}^2 + (T_3 - Q \sin^2 \theta_W) m_Z^2 \cos 2\beta & v(A_b \cos \beta - \mu Y_b \sin \beta) \\ v(A_b \cos \beta - \mu Y_b \sin \beta) & m_{03,R}^2 + (T_3 - Q \sin^2 \theta_W) m_Z^2 \cos 2\beta \end{pmatrix} \\
m_{\tilde{\tau}}^2 &= \begin{pmatrix} m_{03,l}^2 + (T_3 - Q \sin^2 \theta_W) m_Z^2 \cos 2\beta & v(A_\tau \cos \beta - \mu Y_\tau \sin \beta) \\ v(A_\tau \cos \beta - \mu Y_\tau \sin \beta) & m_{03,l}^2 + (T_3 - Q \sin^2 \theta_W) m_Z^2 \cos 2\beta \end{pmatrix}
\end{aligned}
\tag{4.27}
$$

A coannihilation scenario may be realized in case of sizable off-diagonal entries, governed by the trilinear couplings as well as by μ and $\tan \beta$, in the matrix above since they produce an additional mass splitting in the the eigenstates which drives the lightest one close to the DM mass, provided that the scale of the soft mass term is not too high. In the case of the stop mass matrix the off-diagonal terms are mainly determined by the trilinear coupling A_t, for the other to cases the dominant contribution is proportional to the combination $\mu \tan \beta$. We also notice that a sizable

mixing between left-handed a right-handed squark states enhances the contribution of squark mediated interactions in eq. (4.19).

Fig. (4.1) reports the main results of a dedicated scan with the aim of evidencing the relation among the SI cross section and the parameters relevant for coannihilation[4]. We have in particular evidenced the relative importance of the two kinds of contributions, namely higgs and squark mediated interactions, involved in the SI cross section. As evident from the plot squark interaction can very hardly dominate the DM-nucleon interactions unless the higgsino fraction is suppressed much below the order of percent. We also notice that the strongest impact on the scattering cross section is exerted by sbottom mediated interactions. Computing indeed eq. (4.19) in the limit of negligible higgsino fraction the sbottom contribution results enhanced by a factor m_p/m_b compared the ratio m_p/m_t multiplying stop contribution. Moreover the presence of the top mass in the propagators of (4.19) disfavors the contribution of stop squarks very close in mass with the DM.

We can finally anticipate that the coannihilation scenario is deeply influenced by the bounds coming from flavor physics and the higgs mass. Despite lower values, especially regarding the stops, are not strictly forbidden by these bounds we will consider only stop and sbottom masses above 200 GeV in order to avoid an excessive tuning of the parameters, also in view of the bounds on SUSY searches discussed in the next sections.

Together with the one just described, a scenario showing strong correlation between DD and relic density is probably the one in which both these two observables are controlled by the DM higgsino fraction. As evident from fig. 4.2 the strongest constraints come from the current limit on DM direct detection which can be easily exceeded by an excessive higgsino fraction. This problem becomes more severe as the DM mass gets low (see fig. 4.2). This implies that we have to rely on the remaining two scenarios in order to have viable dark matter candidates with mass lower than about 150 GeV. We also remind that the μ parameter is constrained by the LEP bound to lie above 100 GeV.

Despite the two mechanisms showing the greater impact on the SI cross section result not viable, low DM scenarios will deserve anyway attention in our analysis since they guarantee a larger number of signal events in a realization of a DD experiment and hence have the best prospects of reconstruction. Also in this case, anyway, dark matter properties can influence the collider phenomenology.

The annihilations of light DM candidates are dominated by s-channel exchange of higgs or Z-bosons and t-channel slepton (only the stau in our setup) exchange. Fig. (4.3) shows that the formers dominates the mass region $40 - 60$ GeV while the latter becomes relevant at higher masses. This scenario is also very constrained by the flavor process $B_s \to \mu^+\mu^-$ and $b \to s\gamma$ (see next section). The impact of this constraints have been evidenced in the plot by indicating in green the points passing these constraints.

---

[4]The spectra have been generated with the additional conditions $M_1 > 100 GeV$, $\mu, m_A > 2M_1$ in order to avoid resonant annihilations as well as a high dark matter higgsino fraction
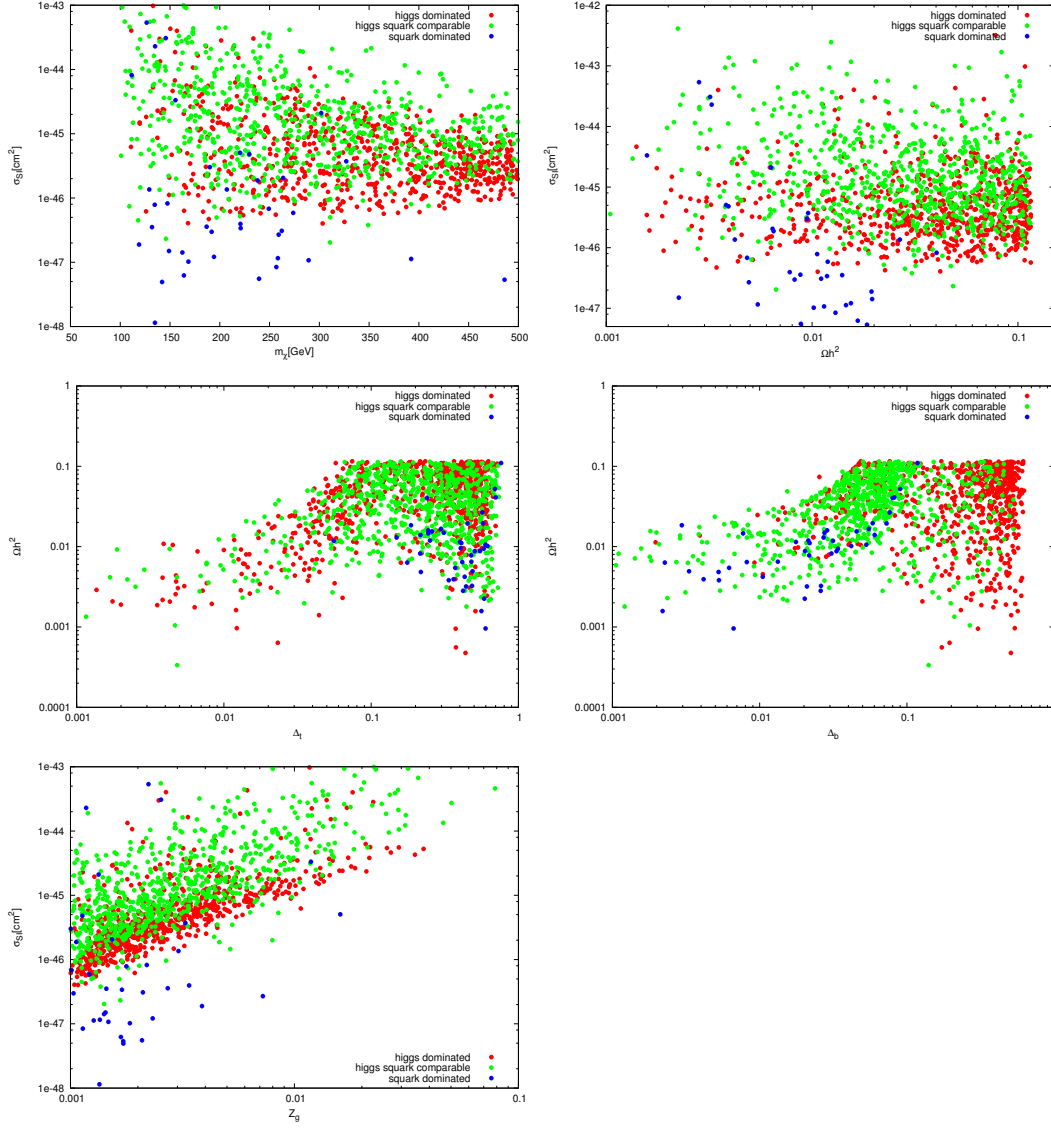
Figure 4.1: First panel:Behavior of σ_{SI} with the DM mass for the points with relic density below the cosmological limit. Second panel: points satisfying the cosmological limit Third and fourth panel: DM relic density with respect to $\Delta_t = \frac{m_{\tilde{t}_1} - m_\chi}{m_{\tilde{t}_1}}$ and $\Delta_b = \frac{m_{\tilde{b}_1} - m_\chi}{m_{\tilde{b}_1}}$.
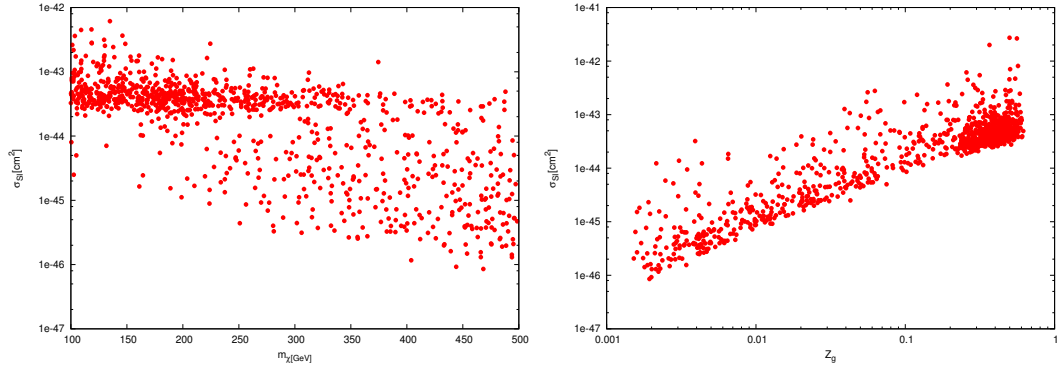
Figure 4.2: Behaviour of the SI cross section and the relic density with DM mass and with the DM higgsino fraction
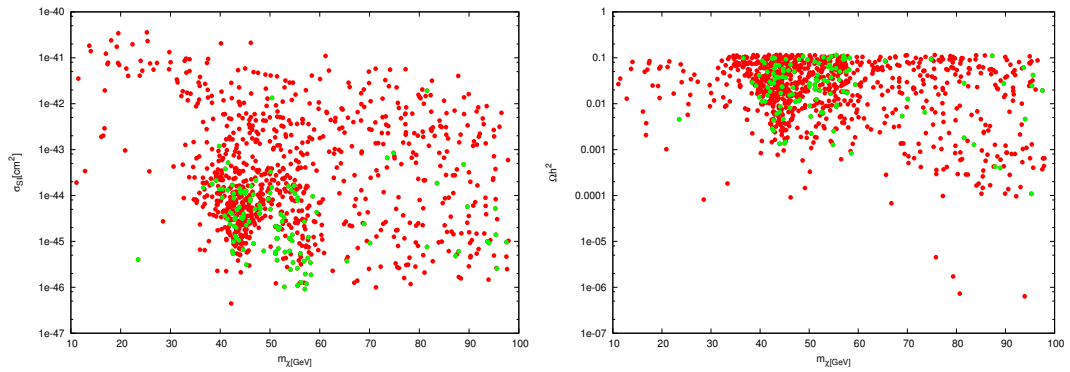
Figure 4.3: Behavior of the SI cross section and relic density in the light DM scenario. In all plots green points are the ones which satisfy the flavor constraints.

We also notice that pratically no viable points are found for DM masses below 30 GeV. To achieve the correct relic density at such low masses one has to rely on interactions mediated by a relatively light CP-odd higgs boson obtaining that [Bottino 2012]:

$$\Omega h^2 \simeq \frac{4.8 \times 10^{-6}}{\text{GeV}^2} \frac{x_f}{g_*^{1/2}(x_f)} \frac{1}{N_{11}^2 N_{13}^2 \tan^2 \beta} m_A^4 \frac{\left[1 - (2m_\chi)^2/m_A^2\right]^2}{m_\chi^2 \left[1 - m_b^2/m_\chi^2\right]^{1/2}} \tag{4.28}$$

with the product $N_{11}^2 N_{13}^2$ limited to be lower than 0.13 by the constraints on the process $Z \to \chi\chi$ [Komatsu 1986, Barbieri 1987]. From the previous expression we can extrapolate a lower limit on the DM mass of the form:

$$m_\chi \frac{\left(1 - m_b^2/m_\chi^2\right)^{1/4}}{1 - (2m_\chi)^2/m_A^2} \gtrsim 21\text{GeV}\left(\frac{m_A}{90\text{GeV}}\right)^2 \left(\frac{12}{\tan\beta}\right) \left(\frac{0.12}{N_{11}^2 N_{13}^2}\right)^{1/2} \left(\frac{0.12}{\Omega h^2}\right)^{1/2} \tag{4.29}$$

excluding masses lighter than 21 GeV in view of the existing limits on m_A and $\tan\beta$ coming from the LHC searches of the higgs decaying into two τ (see [Chatrchyan 2012b] and also next section). The DM relic density results then related to the SI cross section by the relation:

$$\sigma_{SI} \simeq 9.7 \times 10^{-42}\text{cm}^2 \left(\frac{N_{11}^2 N_{13}^2}{0.13}\right) \left(\frac{\tan\beta}{15}\right)^2 \left(\frac{90\text{GeV}}{m_h}\right)^4 \left(\frac{g_d}{390\text{MeV}}\right)^2 \tag{4.30}$$

with

$$g_d \equiv \left[m_d \langle N|\bar{d}d|N\rangle + m_s \langle N|\bar{s}s|N\rangle + m_b \langle N|\bar{d}d|N\rangle\right] \tag{4.31}$$

which evidences large values of the cross section already excluded by XENON experiment.

An alternative would rely on stau mediated interactions but requires for this last particle masses at the edge of the LEP thus resulting trublesome.

The final mention is devoted to the scenario in which the correct relic density is achieved by resonant annihilation processes mediated by CP-odd higgs (cfr. 4.4). This is a viable option for dark matter candidates above around 100 GeV but we will not put particular attention on it since does not provide peculiar indications regarding collider physics

4.2.3   Collider constraints on the higgs mass

The ATLAS and CMS collaboration have recently reported the discovery of a neutral boson of mass of around 125 GeV. Its couplings result fully compatible with the ones of the SM higgs boson despite there are still slight indications, non statistically decisive, of some deviation from the standard values (see for details [Giardino 2012a, Carmi 2012]).

The MSSM setup most likely in agreement with this result is the so called decoupling regime [Haber 1995] in which the light CP-even higgs state h saturates the condition (2.49) and has SM-like couplings while all the other higgs states are
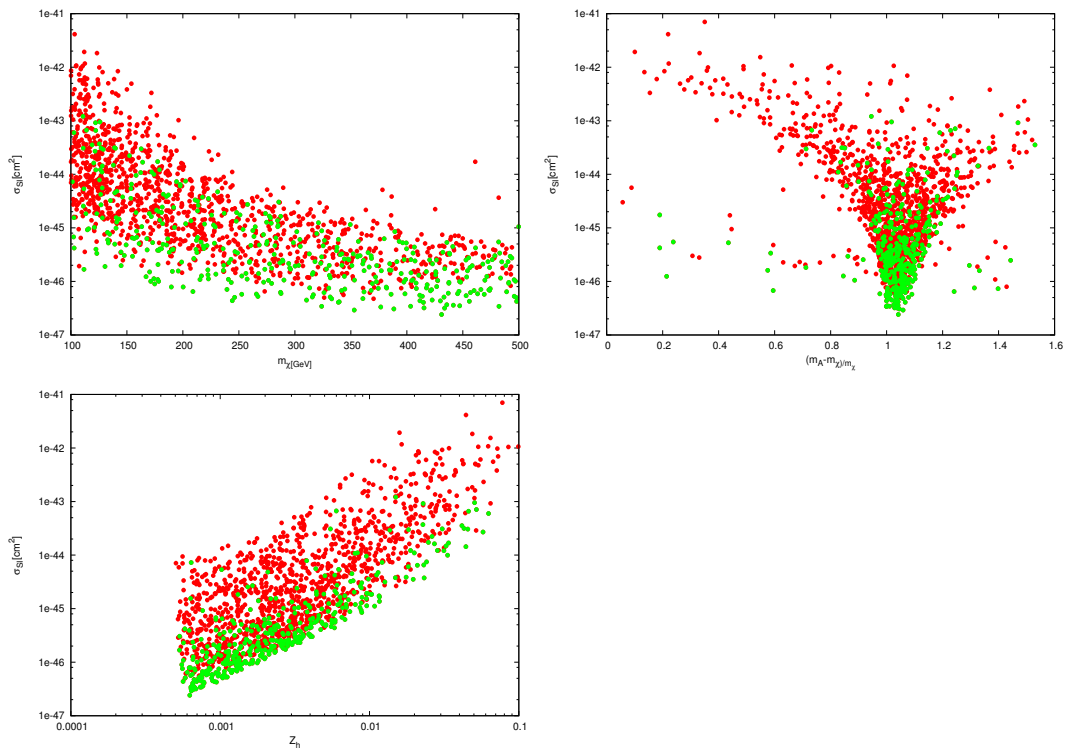
Figure 4.4: Behaviour of Ωh^2 and σ_{SI} in the scenario in which the mass of the CP-odd higgs is close to resonace. Green points satisfy flavor constraints as well.

degenerate in mass and lie at a sensitively higher scale. In this regime the higgs mass m_h is given by the following combination of tree-level and loop contribution, with the latter dominated by stop-top loops:

$$m_h \approx m_Z \cos 2\beta + \frac{3G_F}{\sqrt{2}\pi^2} m_t^4 \left(\log\left(\frac{M_s^2}{m_t^2}\right) + \frac{X_t^2}{M_s^2}\left(1 - \frac{X_t^2}{12M_s^2}\right)\right) \qquad (4.32)$$

where $X_t = A_t - \mu \cot\beta$ and $M_s = \sqrt{m_{\tilde{t}_1} m_{\tilde{t}_2}}$ with $\tilde{t}_1$ and $\tilde{t}_2$ being the two stop eigenstates. Matching the experimental value of the higgs mass is rather challenging for the MSSM. Indeed it requires a large contribution from loop-corrections which achieves the correct value only in the case the stop mass scale lies above around 3 TeV unless the stop mixing parameter $X_t = A_t - \mu \tan\beta$ fulfills the so called maximal mixing condition. [Baer 2012c, Arbey 2012a], namely $X_t \approx \sqrt{6}M_s$ [5].

In all the scans of the MSSM parameter space we are presenting, as well as in the Montecarlo analysis, presented in the next section we have adopted for the higgs mass, according to [Arbey 2012b], the constraint:

$$123 \leq m_h \leq 129\,\text{GeV} \qquad (4.33)$$

which take into account the experimental uncertainties in the determination of the mass as well as the ones affecting the numerical computation performed by SUSPECT.

As evident from the parametric dependence of (4.32) the constraints on the higgs mass influence in particular the coannihilation scenario. In figure 4.5 we study the behaviour of the higgs mass respect to the relevant parameters confirming the requirement of X_t close to the maximal mixing value. Furthermore we notice that maximal mixing allows to achieve rather low values for the mass of the lightest stop with a lower bound of around 200 GeV.

LHC results can be also fitted by the heavy higgs state H. In this case the neutral higgs states are all rather light with the CP-odd higgs having mass $\lesssim 160$ GeV and the lightest neutral CP-even state lying below the LHC favored region. This kind of scenario can be relevant in setups with light DM (see fig. 4.6); however it is severely affected by the constraints arising form searches of CP-odd higgs decays into tau pair which exclude the low values needed unless $\tan\beta \lesssim 10$ [Chatrchyan 2012b]. In view of this results only the so called intense coupling regime [Boos 2002], characterized by all the three higgs states very close in mass (within 20 GeV), results still partially viable [Arbey 2012b].

All over our DD detection and collider studies we will assume the decoupling regime for the higgs mass, explicitly mentioning the cases in which we will consider deviations from it.

---

[5]Milder constraints are obtained in the minimal extension of the MSSM, the so called NMSSM, in which the higgs couples with and additional superfield which provide an additional one-loop contribution to its mass [Hall 2012].
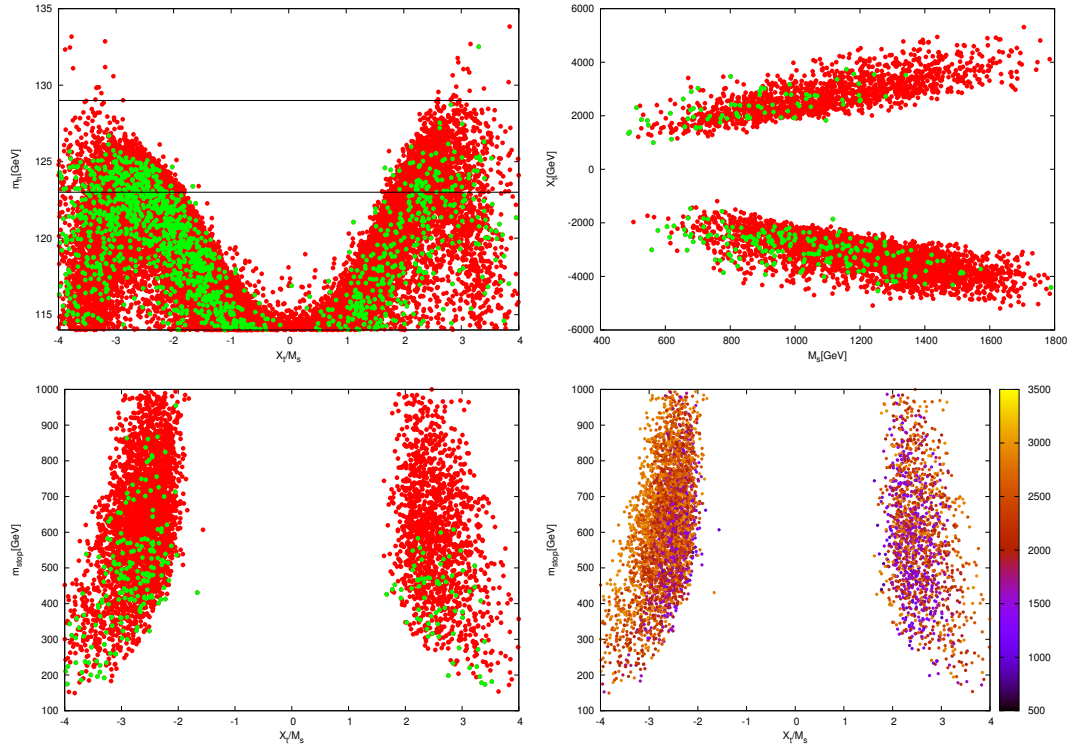
Figure 4.5: Upper left panel: Value of the higgs mass m_h, assuming the decoupling limit, with respect to the parameter X_t. Green points have as well DM relic density compatible with the cosmological limit. Upper right panel: Models with higgs mass in the range 123-129 GeV represented in the plane (M_s, X_t). The ones with DM relic density below the cosmological limit are represented again by green points. Lower left plot: Models with higgs mass in the range 123-129 GeV represented in the plane $(X_t/M_s, m_{\tilde{t}_1})$. The ones with DM relic density below the cosmological limit are represented again by green points. Lower right plot: the same as the previous plot but with an additional chromatic palette related to the mass of the second stop state $\tilde{t}_2$.
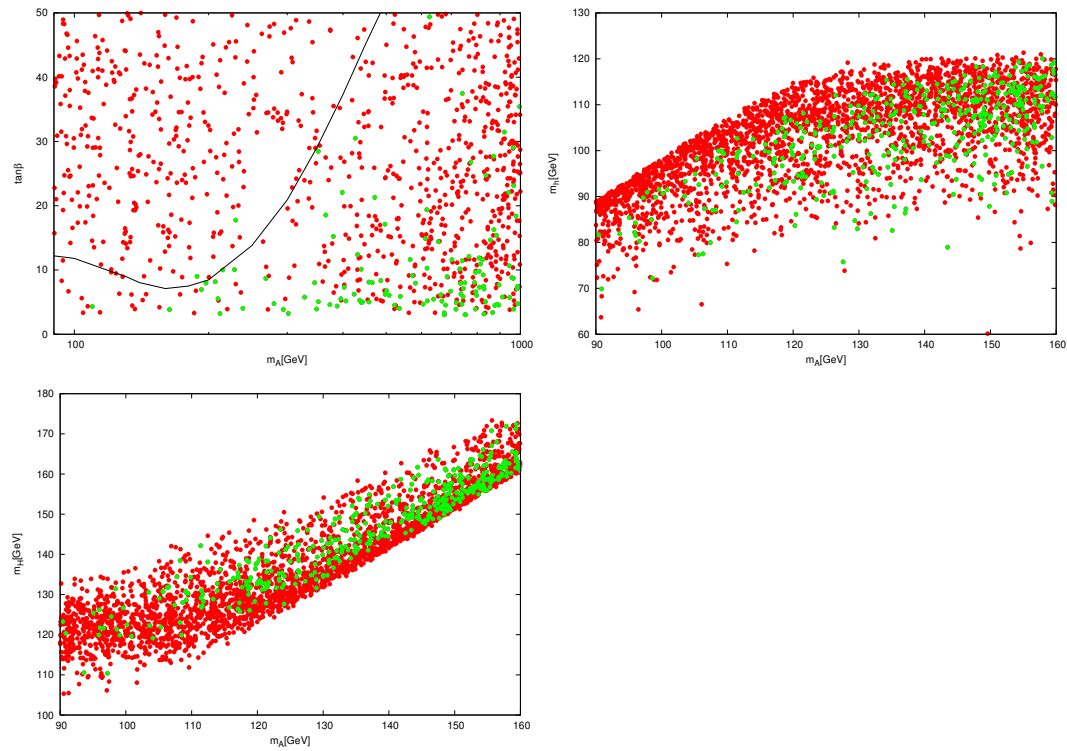
Figure 4.6: Upper left plot: points in the $(m_A, \tan\beta)$ plane relative to the low DM mass scenario. The black line represents the LHC limit relative to the process $A \to \tau^+\tau^-$ as given in [Chatrchyan 2012b]. The other two plots report the values of the masses of the CP-even higgs bosons with respect to the CP-odd one.

4.2.4   Flavor constraints

In this section we discuss the constraints on the MSSM parameter space coming from the searches of FCNC processes, focussing on the three most important ones, namely the anomalous magnetic moment a_μ and the decay processes $b \to s\gamma$ and $B_s \to \mu^+\mu^-$.

Regarding the anomalous moment of the muon, it receives contributions from neutralino-slepton loops and chargino-sneutrino loops [Moroi 1996] with the latters typically dominating [Calibbi 2012]. For illustrative purposes we report an approximate expression of the $\tan\beta$ enhanced chargino diagram:

$$\delta a_\mu \approx \frac{g^2}{32\pi^2} \frac{m_\mu^2}{m_{\tilde{\nu}}^2} \frac{Re(\mu M_2)\tan\beta}{m_{\tilde{\nu}}^2} \qquad (4.34)$$

which evidences that δa_μ is controlled by the mass scale of the sleptons of the first two generations. In our setup this is not anyhow related to DD detection and is kept fixed at a high scale. Consequently we will not aim in our analysis to fit the experimental value of δa_μ just imposing the condition $\mu > 0$ in agreement with the favored sign for the SUSY contribution.

The $b \to s\gamma$ process, as well, already predicted in the SM model with a branching fraction of the order of 3×10^{-4}, receives additional contributions form loops involving SUSY particles. In absences of large flavor mixing in the squark sector, these contributions come from charged Higgs-top loops and chargino-stop loops [Lunghi 2007]. The formers always add constructively to the SM model contribution. The latters have sign dipending from the one of the product $Re(\mu A_t)$. In our scans, being μ parameter is always positice, this contribution adds destructively to the SM contribution when $A_t < 0$ and constructively when $A_t > 0$. Moreover the chargino-stop loop contribution is enhanced at high $\tan\beta$. In our setup, the stronger impact from this process is expected in the coannihilation scenario, where rather low values of the stop mass, combined with the high value of the trilinear coupling A_t needed to match the higgs mass value, can make $Br(b \to s\gamma)$ deviate the experimental limits (see fig. 4.7), unless their contribution is compensated by charged higgs loops.

Another interesting process is $B_s \to \mu^+\mu^-$, especially in view limit $BR(B_s \to \mu^+\mu^-) < 4.5 \times 10^{-9}$ recently updated by LHCb. The SUSY contribution to $B_s \to \mu^+\mu^-$ is given by heavy neutral higgs loops and results proportional to $\tan^3\beta$ and to $A_t\mu$. This process is thus mainly relevant in scenarios with low mass higgs bosons, coinciding with low DM mass scenarios in our setup, but can also influence the coannihilation scenario since the limit can be exceeded for large values of the parameter X_t (see last panel of fig. 4.7).

4.2.5   Invisible higgs width

If the dark matter mass is lower than twice the higgs one the latter acquires an invisible decay rate $\Gamma(h \to \chi\chi)$ which can be constrained by collider studies. The
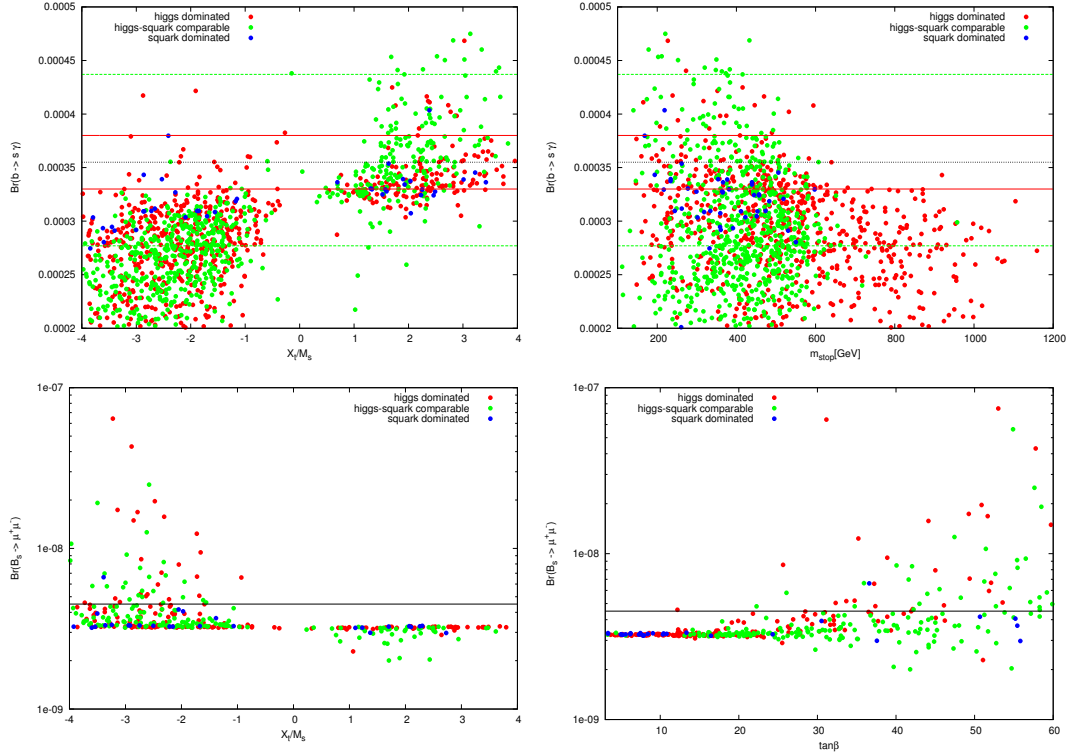
Figure 4.7: Values of the main flavor observables for the points of our scan respect the value of the lightest stop mass (left panels) and of the parameter X_t. In the case of $b \to s\gamma$ the red lines represent $1 - \sigma$ interval from the experimetal value while the green ones represent $3 - \sigma$.

invisible decay width of the higgs can be directly tested by studying multijet + missing E_T events originated by the associated production of the higgs with a gauge boson or jet. This kind of studies put an upper bound on the invisible branching ratio of the higgs of the order of 0.5 [Fox 2012]. In alternative one could ask if the current data relying higgs searches are compatible with a non-zero $BR(h \to \chi\chi)$. A study of this type can be found e.g. in [Giardino 2012b] in which a fit of the current data have been performed by adding to the decay channels into visible states a branching ratio into two DM particles made free to vary. The outcome of such analysis is that $BR(h \to \chi\chi) > 0.4$ is excluded at the 95 percent confidence level with the best fit pointing towards values close to zero.

The impact of the higgs invisible decay channel is visualized in fig. (4.8) in which we have associated, in the low mass DM scenario, the value of $BR(h \to \chi\chi)$ to the ones of other relevant observables.
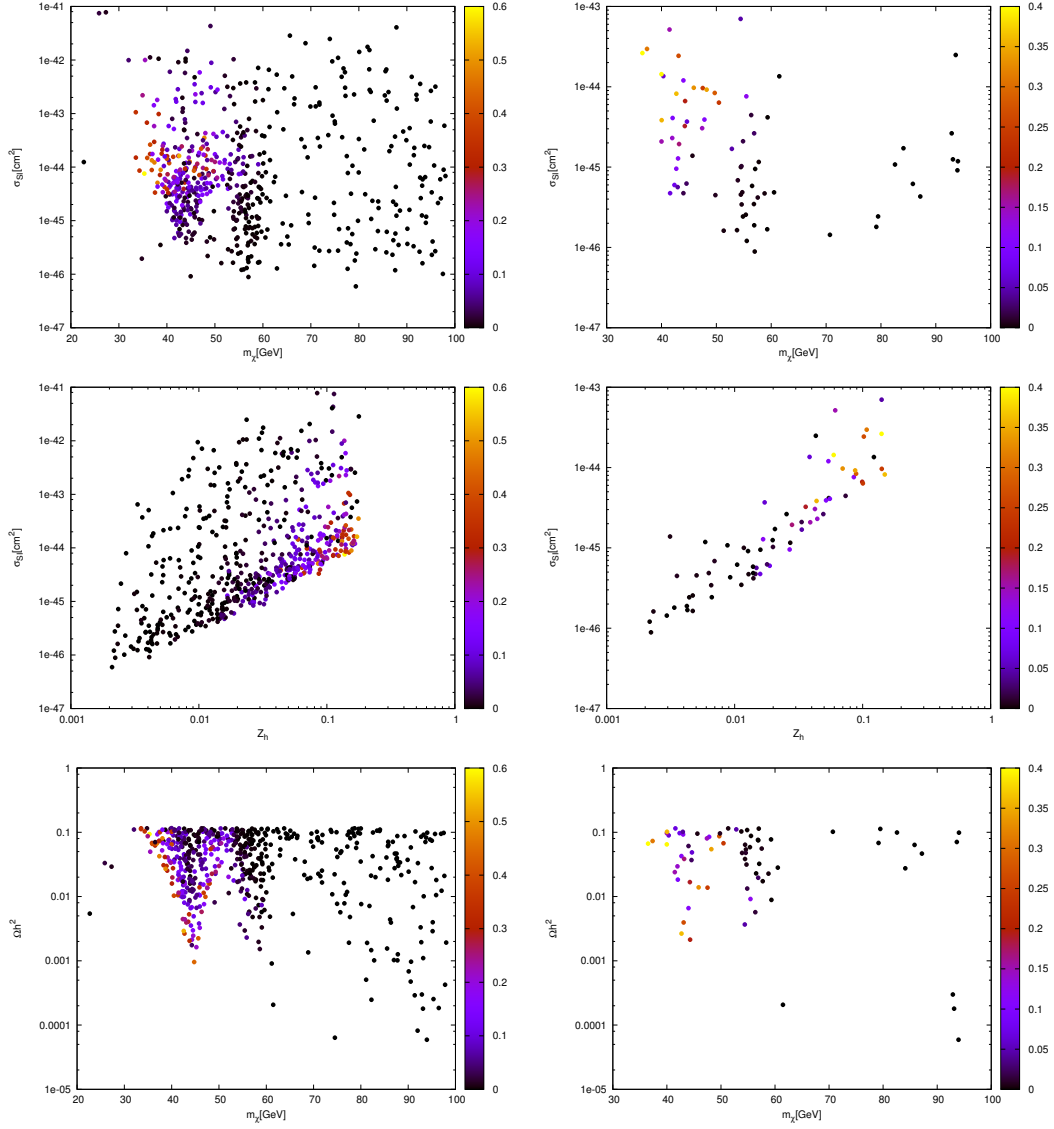
Figure 4.8: Behavior of the SI cross section of the LNM scenario. The points are colored according the value of their corresponding value of $BR(h \to \chi\chi)$. In right plots only the points satisfying the constraints from flavor observables are retained.

4.3   Statistical study of direct detection

In this section we will investigate the capacity of a 1-Ton realization of the Xenon experiment of reconstructing several MSSM benchmark models chosen according the general analysis presented above.

4.3.1   Definition of benchmark points

In view of the outcome of the previous section we can divide the DM mass range under investigation into three regions, depending on the mechanism accounting for the relic density:

- **first region** ($m_\chi \lesssim 70\text{GeV}$): In this region the relic density is determined by Z and higgs boson mediated interactions. This kind of interaction requires anyway a not too-low higgsino fraction. Thus an additional relatively low massive neutralino and chargino are expected in the particle spectrum. The rest of the spectrum can be regarded as decoupled and is just required to pass flavor as well as the current collider constraints. In this setup collider constraints forbid the stop masses below order of 400-500 GeV [ATL 2012a, Aad 2012e, Aad 2012b] and gluino masses up to 900-1000 GeV [Aad 2012a, Aad 2012g]. This limits can be sensitively released in the next scenarios when the mass of the dark matter gets closer to the ones of the colored particles.

- **second region** ($70 \lesssim m_\chi \lesssim 200$ GeV): Here the correct relic density is guaranteed by a certain variety of mechanisms, ranging from the stau mediated annihilations (with possible presence of coannihilation) to higgsino fraction enhanced annihilation and possibly CP-odd mediated annihilations (if allowed by $B_s \rightarrow \mu^+\mu^-$). The typical MSSM spectrum resembles the previous case with a low scale Electroweak sector splitted from the colored sector. The only difference, but relevant for the collider analysis, is that we will explicitly require the presence of at least one stau with mass comparable with the lightest neutralino and charginos.

- **third region** ($200 \lesssim m_\chi \lesssim 500$ GeV): In this scenario the relevant mechanism are the coannihilations with third generation squarks and/or higgsino enhanced annihilations. The lightest particle in this setup are, besides the DM, the lightest stop and sbottom possibly followed by the gluino. Apart, possibly, for a higgsino-like chargino and a neutralino all the rest of the spectrum not relevant for the phenomenology.

Each mass region have been associated to a benchmark point, with the aim of verifying whether a next future DD experiment will be able to reconstruct the relevant properties in view of a collider search. The most relevant features of the corresponding spectra have been summarized in tab. (4.1). All the three benchmark points are compatible with the constraints described in the previous sections and have DM relic density in the range $0.09 \leq \Omega h^2 \leq 0.12$, thus in agreement with the

thermal WIMP paradigm. For what regards the point **bm1** it is determined by interactions mediated by the light CP-even higgs. For the point **bm2** the relevant property is a non negligible higgsino fraction combined with stau coannihilations. The last point, finally, depicts a stop coannihilation scenario. In addition the three benchmark points have been chosen with cross sections very close to the XENON limit in order to maximaze the number of expected events.

benchmark	m_χ	m_A	μ	$m_{\tilde{t}_1}$	$m_{\tilde{b}_1}$	$m_{\tilde{g}}$	$m_{\tilde{\tau}}$	σ_{SI}
bm1	54	890	176	457	665	651	165	$8.92 \times 10^{-45} \mathrm{cm}^2$
bm2	135	651	205	821	985	1530	160	$2.17 \times 10^{-44} \mathrm{cm}^2$
bm3	492	2708	562	533	680	663	663	$3.79 \times 10^{-44} \mathrm{cm}^2$

Table 4.1: Summary table of benchmark points.

During the completion of this analysis an update of Xenon results, relying on a greater exposure time, has been released ruling out the benchmark points which have been substituted with very similar ones reported in tab. (4.2). We have also decided to investigate in more detail the coannihilation scenario by introducing a fourth benchmark point with a low cross section but masses of the lightest stop and sbottom very close to the current collider limits (see sect. 4.4). Before doing this, we will sketch the main features of our Bayesian study.

benchmark	m_χ	m_A	μ	$m_{\tilde{t}_1}$	$m_{\tilde{b}_1}$	$m_{\tilde{g}}$	$m_{\tilde{\tau}}$	σ_{SI}
xen1	56	890	291	557	735	815	165	$2.3 \times 10^{-45} \mathrm{cm}^2$
xen2	155	1550	353	1715	1777	2254	163	$3.12 \times 10^{-45} \mathrm{cm}^2$
xen3	194	2900	1500	340	209	2278	732	$6.1 \times 10^{-46} \mathrm{cm}^2$
xen4	477	2780	718	527	673	665	656	$1.35 \times 10^{-44} \mathrm{cm}^2$

Table 4.2: Table of updated benchmark points in view of the new Xenon results.

4.3.2   Bayes Theorem

The cornerstone of the analysis employed in this chapter is the **Bayes Theorem**, which can be formulated as:

$$p\left(\theta|d\right) = \mathcal{L}\left(\theta\right) \frac{p\left(\theta\right)}{p(d)} \tag{4.35}$$

where $p\left(\theta|d\right)$ is the posterior probability density function (PDF), representing the probability associated to a generic assignment of the N-dimensional set of parameters θ once the data d are given. The posterior is the relevant quantity for Bayesian inference and represents our degree of belief about the most probable value of the parameters θ once the data are taken into account [Trotta 2008a]. It is indeed proportional to the likelihood function $\mathcal{L}(\theta)$, which represents the sampling distribution

of the data given the parameters, and to the prior density function $p(\theta)$ which encodes our prejudice concerning the most probable values of the parameters before seeing the data. The quantity in the denominator is called Bayesian Evidence and in our setup can be regarded as a normalization constant [6]. Notice that the Likelihood can be also a function $\mathcal{L}(\xi)$, with ξ being a set of derived quantities from the parameters θ (the relation between the sets θ and ξ is known). We finally mention that in realistic scenarios the PDF depends also on parameters whose knowledge is imperfect (e.g. within an experimental error). These are represented, in Bayesian statistics, by a set ψ of so called nuisance parameters. The PDF relevant for parameter inference is then obtained by marginalizing, i.e integrating, with respect to the nuisance parameters:

$$p(\theta|d) = \int p(\theta, \psi|d)\, d\psi \qquad (4.36)$$

The prior distribution can be crucial or irrelevant in the inference procedure depending on how peaked is the Likelihood and therefore on how many informations are carried by the used data. If the data have enough constraining power the PDF becomes likelihood dominated while the choice of the prior is irrelevant. If instead, different priors correspond to different values of the posterior the data are not enough informative to constrain the scenario under investigation.

The general procedure of Bayesian inference can be summarized as follows. First of all we identify the scenario under investigation with a set of parameters $\eta = (\theta, \psi)$. The formers are usually the physically relevant quantities under investigation, like, in our case, the pMSSM parameters outlined in section 4.2.1 as well as the SI cross section. Nuisance parameters will be, instead, the astrophysical quantities entering in expression 4.1 or SM parameters like the top mass . The central step, once the prior has been fixed, is the construction of the Likelihood which depends on the measurement of the data, more specifically on the way the data are obtained. In our setup, in which the measurement consists on counts on a detector, we will have a Poisson distribution for the Likelihood. From the Likelihood and the prior is then evaluated the PDF which is representative of the whole set θ. Inference on a single parameter θ_i is obtained by marginalizing with respect to the remaining N-1 parameters the PDF:

$$p(\theta_1|d) = \int p(\theta|d)\, d\theta_2 \cdots d\theta_n; \qquad (4.37)$$

$p(\theta_1|d)$ is referred as marginal posterior for the parameter θ_1. From the PDF of the parameters it is also possible infer the ones of generic functions of the model parameters themselves and compute averages and variances of the relevant quantities with respect to $p(\theta|d)$. It is finally possible to construct $x\%$ credible intervals containing a fraction x of the posterior probability.

Bayesian inference can very rarely carried out analytically but rather relies on numerical sampling of the pdf. The most popular techniques are based on the Markov

---

[6]Bayesian evidence is a central quantity for model comparison [Trotta 2008a] while is irrelevant for parameter inference.

Chain Monte Carlo (MCMC) algorithm. It consists in constructing a sequence of points, called chain, in the parameter space, whose density is proportional to the posterior pdf. On general grounds a Markov chain is defined a sequence of random variables such that the probability of the $(t+1) - th$ element depend only on the value of the $-th$. It can be shown that a Markov chain converges to a stationary state such that the successive elements of the chain are samples of the target distribution, i.e the posterior. The posterior mean, as well as the expectation value of any function of the parameters θ can be straightforwardly obtained as [Trotta 2008a]:

$$\langle \theta \rangle = \int p\left(\theta|d\right)\theta d\theta \approx \frac{1}{M}\sum_{t=0}^{M-1}\theta^{(t)},$$

$$\langle f\left(\theta\right)\rangle \approx \frac{1}{M}\sum_{t=0}^{M-1}f\left(\theta^{(t)}\right) \tag{4.38}$$

In this thesis we have employed Bayesian methods to scan over the pMSSM parameter space to sample PDF relative to simulated data sets obtained from a direct detection experiment.

4.3.3 Likelihood and data generation

In order to examine the prospects, for next future DD experiments, of constraining the SUSY scenarios depicted in (4.3.1) we refer to a 1 Ton extrapolation of the XENON100 experiment. For such experiment we have assumed one year exposure and efficiencies, energy resolutions and energy ranges similar to the present day version. Our setup is totally analogous to the one used in [Akrami 2011].

As discussed in the previous section the key point is the determination of the Likelihood function. The ideal strategy for parameter inference would be to incorporate in this function, in addition to the information relative to direct detection, all the constraints discussed above, like relic density or flavor observables, in a somehow global fit framework. Despite technically achievable (see [Trotta 2008b, Bertone 2010] for some examples) this results computationally troublesome because of the need of repeated lengthy computations of quantities like the DM relic density.

We have thus employed a different strategy, less computationally demanding, motivated by the fact that the we are already referring to some definite scenarios. Our analysis will consist into two steps. We first of all focus on the properties relevant for direct detection, namely the mass and the SI cross section, verifying the constraining power of the data for a Likelihood encoding only the experimental setup and some minimum plausibility requirements for the Susy spectra. We will then verify the inference of the benchmark points by computing the various observables on relevant samples of the PDF's.

The Likelihood of the experimental data is given by the following function:

$$\mathcal{L}_{DD}\left(N|E_R^1,\cdots,E_R^N\right) = P\left(N|\hat{\mu}_S\right)\prod P\left(E_R^i|\theta\right) \tag{4.39}$$

describing the Likelihood of having N detector counts with recoil energy E_R^i $i = 1, N$. $P\left(N|\hat{\mu}_S\right)$ is the probability of seing N events distributed according a Poisson function with average $\hat{\mu}_S$:

$$P\left(N|\hat{\mu}_S\right) = \frac{\hat{\mu}_S^N}{N!}\exp\left[-\hat{\mu}_S\right]; \tag{4.40}$$

$\hat{\mu}_S$ is computed according eq. (4.4). We have neglected the presence of additional recoil events possibly induced by background taking into account the advanced techniques which will be employed in future detectors which expect to reduce the number of background events to < 1 for time exposure [Strege 2012].

$P\left(E_R^i|\theta\right)$ is instead the probability of measuring a recoil energy E_R over the energy range $E_{\min} - E_{\max}$ and is just given by the normalized recoil spectrum:

$$P\left(E_R|\theta\right) = \frac{\frac{dR}{dE_R}\left(E_R,\theta\right)}{\int_{E_{\min}}^{E_{\max}} dE'_R \frac{dR}{dE'_R}\left(E'_R,\theta\right)} \tag{4.41}$$

where the recoil rate is the one given in eq. (4.3) with the factor ϕ computed as in [Akrami 2011]. The detector simulation proceeded as follows: for each benchmark point we have generated, by mean of the Likelihood (4.39) in which the variables θ have been fixed to the value of the considered benchmark, the number N of events detected in the experiment and the associated set of measured recoil energies. These values represent the data sets used to constrain the SUSY parameter space by scanning over the pMSSM realization defined in sec. 4.2.1. The variation ranges have been 100-3000 GeV for the mass parameters, ad exception of M_1 for which a lower limit of 20 GeV have been taken, $|A_{t,b,\tau}| < 9\text{TeV}$ and $3 \leq \tan\beta \leq 60$. The scan have been performed using a Markov Chain Monte Carlo algorithm implemented in a Fortran Code partially based on SuperBayes [de Austri 2006, Trotta 2008b]. The pMSSM parameter space have been explored for two choices of priors, flat and logarithmic, in order to verify the constraining power of the data (see sec. 4.3.2). The generated spectra have been required to satisfy the lower limit on sparticle masses as given by LEP [Beringer 2012] as well as the lower bound on the gluino mass fixed in sec. (4.2.1) and to provide a higgs mass in the range fixed in sec. 4.2.3 according Atlas and CMS measurments. In addition we have employed the limit in the $(m_A, \tan\beta)$ from higgs searches in the $\tau^+\tau^-$ [Chatrchyan 2012b]. All this constraints have been encoded in the Likelihood using the method proposed in [de Austri 2006]. The spectra had finally to satisfy some physicality conditions: EWSB conditions must be fullfilled, no sparticle has tachyonic mass, the neutralino is the LSP. Points not satisfying anyone of these requirement have been automatically associated to a negligible value of the Likelihood. The total Likelihood is then composed by the DD one (4.39), the ones relative to the Susy parameters, and to the SM nuisance parameters (see [de Austri 2006]) and astrophysical nuisance parameters computed according the treatment of [Catena 2010, Catena 2012].

4.3.4 Results

4.3.4.1 DM direct detection

According to the strategy depicted above we will now examine the predictions of a realization of a 1 Ton DD experiment, with the setup described above, regarding the dark matter mass and SI cross section relative to the seven benchmark points introduced above. Although experimentally excluded we will retain the three points **bm1**, **bm2**, **bm3** in order to investigate, by a comparison with their variants **xen1**, **xen2**, **xen4**, the impact of the new constraints on our parameter inference.

Fig. (4.9) reports the marginal 2-D posterior in the (m_χ, σ_{SI}) plane relative to the three original benchmarks, evidencing the 68% and 95% credible intervals. These three benchmarks represent, respectively, examples of good, moderately successful and unsuccessful parameter inference. The lightest mass benchmark point **bm1**, in fact, shows a very good reconstruction with a substantial agreement between flat and log priors. The second benchmark retains the agreement among the true values of the pair (m_χ, σ_{SI}) and the ones expected from the PDF, with the latters still not too sensitively dependent on the priors. On the other hand the credible intervals span a moderately large region of the mass-cross section plane resulting in a lower constraining power of the DD data. The benchmark **bm3** finally evidences a drastic worsening in the performance of parameter reconstruction resulting much more underconstrained with respect to the previous benchmarks.

This decrease in the reconstruction power is originated by a decrease of sensitivity of the nuclear recoil rate (4.3) with respect to the DM mass. Indeed the minimal velocity $v_{\min}$ becomes insensitive to the DM mass as it becomes much larger than the nuclear one and the recoil rate depends on the reconstructed parameters only through the ratio σ_{SI}/m_χ (cfr. eq. 4.3). This results in a degeneracy at higher masses evidenced in the large credible intervals in the second and third panel of fig. (4.9). We also remark that the importance of this effect is expected to increase at lower cross sections since the reduced number of events make troublesome to resolve the recoil energy spectrum making more difficult to trace variations of $v_{\min}$. We finally notice a the dependence of the PDF expectation on the priors possibly indicating that DD data cannot constrain alone the considered scenario.

Additional effects impact parameter reconstruction at lower cross sections decreasing its performace, as evident from fig. (4.10), describing the remaining benchmark points.

A part of the already discussed high mass degeneracy effects affecting the benchmark **xen4** we notice a sensitive decrease in the reconstruction performance also for the lightest DM mass points **xen1** and **xen2**. In particular their 2-D posteriors seem to develop tails towards high values of the DM mass and we also evidence a sensitively worse agreement, with respect to fig. (4.9), between the true and expected values of mass and SI cross section, especially in the case of **xen1** with the true value lying at the boundary of the $1 - \sigma$ credible region. These poor reconstructions are due to unavoidable statistical effects expected at low cross sections [Strege 2012]. Indeed, because of the lower number of counts, the spectrum of recoil energy can
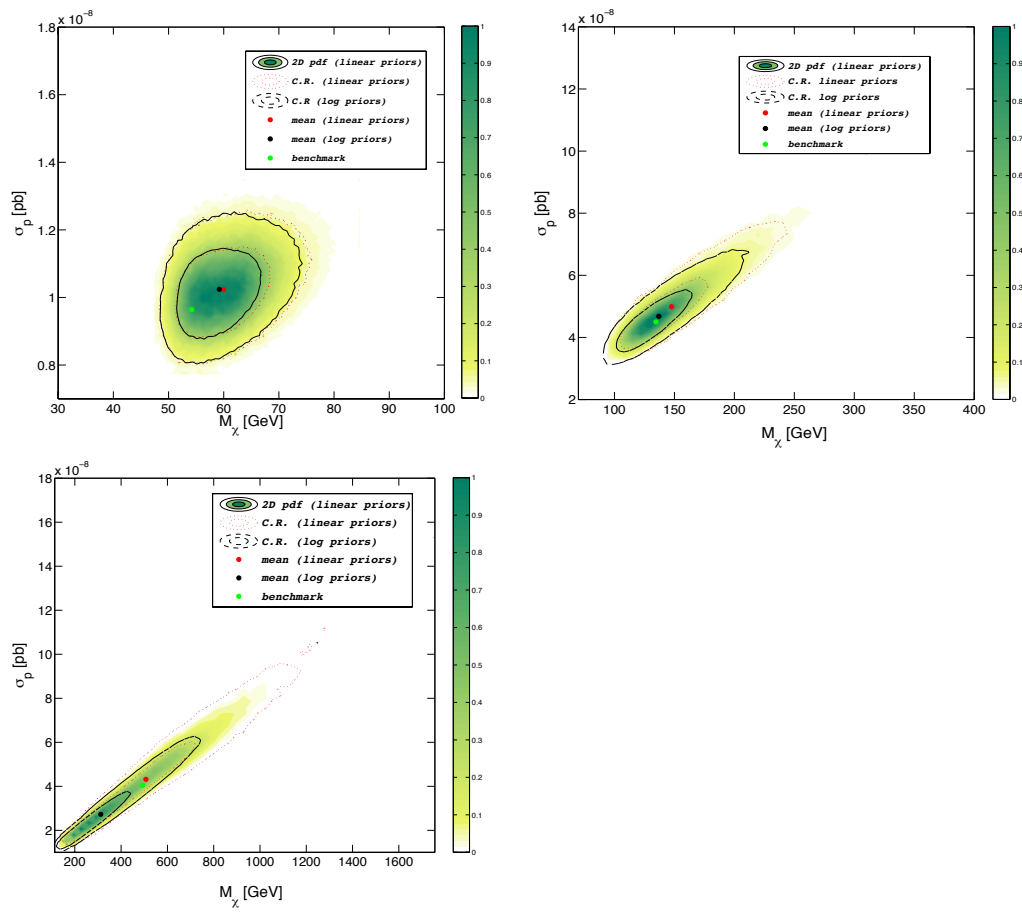
Figure 4.9: 2D marginalized PDF in the plane (m_χ, σ_{SI}) relative to the benchmark points bm1, bm2, bm3

even sensitively deviate from the true one because of statistical fluctuations, thus resulting better fitted by values of the DM mass and cross section very different from the true ones.

In view of this effect one should take into account possible dependence of parameter inference on the mock data sets by performing the pMSSM scans over many realizations of the same experiment. Possible strategies for alleviating this problem could be an increase of the exposure time considered, in order to have a large number of counts, or combining the data set coming from different target detectors (see e.g. [Strege 2012]). All this issues will be object of dedicate forthcoming study.
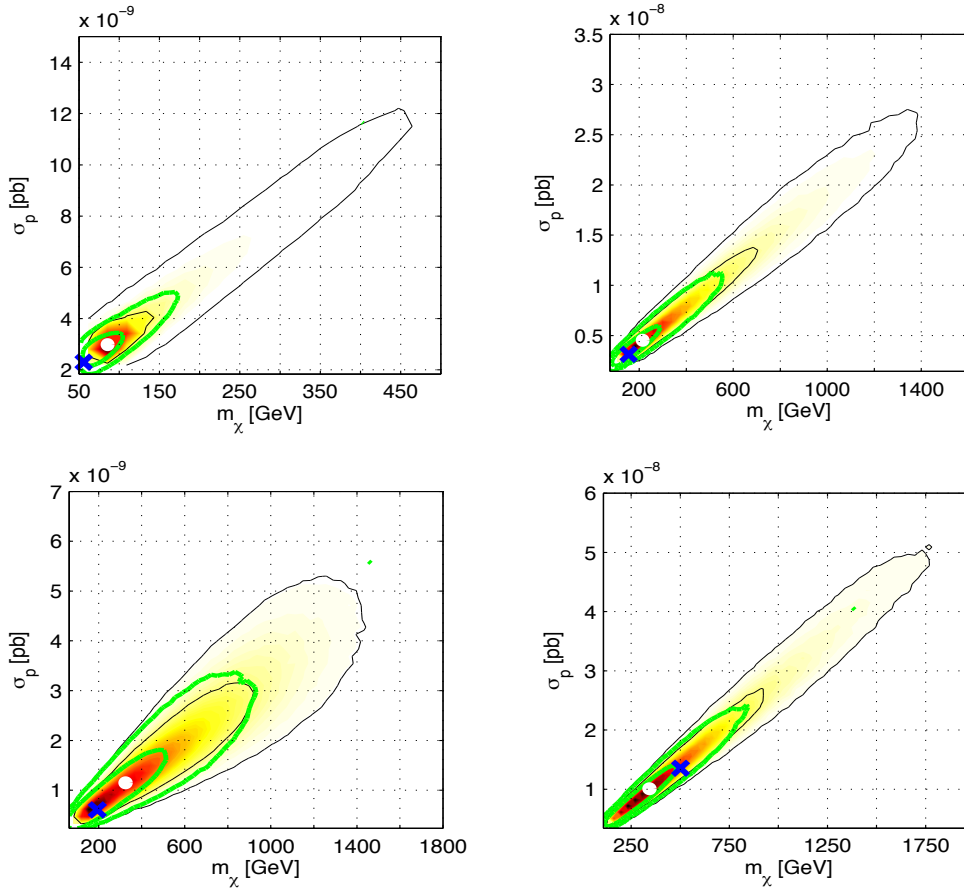
Figure 4.10: 2D marginalized PDF in the plane (m_χ, σ_{SI}) relative to the benchmark points xen1, xen2, xen3 and xen4. The blue crosses represent the true values of m_χ and σ_{SI} while the with points are the expectations according the PDF. The black solid curves are the 68% and 95% contours related to flat priors while the green solid curves refer to logarithmic priors.

We lastly examine the point **xen3** (see third panel of fig. (4.10)). It has the worst detection prospects, being vulnerable to both the two effects discussed above, in view of the moderately large mass and very low cross section.

4.3.4.2   Impact of the other constraints

In this subsection we will examine whether the simulated dark matter signals can be actually associated to the scenarios depicted in the previous section. To this purpose we have computed for the Markov chains [7] , or some their relevant samples, the values of the relic density and of $Br\,(b \to s\gamma)$ and $Br\,(B_s \to \mu^+\mu^-)$. For definiteness we report the results relative to the points **xen1** and **xen3**[8] (see, respectively, fig. (4.11) and (4.12)) representing, respectively, examples of positive and negative outcomes.

Regarding the point **xen1** we notice, in fact, that the high mass tail have been severely reduced by the applied bounds. This is mainly originated by the relic density constraint which severely affects the points of the chain as soon as their mass goes away from the narrow regions in which the annihilations mediated by the light CP-even higgs are relevant. Outside this region the correct relic density can be guaranteed by a light enough stau or CP-odd higgs while a relevant higgsino fraction is forbidden by the low value of the SI cross section. However the stau mass is not constrained anyhow by DD while low values of m_A are disfavored by $B_s \to \mu^+\mu^-$. In view of this result in the next section we will examine the prospects of collider detection referring to the region identified by combining the DD signal with the other constraints (i.e. the one in which most of the points of fig. (4.11) are clustered).
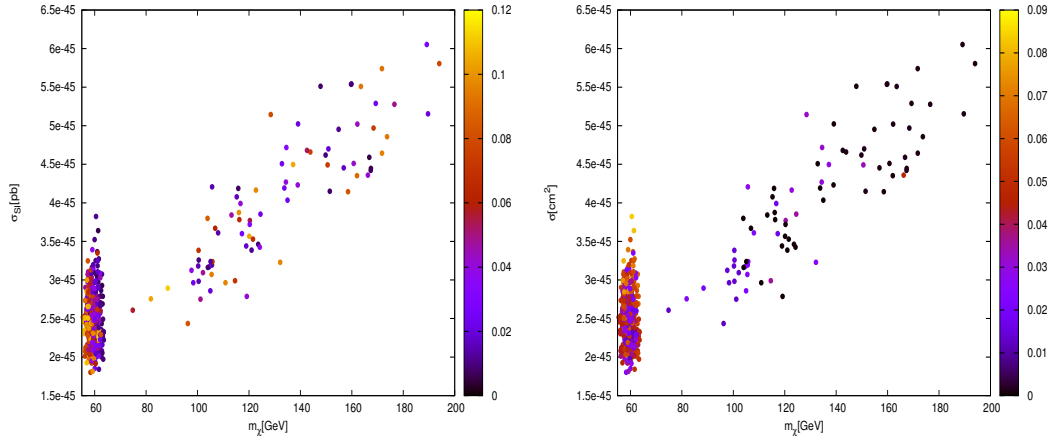
Figure 4.11: Points in the Markov chain associated to the benchmark **xen1** passing flavor and relic density constraints. In the left panel the points are represented in the plane (m_χ, σ_{SI}) following a color patter related to the DM relic density. In the right panel the color pattern is associated to the DM higgsino fraction.

---

[7]A fraction of the points of each chain have been anyway discarded since they are related to the 'convergence' of the chain [Baltz 2006] and are not representative of the PDF.

[8]As already discussed this points describe setups in which the light higgs decay process, can deviate, in some channels, with respect the expectation of the SM. We neglect for the moment this aspect leaving it to a further investigation.

The outcome of the analysis of the benchmark **xen3** is instead more contrived. Fig. (4.12), in fact, evidences a degeneracy between two scenarios. The first is the one described by the original benchmark while the second, corresponding to the totality of points at DM masses greater than 400 GeV but also moderately present at lower values, is characterized by relic density controlled by the resonant CP-odd higgs mediated annihilation, being the mass of the latter around twice the DM mass (see last panel of the plot).

This result is originated by the low constraining power of the DD mock data set, already evident from fig. (4.10), which allows the SUSY mass parameters to vary over a rather wide range of values thus opening different scenarios for what regards the DM relic density. Besides this, the degeneracy among different scenarios may be also originated by a low sensitivity to the DM-stop/sbottom mass splitting due to the fact that squark mediated interactions very rarely dominate the SI cross section (see fig. 4.1) and their contribution can be mimicked by the variation of other SUSY parameters.

This outcome points out that we probably need to encode additional information to DD data in the Likelihood. As evident from fig. 4.12 this kind of information can be only partially provided by the bounds on relic density and flavor physics. A more powerful tool can instead turn to be collider detection. As we can anticipate from the discussion in the next section the coannihilation scenario possesses rather peculiar signatures. From the collider point of view they mainly rely on the direct production and subsequent decay of the coannihilating particles. The production cross-section of these latter particles is steeply decreasing function of their masses; as consequence, for a fixed value of the DM mass, the peculiar signatures under investigation becomes severely suppressed away from coannihilation region. A good strategy for reconstructing the DM properties could be then a global fit of a DD signal combined with a collider signal. This kind of study is, however not in the aim of this thesis and will be possibly leaved for a future investigation. Here we will just illustrate the signatures related to low mass possibly coannihilating third generation squarks.

4.4 Collider analysis

This section is devoted to the prospects of collider detection of the scenarios examined from the point of view DD. In the following we will identify the production processes most likely associated to the SUSY models sharing the characteristics of the four benchmark points **xen1**, **xen2**, **xen3** and **xen4**. We will then employ some of the analysis strategies applied by the ATLAS [Aad 2009] collaboration for these definite processes to few points singled out from the samples of DD PDF's relative to the four reference models. Indeed, for each of these points we will simulate the signal possibly detected by the ATLAS experiment and compute the number of expected signal events for several combinations of final states, as summarized in tab. 4.3.

The signal events have been generated through the numerical package Madgraph
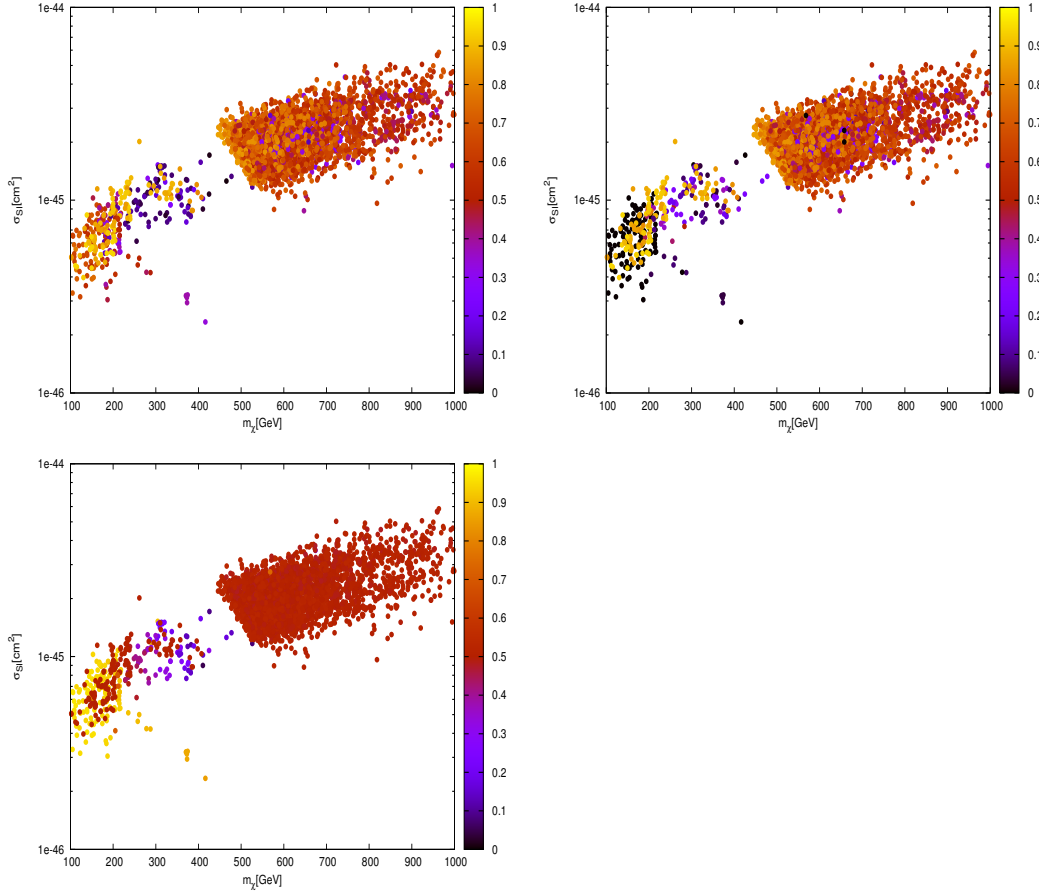
Figure 4.12: Points in the Markov chain associated to the benchmark **xen3** passing flavor and relic density constraints. The points in the three plot follow color patterns determined, respectively, by Δ_t, Δ_b and $(m_A - m_\chi)/m_A$.

Search channel	Main processes	References
3 leptons + E_T^{miss}	$\chi_2^0 \chi_1^\pm \to WZ + \text{E}_T^{\text{miss}}$	[Aad 2012c]
2 leptons + E_T^{miss}	$\chi_1^\pm \chi_2^0,\ \chi_1^\pm \chi_1^\mp,\ \tilde{l}^\pm \tilde{l}^\mp$	[Aad 2012d]
3 b-jets + E_T^{miss}	$\tilde{g}\tilde{g}$	[Aad 2012g]
$\geq$ 1 b-jet + $\geq$ 4 jets + 1 lepton + E_T^{miss}	$\tilde{t}_1 \tilde{t}_1^*$	[Aad 2012e]
1-2 b-jets + 4-5 jets + E_T^{miss}	$\tilde{t}_1 \tilde{t}_1^*$	[Aad 2012b]
monojet + E_T^{miss}	$\tilde{t}_1 \tilde{t}_1^*$	[ATL 2012b]
2 b-jets + E_T^{miss}	$\tilde{b}_1 \tilde{b}_1^*$	[ATL 2012d]
3 leptons + jets + E_T^{miss}	$\tilde{b}_1 \tilde{b}_1^*,\ \tilde{g}\tilde{g}$	[ATL 2012f]

Table 4.3: Summary table of the SUSY searches employed in our collider analysis.

[Alwall 2011] combined with the detector simulator PGS using theoretical cross-sections provided by PROSPINO2.1 [Beenakker 1996]. The simulations have been validated by generating the main backgrounds for the considered search channels and cross-checking our results with the number of background events inferred by the data. The number of events obtained by the simulations has resulted compatible with the expectations.

According to the previous sections we will mostly discuss the results relative to the scenarios associated to **xen1** and **xen3**. In the former case colored particles play no relevant role neither in the SI cross section nor in the relic density while a relevant parameter is instead μ being responsible of the DM higgsino fraction. A good probe is the direct gaugino production $\chi_2^0 \chi_1^\pm$. Assuming that there are no intermediate sleptons between these two states, they can decay either into $W^\pm Z$, with the boson which can be off-shell, and a pair of LSP or in the pair Wh in addition to missing energy. Our study have been focused on the first possibility employing the ATLAS dedicated search through events with 3 leptons in the final state [Aad 2012c]. A strategy for the detection of the Wh channel has been instead proposed in [Baer 2012b] but requires much higher luminosities for the detection with respect to the previous channel.

Tab. 4.4 reports the results relative to 5 models singlet out from the PDF relative to **xen1** and passing relic density and flavor constraints. The table reports, for each model, the values of M_2 and μ, which determine the characteristics of the produced neutralino and chargino, together with the visible cross-section for non-SM processes, i.e. the product $\sigma \, \varepsilon \, A$ of the theoretical production cross-section for the detector efficiency and the acceptance A which accounts for the reduction of the signal strength due to the analysis cuts. DD combined with relic density and flavor requirements has a good constraining power for the μ parameter, which we have found to vary on a moderately restricted range with a lower bound of around 200 GeV, as expected from the functional form of the SI cross section, while leaves substantially M_2 free to vary. Results in the table shows that WZ channel can efficiently probe models with moderate values of M_2 with some regions already excluded and some other which can be detected in the near future with a $O(1)$ increase of the luminosity. At high values of M_2, instead, the chargino and the second neutralino increase their higgsino fraction favoring the decay of into Wh which is not sensitive to the 3-leptons search channel.

We just mention that the benchmark **xen2** is sensitive to the same processes discussed above. Additional peculiar signatures are guaranteed by the presence of a low mass stau, We can get rid off this kind of signature by combining the 3 lepton search channel with searches of final stares containing 2 leptons [Aad 2012d].

Let's now move to the coannihilation scenario **xen3** (see fig. 4.5 for the reference models.). Here the relevant parameters are the masses of the lightest sbottom and stop, namely the particles closest in mass with the LSP, which can be probed by the study of the direct pair production of these particles.

In the following we will mostly focus on the search strategies related to the direct stop production; we just comment that direct sbottom production is customarily

benchmark	M_2	μ	$\sigma_{\text{vis}}[fb]$ SR1	$\sigma_{\text{vis}}[fb]$ SR2
xen1-1	248	259	0.4	1.1
xen1-2	204	231	0.3	2.7
xen1-3	156	245	1.8	0.8
xen1-4	450	273	0.2	0.3
xen1-5	261	203	0.1	0.6

Table 4.4: Values of the non-SM visible cross section associated to 3 leptons + E_T^{miss} search channel for 5 sample points relative to the light DM scenario depicted by the benchmark **xen1**. The results rely on two signal regions associated, respectively, to decay of the gauginos into off-shell and on-shell gauge bosons. The experimental limits are $\sigma_{\text{vis}}^{\text{obs}} = 3\,\text{fb}$ and $\sigma_{\text{vis}}^{\text{obs}} = 2\,\text{fb}$.

benchmark	m_χ	$m_{\tilde{t}_1}$	$m_{\tilde{b}_1}$	
xen3-1	197	210	316	$\tilde{b}_1 \to \tilde{t}_1 W^-,\ \tilde{t}_1 \to c\chi_1^0$
xen3-2	278	497	295	$\tilde{b}_1 \to b\chi_1^0,\ \tilde{t}_1 \to t\chi_1^0$
xen3-3	191	222	349	$\tilde{b}_1 \to \tilde{t}_1 W^-,\ \tilde{t}_1 \to c\chi_1^0$
xen3-4	258	553	278	$\tilde{b}_1 \to b\chi_1^0,\ \tilde{t}_1 \to t\chi_1^0$
xen3-5	195	215	344	$\tilde{b}_1 \to \tilde{t}_1 W^-,\ \tilde{t}_1 \to c\chi_1^0$

Table 4.5: Summary table of the points relative to the scenario **xen3** used for the collider analisis.
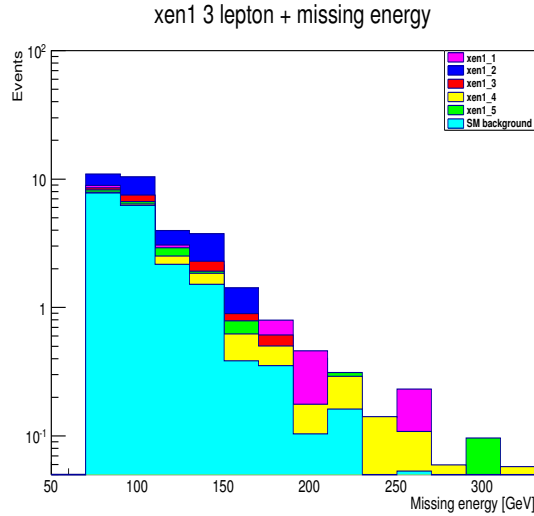
Figure 4.13: Missing energy distribution for the events (signal+background) expected for some sample points extracted from the chain relative to the benchmark **xen1**.

probed by looking at events with b-jets and absence of isolated leptons [Aad 2012f, ATL 2012d] tracing the decay $\tilde{b}_1 \to b\chi_1^0$. We will employ a dedicated study of this signals in a future work.

Direct stop production likely offers the widest variety of signals among the processes here studied, due to the several different decay channels possessed by the stop. Depending on the relative mass splitting with the LSP it can decay into $t\chi_1^0$ or $bW^+\chi_1^0$; if these decay are kinematically forbidden instead the dominant decay channels are $bff'\chi_0^1$ or even $c\chi_1^0$ occurring at the one-loop level. (For some studies of stop production phenomenology see, for example [He 2012, Ajaib 2012, Choudhury 2012]).

Stop masses above around 200 GeV are currently probed by the the two complementary searches [Aad 2012e] and [Aad 2012b] both mostly sensitive to the decay $\tilde{t}_1 \to t\chi_1^0$. Tab. (4.6) and fig. (4.14) describe our study of the search channel relying on jets and one isolated lepton as final states. The models **xen2-2** and **xen2-4**, featuring the process $\tilde{t}_1 \to t\chi_1^0$, show a rather low number of events compared to the current limit. The main reason maybe relies on the rather low mass splitting with the LSP which is still below the sensitivity of the considered search channel. Surprisingly, instead, the three remaining points deminstrate good prospects of being probed in the next future. This is likely due to the fact the in [Aad 2012e] have been implemented analysis cut aimed to detecting the W bosons expected from the top decay. This kind of signal is mimicked by the decay of the sbottom (cf. tab. 4.5) which thus results sensitive to the considered search strategy.

Stop coannihilation scenario, however, cannot be probed, at the moment, by the studies described above since it requires very low mass splitting which forbids

benchmark	SRA	SRB	SRC	SRD	SRE
$N_{\text{events}}^{\text{obs}}$	15.1	10.1	10.8	8.4	8.2
xen3-1	4.0	4.0	3.1	2.7	2.2
xen3-2	0.7	0.5	0.1	0.1	0.1
xen3-3	3.2	3.2	2.2	1.9	1.9
xen3-4	0.7	0.7	0.7	0.4	0.4
xen3-5	13.7	10.9	7.0	5.5	3.1

Table 4.6: Values of the number of expected signal events of the points used for the collider analysis with respect to the 5 signal regions defined in [ATL 2012c] for the searches of stop pair production in events containing jets, one isolated lepton and missing energy.

most of the stop decay channels. The most promising detection strategy is instead the one relying on the search of a single jet and missing energy. This is indeed sensitive to the loop induced decay channel $\tilde{t}_1 \to c\chi_1^0$ with the signal jet originated from the initial states since the charm quark produces soft jets which do not pass the analysis cuts. We have performed a dedicated analysis of this scenario, whose results are reported in tab. 4.7, by generating pairs of stop and sbottom quark with an additional jet; as expected the three points with stop NLSP feature values of the visible cross section close to the current experimental limit and then good prospects for the future investigations.

   Alternative strategies have anyway been proposed for the study of the stop coannihilation scenario, like e.g. [Choudhury 2012] which however relies on slight higher values, with respect to the ones of our five reference models, of the stop-neutralino mass splitting.

benchmark	SR1	SR2	SR3	SR4
$\sigma_{\text{vis}}^{\text{obs}}$[pb]	1.63	0.13	0.026	0.0006
xen3-1	0.70	0.10	0.014	0.003
xen3-2	0.16	0.03	0.005	0.001
xen3-3	0.36	0.05	0.006	0.001
xen3-4	0.19	0.04	0.006	0.0008
xen3-5	0.54	0.07	0.010	0.002

Table 4.7: Values of the non-SM visible cross section of the points used for the collider analysis with respect to the 4 signal regions defined in [ATL 2012b]. This analysis is aimed to explore processes leading to sensitively soft jets and then is particularly suitable to probe coannihilation scenarios.

   In any case the examples here provided evidence that the rich phenomenology associated to stop production deserve a more systematic study. Our purposes is, at the moment, just to demonstrate the possibility of testing in the immediate future
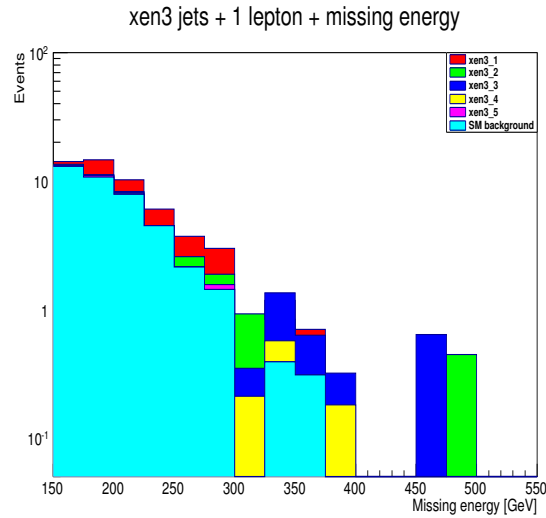
Figure 4.14: Missing energy distribution for the events (signal+background) expected for some sample points extracted from the chain relative to the benchmark **xen3**.

the coannihilation scenarios depicted in this chapter leaving for future investigations this kind of study.

We conclude by briefly mentioning the possible collider behavior of the class of models described by **xen4**. Being as well a coannihilation scenario it features the signatures discussed for **xen3**. In addition the higher value of the DM mass allows for a relevant role played by gluino pair production with subsequent decay into stops or sbottoms. As consequence the analysis employed above should be combined with the ones proposed in [Aad 2012g, ATL 2012d].

Gravitino Dark Matter in Tree Level Gauge Mediation with and without R-parity

Contents

As well known, when promoted to a local symmetry, Supersymmetry allows to embedd gravity into a particle physics framework, leading to a theoretical scenario referred as Supergravity. When Supergravity is taken into account the MSSM spectrum is enriched by a new supermultiplet, containing the gauge boson, the graviton, of the new interaction, and the corresponding superpartner, the spin 3/2 gravitino. The latter remains massless and only gravitationally interacting as long as SUSY is an exact symmetry. On the other hand, Supersymmetry is expected to be spontaneously broken by the v.e.v. of an auxiliary field; as a consequence, the supersymmetric realization of the Higgs mechanism, the so called SuperHiggs mechanism, predicts the existence of a fermionic Nambu-Goldstone particle, the Goldstino, whose degrees of freedom and interactions are eaten by the gravitino itself which becomes massive. The gravitino mass is very sensitive to the mechanism of mediation of SUSY breaking, ranging from few eV up to hundreds of TeV or more. The case of extremely massive gravitinos have been already investigated in the context of non-thermal production of neutralino dark matter. Here we will focus instead on the case in which the gravitino is light enough to be the stable (or quasi-stable) LSP, restricting to a specific particle physics scenario, dubbed as Tree-Level Gauge Mediaton (TGM), which allows for definite predictions regarding the gravitino mass and cosmological origin.

5.1   Gravitino and SUSY breaking

In a large class of models SUSY is broken by the F-term of a chiral superfield $\langle Z \rangle = F\theta^2$. According to the Superhiggs mechanism the mass of the gravitino is related to the SUSY breaking scale F by [Volkov 1973, Deser 1977]:

$$m_{3/2} = \frac{F}{\sqrt{3}M_{Pl}} \qquad (5.1)$$

Whether the gravitino is or not the LSP depends on the scale of the soft terms, which is determined by the ratio $\bar{F}/M$ where $\bar{F}$ is the scale of SUSY breaking felt by the soft terms, whose definition does not necessarily coincides with F [Giudice 1999], while M indicates the typical scale of the interactions communicating the breaking of Supersymmetry to the matter fields. Defining $k = \bar{F}/F$ we can relate the gravitino mass to the scale of the other superpartners:

$$m_{3/2} = \frac{\bar{F}}{\sqrt{3}M_{Pl}} \sim \frac{m_{\text{soft}}}{\sqrt{3}k} \frac{M}{M_{Pl}} \qquad (5.2)$$

The value of k depends on how supersymmetry is mediated. In case of direct mediation is just given by a coupling constant, typically expected to be lower than one in order to maintain perturbativity up to high scales. On the contrary if SUSY breaking is communicated radiatively, k is given by a loop factor and then is much lower than one.

The two most popular mechanisms of mediation of SUSY breaking are gravity and gauge mediation.

In the former case SUSY breaking is communicated directly by mean of gravitational interactions, with the scale M thus coinciding with the Planck scale, M_{Pl}. Then the soft terms and the gravitino mass are expected to be of the order of F/M_{Pl}, implying that the gravitino is not always the LSP and its mass is comparable with $m_{\text{soft}} \sim 1$ TeV. On the other hand, the customary formulation of gauge mediation expects that SUSY breaking is communicated radiatively by messenger fields with characteristic scale M model dependent but, in general, at least several orders of magnitude lower than the Planck scale. In the following sections we will introduce a theory based on gauge mediation in which the communication of SUSY breaking is direct rather than radiative. For this reason, from now on, we will refer the standard realization of gauge mediation as loop gauge mediation. In this framework the soft scale is:

$$m_{\text{soft}} \sim \frac{\alpha}{4\pi} \frac{F}{M}\,, \qquad (5.3)$$

depending on the two parameters F and M. The gravitino is always the LSP with a mass ranging from $\mathcal{O}(\text{eV})$ to $\mathcal{O}(\text{GeV})$.

The high variability of the mass range of the gravitino leads to a very rich but, at the same time, rather model dependent phenomenology given also the fact, as clarified in the following, that many of the relevant interactions are very sensitive to the mass of the gravitino itself. Consequently we are going to restrict to more definite scenarios in which the gravitino, while always being the LSP, has mass varying between few GeV and up to around 100 GeV.

5.2 Gravitino as Dark Matter candidate

In this section we will provide a brief overview of the main features of the gravitino, regarded as the DM candidate. To this purpose we now briefly recall the characteristics of gravitino interactions. Due to their gravitational origin they typcally arise from dimension five non-renormalizable operators and result suppressed by the Planck scale M_{Pl}. On the other hand such operators are sensitive to the energy scale thus resulting enhanced at very high energies. Gravitino can also interact through its Goldstino component. Compared to the previous interactions these are also sensitive to the mass scale of the gravitino, resulting enhanced as the mass of the latter decreases.

All these kind of interactions are typically too weak to make the gravitino a feasible thermal relic, unless is mass its extremely light. Several alternative mechanism have been then proposed in order to explain the primordial origin of the DM candidate. In order to discriminate among the various possibilities, besides the mass the gravitino, we have also to take into account, in principle, the cosmological history as well as the inflation model and in particular the reheating temperature after the inflationary phase. Restricting, however, to the $O(1 - 100)$ GeV mass range, the primordial origin of gravitino mass can be ascribed to a combination of two mechanisms. [1]

The first is the production through thermal scatterings in the primordial plasma. Remembering the energy dependence of the gravitino interactions the dominant production is expected to occur in the earlier stages of the history of the Universe, soon after the inflationary phase. Indeed the relic abundance depends on the reheating temperature as well as on the gravitino mass and other SUSY parameters. Its accurate determination relies on thermal field theory and has been worked out in [Rychkov 2007]. For our purposes, a reliable analytical approximation is provided by the following expression [Olechowski 2009]:

$$\Omega_{DM}^T h^2 =$$
$$\left(\frac{m_{3/2}}{10 \text{ GeV}}\right)\left(\frac{T_{RH}}{10^9 \text{ GeV}}\right) \sum_r y_r' \, g_r^2(T_{RH}) \, (1 + \delta_r)\left(1 + \frac{M_r^2(T_{RH})}{2m_{3/2}^2}\right) \ln\left(\frac{k_r}{g_r(T_{RH})}\right),$$
$$(5.4)$$

where $r = 1, 2, 3$ and the sum runs over the three components $U(1)_Y$, $SU(2)_L$ and $SU(3)_C$ of the SM gauge group. The values of the coefficients k_r, y_r' and δ_r can be found for instance in Ref. [Pradler 2007].

As consequence of R-parity gravitino dark matter can be also produced through decays of the heavier superpartners. Since all the decay rates into gravitinos are expected to be Planck suppressed the production is entirely dominated by the decays of a long-lived NLSP. Particularly interesting is the case of a WIMP NLSP since its long lifetime allows it to freeze-out, according the thermal miracle paradigm, as it

---

[1] Actually alternative mechanisms can be considered, see e.g. [Asaka 2006, Endo 2007]. However, in this thesis, we will neglect this more exotic possibiiities.

was the DM candidate. The relic density of the gravitinos produced in such a way, which from now on we will referred as non-thermal (given the out-of-equilbrium decay of the NLSP), is related the the one of the NLSP by the simple scaling law:

$$\Omega_{3/2}^{NT} = \frac{m_{3/2}}{m_{NLSP}}\Omega_{NLSP} \tag{5.5}$$

For a gravitino with mass above 1 GeV this contribution is always sizable or even dominant with respect to the one coming from (5.4). In this last scenario, analogously to the DM Wimp case, the relic density would be entirely determined by the low energy physics. Moreover the ratio $m_{3/2}/m_{NLSP}$ could compensate the Wimp overproduction without invoking an excessive fine-tuning among the MSSM parameters. In these kind of scenarios gravitinos are referred as SuperWimps [Feng 2003a], [Feng 2003b].

On the other hand the NLSP decays have a much wider impact on the cosmological history. Indeed the production of gravitinos is accompanied by EM and/or hadronic showers which can influence, depending on the lifetime of the NLSP, the primordial abundances of light elements. These result, however, successfully predicted by the Standard Big Bang Nucleosyntesis, thus severely constraining the effects of the NLSP decays. The strength of this kind of constraints is again very model dependent being influenced, besides the NLSP's lifetime, by the nature of the decay products, which depends on the nature of the NLSP, as well as their energy (or equivalently the mass of the NSLP) and abundance (constraining in turn the abundance of the NLSP itself).

In the more definite scenarios we are considering few predictions are anyway possible. For gravitino masses above one GeV the typical NLSP lifetimes largely exceed the time of onset of BBN unless their mass scales lie in the multi-TeV range or above. Neglecting this kind of solution, because of its poor detection prospects, a customary option to limit the impacts on BBN is to require a suppression of the NLSP abundance thus limiting the effects of its decay products [2] . The degree of such suppression depends on the NLSP, which determines their electromagnetic or hadronic nature.

Along this thesis two scenarios will be considered, the only ones relevant for the particle physics scenarios that we are going to depict. The main is the case of a neutralino NLSP. This kind of particle suffers the most severe constraints. Indeed, besides the overproduction problems occurring for Bino-like particles, the decay products are mainly responsible of hadronic showers, affecting the BBN since its early stages with their strong interactions and thus disfavoring also wino and higgsino like particles, although their naturally suppressed abundances [Covi 2009].

As an alternative we mention the case of a non-Wimp NLSP candidate, namely the lightest stau. Differently from the neutralino case this particle is responsible of

---

[2]More contrived solutions have been considered as well, like for example low energetic, and thus more weakly interacting, particle shower in the case of almost degenerate gravitino and NLSP [Boubekeur 2010].

electromagnetic showers which are less efficiently interacting. Accounting also the much lower abundance, guaranteed by the electromagnetically enhanced interactions of the stau, we expect negligible effect from its decays up to lifetimes of the order of $10^5 - 10^6$s; however it has been shown that charged particles can form bound states with the He^4 which can lead to a catalyzed production of Li^6. Requiring that such process does not spoil BBN implies an upper bound on the stau lifetime of around 5×10^3s [Pradler 2008], [Pospelov 2008], which is, anyway a much weaker bound compared to the ones affecting neutralino NLSP.

One of the most interesting possibilities to achieve a cosmologically feasible scenario of gravitino dark matter is to relax the hypothesis of R-parity conservation. In such a case, infact, the NLSP acquires new couplings accounting for faster decay channels, with respect to the ones into gravitino, into only SM particles . In such a way the lifetime is lowered by several orders of magnitude erasing the NLSP abundance before the onset of BBN. At the same time non-thermal gravitinos cannot anymore give sizable account to the DM relic density which now only relies on the thermal production and then on the reheating temperature. Dark matter stability is instead not affected by R-parity violation since it would decay into SM particles through a doubly suppressed rate by the Planck scale and the smallness of RPV couplings [Takayama 2000]. At the same time the small amount of gravitino decays which are anyway possible at the present time open new prospects of detection in cosmic rays.

We conclude by just commenting on the DM relic density in an RPV framework. As already mentioned it is expected to by entirely determined by eq. (5.4) and thus requires the knowledge of the cosmological history as well as, possibly, of the UV completion of the particle physics setup under consideration. On the other hand such dependence on the reheating temperature offers the possibility to correlate the DM phenomenology to several baryogenesis mechanisms, as well sensitive to the reheating temperature. Particularly interesting is the case of the thermal Leptogenesis mechanism [Fukugita 1986]. Indeed it requires a reheating temperature greater than about 10^9 GeV; for this value, the correct DM relic density is achieved, according to (5.4), for a gravitino mass of the order of 10 GeV.

All the various aspects here just sketched will be discussed in detail in the context of a definite scenario: the recently proposed SUSY framework dubbed as Tree-Level-Gauge mediation(TGM) [Nardecchia 2009, Nardecchia 2010, Monaco 2011], which rather naturally allows for a gravitino DM in the range $10 - 100$ GeV.

5.3 Tree Level Gauge Mediation

In this section we will just briefly summarize the general features of TGM models referring, for more details, to the original literature.

TGM relies on the idea of SUSY breaking transmitted to the MSSM fields directly at the Tree Level by gauge interactions. As well known, mediation of SUSY breaking by mean of Tree-Level-interactions is troublesome because of the so called

Supertrace theorem [Ferrara 1979]; indeed for every model in which SUSY break-
ing is mediated by tree-level renormalizable interaction, the sum of all the squared
tree-level mass terms, weighted with the spin degrees of freedom:

$$Str\mathcal{M}^2 \equiv \sum_J (-1)^{2J}(2J+1)\mathcal{M}_J^2 \tag{5.6}$$

follows the following sum rule [Martin 1997]

$$Str\mathcal{M}^2 \equiv Tr(m_S^2) - 2Tr(m_F^\dagger m_F) + 3Tr(m_V^2) = 2g_a Tr(T_a)D_a = 0 \tag{5.7}$$

where m_S, m_F and m_V represent the mass matrices of, respectively, scalars, fermions
and vectors. The index a runs over the components of the gauge group. The last
equality assumes that the traces of the $U(1)$ charges over the chiral superfields is
zero. This condition is satisfied by the $U(1)_Y$ symmetry of the MSSM as well as,
more in general, by any non anomalous gauge symmetry. A simple inspection of this
last expression shows that this theorem would imply the existence of at least one
supersymmetric particle lighter than its SM counter part, against the experimental
evidence. For this reason one typically expects that SUSY masses arise in such a
way that the hyphotesis of the Supertrace thoerem are not fullfilled , implying that
condition (5.7) does not need to hold. In loop gauge mediation, ad example, soft
masses arise radiatively from loop-diagrams involving messenger superfields which
have the role of transmitting SUSY breaking to the ordinary matter [3].

In TGM, instead, the Supertrace condition is satisfied by adding a set of chiral
superfields whose contribution in the sum (5.7) erases the one of ordinary matter
fields. This new fields can be made extremely massive in such a way to end up with
an effective low energy theory coinciding with the MSSM. However, as detailed in
[Nardecchia 2010], if the symmetry group was only the one of the SM, the super-
trace condition would still imply excessively light superpartners. This issue can be
overcome through an additional $U(1)_X$ factor in the gauge group. By definition, the
minimal realization of the TGM is based on the extended gauge group $G_{\mathrm{SM}} \times U(1)_X$.

The additional $U(1)_X$ symmetry is broken at a scale M_X identified with the
mediation scale. The chiral superfield Z, responsible for SUSY breaking, has charge
X_Z with respect to this new symmetry, as well as the MSSM superfields Q which also
carry a non trivial X_Q charge under $U(1)_X$. SUSY breaking is mediated by heavy
vector superfields V_X related to the breaking of the $U(1)_X$ group, which couple both
to the superfields Z and to the matter fields.

Soft sfermion masses arises from an interaction of the type depicted in fig. (5.1),
after integrating out the superfields V_X, through F-term $\langle Z \rangle = F\theta^2$ and read:

$$(\tilde{m}_Q^2)_{\mathrm{tree}} = g_X^2 X_Q X_Z \frac{F^2}{M_X^2} \, , \tag{5.8}$$

where g_X is the gauge coupling relative to $U(1)_X$. The interactions of the field
V_X with the matter are flavor-universal; TGM hence provides a viable solution to

---

[3]Supergravity allows, instead, tree-level mediation of SUSY breaking since soft masses arise
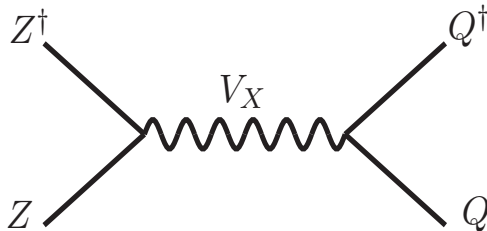from non-renormalizable interactions

Figure 5.1: TGM super-graph generating the bilinear soft masses.

the flavor problem as well as ordinary gauge mediation. From eq. (5.8) it is also evident that the ratios among the soft masses $(\tilde{m}_Q^2)_{\text{tree}}$ depend just on the choice of the $U(1)_X$ charges, thus providing a characteristic signature in view of an eventual future detection at LHC. On the contrary the masses of the gauginos arise at the loop level and are rather model dependent. Finally the gravitino mass is related to m_{soft} according to eq (5.2):

$$ m_{3/2} \sim m_{\text{soft}} \frac{M_X}{M_P} \, . \tag{5.9} $$

From a general point of view the presence of the additional $U(1)_X$ factor in the symmetry group is rather easily motivated in the context of Grand Unified Theories (GUT), which then result the natural framework for TGM models. Particularly interesting is the case in which the scale M_X coincides with the scale of breaking of the larger GUT symmetry group into the SM one, namely $M_{\text{GUT}} \sim 10^{16}$GeV. Relation (5.9), in fact, allows for a rather definite prediction for the gravitino mass, fixing it in the range 10-100 GeV, assuming that the mass scale of the soft term is in the TeV range [4].

The minimal realization of a TGM scenario compatible with Grand Unification is through an embedding into the $SO(10)$ symmetry group. Besides this there are recently proposed realizations based on the group E_6 [Monaco 2011].

In this thesis we are going to explore the aspects of TGM related to the gravitino dark matter phenomenology focusing on a rather precise scenario, namely the $SO(10)$ TGM model presented in [Nardecchia 2009], which we are going to outline in the next subsection.

5.3.1 $SO(10)$ Tree Level Gauge Mediation

The firstly considered and most simple realization of a GUT based TGM model assumes that the SUSY breaking is communicated at the $SO(10) \to G_{SM}$ breaking scale $M_{\text{GUT}} \sim 10^{16}$ GeV. The $U(1)_X$ gauge group responsible for the TGM mechanism is identified with the abelian factor external to $SU(5)$ in the embedding

---

[4]Such value for the gravitino mass is not typically accessible in standard (loop) gauge mediation. On the other hand LSP gravitinos of $\mathcal{O}(10$ GeV$)$ are also achievable in scenarios like gaugino mediated SUSY breaking [Buchmuller 2006b, Buchmuller 2006a].

$SU(5) \otimes U(1)_X \supset SO(10)$. After the one-step breaking $SO(10) \to G_{SM}$ at the scale M_{GUT}, all the effects of TGM and the GUT physics are encoded in the MSSM boundary conditions at the GUT scale.

The ratios among the tree level soft masses $(\tilde{m}_Q^2)_{\text{tree}}$ depend only on the embedding of the MSSM chiral superfields Q into the $SO(10)$ representations. Here we consider an embedding in the 10 and 16 representation of $SO(10)$ which can be decomposed with respect to to the subgroup $SU(5) \otimes U(1)_X$ as:

$$16 = 10_1 \oplus \bar{5}_{-3} \oplus 1_5 \,, \qquad 10 = 5_{-2} \oplus \bar{5}_2 \,, \tag{5.10}$$

while the decomposition of the $\overline{16}$ follows from that of the 16. In order to avoid negative soft terms contributions (cf. Eq. (5.8)), all the MSSM matter superfields (q, u^c, e^c, d^c, ℓ) must have same sign under $U(1)_X$. This condition is fulfilled if [5] :

$$q \oplus u^c \oplus e^c = 10_1 \subset 16 \,, \qquad d^c \oplus \ell = \bar{5}_2 \subset 10 \,. \tag{5.11}$$

The additional chiral superfields, needed to satisfy the supertrace condition, are instead contained in the $\bar{5}_{-2}$ and $\bar{5}_{-3}$ representations. These fields turns to have masses ranging from the order of M_{GUT} to few orders of magnitude below, thus resulting harmless for the phenomenology. [6] The MSSM Higgses are embedded in linear combinations of 10, 16 and $\overline{16}$. According to this discussion the TGM contribution to the bilinear soft masses is

$$(\tilde{m}_Q^2)_{\text{tree}} = \begin{cases} 2\,\tilde{m}_{10}^2 & Q = d^c, \ell \\ \tilde{m}_{10}^2 & Q = q, u^c, e^c \\ -2\,\tilde{m}_{10}^2 < (\tilde{m}_{h_u}^2)_{\text{tree}} < 3\,\tilde{m}_{10}^2 \\ -3\,\tilde{m}_{10}^2 < (\tilde{m}_{h_d}^2)_{\text{tree}} < 2\,\tilde{m}_{10}^2 \end{cases} , \tag{5.12}$$

where $\tilde{m}_{10}^2$ is a universal mass parameter.

Gaugino masses are generated at the one-loop level as in standard gauge mediation. We call $M_{1/2}$ the common gaugino mass at M_{GUT}.

The mechanism responsible for gaugino masses unavoidably generates a two-loop level contribution to the sfermion masses. The final expression at the GUT scale is given by

$$\tilde{m}_Q^2 = (\tilde{m}_Q^2)_{\text{tree}} + 2\,\eta\,C_Q M_{1/2}^2 \,, \tag{5.13}$$

where C_Q is the total SM quadratic Casimir

Q	q	u^c	d^c	ℓ	e^c	h_u	h_d
C_Q	21/10	8/5	7/5	9/10	3/5	9/10	9/10

$\tag{5.14}$

---

[5]The matter fields can also have small projections in the $\bar{5}_{-3}$ ($q \oplus u^c \oplus e^c$) and 5_{-2} ($d^c \oplus \ell$). This however has no relevant implications on the DM phenomenology. We thus stick on the "pure" embedding defined by (**??**). (see also appendix C

[6]This additional heavy states, can actually influence the MSSM spectrum through RGE effects. However this effect turns to be very limited [Monaco 2011, Monaco] and can be, in very good approximation, neglected.

The parameter $\eta > 0$ gives the relations between the two-loop contribution to the sfermion masses and that to the gaugino masses squared[7]. The precise value of η depends on the details of the messenger sector. For instance in standard (loop) gauge mediation with one messenger chiral superfield this parameter is precisely $\eta = 1/n$, where n is the Dynkin index of the vector-like pair of messengers. In most of our analysis we will set $\eta = 1$. Besides being theoretically reasonable this choice is also motivated by the fact that, when also the RGE corrections, mostly dependent on gaugino masses, are taken into account, the tree-level induced term, $\tilde{m}_{10}$, can turn to be subdominant with respect to the loop contribution, making the theory to tend towards the traditional gauge mediation. Higher values of η hence restrict the amount of parameter space in which TGM is the main mechanism responsible for sfermion masses.

From eq. (5.13) we can extrapolate an approximate criterium for determining whether TGM is the dominant mechanism accounting for sfermion masses by requiring that it contributes to the low energy value of each them by an amount of at least 50%. Including also the running effects this translates into the condition:

$$\tilde{m}_{10} \gtrsim (5.2 + 4.2\,\eta)^{1/2}\, M_{1/2}\,, \tag{5.15}$$

which, for $\eta = 1$, reduces to $\tilde{m}_{10} \gtrsim 3.1\, M_{1/2}$ (this criterium will be derived in more detail in appendix B). On top of $\tilde{m}_{10}$ and $M_{1/2}$ the other MSSM parameters relevant at low-energy are $\tan\beta$, μ, $B\mu$ and the A-terms. Relating the μ-term to SUSY breaking is a model-dependent issue[8]. Here we will just fix μ and $B\mu$ in such a way that they satisfy the electroweak symmetry breaking conditions. In addition we assume $\mu > 0$. The A-terms are set to zero at the GUT scale. In general, since they do not arise at the tree level, they are expected to be smaller than the bilinear soft masses.

In the case in which SUSY is broken only by the F-term responsible for sfermion masses, the gravitino mass is directly related to $\tilde{m}_{10}$ by the relation [Nardecchia 2009]

$$m_{3/2} \approx 15\,\text{GeV} \left(\frac{\tilde{m}_{10}}{1\,\text{TeV}} \right)\,. \tag{5.16}$$

We stress again that the magnitude of the gravitino mass is a peculiar prediction of TGM and its embedding into a GUT.

The last comment regards the nature of the NLSP. From the boundary condition 5.13 it immediately turns out that the NLSP is a Bino-like neutralino with the scalars typically heavier than the gauginos. Exceptions to this setup may occur at high values of $\tan\beta$ when third family sfermions, in particular the staus, receive large negative radiative corrections.

---

[7] According to the phenomenological approach of this thesis the η parameter can be regarded as free but definitness its value will be fixed to one. Our results are not sensitively affected by varying this parameter apart from the fact that this parameter influences the regime of TGM dominance which is defined in the text. The origin of the second term of eq (5.13) is discussed, for example, in [Giudice 1999] where the η parameter can be identified with the ratio $\eta = \Lambda_S^2/\Lambda_G^2$.

[8] We just mention that TGM offers a new solution for the μ-problem, where the μ is also responsible for triggering the SUSY breaking [Nardecchia 2010].

5.4   Gravitino Dark Matter with R-parity

In this section we investigate the cosmological aspects of TGM in the R-parity conserving case. As already mentioned the NLSP plays a key role contributing to the DM relic density through its non-thermal decays [9]. This contribution can be expressed in terms of the TGM parameters as:

$$\Omega_{3/2}^{NT} h^2 = \frac{m_{3/2}}{m_{NLSP}} \Omega_{NLSP} h^2 \simeq 3 \times 10^{-2} \frac{\tilde{m}_{10}}{M_{1/2}} \Omega_{NLSP} h^2 \,, \qquad (5.17)$$

with Ω_{NLSP} being the expected NLSP relic density as if it were stable, and should be added to the thermal component Ω_{DM}^T arising from thermal processes in the Early Universe. The behaviour of the DM relic density in a TGM setup is depicted in fig. (5.2), the non thermal component of the DM relic density computed according the scaling formula Eq. (5.17) applied to Ω_{NLSP} numerically evaluated through the numerical code DARKSUSY. For definiteness we have reduced the number of the MSSM parameters by fixing the boundary conditions for higgsino soft masses according to [Nardecchia 2009], thus leaving as free parameters $\tilde{m}_{10}$, $M_{1/2}$ and $\tan\beta$ [10]. The outcome of the analysis is that, especially for low/moderate values of $\tan\beta$ the correct relic density is achieved only in regions where $\tilde{m}_{10} < M_{1/2}$. This is a consequence of an excessive production of non-thermal gravitinos originated by the overabundance of NLSP due to the p-wave suppression of the pair annihilation cross section of a bino-like neutralino. Applying infact eq. (2.59), the NLSP relic density can be estimated as:

$$\Omega_{NLSP} h^2 \approx 0.02 \times 10^3 \left(\frac{m_{\chi_1^0}}{150\,\mathrm{GeV}} \right)^{-2} \left(\frac{\tilde{m}_Q}{1\,\mathrm{TeV}} \right)^4 . \qquad (5.18)$$

The correct value of the DM relic density is hence not exceeded only when too much large sfermion masses are avoided and, at the same time, there is an enhanced hierarchy between the lightest neutralino and the gravitino which suppress the DM relic density with respect to the one of the NLSP. Unfortunately this kind of scenario disfavors TGM (which instead requires $\tilde{m}_{10} > M_{1/2}$ (cfr. eq. 5.13) as the main mechanism responsible for the generation of sfermion masses. The situation slightly improves towards higher values of $\tan\beta$ where is achievable a suppression of the NLSP abundance through CP-odd higgs mediated interaction which can possibly also undergone a resonance. As shown in the second panel of fig. (5.2) the value of $\tilde{m}_{10}$ can be increased to be at most of the order of $M_{1/2}$ thus signaling a still non negligible loop-induced contribution to sfermion masses.

---

[9]In our phenomenological approach the reheating temperature determining the thermal component of gravitino DM is regarded as a free independent parameter. For this reason in the cosmological analysis we will refer only to the non-thermal component assuming that the reheating temperature can be always tuned to the suitable value to match the correct DM relic density.

[10]The analysis that we are going to show has been repeated for different choices of the set δ_u, δ_d, where $\left(\tilde{m}_{h_u,h_d}^2\right)_{\mathrm{tree}} = \delta_{u,d}\tilde{m}_{10}^2$, and we have found that our conclusions are not affected by the choice of these two parameters. For this reason we can restrict to unique choice for the boundary conditions of higgsino soft masses without loss of generality
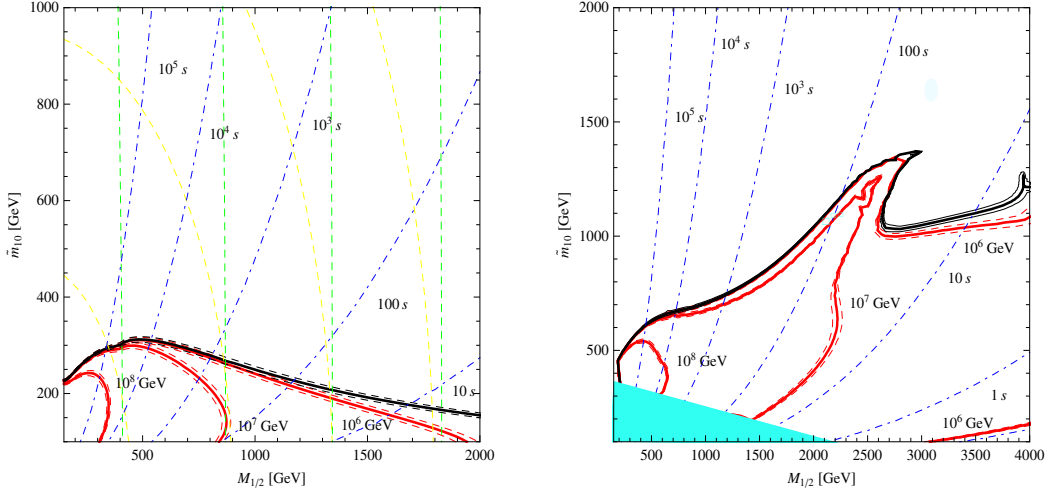
Figure 5.2: Contours of some relevant observables as function of $\tilde{m}_{10}$ and $M_{1/2}$ for two values of $\tan\beta$, 10 (left panel) and 60 (right panel). Red and Black lines are the contours of the cosmological value of the DM relic density within 1σ deviation. For red curves the DM relic density is determined by a combination of thermal (the associated value of the reheating temperature is reporterd in the plot) and non thermal component. The black curve depicts the case in which non-thermal gravitinos match alone the correct value of the relic density. Blu lines are the contours of the NLSP lifetime while yellow and green lines represent, respectively, contours of the stop (the reported values are 500, 1000, 1500, 2000 GeV) and gluino masses (the lowest value is 700 GeV).

In fig. (5.2) are also reported the values of the NLSP lifetime as function of $\tilde{m}_{10}$ and $M_{1/2}$. These largely exceed, ad exclusion of values of $M_{1/2}$ in the multi-TeV range, the typical time scale of onset of BBN thus indicating a potential impact of the NLSP decays on the primordial abundances of light nuclei. As we will show in the next, BBN bounds will further restrict the cosmologically viable regions of parameter space.

As already mentioned, the strongest tensions arise form the decay channels responsible of hadronic showers. For a bino-like neutralino the most important one is the two-body decay channel into a Z boson and a gravitino whose rate is given by [11]:

$$\Gamma(\chi_1^0 \to Z\tilde{G}) = \frac{\sin\theta_W^2}{48\pi M_{Pl}^2} \frac{m_{\chi_1^0}^5}{m_{3/2}^2} F(m_{\chi_1^0}, m_{3/2}, m_Z) \times$$

$$\left(\left(1 - \frac{m_{3/2}^2}{m_{\chi_1^0}^2}\right)^2 \left(1 + 3\frac{m_{3/2}^2}{m_{\chi_1^0}^2}\right) - \frac{m_{\chi_1^0}^2}{m_{3/2}^2} G(m_{\chi_1^0}, m_{3/2}, m_Z) \right) \qquad (5.19)$$

---

[11]The neutralino can also decay into a gravitino and a photon. It is anyway, not responsible of dangerous hadronic showers.

where

$$F(m_{\chi_1^0}, m_{3/2}, m_Z) = \left[\left(1 - \left(\frac{m_{3/2} + m_Z}{m_{\chi_1^0}} \right)^2 \right) \left(1 - \left(\frac{m_{3/2} - m_Z}{m_{\chi_1^0}} \right)^2 \right) \right]^{1/2}$$

(5.20)

$$G(m_{\chi_1^0}, m_{3/2}, m_Z) = 3 + \frac{m_{3/2}^3}{m_{\chi_1^0}^3} \left(-12 + \frac{m_{3/2}}{m_{\chi_1^0}} \right) + \frac{m_Z^4}{m_{\chi_1^0}^4} - \frac{m_Z^2}{m_{\chi_1^0}^2} \left(3 - \frac{m_{3/2}^2}{m_{\chi_1^0}^2} \right)$$

(5.21)

A minor contribution (because suppressed by the higgsino fraction) comes from the decays into a gravitino and a higgs boson:

$$\Gamma(\chi_1^0 \to h\tilde{G}) = \frac{| -N_{13}\cos\alpha + N_{14}\sin\alpha |^2}{96\pi M_{Pl}^2} \frac{m_{\chi_1^0}^5}{m_{3/2}^2} F(m_{\chi_1^0}, m_{3/2}, m_h)$$

$$\times \left(\left(1 - \frac{m_{3/2}}{m_{\chi_1^0}} \right)^2 \left(1 + \frac{m_{3/2}}{m_{\chi_1^0}} \right)^4 - \frac{m_h^2}{m_{\chi_1^0}^2} H(m_{\chi_1^0}, m_{3/2}, m_h) \right)$$

(5.22)

where α is the mixing angle among higgs states and:

$$H(m_{\chi_1^0}, m_{3/2}, m_h) = 3 + 4\frac{m_{3/2}}{m_{\chi_1^0}} + 2\frac{m_{3/2}^2}{m_{\chi_1^0}^2} + 4\frac{m_{3/2}^3}{m_{\chi_1^0}^3} + 3\frac{m_{3/2}^4}{m_{\chi_1^0}^4} + \frac{m_h^4}{m_{\chi_1^0}^4} - \frac{m_h^2}{m_{\chi_1^0}^2} \left(3 + 2\frac{m_{3/2}}{m_{\chi_1^0}} + 3\frac{m_{3/2}^2}{m_{\chi_1^0}^2} \right)$$

(5.23)

In addition to these processes, as the neutralino mass gets lower one has to take into account also three-body decays [Covi 2009] like:

$$\Gamma(\chi_1^0 \to q\bar{q}\tilde{G}) = \frac{\cos^2\theta_W}{27(2\pi)^2 M_{pl}^2} \frac{m_{\chi_1^0}^5}{m_{3/2}^2} log\left(\frac{m_{\chi_1^0}}{2m_q} \right)$$

(5.24)

and

$$\Gamma(\chi_1^0 \to b\bar{b}\tilde{G}) = \frac{| -N_{13}\cos\beta + N_{14}\sin\beta |^2}{48(4\pi)^3 M_{pl}^2} \frac{m_{\chi_1^0}^7}{m_{\tilde{G}}^2} \frac{g_Z^2}{M_Z^2}$$

$$\times \left(\left(\frac{1}{4} - \frac{2}{3}\sin^2\theta_W + \frac{8}{9}\sin^4\theta_W \right) + \frac{3}{10}\frac{\sin^2\beta}{\cos^2\alpha} \frac{| -N_{13}\sin\alpha + N_{14}\cos\alpha |^2}{| -N_{13}\cos\beta + N_{14}\sin\beta |^2} \frac{m_b^2 m_{\chi_1^0}^2}{m_h^4} \right)$$

(5.25)

The total hadronic branching ratio is defined as:

$$B_{had} = B_{3-body} + \frac{\Gamma(\chi_1^0 \to Z\tilde{G})}{\Gamma_{tot}} B_{had}^Z + \frac{\Gamma(\chi_1^0 \to h\tilde{G})}{\Gamma_{tot}} B_{had}^h$$

(5.26)

with $B_{had}^Z \approx 0.7$ and $B_{had}^h \approx 0.9$ [Feng 2004]. The BBN constraints have been applied by performing a scan of the parameter space and computing, for each point, the NLSP lifetime and relic density weighted by the hadronic branching ratio, comparing the results with the general bounds for a decaying particle as derived, for example,

in [Jedamzik 2006]. These bounds are represented by the two lines in fig. (5.3) corresponding, respectively, to the bounds related to a 100 GeV (blue) and 1 TeV (violet) decaying particle.[12] As evident from the plot the regions at low/moderate $\tan\beta$ are disfavored by BBN bounds. The only cosmologically viable regions are the ones at suppressed relic density at high $\tan\beta$. Our results are substantially in
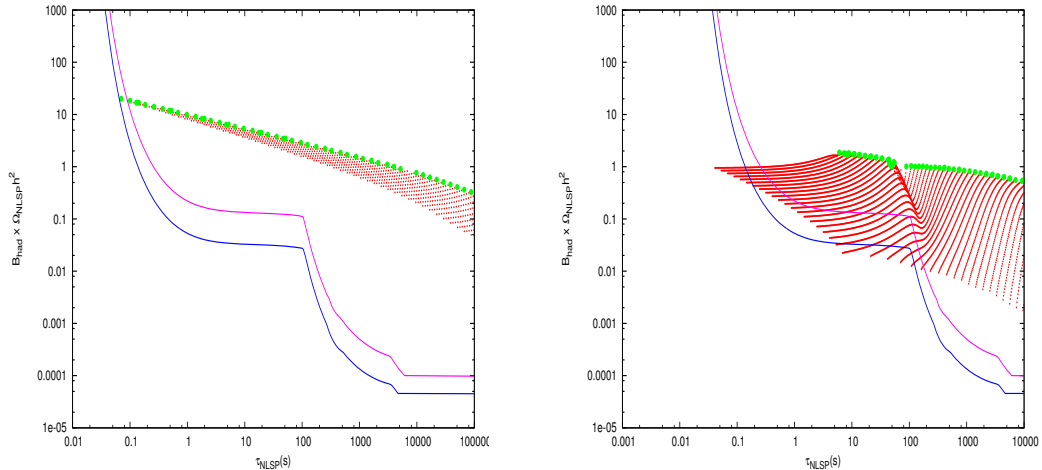

Figure 5.3: BBN bounds for the two reference scenarios depicted in fig. (5.2). The points represent TGM models with non-thermal gravitino relic density below (red points) or within $1-\sigma$ (green points) the cosmological value. The blue and violet lines represents the BBN bounds affecting, respectively a 100 GeV and 1 TeV mass decaying particle. Points above the most external line are ruled-out by BBN.

agreement with the analysis of [Covi 2009], applied to a general neutralino NLSP setup, which basically excludes all neutralinos with a lifetime greater than 10^{-2} s.

It is anyway evident that the BBN bounds, together with the issue of the overabundance of gravitinos, can be evaded in presence of some mechanism which suppresses the NLSP abundance. In the next section we will consider the case of a small amount of R-parity violation[13] .

For completeness we mention, anyway, other possibilities to achieve a cosmological viability within conservation of R-parity. The simplest one is to further enhance the hierarchy between $M_{1/2}$ and $\tilde{m}_{10}$ considering NLSP masses in the multi-TeV range. This allows to lower the NLSP lifetime below the limit just mentioned. On

---

[12]We thank J. Hasenkamp and J. Roberts for having provided the bounds.

[13]As alternative one could also consider scenarios of modified cosmology, like the ones depicted in the previous chapter, in which the NSLP abundance is depleted by the entropy release due to the decay of some heavy state before the onset of BBN. In view of the results already reported these decaying field must have extremely suppressed branching fractions into SUSY particles in order to avoid gravitino overproduction from the cascade decays. Furthermore, the value of the abundance of thermally produced gravitinos should be enhanced in order to get rid off the entropy release. In our study of gravitino dark matter, anyway we will assume a standard cosmological hystory, neglecting this kind of possibility. For an explicit realization of this scenario we instead refer to [Hasenkamp 2010].

the other hand this scenario is not phenomenologically appealing since it requires an high scale spectrum severely limiting or even precluding the possibilities of detection at LHC.

A more interesting scenario is the one with a stau close in mass or possibly lighter than the neutralinos. This possibility, as shown in fig. 5.4 can be achieved only at high values of $\tan\beta$ where the stau mass can be driven even below the one of the lightest neutralino by enhanced radiative corrections proportional to the τ Yukawa coupling. It moreover requires values of the η parameter lower than one and $\tilde{m}_{10}$ lower than $M_{1/2}$.

The scenario of a light stau is described in fig. (5.4). Here, for greater clearness, the thermal and non-thermal contribution have been considered separately, respectively by mean red and black curves. (The formers represent the contours of the cosmological value of the DM relic density for the reheating temperatures reported in the plot and should be regarded as feasible only when the non-thermal component is negligible). In the case that the stau is very close in mass to the neutralino,
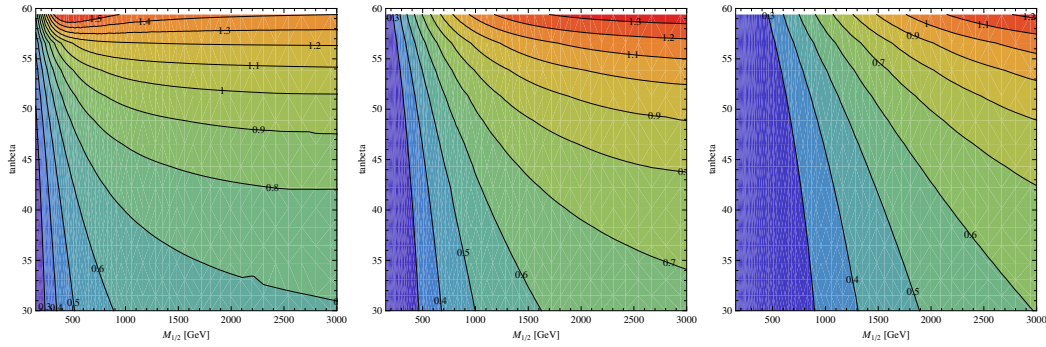
Figure 5.4: Contours of the ratio between the lightest stau and neutralino masses in the plane $(M_{1/2}, \tan\beta)$ for few fixed values of $\tilde{m}_{10}$, respectively 300, 600 and 1200 GeV. This plots have been obtained by fixing $\eta = 1/3$.

with the latter still being the NLSP, the DM relic density results suppressed by coannihilation effects depicting a scenario which resembles, from the point of view of BBN bounds, the one represented in the second panel of (5.3). Very different is instead the case of a stau NLSP since BBN bounds just translate in the upper limit of 5×10^3 s on the lifetime originated by catalyzed BBN. The stau mainly decays into a gravitino and a tau lepton with the following rate [Feng 2004]:

$$\Gamma\left(\tilde{\tau} \to \tau\,\tilde{G}\right) = \frac{1}{48\pi M_{Pl}^2}\frac{m_{\tilde{\tau}}^5}{m_{3/2}^2}\,, \tag{5.27}$$

implying that the BBN constraint is satisfied for masses above $200 \div 300$ GeV. The main features of the light stau scenario are summarized in fig. (5.5). We also notice that stau decay into neutralinos account only for a marginal contribution for the DM relic density, due to the lower stau abundance with respect to the neutralino case.
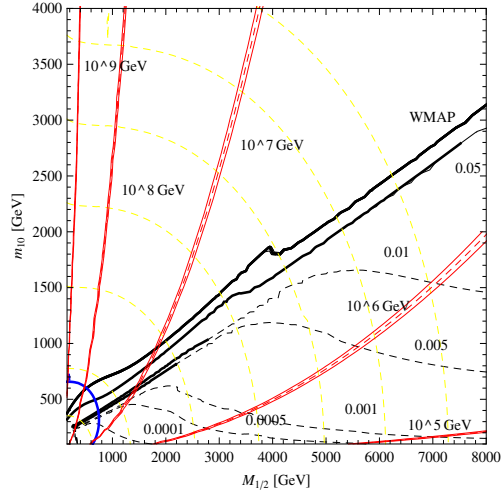
Figure 5.5: Same as fig. (5.2) for the scenario of light stau. Black lines represent the non-thermal gravitino density for the case of neutralino NLSP. Dashed lines represent the stau relic density. The blue solid line is the bound of catalyzed BBN. The yellow contours represent the values of stau mass, from left to right, 200, 500, 1000, 1500, 2000, 2500, 3000 GeV.

The final comment regards the reheating temperature. As already said it has been assumed fixed to the value compatible, depending on the non-thermal contribution, with the cosmological value of the DM relic density. As evident from fig. (5.2), the non thermal relic density grows with the contribution of TGM to sfermion masses. Assuming R-parity conservation neutralino NLSP seems to favor low values of the reheating temperature , at most of order of 10^{4-5} GeV, pointing possibly towards scenarios of thermal inflation [Lyth 1996]. Stau NLSP scenario, on the contrary, favors the dominance of the thermal contribution to the DM relic density, whose correct value is matched for reheating temperatures up to $10^{6\div7}$ GeV.

5.5   Gravitino Dark Matter without R-parity

The outcome of Sect. 5.4 is that cosmological bounds, regarding DM relic density and BBN, cannot be fulfilled by configurations in which TGM is the main mechanism accounting for neutrino masses. On the contrary these bounds can be evaded in presence of a small amount of R-parity breaking (see e.g. Ref. [Buchmuller 2007]). Indeed in such a case the NLSP can decay only into SM particles before the onset of BBN, without contributing to the DM relic density in the form of non-thermal gravitinos. At the same time the thermally produced gravitinos should be stable enough in order to reproduce the correct DM relic density. Then, since the NLSP lifetime does not depend anymore on the gravitino mass, a hierarchy between sfermion and gaugino masses, as expected in TGM, is in principle achievable.

In the following, after briefly depicting the most relevant features (for our purposes) of RPV realizations of the MSSM, we will present and analyze an $SO(10)$ TGM model with explicit R-parity violation. This model is characterized by a more restricted set of operators with respect to the most general case; this choice, as we are going to show, is motivated by the GUT structure of the theory which imposes additional constraints to the RPV operators.

5.5.1 RPV MSSM

In absence of R-parity the most general superpotential compatible with SuperSymmetry gets four additional operators:

$$W_{RPV} = \mu_i h_u l_i + \lambda_{ijk} l_i l_j e_k^c + \lambda'_{ijk} l_i q_j d_k^c + \lambda''_{ijk} u_i^c d_j^c d_k^c \qquad (5.28)$$

At the same time also the set of soft terms is enriched by the following potential:

$$V_{RPV}^{soft} = A_{ijk} \tilde{l}_i \tilde{l}_j \tilde{l}_k^c + A'_{ijk} \tilde{l}_i \tilde{q}_j \tilde{d}_k^c + A''_{ijk} \tilde{u}_i^c \tilde{d}_j^c \tilde{d}_k^c + B_i h_u \tilde{l}_i + \tilde{m}_{h_d l_i}^2 h_d^\dagger \tilde{l}_i + h.c. \quad (5.29)$$

In this section we will investigate several aspects of the broad phenomenology related to RPV realizations of the MSSM relevant for our cosmological analysis. The first aspect that we are going to afford is the origin of the couplings responsible for the decays of the NLSP, assumed from now on to be the lightest neutralino, and then of the depletion of its abundance prior of the onset of BBN.

The starting point is the observation that the new contributions to the superpotential and soft potential induce v.e.v's, here named v_i, in the neutral scalar components of lepton superfields once EW symmetry is broken [Hall 1984, Barbier 2005]. This can be easily understood from the fact that the RPV potential contains terms linear with rispect to the slepton fields $\tilde{l}_i$. A second crucial observation is that, in absence of R-parity, the l_i and h_d superfield, having the same quantum numbers under the gauge transformations, are free to mix each other by mean of a unitary transformation. Under this transformation the couplings of (5.28) and (5.63) are redefined as:

$$\mu'_i = U_{i0}^* \mu + \sum_j U_{ij}^* \mu_j$$

$$\tilde{m}_{h_d l_i}^{2,\prime} = U_{00} U_{i0}^* \tilde{m}_{di}^2 + \sum_{l,m} U_{0l} U_{im}^* \tilde{m}_{lm}^2 + \sum_l \left(U_{00} U_{il}^* \tilde{m}_{dl}^2 + U_{0l} U_{i0}^* (\tilde{m}_{dl}^2)^* \right)$$

$$B'_i = U_{i0}^* B + \sum_j U_{ij}^* B_j$$

$$v'_i = U_{i0} v_d + \sum_j U_{ij} v_j$$

$$(\lambda_{ijk})' = \sum_l \left(U_{i0}^* U_{jl}^* - U_{il}^* U_{j0}^* \right) \lambda_{lk}^e + \sum_{l,m} U_{il}^* U_{jm}^* \lambda_{lmk}$$

$$(\lambda'_{ijk})' = U_{i0}^* \lambda_{jk}^d + \sum_l U_{il}^* \lambda'_{ljk}$$

$$(\lambda''_{ijk})' = \lambda''_{ijk} \qquad (5.30)$$

where the unitary transformation is defined as:

$$\begin{pmatrix} h_d \\ l_i \end{pmatrix} \to \begin{pmatrix} h'_d \\ l'_i \end{pmatrix} = U \begin{pmatrix} h_d \\ l_i \end{pmatrix} \qquad (5.31)$$

as a consequence, in a given model, the parametrization of R-parity violation depends on the definition (or equivalently the choice of basis) of the superfields l_i and h_d. Along this thesis we will define the superfield h_d as the only one possessing the bilinear coupling $\mu h_d h_u$ with the other higgs superfield h_u.

As will be clarified in the following, the various RPV couplings result enough suppressed such the transformation U is well approximated by a linear one; given our choice of basis its form results particularly simple being:

$$
\begin{aligned}
h'_d &= h_d + \varepsilon_i l_i \\
l'_i &= l_i - \varepsilon_i h_d
\end{aligned}
\tag{5.32}
$$

where $\varepsilon_i = \frac{\mu_i}{\mu} \ll 1$, with the other relevant parameters transforming according to:

$$
\begin{aligned}
m^2_{h'_d} &= m^2_{h_d} + \varepsilon_i Re(m^2_{di}) + O\left(\mid \varepsilon_i \mid^2\right) \\
m^2_{l'_i} &= m^2_{l_i} + \varepsilon_i Re(m^2_{h_d l_i}) + O\left(\mid \varepsilon_i \mid^2\right) \\
B' &= B + B_i \varepsilon_i, \quad B'_i = B_i - B\varepsilon_i \\
m^{2\,\prime}_{h_d l_i} &= m^2_{h_d l_i} + \varepsilon_i \left(m^2_{\tilde{l}_i} - m^2_{h_d}\right) + O\left(\mid \varepsilon_i \mid^2\right) \\
(\lambda_{ijk})' &= \lambda_{ijk} - (Y_e)_{ik}\varepsilon_j + (Y_e)_{jk}\varepsilon_i, \qquad (\lambda'_{ijk})' = \lambda'_{ijk} - (Y_d)_{ik}\varepsilon_j,
\end{aligned}
\tag{5.33}
$$

The minimization of the scalar potential yields vacuum expectation values for the neutral components of the Higgs doublets as well as for the sneutrinos:

$$
v_i \equiv \langle \tilde{\nu}'_i \rangle = -\xi_i \langle h_d \rangle = -\frac{B'_i \tan\beta + m'^2_{h_d l_i}}{m'^2_{\tilde{l}_i} + \frac{1}{2} M_Z^2 \cos 2\beta} \langle h_d \rangle
\tag{5.34}
$$

The sneutrino v.e.v's are one of the main origins of the NLSP decay's. Indeed they induce a mixing between neutralino and neutrinos which can be described by the following 7×7 matrix of the form:

$$
M_N = \begin{pmatrix} m^{ss}_\nu & m_{RPV} \\ m^T_{RPV} & M_N \end{pmatrix}
\tag{5.35}
$$

where m^{ss}_ν and M_N represent, respectively, the neutrino mass matrix and the neutralino mass matrix as given in (2.51). m_{RPV} contains the mixing terms induced by R-parity violation and, in the basis chosen, is of the form [Chun 1999]:

$$
m_{RPV} = \begin{pmatrix} M_Z s_W \xi_1 \cos\beta & -M_Z c_W \xi_1 \cos\beta & 0 & 0 \\ M_Z s_W \xi_2 \cos\beta & -M_Z c_W \xi_2 \cos\beta & 0 & 0 \\ M_Z s_W \xi_3 \cos\beta & -M_Z c_W \xi_3 \cos\beta & 0 & 0 \end{pmatrix}
\tag{5.36}
$$

Similar mixings are also induced for charginos and charged leptons and other sets of SM particles and superpartners (for a detailed treatment we refer, for example, to [Hirsch 2000, Allanach 2004]). Remarkably the matrix (5.35) resembles a see-saw matrix; indeed it can be reduced to a block matrix with a 3×3 block being an

effective neutrino mass matrix, potentially induced only be RPV couplings, of the form:

$$m_{\nu,ij}^{\text{eff}} = m_{\nu,ij}^{ss} - \left(m_{RPV} M_N^{-1} m_{RPV}^T \right)_{ij} \tag{5.37}$$

This transformation is operated by the 3×4 neutralino-neutrino mixing matrix:

$$N_{ij} = - \left(M_N^{-1} m_{RPV}^T \right)_{ij} = \frac{M_Z}{F_N} b_i \xi_j cos\beta, \quad \begin{array}{l} i = \tilde{B}, \tilde{W}, \tilde{h}_u, \tilde{h}_d \\ j = e, \mu, \tau \end{array} \tag{5.38}$$

with:

$$b_1 = - \frac{s_W M_2}{M_1 c_W^2 + M_2 s_W^2} \tag{5.39}$$

$$b_2 = \frac{c_W M_1}{M_1 c_W^2 + M_2 s_W^2} \tag{5.40}$$

$$b_3 = - \sin\beta \frac{M_Z}{\mu} \tag{5.41}$$

$$b_4 = \cos\beta \frac{M_Z}{\mu} \tag{5.42}$$

$$F_N = \frac{M_1 M_2}{M_1 c_W^2 + M_2 s_W^2} + \frac{M_Z^2}{\mu} \sin 2\beta \tag{5.43}$$

with s_W and c_W being the sin and cos of the Weinberg's angle.

This matrix will be the crucial element for the cosmological analysis since it is responsible of mixing of the neutralinos with leptons and gauge bosons thus leading to their decays. Additional decay channels are also provided by the trilinear couplings $\lambda, \lambda', \lambda''$ and will be discussed directly in the context of the TGM model presented in the next sections.

In conclusion of this section we will now discuss some general bounds on the RPV couplings. A first set of constraints is interestingly provided by neutrino masses. As already mentioned R-parity violation can, potentially, completely account for neutrino masses [Bajc 2010] originating from (5.37). In this kind of setup we distinguish two kind of contributions; the first is a direct Majorana mass term, described by the matrix m_ν^{ss}, arising at the one-loop level and proportional to various combination of ξ, λ and λ' parameters as well as soft parameters B_i [Chun 2000, Davidson 2002]. As an example we just quote a contribution related to the trilinear couplings which turn to the most relevant in several setups:

$$\left(m_{\alpha\beta}^\nu \right)_{1-loop} \simeq \frac{3\lambda'_{\alpha ij}\lambda'_{\beta lk}}{8\pi^2} \frac{m_{ik}^d \left(\tilde{m}_{jl}^d \right)_{LR}^2}{\tilde{m}^2} + \frac{3\lambda_{\alpha\gamma j}\lambda_{\beta\sigma k}}{8\pi^2} \frac{m_{\gamma k}^l \left(\tilde{m}_{j\sigma}^l \right)_{LR}^2}{\tilde{m}^2} \tag{5.44}$$

where $\tilde{m}^2$ represent the sfermion mass scale, assumed unique for simplicity. The second contribution, arising from the second term of eq. (5.37), comes from the electroweak see-saw induced by the neutralino mass matrix and can be expressed as a rank one matrix:

$$m_{\nu,ij}^{\text{eff}} = \frac{M_Z^2}{F_N} \xi_i \xi_j cos^2\beta \tag{5.45}$$

Assuming for semplicity that the neutrino mass spectum is hierarchical with the dominant contribution given by (5.74) (this can be motivated by the tree-level origin of this term) we can derive a bound on the sneutrino v.e.v.'s. Indeed the only non zero eigenvalue of the tree-level mass matrix,

$$m_{\nu_3} = \frac{M_Z^2 \xi^2 cos^2\beta}{F_N}, \ \ \xi = \sqrt{\xi_1^2 + \xi_2^2 + \xi_3^2} \tag{5.46}$$

has to satisfy the cosmological bound on the sum of neutrino masses of around 0.3 eV. This implies:

$$\xi \lesssim 2.8 \cdot 10^{-7} \left(\frac{F_N}{M_Z}\right)^{1/2} \left(\frac{m_{\nu_3}}{0.3\text{eV}}\right)^{1/2} \left(\frac{\tan\beta}{10}\right)^{-1} \tag{5.47}$$

More stringent bounds, also involving the trilinear couplings, can be derived by imposing a fit of the neutrino observables, namely the mass splitting and missing angles, but they are, however, rather model dependent. We refer to this kind of limits while investigating the definite model which will be proposed in the next.

The most stringent bound on a generic RPV models comes however from the stability of the proton. Proton decay is induced by the baryon number violating coupling λ'' in combination with one of the lepton number violating couplings. The most commonly considered bounds are the ones involving products of trilinear couplings λ' or λ'' and depend, as well, on the sfermion mass scale. The tightest limits apply to the coupling carrying flavor indices related to the first generation which induce proton decay at the tree level. As an example we cite the bound from the decay process $p \to \pi^0 e^+$:

$$\lambda'_{k11}\lambda''_{k11} \lesssim 10^{-26} \left(\frac{\tilde{m}}{1\text{ TeV}}\right)^2, \tag{5.48}$$

All the other trilinear couplings give anyway contributions at one loop level. For 1 TeV scalars we have to satisfy [Smirnov 1996b]:

$$\lambda'_{ijk}\lambda''_{lmn} \lesssim 10^{-9} \tag{5.49}$$

(For a rather complete least list of the bounds coming from proton decay see also [Fileviez Perez 2005].) Proton decay can also arise from the combination of baryon violating couplings with quark-squark-gaugino/higgsino coupling, as, for example, in the following effective lagrangian:

$$\frac{\sqrt{2}g\lambda''_{112}}{m_{\tilde{u}_R}^2} \bar{s}^c P_R d \left[(2Q_u t_W)\,\bar{\tilde{B}}P_R u - \frac{m_u}{M_W sin\beta}\bar{\tilde{h}}_u^0 P_L u\right]$$

$$+ \frac{\sqrt{2}g\lambda''_{112}}{m_{\tilde{d}_R}^2} \bar{u}^c P_R s \left[(2Q_d t_W)\,\bar{\tilde{B}}P_R d - \frac{m_d}{M_W cos\beta}\bar{\tilde{h}}_d^0 P_L d\right]$$

$$+ \frac{\sqrt{2}q\lambda''_{112}}{m_{\tilde{s}_R}^2} \bar{u}^c P_R d \left[(2Q_d t_W)\,\bar{\tilde{B}}P_R s - \frac{m_s}{M_W cos\beta}\bar{\tilde{h}}_d^0 P_L s\right] \tag{5.50}$$

which describes the proton decay into a Kaon as consequence of the neutralino-neutrino mixing. The resulting bounds affect the combination $\lambda''\xi$ and are analogous to the ones just quoted.

RPV coulings are also costrained by lepton number violating processes like $\mu \to e\gamma$ (see [Barbier 2005] and references therein). These however result irrelevant for the model we are going to consider, thus we will not explicitly refer to them.

5.5.2   An R-parity violating $SO(10)$ model

On very simple ground, the R-parity can be viewed as a Z_2 symmetry which distinguishes the SM fields from their super-partners. By assigning a positive charge to the former and negative one to the latter it provides for instance the stability of the LSP. It is useful to rephrase the R-parity in a slightly different language [Martin 1992]

$$R_p = (-)^{3(B-L)+2s}\,, \tag{5.51}$$

where s is the spin and $(B-L)$ is the global $B-L$ quantum number. Eq. (5.51) suggests that in theories in which $B-L$ is gauged the R-parity can be viewed as the discrete subgroup of a local $U(1)_{B-L}$, thus providing a link between the amount of R-parity violation and the $B-L$ breaking scale.

Actually one of the five Cartan generators of $SO(10)$ can be identified with $B-L$ when acting on the spinorial matter representation 16_F. However this does not apply to TGM where the peculiar embedding of the SM fermions is such that some of them reside into a 10_F, as we have seen in Sect. 5.3. Hence the $SO(10)$ gauge symmetry does not protect against the appearance of R-parity violating interactions and the simplest way to forbid those operators is to impose a Z_2 Matter (M)-parity which distinguishes the matter superfields (with a negative charge) from the Higgs ones (carrying a positive charge) [Nardecchia 2009]. As soon as the Lorentz group is unbroken the M-parity is essentially equivalent to the R-parity.

Our approach will be that of relaxing the presence of the M-parity and, by considering all the operators compatible with the $SO(10)$ symmetry, we will prove the existence of R-parity violation in the low-energy effective theory. In addition we will assume that the R-parity violating operators are suppressed when compared to their R-parity conserving counterparts, in order to avoid an unacceptable amount of lepton and baryon number violation. Addressing the issue of the origin of such a small amount of R-parity breaking is anyway beyond the scopes of this work.

For definiteness let us focus on a supersymmetric $SO(10)$ model featuring the following minimal set of Higgs representations: $54_H \oplus 45_H \oplus 16_H \oplus \overline{16}_H \oplus 10_H$. As shown in Appendix C this field content is sufficient in order to break $SO(10)$ down to the SM at the renormalizable level (cf. Appendix C.1.1) and to give mass to the SM fermions (cf. Appendix C.1.2)[14]. As already mentioned the MSSM matter superfields

---

[14]To be complete one should also add a $16'_H \oplus \overline{16}'_H$ representation which is responsible for the SUSY breaking [Nardecchia 2009]. For simplicity we will carry on our analysis in the supersymmetric limit, assuming that the conclusions regarding the gauge symmetry breaking and the fermion mass spectrum are only marginally affected by the SUSY breaking sector.

span over three copies of $16_F \oplus 10_F$ in such a way that they are embedded in the $SU(5)$ representations $10 \supset 16_F$ and $\bar{5} \supset 10_F$ (cf. Eq. (5.11)). The conditions to be fulfilled in order to obtain such a "pure" embedding are detailed in Appendix C.1.2.

The superpotential can be schematically written as

$$W = W_H + W_Y + \delta W_{RPV} \,, \qquad (5.52)$$

where W_H and W_Y are the Higgs and the Yukawa components:

$$
\begin{aligned}
W_H &= \left(\mu_{54} + \eta_{54} 45_H + \lambda_{54} 54_H \right) 54_H^2 + \mu_{45} 45_H^2 + \left(\mu_{10} + \lambda_{10} 54_H \right) 10_H^2 \\
&\quad + \left(\mu_{16} + \lambda_{16} 45_H \right) 16_H \overline{16}_H + \lambda_{16-10} 16_H^2 10_H + \overline{\lambda}_{16-10} \overline{16}_H^2 10_H \,, \qquad (5.53)
\end{aligned}
$$

$$
W_Y = Y_{10}^{ij} 16_F^i 16_F^j 10_H + Y_{16}^{ij} 16_F^i 10_F^j 16_H + \left(M_{10}^{ij} + \eta^{ij} 45_H + \lambda^{ij} 54_H \right) 10_F^i 10_F^j \,, \qquad (5.54)
$$

while δW_{RPV} is the R-parity violating piece:

$$
\begin{aligned}
\delta W_{RPV} &= \left(\tilde{\mu}_{10}^i + \tilde{\eta}_{10}^i 45_H + \tilde{\lambda}_{10}^i 54_H \right) 10_F^i 10_H + \left(\tilde{\mu}_{16}^i + \tilde{\lambda}_{16}^i 45_H \right) 16_F^i \overline{16}_H \\
&\quad + \tilde{\rho}^i 16_F^i 16_H 10_H + \tilde{\sigma}^i 10_F^i 16_H 16_H + \tilde{\bar{\sigma}}^i 10_F^i \overline{16}_H \overline{16}_H + \tilde{\Lambda}^{ijk} 16_F^i 16_F^j 10_F^k \,. \qquad (5.55)
\end{aligned}
$$

Notice that without M-parity the separation between the F and the H superfields is somehow artificial. However, since we consider δW_{RPV} as a perturbation, we can still retain W_H responsible for the symmetry breaking and W_Y for the (charged fermions) Yukawa sector. On the other hand the situation about neutrino masses is subtler, being RPV potentially responsible for sizable contributions to them. We will comment later on the generation of neutrino masses in our model.

In Appendix C.1.3 we provide an existence proof of the R-parity violating operators in the MSSM effective theory. In order to obtain the low-energy superpotential one has to project the operators of Eq. (5.55) on the representations containing the MSSM fields. Here we just report the results of this operation leaving most of the technical details in Appendix C.1.3.

Bilinear R-parity violation in the effective superpotential is induced by operators containing just one F superfield in Eq. (5.55), leading to

$$W_{RPV}^{eff} \supset \mu_i \, \ell_i h_u \,, \qquad (5.56)$$

where the expression of μ_i in terms of the original couplings is given in Eq. (C.25).

Notice that in the "pure" matter embedding of TGM only some of the operators have projections on the MSSM fields. In particular the trilinear operator relative to the coupling $\tilde{\Lambda}^{ijk}$ does not contribute to the effective theory. On the other hand the phenomenological viability of the model, within the minimal choice of representations at hand, requires the presence of non-renormalizable operators (cf. again Appendix C). By relaxing renormalizability there is an additional source of R-parity violation given by the operator

$$
\frac{\tilde{\Lambda}_{ijk}^{NR}}{M_P} 10_F^i 10_F^j 16_F^k \left\langle \overline{16}_H \right\rangle \supset \lambda_{ijk}^{NR} \, \ell_i \ell_j e_k^c + \lambda_{ijk}'^{NR} \, d_i^c \ell_j q_k + \lambda_{ijk}''^{NR} \, d_i^c d_j^c u_k^c \,, \qquad (5.57)
$$

where

$$\lambda_{ijk}^{NR} = \frac{1}{2}\lambda_{ijk}'^{NR} = \lambda_{ijk}''^{NR} = \frac{\tilde{\Lambda}_{ijk}^{NR} V^{16}}{M_P} \equiv \Lambda_{ijk} \,. \tag{5.58}$$

Notice that the relation in Eq. (5.58) gives a correlation between the baryon (λ'') and lepton number (λ, λ') violating couplings.

Actually one should also mention that λ'' receives an additional contribution when combining the bilinear operators in Eq. (5.55) with the Yukawa ones, where the Higgs fields have been projected on the heavy triplet components and integrated out. This last contribution labeled as λ_T'' is showed in Eq. (C.29).

In the end the structure of the induced superpotential in the MSSM effective theory is given by:

$$W_{RPV}^{eff} = \mu_i \, \ell_i h_u + \lambda_{ijk} \, \ell_i \ell_j e_k^c + \lambda_{ijk}' \, d_i^c \ell_j q_k + \lambda_{ijk}'' \, d_i^c d_j^c u_k^c \,, \tag{5.59}$$

where

$$\lambda = \Lambda \,, \qquad \lambda' = 2\Lambda \,, \qquad \lambda'' = \Lambda + \lambda_T'' \,. \tag{5.60}$$

As already mentioned severe bounds on the products of couplings $\lambda\lambda''$, $\lambda'\lambda''$ are enforced by proton decay. This bounds, moreover, are strengthened by the GUT structure of the theory which relates the flavor indices of the trilinear couplings.

The most conservative bound on all the R-parity violating trilinear couplings in the presence of a GUT relation such as that in Eq. (5.58) is given by [Smirnov 1996a]:

$$\Lambda \lesssim 10^{-10} \left(\frac{\tilde{m}}{1 \text{ TeV}}\right)^2 \,. \tag{5.61}$$

Barring extremely accurate cancellations between the two unrelated components Λ and λ_T in the expression for λ'' (cf. Eq. (5.60)), the bound in Eq. (5.61) is automatically translated onto λ and λ'.

The bounds on the trilinear RPV couplings just derived are very strong, making them harmless for the cosmological analysis. In light of this result, we can restrict the superpotential to the unique operator:

$$W_{RPV}^{eff} = \mu_i \, \ell_i h_u \,. \tag{5.62}$$

In the effective theory one also expects R-parity violating couplings in the soft scalar potential, whose values depend on the details of the SUSY breaking sector. However, as we will show in the next section, the main cosmological constraints apply to the bilinear soft terms

$$V_{RPV}^{\text{soft}} = B_i \, \tilde{\ell}_i h_u + \tilde{m}_{h_d \ell_i}^2 h_d^\dagger \tilde{\ell}_i + \text{h.c.} \,. \tag{5.63}$$

5.5.3 Cosmological analysis

The framework depicted by Eqs. (5.62)–(5.63) is customarily dubbed as bilinear R-parity violation. Having in mind the discussion of sect. 5.5, we have still the freedom to fix a basis for the superfields h_d, l_i. We thus use the linear transformation (5.32) to rotate away, up to $O\left(|\,\varepsilon_i\,|^2\right)$, the RPV couplings μ_i. Notice that in

this new basis lepton number violating couplings λ and λ' are reintroduced according to eq. (5.33) while the baryon number violating coupling λ'' remains zero, being invariant with respect to the unitary transformations involving l_i and h_d. The new trilinear couplings are not, anyway, new free parameters, depending only on ε_i and the SM Yukawas.

In our setup, the parameters ξ_i, relating the sneturino and the higgs v.e.v's can be written, at the leading order in ε_i, in the from:

$$\xi_i \approx \frac{(B_i - \varepsilon_i B)\tan\beta + \tilde{m}_{h_d \ell_i}^2 + \varepsilon_i(\tilde{m}_{\ell_i}^2 - \tilde{m}_{h_d}^2)}{\tilde{m}_{\ell_i}^2 + \frac{1}{2}M_Z^2 \cos 2\beta} \, . \tag{5.64}$$

Given the model dependence of the soft terms b_i and $\tilde{m}_{h_d \ell_i}$, RPV is described at low-energy by the six parameters ξ_i and ε_i. On the other hand, by inspecting Eq. (5.64) and Eq. (5.12) it turns out that, barring cancellations, the parameters ξ_i are at least of the order of ε_i.

In what follows we will analyze the bilinear RPV model introduced in the previous section and identify the range of viability of the R-parity violating couplings. The analysis is organized according to the following points:

- NLSP lifetime and BBN.

- Gravitino lifetime and cosmic rays.

- Neutrino masses through RPV.

- Gravitino relic density and thermal leptogenesis.

NLSP lifetime and BBN

The main motivation for the introduction of R-parity violation is to restore the agreement between the decay of the NLSP and BBN. In our setup the most efficient processes are induced by the sneutrino VEVs which mixes the Z (W) boson with a neutrino (charged-lepton) and a neutralino.

A Bino can decay into a W boson and a charged-lepton or into a Z boson and a neutrino with the typical rates [Bobrovskyi 2010]

$$\Gamma\left(\chi_1^0 \to Z\,\nu\right) = \frac{G_F\, m_{\chi_1^0}^3}{4\pi\sqrt{2}} \frac{\sin^2\theta_W \cos^2\beta}{M_1^2} \xi^2 \, , \tag{5.65}$$

$$\Gamma\left(\chi_1^0 \to W^\pm l^\mp\right) = \frac{G_F\, m_{\chi_1^0}^3}{2\pi\sqrt{2}} \frac{\sin^2\theta_W \cos^2\beta}{M_1^2} \xi^2 \, , \tag{5.66}$$

The NLSP may also decay into three fermions by means of the couplings λ and λ' in Eq. (5.33) with a typical rate of the form

$$\Gamma_{3-\text{body}} = \frac{g^2 |\hat{\lambda}'|^2}{1024\,\pi^3} \frac{m_{\chi_1^0}^5}{\tilde{m}_Q^4} \, . \tag{5.67}$$

The same expression, divided by a factor of three, holds for the rates involving the coupling $\hat{\lambda}$. However the 3-body processes are highly suppressed with respect to the 2-body decay

$$BR(3-\text{body}/2-\text{body}) \approx 1.3 \times 10^{-5} \left(\frac{\varepsilon}{\xi}\right)^2 \left(\frac{\tan\beta}{10}\right)^4 \left(\frac{\tilde{m}_Q}{1 \text{ TeV}}\right)^{-4} \left(\frac{m_{\chi_1^0}}{150 \text{ GeV}}\right)^4 .$$
(5.68)

In writing this expression we used Eq. (5.33) and assumed $\varepsilon_i \sim \varepsilon$ for $i = 1, 2, 3$. Hence the 3-body processes can be neglected for a typical TGM spectrum, barring cancellations in the sneutrino VEVs. The NLSP lifetime is then determined by Eqs. (5.65)–(5.66)

$$\tau_{\text{NLSP, 2-body}} \approx 0.02 \text{ s} \left(\frac{m_{\chi_1^0}}{150 \text{ GeV}}\right)^{-1} \left(\frac{\tan\beta}{10}\right)^2 \left(\frac{\xi}{10^{-10}}\right)^{-2} ,$$
(5.69)

which satisfies the BBN bounds, as reproduced in Fig. 5.3 for $\tau_{\text{NLSP}} \gtrsim 10^{-2}$ s, thus implying $\xi \gtrsim 10^{-(10 \div 11)}$ depending on $m_{\chi_1^0}$. This is actually a rather conservative bound; lower values of ξ are allowed depending on the NLSP abundance[15].

Gravitino lifetime and cosmic rays

The amount of R-parity violation is also constrained from above since the DM is not stable anymore. As it will be evident from the expressions below the gravitino is stable on cosmological time-scales, being its decay rate doubly suppressed both by the R-parity violating couplings and the Planck mass. On the other hand the small portion of the decaying gravitinos is able to leave an imprint on the cosmic ray spectrum.

In our setup the main decay channel of the gravitino is into a neutrino and a photon [Takayama 2000]

$$\Gamma(\tilde{G} \to \gamma\,\nu) = \frac{1}{32\pi} \frac{(M_2 - M_1)^2}{M_1^2 M_2^2} M_Z^2 \sin^2\theta_W \cos^2\theta_W \cos^2\beta\, \xi^2 \frac{m_{3/2}^3}{M_{Pl}^2} .$$
(5.70)

---

[15] On the other hand the given bound takes also into account the fact that a population of NLSP, potentially dangerous for BBN, could survive despite the low branching ratio of 3-body decays. From Eq. (5.68) we see that this scenario does not occur for low/moderate values of $\tan\beta$ (cf. also the lines in Fig. 5.3). Eventually it could be necessary to assume an even more conservative limit $\xi > 10^{-9}$.

Then the associated lifetime can be estimated by[16]

$$\tau \simeq 7.3 \times 10^{28} \text{ s} \left(\frac{\tan\beta}{10}\right)^2 \left(\frac{M_{1/2}}{300 \text{ GeV}}\right)^2 \left(\frac{m_{3/2}}{15 \text{ GeV}}\right)^{-3} \left(\frac{\xi}{10^{-7}}\right)^{-2}. \quad (5.73)$$

This process is expected to leave an imprint on the cosmic gamma ray spectrum in the form of an approximately monochromatic line at an energy depending on the gravitino mass. For higher values of $M_{1/2}$ and $m_{3/2}$ the 3-body processes mediated by off-shell gauge bosons become also important and eventually dominant [Choi 2010], implying the presence of an additional continuos component in the gamma ray spectrum. This kind of signals have been the subject of dedicated searches performed by the Fermi Large Area Telescope (LAT) collaboration [Abdo 2010a, Abdo 2010b]. Since none of the expected excesses in the gamma ray spectrum have been detected so far one obtains a lower bound on the gravitino lifetime.

According to Refs. [Choi 2010, Vertongen 2011] the lower bound on the gravitino lifetime is approximatively of $10^{27\div 29}$ s for gravitino masses in the range $10\div 80$ GeV and $M_{1/2}$ in the range $100\div 1000$ GeV. This translates into an upper bound for ξ of about $\xi \lesssim 10^{-(6\div 8)}$.

For definiteness we mention that for the central values of $M_{1/2}$ and $m_{3/2}$ in Eq. (5.73), which roughly correspond to the LHC bound quoted in Sect. 5.3, the limit on the gravitino lifetime is 10^{28} s which is satisfied for $\xi \lesssim 3 \times 10^{-7}$.

Neutrino masses trough RPV

Summing up the results obtained until now, the outcome of the cosmological analysis is that the RPV coupling ξ must lie in the window $10^{-6} < \xi < 10^{-11}$. R-parity violation can have, however, a wider impact on the phenomenology, like the one, already discussed, on neutrino masses. In our bilinear setup the neutrino mass matrix (5.37) is dominated by the tree-level see-saw like contribution and can be diagonalized along the lines of [Hirsch 2000, Diaz 2003] leading to a hierarchical spectrum. The highest eigenvalue basically coincides with the non-zero eigenvalue of the tree level matrix [Chun 1999]:

$$m_{\nu_3} = M_Z^2\, \xi^2 \cos^2\beta \left(\frac{M_1 M_2}{M_1 c_W^2 + M_2 s_W^2} - \frac{M_Z^2}{\mu} \sin 2\beta\right)^{-1}. \quad (5.74)$$

---

[16]The trilinear couplings λ and λ' yield a negligible contribution to the gravitino lifetime. Indeed the typical rates are [Moreau 2002]

$$\Gamma_{3/2,3-\text{body}} = \frac{\bar{\lambda}^2}{18432\,\pi^3} \frac{m_{3/2}^7}{\tilde{m}_Q^4}, \qquad \bar{\lambda} = 3\,\lambda', \lambda \quad (5.71)$$

which lead to the following lifetime:

$$\tau_{3/2,3-\text{body}} \approx 6.5 \times 10^{37} \text{ s} \left(\frac{\varepsilon}{10^{-4}}\right)^{-2} \left(\frac{m_{3/2}}{10 \text{ GeV}}\right)^{-7} \left(\frac{\tan\beta}{10}\right)^{-2} \left(\frac{\tilde{m}_Q}{1 \text{ TeV}}\right)^4. \quad (5.72)$$

and must not exceed the atmospheric mass splitting. A second eigenvalue is instead given by:

$$m_{\nu_2} \approx \frac{3}{8\pi^2} \frac{m_b^2 \tilde{m}_{LR}^{b2}}{m_{\tilde{b}_R}^2 - m_{\tilde{b}_L}^2} \ln\left(\frac{m_{\tilde{b}_R}^2}{m_{\tilde{b}_L}^2}\right) \frac{|\vec{\xi} \times \vec{\lambda}'|^2}{|\vec{\xi}|^2} \tag{5.75}$$

where $\vec{\lambda}' \equiv (\lambda'_{133}, \lambda'_{233}, \lambda'_{333})$ and $m_{b,LR}^2$ is the off-diagonal part of the sbottom mass matrix and can be constrained by the solar mass splitting. Additional constraints are obtained by the fitting of the neutrino mixing angles [Hirsch 2000]. From the condition $m_{\nu_3} \simeq \sqrt{\Delta m_{\text{atm}}^2}$, implying:

$$\xi \simeq 1.5 \times 10^{-5} \left(\frac{\sqrt{\Delta m_{\text{atm}}^2}}{0.05 \text{ eV}}\right)^{1/2} \left(\frac{\tan\beta}{10}\right) \left(\frac{M_{1/2}}{300 \text{ GeV}}\right)^{1/2}. \tag{5.76}$$

it is however evident that the contribution from RPV neutrino masses should be suppressed well below the experimental constraints to be in agreement with the outcome of the analysis of cosmic ray bounds ($\xi < 10^{-6}$). This result is in agreement with the recent analysis of Ref. [Restrepo 2011] which rules out bilinear RPV as the mechanism responsible for neutrino masses for gravitinos heavier than 1 GeV. Such low vales of the gravitino mass are not achievable if TGM is the dominant mechanism originating sfermion masses (cf. Eq. (5.16)). In our model, neutrino masses have to be generated by means of another mechanism (see Appendix C.1.2 for the discussion on neutrino masses).

Gravitino relic density and thermal leptogenesis

At this point we turn to the relic density of DM. For the range $10^{-(10\div11)} \lesssim \xi \lesssim 10^{-(7\div8)}$ the NLSP decays only into SM particles at a much faster rate with respect to the decay into gravitinos. The branching ratio between the R-parity conserving decays (into SM particles) and the R-parity violating ones (into SM particles and gravitinos),

$$BR(RPC/RPV) \approx 10^{-8} \left(\frac{m_{\chi_1^0}}{150 \text{ GeV}}\right)^4 \left(\frac{m_{3/2}}{15 \text{ GeV}}\right)^{-2} \left(\frac{\tan\beta}{10}\right)^2 \left(\frac{\xi}{10^{-10}}\right)^{-2}, \tag{5.77}$$

indicates that the DM relic density is completely determined by its thermal component.

As shown in Fig. 5.6 the DM relic density matches the cosmological value, depending on the values of $M_{1/2}$ and $\tilde{m}_{10}$, for reheating temperatures up to $\sim 10^9$ GeV. By estimating Eq. (5.4) in the following way:

$$\Omega_{DM}^T h^2 \approx 0.12 \left(\frac{T_{RH}}{10^9 \text{ GeV}}\right) \left(\frac{30 \text{ GeV}}{m_{3/2}}\right) \left(\frac{M_{1/2}}{300 \text{ GeV}}\right)^2, \tag{5.78}$$

and considering the relation in Eq. (5.16), we can see that the increase in the contribution of TGM to sfermion masses (with respect to standard gauge mediation)
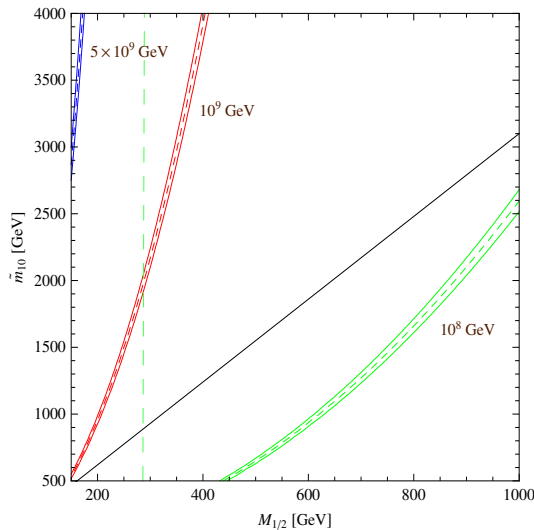
Figure 5.6: Contours of the gravitino relic density in the plane $(M_{1/2}, \tilde{m}_{10})$ computed, according to Eq. (5.4), for the values of the reheating temperature reported. The black line represent the condition of TGM dominace eq. (5.15). The green dashed line represent the value 700 GeV of the gluino mass.

coincides with an increase of the reheating temperature needed to fit the cosmological value of the DM relic density. Moreover values of the reheating temperature of the order of 10^9 GeV are welcome in the standard thermal leptogenesis scenarios [Fukugita 1986]. We stress that this result is obtained thanks to the natural prediction of TGM of a gravitino mass of the order of 10 GeV. On the contrary theories based on standard (loop) gauge mediation predicts much lower reheating temperatures due to lower gravitino masses. By rescaling Eq. (5.78), in terms of $\tilde{m}_{10}$ and the gluino mass

$$\Omega_{DM}^T h^2 \approx 0.12 \ \left(\frac{T_{RH}}{10^9 \ \text{GeV}} \right) \left(\frac{2 \ \text{TeV}}{\tilde{m}_{10}} \right) \left(\frac{M_3}{700 \ \text{GeV}} \right)^2 , \qquad (5.79)$$

we see that a reheating temperature of the order of 10^9 GeV requires sfermion masses in the multi TeV range.

We conclude by mentioning that, in presence of a leptogenesis mechanism, the theory is subject to additional constraints on the amount of RPV. Indeed baryon and lepton number violating interactions due to RPV could erase the $B - L$ asymmetry generated by leptogenesis. This can be avoided by requiring that the dangerous processes are not efficient, i.e. $\Gamma_{\text{RPV}} < H$, when the asymmetry is generated. The general expression for these rates has been studied in [Campbell 1991, Campbell 1992]. In case of bilinear R-parity violation the baryogenesis bound can be summarized by the condition [Buchmuller 2007]

$$\varepsilon \lesssim 10^{-6} \left(\frac{\tan \beta}{10} \right)^{-1} , \qquad (5.80)$$

which implies a similar bound on ξ, barring cancellations in Eq. (5.64).

The bounds emerging from the cosmological analysis are collectively summarized in Table 5.1.

Observable	Bound	References
Proton decay	$\lambda, \lambda', \lambda'' < 10^{-10}$	[Smirnov 1996a]
BBN (NLSP lifetime)	$\xi > 10^{-(10 \div 11)}$	[Ishiwata 2008]
Cosmic rays	$\xi < 10^{-(6 \div 8)}$	[Choi 2010],[Vertongen 2011]
Neutrino masses	$\xi \simeq 10^{-5}$	[Barbier 2005]
Baryogenesis	$\varepsilon < 10^{-6}$	[Campbell 1991, Campbell 1992]

Table 5.1: Summary of the bounds on the R-parity violating couplings.

Conclusions

In this thesis we have reconsidered some of the main aspects regarding the Dark Matter generation mechanisms in the context of the Minimal Supersymmetric Standard Model. This class of models naturally provides two DM candidates, featuring a very different phenomenology.

Our focus has been firstly dedicated to its WIMP Dark Matter candidate, namely the lightest neutralino.

We have, in particular, evidenced the constraining power of the requirement a relic abundance compatible with the experimental determination. Assuming the DM to be a thermal relic, indeed, overproduction or underproduction can be avoided only by precise relations among the SUSY parameters entering in its effective thermally averaged pair annihilation cross section.

We have then considered, as viable alternative, non-thermal dark matter production, a well-motivated scenario arising naturally in several particle physics frameworks, including SUSY standard model extensions within supergravity and superstring theories. After reviewing how to introduce a system of differential equations to treat a generic case of non-thermal dark matter generation, we have implemented an efficient and accurate numerical scheme for the computation; such scheme has been interfaced to DarkSUSY numerical package and will be released together a future version of the code.

On general grounds this kind of scenario results interesting thanks to the fact that, generically, it favors dark matter candidates with pair annihilation cross sections larger than in the thermal WIMP framework, which can be efficiently probed by current Indirect Detection experiments. In particular non-thermal dark matter models possibly suggest a connection with the very large annihilation rates which would be needed to explain with a dark matter induced component recently detected anomalies in cosmic-ray lepton fluxes, such as the rise in the positron fraction measured by the PAMELA detector; we have considered, within a toy model, what range of reheating temperatures would follow from such identification.

Our main interest has been, however, the impact of non-thermal DM production on SUSY models. The most relevant effect is the selection of the preferred mass scale of the lightest SUSY particle as dark matter candidate; in particular we have found a sensitive reduction of the preferred mass scale for wino-like and higgsino-like neutralinos. In addition we remark that a partial influence on the Supersymmetric spectrum is retained also in this kind of scenario, again through the pair annihilation cross section which selects, together with the production efficiency,

the possible trends of the numerical solution of the Boltzmann equations of the DM relic abundance.

In view of these effect, the issue of non-thermal DM production, as opposed to the standard thermal paradigm has a direct impact on the interpretation of new physics eventually discovered at accelerators including LHC.

On top of this general study we have also applied our numerical scheme to a more definite framework, a rather predicting class of models, featuring non thermal production, dubbed as G2-MSSM.

As final step of our examination of WIMP DM production we have questioned the underlying assumptions in the standard solution of the Boltzmann equation for the dark matter component; in particular, we discussed how to verify whether kinetic equilibrium holds along the whole phase of dark matter generation, as well as the validity of the factorization usually implemented to rewrite a system of coupled Boltzmann equation for each number density of a set coannihilating particles as a single equation for the sum of all the number densities. As a byproduct we also developed a formalism to compute the kinetic decoupling temperature for a system of coannihilating species. Despite this formalism have been mostly applied to non-thermal dark matter scenario, in particular to realization of the G2-MSSM, it is valid also in case standard thermal relics within a standard cosmology.

The second main topic has been, as mentioned just before, the impact of the DM phenomenology on the prospects of SUSY detection at LHC. Our purpose was to show as the relations among SUSY parameters enforced by the mechanism accounting for the DM relic density, combined with the information about the DM mass scale and intrinsic properties which can be potentially provided in the near future by a direct detection experiment can be used as guidelines for the future searches of production processes of Supersymmetric particles. We have indeed examined the capability of a 1Ton realization of the Xenon experiment of identifying , once a signal is detected, some peculiar MSSM realization featuring some peculiar DM scenarios. These particular scenarios, as emerged from our simulation of the ATLAS detector, will be effectively probed even in the next months.

Unfortunately the outcome of our DD analysis have resulted troublesome in several setups, evidencing that the direct detection signal cannot reconstruct alone the properties relevant for a collider detection. A partial improvement is obtained by noticing that in the considered scenarios some dark matter properties influence the rates of rare processes like $b \rightarrow s\gamma$ and $B_s \rightarrow \mu^+\mu^-$ as well as the value of the mass of the SM-like higgs state, recently determined by the LHC collaboration; as a consequence the constraints associated to these observables can be used as additional source of information. Also accounting for these features, the reconstruction prospects of the models with DM masses of the order of few hundreds of GeV are still very poor because statistical effects in the measure of the recoil energies. This last issue has become more pressing in view of the recent update of the limits on the DM SI cross-section.

A possible strategy is to include information from the third DM search strategy, potentially complementary to direct and collider detection, namely indirect

detection, also in view of the growing attention gained after the recent claim of the identification of a line in the galactic γ-ray spectrum. This issue, together with a more systematic investigation of the detection prospects of viable dark matter scenarios will be object of future investigations.

In conclusion of this thesis we have afforded the main cosmological aspects of the alternative MSSM DM candidate, the gravitino. The playground of our study has been the $SO(10)$ realization of the TGM mechanism. This kind of model guarantees peculiar predictions for the supersymmetric spectrum; in particular, once the messenger scale is fixed at the GUT scale one obtains a definite prediction for the value of the gravitino mass to be of $\mathcal{O}(10\text{ GeV})$ by assuming the sfermion masses in the TeV range. Another consequence of the model is the fact that the NLSP is a Bino-like neutralino over most of the parameter space.

This scenario is highly disfavored if R-parity is conserved, being the DM overproduced by the NLSP decays. Moreover the gravitino production is accompanied by hadronic and/or electromagnetic showers which spoil the predictions of BBN.

On the contrary the TGM model is naturally feasible in presence of a small amount of R-parity violation. Furthermore the GUT structure of the theory and the constraints from the proton decay motivates the restriction to a scenario of bilinear R-parity violation which allows to describe the relevant phenomenology in terms of a limited number of parameters. Given the correct amount of RPV, the NLSP is allowed to decay much before the onset of BBN without overproducing gravitinos. The latter, at the same time, remains stable over cosmological times, being their decay rate doubly suppressed both by the R-parity violating couplings and by the Planck scale. Interestingly the small amount of decays which can take place at the present time is in principle detectable by the current cosmic ray experiments such as FERMI-LAT.

The same RPV couplings responsible for the NSLP and gravitino decay could be at the origin of neutrino masses. However the value required for these couplings is not compatible with the bounds from cosmic rays, at least for the gravitino masses predicted by TGM.

On the other hand a gravitino with mass of $\mathcal{O}(10\text{ GeV})$, combined with a natural TGM spectrum with sfermions in the multi TeV region, allows the DM relic density to match the cosmological value for a reheating temperature of $\mathcal{O}(10^9\text{ GeV})$ relevant for leptogenesis. This improves the situation with respect to the case of the standard (loop) gauge mediation, where the gravitino mass can be at most of $\mathcal{O}(1\text{ GeV})$ implying a lower reheating temperature.

Evaluation of collisional operator

In this appendix we will sketch how to compute the operators $\hat{\mathbf{C}}$, as introduced in 2.1 and then in the system of coupled Boltzmann equations (3.24), in two sample scenarios. First of all we will briefly review the treatment introduced in [Bringmann 2007], for the case of a single species only elastically scattering, with explicit reference to a Bino-like dark matter. Then we discuss how this formalism should be modified in the case of inelastic scattering processes involving more than one particle species.

A.1 Elastic scattering case

In this section we will discuss the collision term referring to the elastic scattering of a non-relativistic neutralino with relativistic SM states. Most of the results here reported, as well as the ones of the next section, are valid in more general particle physics frameworks, possibly other than SUSY theories. The collision term involving elastic scattering can be written as:

$$
\begin{aligned}
\frac{\hat{\mathbf{C}}_{\chi^0,\mathrm{es}}}{E}[f_{\chi^0}] &= \sum_i \tilde{g}_i g_{\chi^0} \int \frac{d^3k}{(2\pi)^3 2k} \int \frac{d^3k'}{(2\pi)^3 2k'} \int \frac{d^3p'}{(2\pi)^3 2E'} \frac{|\bar{M}|_i^2}{2E} \\
&\quad \cdot (2\pi)^4 \delta^4(P' + K' - P - K) \cdot \\
&\quad \cdot \left[f_i(k')(1 - f_i(k)) f_{\chi^0}(p') - f_i(1 - f_i(k')) f_{\chi^0}(p) \right]
\end{aligned}
\tag{A.1}
$$

with $K \equiv (k, \mathbf{k})$ and $K' \equiv (k', \mathbf{k}')$ identifying the initial and final state four-momentum of the SM particle while , while $P \equiv (E, \mathbf{p})$ and $P' \equiv (E', \mathbf{p}')$ denote the four-momenta of the initial and final neutralino. $\tilde{g}_i$ represent the internal degrees of freedom of the SM state i assumed to have a thermal distribution function $f_i(k) = 1/\left(e^{\frac{k}{T}} \pm 1\right)$. The dark matter distribution function is assumed to be generic apart from the fact that it allows to neglect the Pauli blocking factor. $|\bar{M}|_i^2$ is the modulus squared of the scattering amplitude, averaged over the initial spin states and summed over the final spin states. The exchanged four-momentum is indicated as $(\omega, \mathbf{q}) \equiv (E - E', \mathbf{p} - \mathbf{p}')$; for kinematical reasons, the transferred momentum is constrained to be of the order of the heat bath temperature and is small compared to the initial energy and mass of the neutralino. Furthermore we have initial conditions such that neutralinos have nearly thermal distributions. Under such conditions, we can just take the non-relativistic limit of the collision term. In addition, we can expand it in the limit of zero momentum transfer between the DM and the SM

particles:

$$\hat{C} = \sum_{j=0}^{\infty} \hat{C}_j \tag{A.2}$$

with:

$$
\begin{aligned}
\hat{C}_j \;\equiv\; & \sum_i \tilde{g}_i g_{\chi^0} \int \frac{d^3 k}{(2\pi)^3 2k} \int \frac{d^3 k'}{(2\pi)^3 2k'} \int \frac{d^3 p'}{(2\pi)^3 2E'} \frac{|\bar{M}|^2_{ab}}{2E} \\
& \cdot (2\pi)^4 \delta(E' + k' - E - k) \cdot \\
& \cdot \left[f_i(k') f_i(k) f_{\chi_0}(p') - f_i(k)(1 - f_i(k')) f_{\chi^0}(p) \right] \\
& \cdot \left[\frac{1}{j!} D^j_{\mathbf{q}}(\mathbf{p}' - \mathbf{p}) \right]
\end{aligned} \tag{A.3}
$$

where:

$$D_{\mathbf{q}}(\mathbf{p}') \equiv \mathbf{q} \cdot \nabla_{\mathbf{p}'} \equiv (\mathbf{k}' - \mathbf{k}) \cdot \nabla_{\mathbf{p}'} \tag{A.4}$$

For the detailed computation off the terms of the expansion we refer to [Bringmann 2007]. We just remark that the zero-th order term C_0 is null for $\mathbf{p} \to \mathbf{p}', k \to k'$. The leading contributions are then provided by the terms C_1 and C_2 which can be written as:

$$
\begin{aligned}
C_1 \;=\; & -2\pi \int \frac{d^3 k}{(2\pi)^3 2k} \int \frac{d^3 k'}{(2\pi)^3 2k'} \mathbf{q} \cdot \nabla_{\mathbf{p}'} \\
& \left[\frac{|\bar{M}|^2}{2E'} J \delta(E' + k' - E - k) \right]_{\mathbf{p}'=\mathbf{p}} \\
=\; & -\pi \int \frac{d^3 k}{(2\pi)^3 2k} \int \frac{d^3 k'}{(2\pi)^3 2k'} \delta(k' - k) \frac{|\bar{M}_{t=0}|^2}{E} \\
& \left[\mathbf{q} \cdot \nabla_{\mathbf{p}'} J - \frac{\mathbf{q} \cdot \mathbf{p}}{E} \partial_{k'} J \right]
\end{aligned} \tag{A.5}
$$

$$
\begin{aligned}
C_2 \;=\; & \pi \int \frac{d^3 k}{(2\pi)^3 2k} \int \frac{d^3 k'}{(2\pi)^3 2k'} \left(\mathbf{q} \cdot \nabla_{\mathbf{p}'} \right)^2 \\
& \left[\frac{|\bar{M}|^2}{2E'} J \delta(E' + k' - E - k) \right]_{\mathbf{p}'=\mathbf{p}} \\
=\; & \frac{\pi}{2} \int \frac{d^3 k}{(2\pi)^3 2k} \int \frac{d^3 k'}{(2\pi)^3 2k'} |M|^2_{t=0} \\
\times \; & \left[\left(\frac{(\mathbf{q} \cdot \nabla_{\mathbf{p}'})^2 J}{E} - 2 \frac{(\mathbf{q} \cdot \mathbf{p})(\mathbf{q} \cdot \nabla_{\mathbf{p}'}) J}{E^3} \right) \delta(k' - k) \right. \\
+ \; & \frac{(\mathbf{q} \cdot \mathbf{p})^2}{E^3} J \partial^2_{k'} \delta(k' - k) \\
+ \; & \left. \left(2 \frac{(\mathbf{q} \cdot \mathbf{p})(\mathbf{q} \cdot \nabla_{\mathbf{p}'}) J}{E^2} + \frac{\mathbf{q}^2}{E^2} J - \frac{(\mathbf{q} \cdot \mathbf{p})^2}{E^4} J \right) \partial_{k'} \delta(k' - k) \right]
\end{aligned} \tag{A.6}
$$

where:

$$J = \left(f_{\chi^0}(p')f(k')(1 - f(k)) - f_{\chi^0}(p)f(k)(1 - f(k')) \right) \tag{A.7}$$

The previous integrals can be partially computed by mean of the Dirac delta and the following angular integrals:

$$\int d\Omega \int d\Omega' |\bar{M}|^2 (\mathbf{q} \cdot \mathbf{l}) = \frac{16\pi^2}{3} \frac{k}{E} (\mathbf{p} \cdot \mathbf{l}) \left\{ \left(\partial_k |\bar{M}|^2_{t=0,\theta=\pi/2} \right) + \mathcal{O}\left(\frac{\mathbf{p}^2}{E^2} \right) \right\} \tag{A.8}$$

$$\int d\Omega \int d\Omega' |\bar{M}|^2 q^i q^j = \frac{16\pi^2}{3} \left(k^2 + k'^2 \right) |\bar{M}|^2_{t=0,\theta=\pi/2} g^{ij} + \mathcal{O}\left(\frac{\mathbf{p}^2}{E^2} \right) \tag{A.9}$$

After a bit lengthy computation, dropping for semplicity the sum over the different possible processes, the collision term, at the leading order in $\mathbf{p}^2/E^2$ and k/E, both corresponding to the order T/m_χ, reduces to the following integral:

$$\begin{aligned}
\hat{C} &= C_1 + C_2 \\
&= \frac{\tilde{g}_{SM}}{6(2\pi)^3} \frac{1}{m_\chi^3} \int dk f(k) \partial_k \left(k^4 |M|^2_{t=0,s=m_\chi^2+2m_\chi k} \right) \\
&\times \left[m_\chi T \Delta_{\mathbf{p}} + \mathbf{p} \cdot \nabla_{\mathbf{p}} + 3 \right] f_{\chi^0}(p)
\end{aligned} \tag{A.10}$$

where with $\tilde{g}_{SM}$ we generically refer to the internal degrees of freedom of the SM states.

A bino-like DM particle interacts with heat bath particles through the mediation of either slepton or squarks. Customarily only the formers are regarded as relevant, given the fact that at lower temperatures, below the QCD phase transition, no free quarks are expected in the thermal bath [1]. The invariant scattering amplitude can be expanded with respect to k/E and, at the leading order, can be written as:

$$|\bar{M}|^2_{t=0} = 32 g_Y^4 (b_L^4 + c_L^4) \left(\frac{m_\chi}{m_{\tilde{l}}^2 - m_\chi^2} \right)^2 k^2, \quad b_L = \frac{Y_e}{2} \tan\theta_W N_{11}, \quad c_L = N_{11} \tan\theta_W \tag{A.11}$$

Inserting this expression into eq.(A.10) and integrating over k one finds that:

$$\hat{C} \propto \left(\frac{T}{m_\chi} \right)^4 [m_\chi T \Delta_{\mathbf{p}} + \mathbf{p} \cdot \nabla_{\mathbf{p}} + 3] f_{\chi^0}(p) \tag{A.12}$$

A straightforward computation shows that:

$$\int d^3p \left[m_\chi T \Delta_{\mathbf{p}} + \mathbf{p} \cdot \nabla_{\mathbf{p}} + 3 \right] f_{\chi^0}(p) = 0 \tag{A.13}$$

in agreement with the fact that elastic scattering processes do not alter the DM number density while:

$$\int d^3p \left[m_\chi T \Delta_{\mathbf{p}} + \mathbf{p} \cdot \nabla_{\mathbf{p}} + 3 \right] p^2 f_{\chi^0}(p) \propto n_{\chi^0}(T - T_\chi) \tag{A.14}$$

---

[1]A more complete treatment, including the contribution of scattering over quarks is considered in [Gondolo 2012]

recovering the general expression (2.39).

We conclude by mentioning that, the equation for the kinetic temperature of a bino-like neutralino can be written as:

$$\frac{dT_\chi}{dT} = \left[2 + a\left(\frac{T}{m_\chi}\right)^4 \right] \frac{T_\chi}{T} - a\left(\frac{T_\chi}{m_\chi}\right)^4 \tag{A.15}$$

with

$$a = \frac{31}{21} \sqrt{\frac{5\pi^3}{g_{\text{eff}}}} \frac{M_{\text{Pl}}}{m_\chi} g_Y^4 g_{SM} (b_L^4 + c_L^4) \left(\frac{m_\chi}{m_{\tilde{l}}^2 - m_\chi^2}\right)^2 \tag{A.16}$$

and analytically solved as shown in [Bringmann 2007]. Here we just point out the two asymptotic solutions:

$$T_\chi = T, \ \ T \to \infty$$
$$T_\chi = \left(\frac{a}{4}\right)^{1/4} \Gamma\left[\frac{3}{4}\right] \frac{T^2}{m_\chi}, \ \ T \to 0 \tag{A.17}$$

from whose matching is defined the kinetic decoupling temperature:

$$\frac{T_{\text{kd}}}{m_\chi} = \left(\left(\frac{a}{4}\right)^{1/4} \Gamma\left[\frac{3}{4}\right] \right)^{-1} \tag{A.18}$$

A.2   Inelastic scattering case

We now discuss how to deal with the contribution to the neutralino collisional operator coming from inelastic processes of the type:

$$\chi^0(P) + a(K) \leftrightarrow \chi^\pm (P') + b(K') \tag{A.19}$$

where a and b are thermal background particles. The four-momenta of the neutralino, chargino and SM particles follow the same notation of the previous section. Summing over all available thermal bath pairs (a, b), such contribution to the collisional operator, normalized to the neutralino energy E, takes the form:

$$\begin{aligned}
\frac{\hat{\mathbf{C}}_{\chi^0,\text{is}}}{E}[f_{\chi^0}, f_{\chi^\pm}] &= \sum_{(a,b)} \tilde{g}_{Wab} g_{\chi^\pm} \int \frac{d^3k}{(2\pi)^3 2k} \int \frac{d^3k'}{(2\pi)^3 2k'} \int \frac{d^3p'}{(2\pi)^3 2E'} \frac{|\bar{M}|_{ab}^2}{2E} \\
&\quad \cdot (2\pi)^4 \delta^4(P' + K' - P - K) \cdot \\
&\quad \cdot \left[f_b(k')(1 - f_a(k)) f_{\chi^\pm}(p') - f_a(k)(1 - f_b(k')) f_{\chi^0}(p) \right]
\end{aligned} \tag{A.20}$$

In the following we assume that a and b are massless and described by Fermi-Dirac distribution functions $f_a(k, t)$ and $f_b(k', t)$ (to shorten the notation the indices a and b will be dropped). The expansion depicted in the previous section cannot rigorously performed in the case of inelastic scattering since the energy-momentum exchange between the chargino-neutralino system and the SM states is constrained by the finite mass-splitting of the two SUSY states. On the other hand, in the

case of a Wino-like particle the ratio between the mass splitting chargino-neutralino and the neutralino mass can be safely assumed as a small parameter. Under this assumption we can obtain an analogous expression of the collisional operator as [Bringmann 2007] by performing an expansion, in the non relativistic limit, in terms of T/E and of the additional parameter $\Delta m_\chi / m_\chi$.

In order to take the non relativistic limit it is also useful to to introduce the neutralino velocity defined as $\mathbf{v} \equiv \mathbf{p}/E$; considering initial conditions such that neutralinos have nearly thermal distributions, their velocity can be also expressed as $v \sim \sqrt{T/m_\chi} \ll 1$.

Under the above conditions we can eliminate the dependence on $\mathbf{p}'$ by Taylor expanding $f_{\chi^\pm}(p')$ as:

$$f_{\chi^\pm}(p') \simeq f_{\chi^\pm}(p) - \mathbf{q} \cdot \nabla_\mathbf{p} f_{\chi^\pm}(p) + \frac{1}{2}(\mathbf{q} \cdot \nabla_\mathbf{p})^2 f_{\chi^\pm}(p) + ... \qquad (A.21)$$

This allows us to freely integrate over the three-momentum component of the delta function in Eq. (A.20). Using now the relation:

$$f(k')(1 - f(k)) = \exp\left(-\frac{\omega}{T}\right) f(k)(1 - f(k')) \simeq \exp\left(-\frac{\omega}{T}\right) f(k) \qquad (A.22)$$

with:

$$\exp\left(-\frac{\omega}{T}\right) \simeq \exp\left(\frac{\Delta m_\chi}{T}\right) \left(1 - \frac{\Delta m_\chi v^2}{2T} - \frac{\mathbf{q} \cdot \mathbf{v}}{T} + \frac{q^2}{2m_\chi T} + \frac{(\mathbf{q} \cdot \mathbf{v})(\mathbf{q} \cdot \mathbf{v})}{2T^2}\right) \qquad (A.23)$$

we need to compute:

$$
\begin{aligned}
\frac{\hat{\mathbf{C}}_{\chi^0,\text{is}}[f_{\chi^0}]}{E} =& \sum_{(a,b)} \frac{\tilde{g}_{Wab} g_{\chi^\pm}}{256\pi^5 EE'} \int \frac{d^3k}{k} f(k) \int \frac{d^3k'}{k'} |\bar{M}|^2_{ab} \, \delta\left(E' + k' - E - k\right) \\
& \left[\left(f_{\chi^\pm}(p)e^{\frac{\Delta m_\chi}{T}} - f_{\chi^0}(p)\right) - \left(\frac{\Delta m_\chi v^2}{2T} f_{\chi^\pm}(p) + \frac{\mathbf{q} \cdot \mathbf{v}}{v} \frac{df_{\chi^\pm}}{dp} + \frac{\mathbf{q} \cdot \mathbf{v}}{T} f_{\chi^\pm}(p)\right) e^{\frac{\Delta m_\chi}{T}}\right. \\
& + \left(\frac{q^2}{2m_\chi T} f_{\chi^\pm}(p) + \frac{(\mathbf{q} \cdot \mathbf{v})(\mathbf{q} \cdot \mathbf{v})}{2T^2} f_{\chi^\pm}(p) \right. \qquad (A.24) \\
& \left. + \frac{(\mathbf{q} \cdot \mathbf{v})(\mathbf{q} \cdot \mathbf{v})}{vT} \frac{df_{\chi^\pm}}{dp} + \frac{(\mathbf{q} \cdot \mathbf{v})(\mathbf{q} \cdot \mathbf{v})}{2v^2} \Delta_\mathbf{p} f_{\chi^\pm}\right) e^{\frac{\Delta m_\chi}{T}} \\
& \left. + \frac{1}{2}\left(\frac{q^2}{v} - \frac{3(\mathbf{q} \cdot \mathbf{v})(\mathbf{q} \cdot \mathbf{v})}{v^3}\right) \frac{df_{\chi^\pm}}{dp} e^{\frac{\Delta m_\chi}{T}}\right] \qquad (A.25)
\end{aligned}
$$

which is the analogous to the expression for the expansion of the collisional operator obtained in [Bringmann 2007]. Notice that the leading order term of the expansion above is not suppressed as T/m_χ. It indeed corresponds to the term C_0 of the expansion (A.2) and can be non-zero when the distribution functions of neutralino and/or chargino deviate from thermal equilibrium.

As an example we sketch the calculus of the first term in the square bracket. The invariant amplitude takes the form:

$$|\bar{M}|^2_{ab} = 64G_\text{F}^2 \left((PK)(P'K') + (PK')(P'K) - (m_\chi + \Delta m_\chi)m_\chi KK'\right) \qquad (A.26)$$

At the leading order in T/m_χ and $\Delta m_\chi/m_\chi$ we can write:

$$\int \frac{d^3k}{k} f(k) \int \frac{d^3k'}{k'} |\bar{M}|^2_{ab} \delta \left(E' + k' - E - k\right) = \int \frac{d^3k}{k} f(k) \int \frac{d^3k'}{k'} \delta(\omega + \sqrt{1-v^2}\Delta m_\chi - \mathbf{v} \cdot \mathbf{q}) \cdot$$

$$\cdot \left[\left(2(k - \mathbf{v}\cdot\mathbf{k})(k' - \mathbf{v}\cdot\mathbf{k}') + \frac{1}{2}(\omega^2 - q^2)(1-v^2)\right) \right. \tag{A.27}$$

$$+\sqrt{1-v^2}\left(-k'\frac{\mathbf{k}\cdot\mathbf{q}}{m_\chi} - k\frac{\mathbf{k}'\cdot\mathbf{q}}{m_\chi} + 2\mathbf{v}\cdot\mathbf{k}\,\mathbf{v}\cdot\mathbf{k}'\frac{\mathbf{v}\cdot\mathbf{q}}{m_\chi}+\right.$$

$$\left.-k\mathbf{v}\cdot\mathbf{k}'\frac{\Delta m_\chi}{m_\chi} - k'\mathbf{v}\cdot\mathbf{k}\frac{\Delta m_\chi}{m_\chi}\right) + \frac{1}{2}\left(\omega^2 - q^2\right)\left(-v^2\frac{\Delta m_\chi}{m_\chi} + (1 - \frac{3}{2}v^2)\frac{(\mathbf{v}\cdot\mathbf{q})}{m_\chi}\right)\right] \tag{A.28}$$

The first step of the integration is an average over the directions of v. It can be done by use of the following results:

$$\int \frac{d\Omega}{4\pi} \delta(W - \mathbf{v}\cdot\mathbf{q}) = \frac{1}{2vq}\theta(v^2q^2 - W^2) \tag{A.29}$$

$$\int \frac{d\Omega}{4\pi} \delta(W - \mathbf{v}\cdot\mathbf{q})v^i = \frac{1}{2vq}\theta(v^2q^2 - W^2)\frac{W}{q^2}q^i$$

$$\int \frac{d\Omega}{4\pi} \delta(W - \mathbf{v}\cdot\mathbf{q})v^iv^j = \frac{1}{2vq}\theta(v^2q^2 - W^2)\left(\frac{W^2 - v^2q^2}{2q^2}\delta^{ij} + \frac{3W^2 - v^2q^2}{2q^4}q^iq^j\right)$$

$$\int \frac{d\Omega}{4\pi} \delta(W - \mathbf{v}\cdot\mathbf{q})v^iv^jv^k = \frac{1}{2vq}\theta(v^2q^2 - W^2) \tag{A.30}$$

$$\left(\frac{v^2q^2W - W^3}{2q^4}\left(q^i\delta^{jk} + q^j\delta^{ik} + q^k\delta^{ij}\right) + \frac{5W^3 - 3v^2q^2W}{2q^6}q^iq^jq^k\right)$$

where we defined $W \equiv \omega + \sqrt{1-v^2}\Delta m_\chi$. The further 3 integrals in Eq. (A.28) are most easily performed in in the variables ω, q and k. Actually the last step, the integral in the variable k needs to be performed numerically; an analytic expression, which traces rather accurately the numerical result, can be obtained by replacing the Fermi-Dirac distribution $f(k)$ with the exponential scaling $\exp(-k/T)$. At the first order in T/m_χ and $\Delta m_\chi/m_\chi$, also remembering that, under our assumptions, $p^2/m_\chi^2 \simeq T/m_\chi$ this gives:

$$\int \frac{d^3k}{k} f(k) \int \frac{d^3k'}{k'} |\bar{M}|^2_{ab} \delta \left(E' + k' - E - k\right) = \left[4T^3\left(\Delta m_\chi^2 + 6\Delta m_\chi T + 12T^2\right)\left(1 + \frac{\Delta m_\chi}{m_\chi}\right) + \right.$$

$$-2\Delta m_\chi^2 T^2 \left(\Delta m_\chi + 2T\right)\frac{p}{m_\chi} \tag{A.31}$$

$$\left.+\frac{2}{3}T\left(\Delta m_\chi^4 + 3\Delta m_\chi^3 T + 32\Delta m_\chi^2 T^2 + 114\Delta m_\chi T^3 + 144T^4\right)\frac{p^2}{m_\chi^2}\right] e^{\frac{\Delta m_\chi}{T}} .$$

After computing all integrals, the inelastic scattering contributions to the neutralino

and chargino collision terms are then found to be:

$$
\frac{\hat{\mathbf{C}}_{\chi 0,\mathrm{is}}\left[f_{\chi^0}, f_{\chi^\pm}\right]}{E} = \sum \frac{2G_{\mathrm{F}}^2 \tilde{g}_{Wab} g_{\chi^\pm}}{\pi^3} \left\{ \left[4T^3 \left(\Delta m_\chi^2 + 6\Delta m_\chi T + 12T^2\right) \left(1 + \frac{\Delta m_\chi}{m_\chi}\right) \right.\right.
$$

$$
\left. -2\Delta m_\chi^2 T^2 \left(\Delta m_\chi + 2T\right) \frac{p}{m_\chi} + \frac{2}{3} T \left(\Delta m_\chi^4 + 3\Delta m_\chi^3 T + 32\Delta m_\chi^2 T^2 + 114\Delta m_\chi T^3 + 144T^4\right) \frac{p^2}{m_\chi^2} \right]
$$

$$
\left(f_{\chi^\pm} - f_{\chi^0} e^{-\frac{\Delta m_\chi}{T}} \right)
$$

$$
- \frac{8}{3} \Delta m_\chi T^3 \left(\Delta m_\chi^2 + 6\Delta m_\chi T + 12T^2\right) \left(\frac{p^2}{T m_\chi^2} f_{\chi^\pm} + \frac{\mathbf{p} \cdot \nabla_{\mathbf{p}} f_{\chi^\pm}}{m_\chi} \right)
$$

$$
+ \frac{2}{3} T^3 \left(\Delta m_\chi^4 + 10\Delta m_\chi^3 T + 60\Delta m_\chi^2 T^2 + 240\Delta m_\chi T^3 + 480T^4\right) \left(\Delta_{\mathbf{p}} f_{\chi^\pm} + \frac{\mathbf{p} \cdot \nabla_{\mathbf{p}} f_{\chi^\pm}}{m_\chi T} + \frac{3}{m_\chi T} f_{\chi^\pm} \right)
$$

$$
\left. -2T^2 \Delta m_\chi \left(\Delta m_\chi^2 + 6\Delta m_\chi T + 12T^2\right) \frac{p^2}{m_\chi^2} f_{\chi^\pm} \right\} \tag{A.32}
$$

$$
\frac{\hat{\mathbf{C}}_{\chi^\pm,\mathrm{is}}\left[f_{\chi^0}, f_{\chi^\pm}\right]}{E} = \sum \frac{2G_{\mathrm{F}}^2 \tilde{g}_{Wab} g_{\chi^0}}{\pi^3} \left\{ \left[4T^3 \left(\Delta m_\chi^2 + 6\Delta m_\chi T + 12T^2\right) \left(1 - \frac{\Delta m_\chi}{m_\chi}\right) \right.\right.
$$

$$
\left. -2\Delta m_\chi^2 T^2 \left(\Delta m_\chi + 2T\right) \frac{p}{m_\chi} + \frac{2}{3} T \left(\Delta m_\chi^4 - 4\Delta m_\chi^3 T - 10\Delta m_\chi^2 T^2 + 30\Delta m_\chi T^3 + 144T^4\right) \frac{p^2}{m_\chi^2} \right]
$$

$$
\tag{A.33}
$$

$$
\left(f_{\chi^0} e^{-\frac{\Delta m_\chi}{T}} - f_{\chi^\pm} \right)
$$

$$
+ \frac{8}{3} \Delta m_\chi T^3 \left(\Delta m_\chi^2 + 6\Delta m_\chi T + 12T^2\right) \left(\frac{p^2}{T m_\chi^2} f_{\chi^0} + \frac{\mathbf{p} \cdot \nabla_{\mathbf{p}} f_{\chi^0}}{m_\chi} \right) e^{-\frac{\Delta m_\chi}{T}}
$$

$$
+ \frac{2}{3} T^3 \left(\Delta m_\chi^4 + 10\Delta m_\chi^3 T + 60\Delta m_\chi^2 T^2 + 240\Delta m_\chi T^3 + 480T^4\right) \left(\Delta_{\mathbf{p}} f_{\chi^0} + \frac{\mathbf{p} \cdot \nabla_{\mathbf{p}} f_{\chi^0}}{m_\chi T} + \frac{3}{m_\chi T} f_{\chi^0} \right) e^{-\frac{\Delta m}{T}}
$$

$$
\left. +2T^2 \Delta m_\chi \left(\Delta m_\chi^2 + 6\Delta m_\chi T + 12T^2\right) \frac{p^2}{m_\chi^2} f_{\chi^0} e^{-\frac{\Delta m_\chi}{T}} \right\} \tag{A.34}
$$

The ordering of the terms is such that, when integrated over the momentum $\mathbf{p}$ of the neutralino (first equation) or the chargino (second equation), the terms on the third and forth row of the two expressions cancel out while, for what regards the others, it can be seen that once summing the two equations one obtains a term proportional to $\left(\frac{p^2}{m_\chi^2} - 3\right)\left(f_{\chi 0} e^{-\frac{\Delta m_\chi}{T}} - f_{\chi^\pm}\right)$ which cancels out too. The Boltzmann equation in (3.26) are then obtained after the momentum integration $\mathbf{p}$ and using the fact that $T/m_\chi, \Delta m_\chi/m_\chi \ll 1$ which allows to keep just the 0th order terms in both (A.32) and (A.33).

The equation for the neutralino temperature can be obtained from the second moment of the Boltzmann equation in phase space:

$$
\int \frac{d^3 p}{(2\pi)^3} g_{\chi^0} p^2 \left(\partial_t - H\mathbf{p} \cdot \nabla_{\mathbf{p}}\right) f_{\chi^0}(p) = \int \frac{d^3 p}{(2\pi)^3} g_{\chi^0} \frac{p^2}{E} \hat{\mathbf{C}}_{\chi^0}[f_{\chi^0}] \tag{A.35}
$$

The left hand side can be rewritten as:

$$3n_{\chi^0}\frac{dT_N}{dt} + 15HT_{\chi_0}n_{\chi^0} + 3T_{\chi^0}\frac{dn_{\chi^0}}{dt} \tag{A.36}$$

For what regards the right-hand side, we have that the contribution from annihilations, can be computed using the S-wave approximation. In this case in fact we can assume that the dipendence of the pair annihilation cross section on the momentum can be neglected and use the same factorization implemented when assuming kinetic equilibrium, i.e. :

$$\int \frac{d^3p_1}{(2\pi)^3}\frac{d^3p_2}{(2\pi)^3}g_1g_2\,(\sigma v)\,(f_1f_2 - f_1^{eq}f_2^{eq}) = \langle\sigma v\rangle\,(n_1n_2 - n_{1,eq}n_{2,eq}) \tag{A.37}$$

with

$$\langle\sigma v\rangle = \frac{\int d^3p_1 d^3p_2(\sigma v)f_1f_2}{\int d^3p_1 d^3p_2 f_1 f_2}\;. \tag{A.38}$$

taking second moments of the distribution functions, one gets a the term:

$$3M_{\chi^0}T_{\chi_0}\left(\langle\sigma v\rangle_{\chi^0\chi^0}\left(n_{\chi^0}^2 - n_{\chi^0,eq}^2\right) + \langle\sigma v\rangle_{\chi^0\chi^\pm}\left(n_{\chi^0}n_{\chi^\pm} - n_{\chi^0,eq}n_{\chi^\pm,eq}\right)\right) \tag{A.39}$$

which cancels out against the term on the left hand-side proportional to dn_{χ_0}/dt.

Appendix 2

B.1 TGM dominance for sfermion masses

In this appendix we will derive eq. (5.15) which provides a criterium for the determination of the TGM dominance to sfermion masses. In order to do this we perform an analytical study of the one-loop renormalization group equations (RGEs) for the relevant MSSM parameters.

Defining $t = \log(\mu/\mu_0)$ (here μ and μ_0 represent, respectively, a generic energy scale and a the EW scale $\mu_0 = m_Z$), the running of gaugino masses for $a = 1, 2, 3$ reads

$$M_a(t) = M_{1/2} \frac{g_a^2(t)}{g_0^2}\,, \tag{B.1}$$

where g_0 and $M_{1/2}$ are evaluated at the GUT scale and $g_a(t)$ obeys the RGE

$$g_a^{-2}(t) = g_0^{-2} - \frac{b_a}{8\pi^2}\,t\,, \tag{B.2}$$

with $b_a = (33/5, 1, -3)$ being the one-loop MSSM beta-functions. Assuming flavor universality at the GUT scale and neglecting the contributions from the Yukawa couplings and the A-terms, the one-loop RGEs for the scalar soft masses can be written as [Martin 1997]

$$16\pi^2 \frac{d}{dt}\tilde{m}_Q^2 = -\sum_{a=1,2,3} 8\,C_a(Q)\,g_a^2 M_a^2 + \frac{6}{5}Y_Q\,g_1^2 S\,, \tag{B.3}$$

where $C_a(Q)$ is the quadratic Casimir relative to the representation Q and to the gauge group a, and the factor S reads

$$S = \tilde{m}_{h_u}^2 - \tilde{m}_{h_d}^2 + 3\left(\tilde{m}_q^2 - \tilde{m}_\ell^2 - 2\tilde{m}_{u^c}^2 + \tilde{m}_{d^c}^2 + \tilde{m}_{e^c}^2\right)\,. \tag{B.4}$$

Then, by combining Eq. (B.3) and Eq. (B.4) we obtain

$$16\pi^2 \frac{d}{dt}S = \frac{66}{5}g_1^2 S\,, \tag{B.5}$$

whose integration yields

$$S(t) = S_0 \frac{g_1^2(t)}{g_0^2}\,, \tag{B.6}$$

where S_0 is evaluated at the GUT scale. Given the $SO(10)$ embedding of the matter superfields in Eq. (5.12) one gets $S_0 \equiv S(0) = \tilde{m}_{h_u}^2(0) - \tilde{m}_{h_d}^2(0)$.

The assumption regarding the RGE corrections related to Yukawa and trilinear couplings is generally viable for the sfermions of the first two families while it is not generally true in the case of the third family where this corrections can be large, due e.g. to the top Yukawa coupling. For this reason 5.15 should regarded as a simple analytical estimate, useful as general guideline, rather than a stringent condition.

We can now integrate Eq. (B.3) with the help of Eq. (B.1), Eq. (B.2), Eq. (B.6) and the GUT boundary conditions in Eq. (5.13), obtaining

$$\tilde{m}_Q^2(t) = A_Q\,\tilde{m}_{10}^2 + (B_Q(t) + 2\,C_Q\,\eta)\,M_{1/2}^2 + D_Q(t)\,S_0\,, \tag{B.7}$$

where A_Q is equal to 1 for $i = q, u^c, e^c$ and 2 for $i = \ell, d^c$ (cf. Eq. (5.12)) and C_Q is the total SM quadratic Casimir relative to the representation Q (cf. Eq. (5.14)). The coefficients B_Q and D_Q parametrize the effects of the running and can be analytically expressed as

$$B_Q(t) = \sum_{a=1,2,3} 2\,C_a(Q)\frac{1}{b_a}\left(1 - \frac{g_a^4(t)}{g_0^4}\right) \quad \text{and} \quad D_Q(t) = \frac{Y_Q}{11}\left(\frac{g_1^2(t)}{g_0^2} - 1\right)\,. \tag{B.8}$$

Evaluating Eq. (B.1) and Eq. (B.7) at the TeV scale one obtains

$$M_1 \simeq 0.4\,M_{1/2}\,, \tag{B.9}$$
$$M_2 \simeq 0.8\,M_{1/2}\,, \tag{B.10}$$
$$M_3 \simeq 2.5\,M_{1/2}\,, \tag{B.11}$$
$$\tilde{m}_q^2 \simeq \tilde{m}_{10}^2 + (5.2 + 4.2\,\eta)\,M_{1/2}^2 - 0.009\,S_0\,, \tag{B.12}$$
$$\tilde{m}_{u^c}^2 \simeq \tilde{m}_{10}^2 + (4.7 + 3.2\,\eta)\,M_{1/2}^2 - 0.02\,S_0\,, \tag{B.13}$$
$$\tilde{m}_{e^c}^2 \simeq \tilde{m}_{10}^2 + (0.1 + 1.2\,\eta)\,M_{1/2}^2 - 0.05\,S_0\,, \tag{B.14}$$
$$\tilde{m}_{d^c}^2 \simeq 2\,\tilde{m}_{10}^2 + (4.8 + 2.8\,\eta)\,M_{1/2}^2 + 0.03\,S_0\,, \tag{B.15}$$
$$\tilde{m}_\ell^2 \simeq 2\,\tilde{m}_{10}^2 + (0.5 + 1.8\,\eta)\,M_{1/2}^2 - 0.03\,S_0\,. \tag{B.16}$$

The presence of the contributions due to $M_{1/2}$ makes TGM the leading mechanism for sfermion masses only in some portions of the MSSM parameter space. We can define operatively the dominance of TGM by requiring that at least the 50% of the low-energy value of the sfermion masses is due to TGM. Neglecting S_0 the worst case scenario in Eq. (B.12) translates into

$$\tilde{m}_{10}^2 \gtrsim (5.2 + 4.2\,\eta)\,M_{1/2}^2\,, \tag{B.17}$$

that is

$$\tilde{m}_{10} \gtrsim 3.1\,M_{1/2}\,, \tag{B.18}$$

for $\eta = 1$. From this relation it is evident that the NLSP is always the lightest gaugino if TGM is the dominant mechanism generating sfermion masses.

Appendix 3

C.1 Details of the $SO(10)$ model

In this Appendix we give the details of the $SO(10)$ model presented in Sect. 5.5.2. For later convenience let us set the following notation for the SM components of the $SO(10)$ fields relevant for the Yukawa sector

$$16_F = (D^c \oplus L)_{\overline{5}_{-3}} \oplus (u^c \oplus q \oplus e^c)_{10_{+1}} \oplus (\nu^c)_{1_{+5}} \tag{C.1}$$

$$10_F = (D \oplus L^c)_{5_{-2}} \oplus (d^c \oplus \ell)_{\overline{5}_{+2}} \tag{C.2}$$

$$16_H = (T_d^{16} \oplus h_d^{16})_{\overline{5}_{-3}} \oplus (\ldots)_{10_{+1}} \oplus (\ldots)_{1_{+5}} \tag{C.3}$$

$$\overline{16}_H = (T_u^{\overline{16}} \oplus h_u^{\overline{16}})_{5_{+3}} \oplus (\ldots)_{\overline{10}_{-1}} \oplus (\ldots)_{1_{-5}} \tag{C.4}$$

$$10_H = (T_u^{10} \oplus h_u^{10})_{5_{-2}} \oplus (T_d^{10} \oplus h_d^{10})_{\overline{5}_{+2}} \tag{C.5}$$

where a self-explanatory SM notation is employed and the outer subscripts label the $SU(5) \otimes U(1)_X$ origin. The $SU(2)_L$ doublets decompose as $q = (u \oplus d)$, $\ell = (\nu \oplus e)$, $L = (N \oplus E)$, $L^c = (E^c \oplus N^c)$, $h_u = (h_u^+ \oplus h_u^0)$ and $h_d = (h_d^0 \oplus h_d^-)$.

C.1.1 Symmetry breaking and doublet-triplet splitting

The set of Higgs fields $54_H \oplus 45_H \oplus 16_H \oplus \overline{16}_H$ is sufficient in order to achieve a renormalizable[1] breaking of $SO(10)$ down to the SM (see e.g. Ref. [Buccella 2002] for the study of the vacuum patterns). In particular, the SM gauge group is obtained as the intersection of the little groups preserved by the following VEVs:

$$\langle 54_H \rangle \equiv V^{54} \qquad SU(4)_C \otimes SU(2)_L \otimes SU(2)_R \,, \tag{C.6}$$

$$\langle 45 \rangle_{B-L} \equiv V_{B-L}^{45} \qquad SU(3)_C \otimes SU(2)_L \otimes SU(2)_R \otimes U(1)_{B-L} \,, \tag{C.7}$$

$$\langle 45 \rangle_R \equiv V_R^{45} \qquad SU(4)_C \otimes SU(2)_L \otimes U(1)_R \,, \tag{C.8}$$

$$\langle 16_H \rangle \equiv V^{16} \qquad SU(5) \,. \tag{C.9}$$

With the minimal set of Higgs representations at hand we can explicitly check the feasibility of the doublet-triplet (DT) splitting. To this end we compute the mass

---

[1]With only $45_H \oplus 16_H \oplus \overline{16}_H$ at play the requirement of a supersymmetric vacuum at the GUT scale is such that the little group is $SU(5)$ [Buccella 1981, Babu 1995, Aulakh 2001]. In order to reach the SM gauge group one can either relax renormalizability [Babu 1995] or add a 54_H [Buccella 1981, Aulakh 2001]. Since the first option introduces a delicate interplay between the GUT and the Planck scale which may be an issue for unification and proton decay (see e.g. Ref. [Bertolini 2011]), we choose the second option.

matrices for the doublets ($\mathcal{M}_D$) and the triplets ($\mathcal{M}_T$). From W_H in Eq. (5.53) we get

$$\mathcal{M}_D = \begin{pmatrix} \mu_{10} + \frac{1}{2}\sqrt{\frac{3}{5}}\lambda_{10}V^{54} & \lambda_{16-10}V^{16} \\ \overline{\lambda}_{16-10}V^{16} & \mu_{16} + \lambda_{16}V_{B-L}^{45} \end{pmatrix}, \tag{C.10}$$

$$\mathcal{M}_T = \begin{pmatrix} \mu_{10} - \frac{1}{\sqrt{15}}\lambda_{10}V^{54} & \lambda_{16-10}V^{16} \\ \overline{\lambda}_{16-10}V^{16} & \mu_{16} + \lambda_{16}V_{R}^{45} \end{pmatrix}, \tag{C.11}$$

defined, respectively, on the basis $(h_u^{10},\ h_u^{\overline{16}})(h_d^{10},\ h_d^{16})$ and $(T_u^{10},\ T_u^{\overline{16}})(T_d^{10},\ T_d^{16})$. The relevant Clebsch-Gordan coefficients can be found for instance in Ref. [Fukuyama 2005].

Two light Higgs doublets, h_u and h_d, can be obtained by imposing the minimal fine-tuning condition $\det \mathcal{M}_D \sim 0$ in Eq. (C.10), while leaving at the same time the triplets at the GUT scale (cf. Eq. (C.11)). Working for simplicity in the real approximation the light components read

$$h_u = \cos\theta_u h_u^{10} + \sin\theta_u h_u^{\overline{16}}, \qquad h_d = \cos\theta_d h_d^{10} + \sin\theta_d h_d^{16}, \tag{C.12}$$

where, taking into account the minimal fine-tuning condition, $\theta_{u,d}$ are fixed in the following way in terms of the superpotential parameters

$$\tan\theta_u = -\frac{\lambda_{16-10}V^{16}}{\mu_{16} + \lambda_{16}V_{B-L}^{45}}, \qquad \tan\theta_d = -\frac{\overline{\lambda}_{16-10}V^{16}}{\mu_{16} + \lambda_{16}V_{B-L}^{45}}. \tag{C.13}$$

Notice that in general $\theta_u \neq \theta_d$. In particular, the projection of $v_u^{10,\overline{16}}$ and $v_d^{10,16}$ on the electroweak VEVs $v_u \equiv \langle h_u \rangle$ and $v_d \equiv \langle h_d \rangle$ is

$$v_u^{10} = v_u\cos\theta_u, \quad v_u^{\overline{16}} = v_u\sin\theta_u, \quad v_d^{10} = v_d\cos\theta_d, \quad v_d^{16} = v_d\sin\theta_d. \tag{C.14}$$

Worth of a comment is the fact that the natural (without fine-tuning) implementation of the DT splitting requires the introduction of additional representations. A solution along these lines, in the context of an $SO(10)$ model of TGM, has been put forward in Ref. [Nardecchia 2010].

C.1.2   Yukawa sector in the pure embedding

Let us turn now to the Yukawa sector of the model. The flavor structure of supersymmetric $SO(10)$ GUTs with extended matter sector $(16_F \oplus 10_F)$ has been extensively studied in Refs. [Malinsky 2008, Heinze 2011]. On the other hand the mechanism of TGM requires a peculiar embedding of the MSSM fields which must fit into $SU(5)$ representations with positive X-charge where $SU(5)\otimes U(1)_X \subset SO(10)$. This is needed in order to guarantee positive sfermion masses[2] (cf. e.g. Eq. (5.8)).

---

[2] Strictly speaking what one has to require from a phenomenological point of view is that possible negative contribution to sfermion masses, originating from a non-pure embedding, are anyway subleading with respect to the positive ones [Nardecchia 2010]. For simplicity we stick here to the pure embedding limit.

Such an embedding is explicitly shown in Eqs. (C.1)–(C.2), with the lower-case fields $(q,\ u^c,\ d^c,\ \ell,\ e^c,\ \nu^c)$ labeling the MSSM degrees of freedom. In order for this to work one has to ensure that the vector-like pairs $D^c \oplus L$ and $D \oplus L^c$ (cf. again Eqs. (C.1)–(C.2)) pick up a super-heavy mass term, thus decoupling from the low-energy spectrum.

After the electroweak symmetry breaking the fields with the same unbroken quantum numbers mix among themselves. As far as the charged fermions are concerned the superpotential W_Y in Eq. (5.54) yields the following mass matrices

$$
M_u = Y_{10} v_u^{10}, \qquad
M_d = \begin{pmatrix} Y_{10} v_d^{10} & Y_{16} v_d^{16} \\ Y_{16}^T V^{16} & M_\Delta \end{pmatrix}, \qquad
M_e = \begin{pmatrix} Y_{10} v_d^{10} & Y_{16} V^{16} \\ Y_{16}^T v_d^{16} & M_\Lambda \end{pmatrix},
\tag{C.15}
$$

defined respectively on the basis $(u)(u^c)$, $(d,\ D)(D^c,\ d^c)$ and $(E,\ e)(e^c,\ E^c)$. We also defined (see e.g. Refs. [Malinsky 2008, Heinze 2011])

$$
M_\Delta \equiv M_{10} + \eta V_{B-L}^{45} - \tfrac{1}{\sqrt{15}}\lambda V^{54}, \tag{C.16}
$$

$$
M_\Lambda \equiv M_{10} - \eta V_R^{45} + \tfrac{1}{2}\sqrt{\tfrac{3}{5}}\lambda V^{54}, \tag{C.17}
$$

where M_{10} and λ (η) are symmetric (antisymmetric) matrices in flavor space[3]. Thus, by inspecting Eq. (C.15), the decoupling of the vector-like pairs $D^c \oplus L$ and $D \oplus L^c$ is achieved by requiring

$$
M_\Delta = M_\Lambda = 0. \tag{C.18}
$$

We call this the pure embedding condition which gives the desired embedding up to $v_d/V^{16} \ll 1$ corrections. Given the symmetry properties of the matrices M_{10}, η and λ and the need to keep the VEVs of the 45_H and 54_H switched on for the $SO(10)$ symmetry breaking, the pure embedding condition translates into $M_{10} = \eta = \lambda = 0$.

Let us consider now neutrino masses. In this case Eq. (5.54) is responsible for the following Majorana mass matrix

$$
M_\nu = \begin{pmatrix} 0 & Y_{10} v_u^{10} & 0 & Y_{16} V^{16} \\ \cdot & 0 & 0 & Y_{16} v_d^{16} \\ \cdot & \cdot & \lambda w_+ & M_\Lambda \\ \cdot & \cdot & \cdot & \lambda w_- \end{pmatrix}, \tag{C.19}
$$

defined on the symmetric basis $(N,\ \nu^c, \nu,\ N^c)$. In Eq. (C.19) $w_\pm \equiv \langle (1,3,\pm1)_{54_H}\rangle$ denotes a pair of VEVs induced by W_H. The contribution to neutrino masses due to the VEV of the scalar triplets goes under the name of type-II seesaw.

In order to estimate the order of magnitude of the induced VEVs let us consider the following piece of superpotential evaluated on the vacuum

$$
\langle W_H \rangle \supset \mu_{54}\left((V^{54})^2 + w_+ w_-\right) + \lambda_{54}\left(w_+ w_- V^{54}\right) + \lambda_{10}\left(w_+ (v_d^{10})^2 + w_- (v_u^{10})^2\right)
\tag{C.20}
$$

---

[3]The reason being simply because $10 \otimes 10 = 1_S \oplus 45_A \oplus 54_S$.

and require the F-term conditions $F_{w_\pm} = 0$, which gives

$$w_\mp = -\frac{\lambda_{10}\left(v_{d,u}^{10}\right)^2}{\mu_{54} + \lambda_{54}V^{54}} = \mathcal{O}\left(\frac{M_W^2}{M_G}\right) . \tag{C.21}$$

However, as explained above, the pure embedding condition requires $\lambda = 0$ so that the type-II seesaw contribution to light neutrino masses vanishes (cf. Eq. (C.19)).

Sticking to a pure embedding one can still invoke non-renormalizable operators in order to give a mass to neutrinos through a standard type-I seesaw mechanism[4]. Consider for instance the following Planck-suppressed operators

$$\frac{Y_D}{M_P}16_F10_F\overline{16}_H10_H \supset \frac{Y_DV^{16}}{M_P}\,\ell\,\nu^c h_u^{\overline{16}}\,, \tag{C.22}$$

and

$$\frac{Y_N}{M_P}16_F16_F\overline{16}_H\overline{16}_H \supset \frac{Y_N(V^{16})^2}{M_P}\,\nu^c\nu^c\,. \tag{C.23}$$

They contribute to the light neutrino mass matrix after integrating out ν^c, yielding

$$m_\nu^I = \left(Y_DY_N^{-1}Y_D^T\right)(\sin^2\theta_u)^2\frac{v_u^2}{M_P} \sim \left(Y_DY_N^{-1}Y_D^T\right)(\sin\theta_u)^2\,10^{-5}\text{ eV}\,. \tag{C.24}$$

This value is naturally too small and requires a fine-tuning in the Yukawa structure in order to restore the agreement with the experimental data.

One should also keep in mind that in an R-parity breaking scenario there are new lepton number violating operators which contribute to neutrino masses as well. However the issue of neutrino masses with R-parity violation is tightly correlated with cosmology and it turns out that the size of the RPV couplings needed by neutrino masses leads, for the range of gravitino masses expected in TGM, to an unacceptable decay rate of gravitinos in view of the recent bounds on cosmic rays (cf. Sect. 5.5.3).

The bottom line about neutrino masses is that they are naturally too small in the minimal $SO(10)$ model at stake, though it is always possible to fit them with a standard type-I seesaw mechanism (cf. Eq. (C.24)) due to the presence of unknown Yukawa structures which are not correlated with the charged fermion sector.

On the other hand it is also easy to understand that by introducing additional representations in the game one can fit neutrino masses without too much fine-tuning. An interesting possibility is the introduction of a $54'_H$ that couples to 10_H^2 with strength γ. If the $54'_H$ does not develop a GUT scale VEV then the pure embedding condition in Eq. (C.18) is automatically fulfilled with $\gamma \neq 0$, yielding a type-II seesaw contribution to neutrino masses [Frigerio 2009, Calibbi 2009]. The latter also provides an interesting leptogenesis mechanism based on the out-of-equilibrium decay of the Higgs triplets. On the other hand it has been pointed out

---

[4]Notice that in the pure embedding one has the $SU(5)$ relation $M_d = M_e^T$ (cf. Eq. (C.15)) which is phenomenologically unacceptable. In this respect the presence of non-renormalizable operators is welcome in order to unlock that relation.

in Ref. [Frigerio 2009] that this mechanism requires an high reheating temperature of at least $\mathcal{O}(10^{11}\ \mathrm{GeV})$, while the cosmological value of the DM relic density is fitted by reheating temperatures pointing towards a standard thermal leptogenesis mechanism based on a type-I seesaw (see Sect. 5.5.3 for more details).

C.1.3 Origin of the R-parity violating operators

This last section is devoted to the derivation of the R-parity violating operators in the effective MSSM theory. Starting from δW_{RPV} in Eq. (5.55) and by projecting the $SO(10)$ representations onto the light components (cf. Eqs. (C.1)–(C.2)) one finds:

- A bilinear operator of the type $\mu_i\,\ell_i h_u$, where

$$\mu^i = \cos\theta_u\left(\tilde{\mu}_{10}^i - \tilde{\eta}_{10}^i V_R^{45} + \tfrac{1}{2}\sqrt{\tfrac{3}{5}}\tilde{\lambda}_{10}^i V^{54}\right) + \sin\theta_u\tilde{\tilde{\sigma}}^i V^{16}\,. \qquad (C.25)$$

- Two bilinear operators of the type $\mu_{Ti}^{10}d_i^c T_u^{10}$ and $\mu_{Ti}^{\overline{16}}d_i^c T_u^{\overline{16}}$, where

$$\mu_T^{10i} = \tilde{\mu}_{10}^i + \tilde{\eta}_{10}^i V_{B-L}^{45} - \frac{1}{\sqrt{15}}\tilde{\lambda}_{10}^i V^{54} \qquad \text{and} \qquad \mu_T^{\overline{16}i} = \tilde{\tilde{\sigma}}^i V^{16}\,. \qquad (C.26)$$

The triplet bilinears can actually generate effective baryon violating trilinears when combined with the Yukawas (see e.g. [Smirnov 1996a, Giudice 1997]). This can be easily seen working at the $SO(10)$ level. Take for instance the terms

$$W \supset Y_{10}^{ij}16_F^i 16_F^j 10_H + Y_{16}^{ij}16_F^i 10_F^j 16_H + \tilde{\mu}^k 10_F^k 10_H + \tilde{\tilde{\sigma}}^k 10_F^k \overline{16}_H \overline{16}_H\,, \qquad (C.27)$$

where $\tilde{\mu}^k = \left(\tilde{\mu}_{10}^k + \tilde{\eta}_{10}^k\langle 45_H\rangle + \tilde{\lambda}_{10}^k\langle 54_H\rangle\right)$ and by integrating out the pairs $10_H - 10_H$ and $16_H - \overline{16}_H$ one gets[5]

$$\frac{Y_{10}^{ij}\tilde{\mu}^k}{\mu_{10}}16_F^i 16_F^j 10_F^k + \frac{Y_{16}^{ij}\tilde{\tilde{\sigma}}^k}{\mu_{16}}16_F^i 10_F^j 10_F^k\langle\overline{16}_H\rangle\,. \qquad (C.28)$$

After projecting these operators on the MSSM fields, only the second one gives a low-energy contribution, leading to the trilinear operator $(\lambda_T'')^{ijk}\,u_i^c d_j^c d_k^c$ with

$$\left(\lambda_T''\right)^{ijk} = \frac{V^{16}}{\mu_{16}}Y_{16}^{ij}\tilde{\tilde{\sigma}}^k\,. \qquad (C.29)$$

The $SO(10)$ trilinear operator $\tilde{\Lambda}^{ijk}16_F^i 16_F^j 10_F^k$ has no projection on the light MSSM fields as well and thus does not contribute to the effective low-energy RPV superpotential. On the other hand RPV trilinear couplings can arise at the non-renormalizable level from the following operator

$$\frac{\tilde{\Lambda}_{NR}^{ijk}}{M_P}10_F^i 10_F^j 16_F^k\langle\overline{16}_H\rangle \supset \frac{\tilde{\Lambda}_{NR}^{ijk}}{M_P}\bar{5}_{10_F}^i \bar{5}_{10_F}^j 10_{16_F}^k\langle 1_{\overline{16}_H}\rangle$$

$$= \frac{\tilde{\Lambda}_{NR}^{ijk}V^{16}}{M_P}\left(\ell_i\ell_j e_k^c + 2\,d_i^c\ell_j q_k + d_i^c d_j^c u_k^c\right)\,. \qquad (C.30)$$

---

[5]The argument should be formally carried on at the SM level by integrating out the heavy triplets.

Notice that due to the antisymmetry of the $10^k_{16_F}$ in the $SU(5)$ space the interactions in Eq. (C.30) are antisymmetric in the first two generation indices: $\Lambda^{ijk}_{NR} = -\Lambda^{jik}_{NR}$.

Bibliography

[2003]   *A Combination of preliminary electroweak measurements and constraints on the standard model.* 2003. (Cited on page 24.)

[2012]   *et al. Dark Matter Results from 225 Live Days of XENON100 Data.* 2012. (Cited on pages 4 and 65.)

[Aad 2009] G. Aad*et al. Expected Performance of the ATLAS Experiment - Detector, Trigger and Physics.* 2009. (Cited on page 87.)

[Aad 2011a] Georges Aad*et al. Search for neutral MSSM Higgs bosons decaying to* $\tau^+\tau^-$ *pairs in proton-proton collisions at sqrt(s) = 7 TeV with the ATLAS detector.* Phys.Lett., vol. B705, pages 174–192, 2011. (Cited on page 65.)

[Aad 2011b] Georges Aad*et al. Search for squarks and gluinos using final states with jets and missing transverse momentum with the ATLAS detector in sqrt(s) = 7 TeV proton-proton collisions.* 2011. (Cited on page 64.)

[Aad 2012a] Georges Aad*et al. Hunt for new phenomena using large jet multiplicities and missing transverse momentum with ATLAS in 4.7 fb$^-$1 of sqrt(s) = 7 TeV proton-proton collisions.* 2012. (Cited on page 78.)

[Aad 2012b] Georges Aad*et al. Search for a supersymmetric partner to the top quark in final states with jets and missing transverse momentum at sqrt(s) = 7 TeV with the ATLAS detector.* 2012. (Cited on pages 78, 88 and 91.)

[Aad 2012c] Georges Aad*et al. Search for direct production of charginos and neutralinos in events with three leptons and missing transverse momentum in sqrt(s) = 7 TeV pp collisions with the ATLAS detector.* 2012. (Cited on pages 88 and 89.)

[Aad 2012d] Georges Aad*et al. Search for direct slepton and gaugino production in final states with two leptons and missing transverse momentum with the ATLAS detector in pp collisions at sqrt(s) = 7 TeV.* 2012. (Cited on pages 88 and 89.)

[Aad 2012e] Georges Aad*et al. Search for direct top squark pair production in final states with one isolated lepton, jets, and missing transverse momentum in sqrt(s) = 7 TeV pp collisions using 4.7 fb-1 of ATLAS data.* 2012. (Cited on pages 78, 88 and 91.)

[Aad 2012f] Georges Aad*et al. Search for scalar bottom pair production with the ATLAS detector in pp Collisions at sqrts = 7 TeV.* Phys.Rev.Lett., vol. 108, page 181802, 2012. (Cited on page 91.)

[Aad 2012g] Georges Aad *et al. Search for top and bottom squarks from gluino pair production in final states with missing transverse energy and at least three b-jets with the ATLAS detector.* 2012. (Cited on pages 78, 88 and 93.)

[Aaij 2012] R. Aaij *et al. Strong constraints on the rare decays* $B_s \rightarrow \mu^+\mu^-$ *and* $B^0 \rightarrow \mu^+\mu^-$. Phys.Rev.Lett., vol. 108, page 231801, 2012. (Cited on page 65.)

[Aalseth 2011] C.E. Aalseth, P.S. Barbeau, J. Colaresi, J.I. Collar, J. Diaz Leon *et al. Search for an Annual Modulation in a P-type Point Contact Germanium Dark Matter Detector.* Phys.Rev.Lett., vol. 107, page 141301, 2011. (Cited on page 4.)

[Abdo 2010a] A.A. Abdo, M. Ackermann, M. Ajello, W.B. Atwood, L. Baldini *et al. Fermi LAT Search for Photon Lines from 30 to 200 GeV and Dark Matter Implications.* Phys.Rev.Lett., vol. 104, page 091302, 2010. (Cited on page 119.)

[Abdo 2010b] A.A. Abdo *et al. The Spectrum of the Isotropic Diffuse Gamma-Ray Emission Derived From First-Year Fermi Large Area Telescope Data.* Phys.Rev.Lett., vol. 104, page 101101, 2010. (Cited on page 119.)

[Acharya 2007] Bobby Samir Acharya, Konstantin Bobkov, Gordon L. Kane, Piyush Kumar and Jing Shao. *Explaining the electroweak scale and stabilizing moduli in M theory.* Phys. Rev., vol. D76, page 126010, 2007. (Cited on pages 30, 44 and 46.)

[Acharya 2008a] Bobby Samir Acharya, Konstantin Bobkov, Gordon L. Kane, Jing Shao and Piyush Kumar. *The* G_2-*MSSM - An M Theory motivated model of Particle Physics.* Phys. Rev., vol. D78, page 065038, 2008. (Cited on pages 13, 44 and 45.)

[Acharya 2008b] Bobby Samir Acharya *et al. Non-thermal Dark Matter and the Moduli Problem in String Frameworks.* JHEP, vol. 06, page 064, 2008. (Cited on pages 32, 45 and 47.)

[Acharya 2009a] Bobby Samir Acharya *et al. Identifying Multi-Top Events from Gluino Decay at the LHC.* 2009. (Cited on page 44.)

[Acharya 2009b] Bobby Samir Acharya, Gordon Kane, Scott Watson and Piyush Kumar. *A Non-thermal WIMP Miracle.* Phys. Rev., vol. D80, page 083529, 2009. (Cited on page 38.)

[Acharya 2010a] Bobby Samir Acharya and Konstantin Bobkov. *Kahler Independence of the G(2)-MSSM.* JHEP, vol. 1009, page 001, 2010. (Cited on page 44.)

[Acharya 2010b] Bobby Samir Acharya, Gordon Kane and Eric Kuflik. *String Theories with Moduli Stabilization Imply Non- Thermal Cosmological History, and Particular Dark Matter.* 2010. (Cited on page 38.)

[Adriani 2009] Oscar Adriani *et al. An anomalous positron abundance in cosmic rays with energies 1.5-100 GeV.* Nature, vol. 458, pages 607–609, 2009. (Cited on pages 2 and 3.)

[Ahmed 2010] Z. Ahmed *et al. Dark Matter Search Results from the CDMS II Experiment.* Science, vol. 327, pages 1619–1621, 2010. (Cited on page 4.)

[Ahrens 2003] J. Ahrens *et al. Icecube - the next generation neutrino telescope at the south pole.* Nucl.Phys.Proc.Suppl., vol. 118, pages 388–395, 2003. (Cited on page 3.)

[Ajaib 2012] M. Adeel Ajaib, Tong Li and Qaisar Shafi. *Stop-Neutralino Coannihilation in the Light of LHC.* Phys.Rev., vol. D85, page 055021, 2012. (Cited on page 91.)

[Akrami 2011] Yashar Akrami, Christopher Savage, Pat Scott, Jan Conrad and Joakim Edsjo. *How well will ton-scale dark matter direct detection experiments constrain minimal supersymmetry?* JCAP, vol. 1104, page 012, 2011. (Cited on pages 59, 62, 81 and 82.)

[Allanach 2004] B.C. Allanach, A. Dedes and H.K. Dreiner. *R parity violating minimal supergravity model.* Phys.Rev., vol. D69, page 115002, 2004. (Cited on page 111.)

[Alwall 2011] Johan Alwall, Michel Herquet, Fabio Maltoni, Olivier Mattelaer and Tim Stelzer. *MadGraph 5 : Going Beyond.* JHEP, vol. 1106, page 128, 2011. (Cited on page 89.)

[Angloher 2012] G. Angloher, M. Bauer, I. Bavykina, A. Bento, C. Bucci *et al. Results from 730 kg days of the CRESST-II Dark Matter Search.* Eur.Phys.J., vol. C72, page 1971, 2012. (Cited on page 4.)

[Antoniadis 2005] I. Antoniadis and S. Dimopoulos. *Splitting supersymmetry in string theory.* Nucl. Phys., vol. B715, pages 120–140, 2005. (Cited on page 39.)

[Aprile 2011] E. Aprile *et al. Dark Matter Results from 100 Live Days of XENON100 Data.* Phys.Rev.Lett., vol. 107, page 131302, 2011. (Cited on page 65.)

[Arbey 2012a] A. Arbey, M. Battaglia, A. Djouadi, F. Mahmoudi and J. Quevillon. *Implications of a 125 GeV Higgs for supersymmetric models.* Phys.Lett., vol. B708, pages 162–169, 2012. (Cited on pages 40 and 72.)

[Arbey 2012b] Alexandre Arbey, Marco Battaglia, Abdelhak Djouadi and Farvah Mahmoudi. *The Higgs sector of the phenomenological MSSM in the light of the Higgs boson discovery.* 2012. (Cited on pages 63 and 72.)

[Arkani-Hamed 2005a] N. Arkani-Hamed, S. Dimopoulos, G. F. Giudice and A. Romanino. *Aspects of split supersymmetry.* Nucl. Phys., vol. B709, pages 3–46, 2005. (Cited on page 39.)

[Arkani-Hamed 2005b] Nima Arkani-Hamed and Savas Dimopoulos. *Supersymmetric unification without low energy supersymmetry and signatures for fine-tuning at the LHC.* JHEP, vol. 06, page 073, 2005. (Cited on pages 29 and 39.)

[Arkani-Hamed 2006] N. Arkani-Hamed, A. Delgado and G.F. Giudice. *The Well-tempered neutralino.* Nucl.Phys., vol. B741, pages 108–130, 2006. (Cited on page 26.)

[Asaka 1998] T. Asaka, J. Hashiba, M. Kawasaki and T. Yanagida. *Cosmological moduli problem in gauge-mediated supersymmetry breaking theories.* Phys. Rev., vol. D58, page 083509, 1998. (Cited on page 38.)

[Asaka 2006] Takehiko Asaka, Shuntaro Nakamura and Masahiro Yamaguchi. *Gravitinos from heavy scalar decay.* Phys.Rev., vol. D74, page 023520, 2006. (Cited on page 97.)

[ATL 2012a] *Search for a heavy top partner in final states with two leptons with the ATLAS detector.* Rapport technique ATLAS-CONF-2012-071, CERN, Geneva, Jul 2012. (Cited on page 78.)

[ATL 2012b] *Search for dark matter candidates and large extra dimensions in events with a jet and missing transverse momentum with the ATLAS detector.* Rapport technique ATLAS-CONF-2012-084, CERN, Geneva, Jul 2012. (Cited on pages 88 and 92.)

[ATL 2012c] *Search for direct top squark pair production in final states with one isolated lepton, jets, and missing transverse momentum in sqrt(s) = 7 TeV pp collisions using 4.7 ifb of ATLAS data.* Rapport technique ATLAS-CONF-2012-073, CERN, Geneva, Jul 2012. (Cited on page 92.)

[ATL 2012d] *Search for scalar bottom pair production in Þnal states with missing transverse momentum and two b-jets in pp collisions at $\tilde{A}s$=7 TeV with the ATLAS Detector.* Rapport technique ATLAS-CONF-2012-106, CERN, Geneva, Aug 2012. (Cited on pages 88, 91 and 93.)

[ATL 2012e] *Search for squarks and gluinos using final states with jets and missing transverse momentum with the ATLAS detector in $\tilde{A}s$ = 7 TeV proton-proton collisions.* Rapport technique ATLAS-CONF-2012-033, CERN, Geneva, Mar 2012. (Cited on page 25.)

[ATL 2012f] *Search for supersymmetry using events with three leptons, multiple jets, and missing transverse momentum with the ATLAS detector.* Rapport technique ATLAS-CONF-2012-108, CERN, Geneva, Aug 2012. (Cited on page 88.)

[Atwood 2009] W.B. Atwood *et al. The Large Area Telescope on the Fermi Gamma-ray Space Telescope Mission.* Astrophys.J., vol. 697, pages 1071–1102, 2009. (Cited on page 3.)

[Aulakh 2001] Charanjit S. Aulakh, Borut Bajc, Alejandra Melfo, Andrija Rasin and Goran Senjanovic. *SO(10) theory of R-parity and neutrino mass.* Nucl.Phys., vol. B597, pages 89–109, 2001. (Cited on page 137.)

[Babu 1995] K.S. Babu and Stephen M. Barr. *Supersymmetric SO(10) simplified.* Phys.Rev., vol. D51, pages 2463–2470, 1995. (Cited on page 137.)

[Baer 2012a] Howard Baer, Vernon Barger, Peisi Huang and Xerxes Tata. *Natural Supersymmetry: LHC, dark matter and ILC searches.* 2012. (Cited on page 20.)

[Baer 2012b] Howard Baer, Vernon Barger, Andre Lessa, Warintorn Sreethawong and Xerxes Tata. *Wh plus missing-E_T signature from gaugino pair production at the LHC.* Phys.Rev., vol. D85, page 055022, 2012. (Cited on page 89.)

[Baer 2012c] Howard Baer, Vernon Barger and Azar Mustafayev. *Implications of a 125 GeV Higgs scalar for LHC SUSY and neutralino dark matter searches.* Phys.Rev., vol. D85, page 075010, 2012. (Cited on page 72.)

[Bajc 2010] Borut Bajc, Tsedenbaljir Enkhbat, Dilip Kumar Ghosh, Goran Senjanovic and Yue Zhang. *MSSM in view of PAMELA and Fermi-LAT.* JHEP, vol. 1005, page 048, 2010. (Cited on page 112.)

[Baltz 2006] Edward A. Baltz, Marco Battaglia, Michael E. Peskin and Tommer Wizansky. *Determination of dark matter properties at high-energy colliders.* Phys.Rev., vol. D74, page 103521, 2006. (Cited on page 86.)

[Barbier 2005] R. Barbier, C. Berat, M. Besancon, M. Chemtob, A. Deandrea *et al. R-parity violating supersymmetry.* Phys.Rept., vol. 420, pages 1–202, 2005. (Cited on pages 110, 114 and 122.)

[Barbieri 1987] Riccardo Barbieri, Giorgio Gamberini, Gian Francesco Giudice and Giovanni Ridolfi. *NEUTRALINO PRODUCTION AT (AND CLOSE TO) THE Z0 PEAK.* Phys.Lett., vol. B195, page 500, 1987. (Cited on page 70.)

[Beenakker 1996] W. Beenakker, R. Hopker and M. Spira. *PROSPINO: A Program for the production of supersymmetric particles in next-to-leading order QCD.* 1996. (Cited on page 89.)

[Berezinsky 2008] Veniamin Berezinsky, Vyacheslav Dokuchaev and Yury Eroshenko. *Remnants of dark matter clumps.* Phys.Rev., vol. D77, page 083519, 2008. (Cited on page 17.)

[Beringer 2012] J. Beringer, J. F. Arguin, R. M. Barnett, K. Copic, O. Dahl, D. E. Groom, C. J. Lin, J. Lys, H. Murayama, C. G. Wohl, W. M. Yao, P. A. Zyla, C. Amsler, M. Antonelli, D. M. Asner, H. Baer, H. R. Band, T. Basaglia, C. W. Bauer, J. J. Beatty, V. I. Belousov, E. Bergren, G. Bernardi, W. Bertl, S. Bethke, H. Bichsel, O. Biebel, E. Blucher, S. Blusk, G. Brooijmans, O. Buchmueller, R. N. Cahn, M. Carena, A. Ceccucci, D. Chakraborty, M. C. Chen, R. S. Chivukula, G. Cowan, G. D'Ambrosio, T. Damour, D. de Florian, A. de Gouvêa, T. DeGrand, P. de Jong, G. Dissertori, B. Dobrescu, M. Doser, M. Drees, D. A. Edwards, S. Eidelman, J. Erler, V. V. Ezhela, W. Fetscher, B. D. Fields, B. Foster, T. K. Gaisser, L. Garren, H. J. Gerber, G. Gerbier, T. Gherghetta, S. Golwala, M. Goodman, C. Grab, A. V. Gritsan, J. F. Grivaz, M. Grünewald, A. Gurtu, T. Gutsche, H. E. Haber, K. Hagiwara, C. Hagmann, C. Hanhart, S. Hashimoto, K. G. Hayes, M. Heffner, B. Heltsley, J. J. Hernández-Rey, K. Hikasa, A. Höcker, J. Holder, A. Holtkamp, J. Huston, J. D. Jackson, K. F. Johnson, T. Junk, D. Karlen, D. Kirkby, S. R. Klein, E. Klempt, R. V. Kowalewski, F. Krauss, M. Kreps, B. Krusche, Yu. V. Kuyanov, Y. Kwon, O. Lahav, J. Laiho, P. Langacker, A. Liddle, Z. Ligeti, T. M. Liss, L. Littenberg, K. S. Lugovsky, S. B. Lugovsky, T. Mannel, A. V. Manohar, W. J. Marciano, A. D. Martin, A. Masoni, J. Matthews, D. Milstead, R. Miquel, K. Mönig, F. Moortgat, K. Nakamura, M. Narain, P. Nason, S. Navas, M. Neubert, P. Nevski, Y. Nir, K. A. Olive, L. Pape, J. Parsons, C. Patrignani, J. A. Peacock, S. T. Petcov, A. Piepke, A. Pomarol, G. Punzi, A. Quadt, S. Raby, G. Raffelt, B. N. Ratcliff, P. Richardson, S. Roesler, S. Rolli, A. Romaniouk, L. J. Rosenberg, J. L. Rosner, C. T. Sachrajda, Y. Sakai, G. P. Salam, S. Sarkar, F. Sauli, O. Schneider, K. Scholberg, D. Scott, W. G. Seligman, M. H. Shaevitz, S. R. Sharpe, M. Silari, T. Sjöstrand, P. Skands, J. G. Smith, G. F. Smoot, S. Spanier, H. Spieler, A. Stahl, T. Stanev, S. L. Stone, T. Sumiyoshi, M. J. Syphers, F. Takahashi, M. Tanabashi, J. Terning, M. Titov, N. P. Tkachenko, N. A. Törnqvist, D. Tovey, G. Valencia, K. van Bibber, G. Venanzoni, M. G. Vincter, P. Vogel, A. Vogt, W. Walkowiak, C. W. Walter, D. R. Ward, T. Watari, G. Weiglein, E. J. Weinberg, L. R. Wiencke, L. Wolfenstein, J. Womersley, C. L. Woody, R. L. Workman, A. Yamamoto, G. P. Zeller, O. V. Zenin, J. Zhang, R. Y. Zhu, G. Harper, V. S. Lugovsky and P. Schaffner. *Review of Particle Physics.* Phys. Rev. D, vol. 86, page 010001, Jul 2012. (Cited on page 82.)

[Bernabei 2008] R. Bernabei *et al. First results from DAMA/LIBRA and the combined results with DAMA/NaI.* Eur.Phys.J., vol. C56, pages 333–355, 2008. (Cited on page 4.)

[Bertolini 2011] Stefano Bertolini, Luca Di Luzio and Michal Malinsky. *Minimal Flipped SO(10) x U(1) Supersymmetric Higgs Model.* Phys.Rev., vol. D83, page 035002, 2011. (Cited on page 137.)

[Bertone 2010] Gianfranco Bertone, David G. Cerdeno, Mattia Fornasa, Roberto Ruiz de Austri and Roberto Trotta. *Identification of Dark Matter particles with LHC and direct detection data.* Phys.Rev., vol. D82, page 055008, 2010. (Cited on pages 4 and 81.)

[Birkedal 2006] Andreas Birkedal, Andrew Noble, Maxim Perelstein and Andrew Spray. *Little Higgs Dark Matter.* Phys. Rev., vol. D74, page 035002, 2006. (Cited on page 3.)

[Bobrovskyi 2010] Sergei Bobrovskyi, Wilfried Buchmuller, Jan Hajer and Jonas Schmidt. *Broken R-Parity in the Sky and at the LHC.* JHEP, vol. 1010, page 061, 2010. (Cited on page 117.)

[Boehm 2001] C. Boehm, Pierre Fayet and R. Schaeffer. *Constraining dark matter candidates from structure formation.* Phys.Lett., vol. B518, pages 8–14, 2001. (Cited on page 17.)

[Boos 2002] Edward Boos, Abdelhak Djouadi, Margarete Muhlleitner and Alexander Vologdin. *The MSSM Higgs bosons in the intense coupling regime.* Phys.Rev., vol. D66, page 055004, 2002. (Cited on page 72.)

[Borasoy 1997] B. Borasoy and Ulf-G. Meissner. *Chiral expansion of baryon masses and sigma terms.* Annals Phys., vol. 254, pages 192–232, 1997. (Cited on page 61.)

[Bottino 2012] A. Bottino, N. Fornengo and S. Scopel. *Phenomenology of light neutralinos in view of recent results at the CERN Large Hadron Collider.* Phys.Rev., vol. D85, page 095013, 2012. (Cited on page 70.)

[Boubekeur 2010] Lotfi Boubekeur, Ki Young Choi, Roberto Ruiz de Austri and Oscar Vives. *The degenerate gravitino scenario.* JCAP, vol. 1004, page 005, 2010. (Cited on page 98.)

[Braaten 1991] Eric Braaten and Markus H. Thoma. *Energy loss of a heavy fermion in a hot plasma.* Phys. Rev., vol. D44, pages 1298–1310, 1991. (Cited on page 49.)

[Bringmann 2007] Torsten Bringmann and Stefan Hofmann. *Thermal decoupling of WIMPs from first principles.* JCAP, vol. 0407, page 016, 2007. (Cited on pages 3, 17, 18, 27, 52, 53, 127, 128, 130 and 131.)

[Bringmann 2009] Torsten Bringmann. *Particle Models and the Small-Scale Structure of Dark Matter.* New J. Phys., vol. 11, page 105027, 2009. (Cited on pages 17, 19, 52 and 53.)

[Buccella 1981] F. Buccella, J.P. Derendinger, Carlos A. Savoy and S. Ferrara. *Symmetry breaking in supersymmetric GUTs.* 1981. Second Europhysics Study Conference on the Unification of the Fundamental Interactions, Erice, Italy, 1981. (Cited on page 137.)

[Buccella 2002] F. Buccella and Carlos A. Savoy. *Intermediate symmetries in the spontaneous breaking of supersymmetric SO(10).* Mod.Phys.Lett., vol. A17, pages 1239–1248, 2002. (Cited on page 137.)

[Buchmuller 2006a] Wilfried Buchmuller, Laura Covi, Joern Kersten and Kai Schmidt-Hoberg. *Dark Matter from Gaugino Mediation.* JCAP, vol. 0611, page 007, 2006. (Cited on page 101.)

[Buchmuller 2006b] Wilfried Buchmuller, Koichi Hamaguchi and Joern Kersten. *The Gravitino in gaugino mediation.* Phys.Lett., vol. B632, pages 366–370, 2006. (Cited on page 101.)

[Buchmuller 2007] Wilfried Buchmuller, Laura Covi, Koichi Hamaguchi, Alejandro Ibarra and Tsutomu Yanagida. *Gravitino Dark Matter in R-Parity Breaking Vacua.* JHEP, vol. 0703, page 037, 2007. (Cited on pages 109 and 121.)

[Caldwell 1981] J.A.R. Caldwell and J.P. Ostriker. *The Mass distribution within our Galaxy: A Three component model.* Astrophys.J., vol. 251, pages 61–87, 1981. (Cited on page 59.)

[Calibbi 2009] Lorenzo Calibbi, Michele Frigerio, Stephane Lavignac and Andrea Romanino. *Flavour violation in supersymmetric SO(10) unification with a type II seesaw mechanism.* JHEP, vol. 0912, page 057, 2009. (Cited on page 140.)

[Calibbi 2012] L. Calibbi, R.N. Hodgkinson, J. Jones Perez, A. Masiero and O. Vives. *Flavour and Collider Interplay for SUSY at LHC7.* Eur.Phys.J., vol. C72, page 1863, 2012. (Cited on page 75.)

[Campbell 1991] Bruce A. Campbell, Sacha Davidson, John R. Ellis and Keith A. Olive. *Cosmological baryon asymmetry constraints on extensions of the standard model.* Phys.Lett., vol. B256, page 457, 1991. (Cited on pages 121 and 122.)

[Campbell 1992] Bruce A. Campbell, Sacha Davidson, John R. Ellis and Keith A. Olive. *On B+L violation in the laboratory in the light of cosmological and astrophysical constraints.* Astropart.Phys., vol. 1, pages 77–98, 1992. (Cited on pages 121 and 122.)

[Carmi 2012] Dean Carmi, Adam Falkowski, Eric Kuflik, Tomer Volansky and Jure Zupan. *Higgs After the Discovery: A Status Report.* 2012. (Cited on page 70.)

[Catena 2004] Riccardo Catena, N. Fornengo, A. Masiero, Massimo Pietroni and Francesca Rosati. *Dark matter relic abundance and scalar-tensor dark energy.* Phys. Rev., vol. D70, page 063519, 2004. (Cited on page 42.)

[Catena 2010] Riccardo Catena and Piero Ullio. *A novel determination of the local dark matter density.* JCAP, vol. 1008, page 004, 2010. (Cited on pages 59, 60, 62 and 82.)

[Catena 2012] Riccardo Catena and Piero Ullio. *The local dark matter phase-space density and impact on WIMP direct detection.* JCAP, vol. 1205, page 005, 2012. (Cited on pages 60, 62 and 82.)

[Chatrchyan 2011] Serguei Chatrchyan *et al. Search for Supersymmetry at the LHC in Events with Jets and Missing Transverse Energy.* Phys.Rev.Lett., vol. 107, page 221804, 2011. (Cited on page 64.)

[Chatrchyan 2012a] Serguei Chatrchyan *et al. Search for $B_s^0 to \mu^+\mu^-$ and $B^0 to \mu^+\mu^-$ decays.* JHEP, vol. 1204, page 033, 2012. (Cited on page 65.)

[Chatrchyan 2012b] Serguei Chatrchyan *et al. Search for neutral Higgs bosons decaying to tau pairs in pp collisions at sqrt(s)=7 TeV.* Phys.Lett., vol. B713, pages 68–90, 2012. (Cited on pages 65, 70, 72, 74 and 82.)

[Chen 1996] C. H. Chen, Manuel Drees and J. F. Gunion. *Searching for Invisible and Almost Invisible Particles at $e +e -$ Colliders.* Phys. Rev. Lett., vol. 76, pages 2002–2005, 1996. (Cited on page 48.)

[Chen 1997] C. H. Chen, Manuel Drees and J. F. Gunion. *A non-standard string/SUSY scenario and its phenomenological implications.* Phys. Rev., vol. D55, pages 330–347, 1997. (Cited on page 48.)

[Cheng 1989] Hai-Yang Cheng. *LOW-ENERGY INTERACTIONS OF SCALAR AND PSEUDOSCALAR HIGGS BOSONS WITH BARYONS.* Phys.Lett., vol. B219, page 347, 1989. (Cited on page 61.)

[Cheung 2011] Clifford Cheung, Gilly Elor, Lawrence J. Hall and Piyush Kumar. *Origins of Hidden Sector Dark Matter I: Cosmology.* JHEP, vol. 03, page 042, 2011. (Cited on page 33.)

[Choi 2010] Ki-Young Choi, Diego Restrepo, Carlos E. Yaguna and Oscar Zapata. *Indirect detection of gravitino dark matter including its three-body decays.* JCAP, vol. 1010, page 033, 2010. (Cited on pages 119 and 122.)

[Choudhury 2012] Arghya Choudhury and Amitava Datta. *New limits on top squark NLSP from LHC 4.7 fb^{-1} data.* 2012. (Cited on pages 91 and 92.)

[Chun 1999] Eung Jin Chun and Jae Sik Lee. *Implication of Super-Kamiokande data on R-parity violation.* Phys.Rev., vol. D60, page 075006, 1999. (Cited on pages 111 and 119.)

[Chun 2000]   Eung Jin Chun and Sin Kyu Kang. *One loop corrected neutrino masses and mixing in supersymmetric standard model without R-parity.* Phys.Rev., vol. D61, page 075012, 2000. (Cited on page 112.)

[Chung 1998]   Daniel J. H. Chung, Edward W. Kolb and Antonio Riotto. *Nonthermal supermassive dark matter.* Phys. Rev. Lett., vol. 81, pages 4048–4051, 1998. (Cited on page 1.)

[Coughlan 1983]   G. D. Coughlan, W. Fischler, Edward W. Kolb, S. Raby and Graham G. Ross. *Cosmological Problems for the Polonyi Potential.* Phys. Lett., vol. B131, page 59, 1983. (Cited on page 38.)

[Covi 2009]   Laura Covi, Jasper Hasenkamp, Stefan Pokorski and Jonathan Roberts. *Gravitino Dark Matter and general neutralino NLSP.* JHEP, vol. 0911, page 003, 2009. (Cited on pages 98, 106 and 107.)

[Davidson 2002]   Sacha Davidson and Marta Losada. *Basis independent neutrino masses in the R(p) violating MSSM.* Phys. Rev., vol. D65, page 075025, 2002. (Cited on page 112.)

[de Austri 2006]   Roberto Ruiz de Austri, Roberto Trotta and Leszek Roszkowski. *A Markov chain Monte Carlo analysis of the CMSSM.* JHEP, vol. 0605, page 002, 2006. (Cited on page 82.)

[Deser 1977]   Stanley Deser and B. Zumino. *Broken Supersymmetry and Supergravity.* Phys.Rev.Lett., vol. 38, page 1433, 1977. (Cited on page 96.)

[Diaz 2003]   M.A. Diaz, M. Hirsch, W. Porod, J.C. Romao and J.W.F. Valle. *Solar neutrino masses and mixing from bilinear R parity broken supersymmetry: Analytical versus numerical results.* Phys.Rev., vol. D68, page 013009, 2003. (Cited on page 119.)

[Diemand 2005]   Jurg Diemand, Ben Moore and Joachim Stadel. *Earth-mass dark-matter haloes as the first structures in the early Universe.* Nature, vol. 433, pages 389–391, 2005. (Cited on page 17.)

[Diemand 2008]   J. Diemand, M. Kuhlen, P. Madau, M. Zemp, B. Moore *et al.* *Clumps and streams in the local dark matter distribution.* Nature, vol. 454, pages 735–738, 2008. (Cited on page 60.)

[Dine 1984]   Michael Dine, Willy Fischler and Dennis Nemeschansky. *Solution of the Entropy Crisis of Supersymmetric Theories.* Phys. Lett., vol. B136, page 169, 1984. (Cited on page 38.)

[Dine 1996]   Michael Dine, Lisa Randall and Scott D. Thomas. *Baryogenesis from flat directions of the supersymmetric standard model.* Nucl. Phys., vol. B458, pages 291–326, 1996. (Cited on pages 13 and 32.)

[Dine 2006] Michael Dine, Ryuichiro Kitano, Alexander Morisse and Yuri Shirman. *Moduli decays and gravitinos.* Phys. Rev., vol. D73, page 123518, 2006. (Cited on page 37.)

[Djouadi 1998a] A. Djouadi *et al.* *The Minimal supersymmetric standard model: Group summary report.* 1998. (Cited on page 63.)

[Djouadi 1998b] A. Djouadi, J. Kalinowski and M. Spira. *HDECAY: A Program for Higgs boson decays in the standard model and its supersymmetric extension.* Comput.Phys.Commun., vol. 108, pages 56–74, 1998. (Cited on page 65.)

[Djouadi 2007] Abdelhak Djouadi, Jean-Loic Kneur and Gilbert Moultaka. *SuSpect: A Fortran code for the supersymmetric and Higgs particle spectrum in the MSSM.* Comput. Phys. Commun., vol. 176, pages 426–455, 2007. (Cited on page 65.)

[Djouadi 2008] Abdelhak Djouadi. *The Anatomy of electro-weak symmetry breaking. II. The Higgs bosons in the minimal supersymmetric model.* Phys.Rept., vol. 459, pages 1–241, 2008. (Cited on page 23.)

[Drees 1993a] Manuel Drees and Mihoko Nojiri. *Neutralino - nucleon scattering revisited.* Phys.Rev., vol. D48, pages 3483–3501, 1993. (Cited on page 62.)

[Drees 1993b] Manuel Drees and Mihoko M. Nojiri. *New contributions to coherent neutralino - nucleus scattering.* Phys.Rev., vol. D47, pages 4226–4232, 1993. (Cited on page 62.)

[Dutta 2009] Bhaskar Dutta, Louis Leblond and Kuver Sinha. *Mirage in the Sky: Non-thermal Dark Matter, Gravitino Problem, and Cosmic Ray Anomalies.* Phys.Rev., vol. D80, page 035014, 2009. (Cited on page 35.)

[Edsjo 1997] Joakim Edsjo and Paolo Gondolo. *Neutralino Relic Density including Coannihilations.* Phys. Rev., vol. D56, pages 1879–1894, 1997. (Cited on pages 8 and 9.)

[Edsjo 2003] Joakim Edsjo, Mia Schelke, Piero Ullio and Paolo Gondolo. *Accurate relic densities with neutralino, chargino and sfermion coannihilations in mSUGRA.* JCAP, vol. 0304, page 001, 2003. (Cited on page 42.)

[Ellis 1986] John R. Ellis, Dimitri V. Nanopoulos and M. Quiros. *On the Axion, Dilaton, Polonyi, Gravitino and Shadow Matter Problems in Supergravity and Superstring Models.* Phys. Lett., vol. B174, page 176, 1986. (Cited on page 38.)

[Ellis 2005] John R. Ellis, Keith A. Olive, Yudi Santoso and Vassilis C. Spanos. *Update on the direct detection of supersymmetric dark matter.* Phys.Rev., vol. D71, page 095007, 2005. (Cited on page 62.)

[Endo 2006]   Motoi Endo, Koichi Hamaguchi and Fuminobu Takahashi.   *Moduli-induced gravitino problem*.   Phys. Rev. Lett., vol. 96, page 211301, 2006. (Cited on pages 37 and 42.)

[Endo 2007]   Motoi Endo, Fuminobu Takahashi and T.T. Yanagida. *Inflaton Decay in Supergravity*. Phys.Rev., vol. D76, page 083509, 2007. (Cited on page 97.)

[Falk 1994]   Toby Falk, Keith A. Olive and Mark Srednicki.   *Heavy sneutrinos as dark matter*. Phys.Lett., vol. B339, pages 248–251, 1994. (Cited on page 24.)

[Falk 1999]   Toby Falk, Andrew Ferstl and Keith A. Olive.   *New contributions to neutralino elastic cross-sections from CP violating phases in the MSSM*. Phys.Rev., vol. D59, page 055009, 1999. (Cited on page 60.)

[Feldman 2010]   Daniel Feldman, Gordon Kane, Ran Lu and Brent D. Nelson. *Dark Matter as a Guide Toward a Light Gluino at the LHC*. Phys. Lett., vol. B687, pages 363–370, 2010. (Cited on pages 44 and 47.)

[Feng 1999]   Jonathan L. Feng, Takeo Moroi, Lisa Randall, Matthew Strassler and Shu-fang Su. *Discovering supersymmetry at the Tevatron in Wino LSP scenarios*. Phys. Rev. Lett., vol. 83, pages 1731–1734, 1999. (Cited on pages 44, 45 and 48.)

[Feng 2003a]   Jonathan L. Feng, Arvind Rajaraman and Fumihiro Takayama. *Superweakly interacting massive particles*. Phys.Rev.Lett., vol. 91, page 011302, 2003. (Cited on page 98.)

[Feng 2003b]   Jonathan L. Feng, Arvind Rajaraman and Fumihiro Takayama. *SuperWIMP dark matter signals from the early universe*. Phys.Rev., vol. D68, page 063504, 2003. (Cited on page 98.)

[Feng 2004]   Jonathan L. Feng, Shufang Su and Fumihiro Takayama. *Supergravity with a gravitino LSP*. Phys.Rev., vol. D70, page 075019, 2004. (Cited on pages 106 and 108.)

[Ferrara 1979]   S. Ferrara, L. Girardello and F. Palumbo. *A General Mass Formula in Broken Supersymmetry*. Phys.Rev., vol. D20, page 403, 1979. (Cited on page 100.)

[Fileviez Perez 2005]   Pavel Fileviez Perez.   *How large could the R-parity violating couplings be?* J.Phys.G, vol. G31, pages 1025–1030, 2005. (Cited on pages 21 and 113.)

[Fox 2012]   Patrick J. Fox, Roni Harnik, Joachim Kopp and Yuhsin Tsai. *Missing Energy Signatures of Dark Matter at the LHC*. Phys.Rev., vol. D85, page 056011, 2012. (Cited on page 76.)

[Frigerio 2009] Michele Frigerio, Pierre Hosteins, Stephane Lavignac and Andrea Romanino. *A New, direct link between the baryon asymmetry and neutrino masses.* Nucl.Phys., vol. B806, pages 84–102, 2009. (Cited on pages 140 and 141.)

[Fukugita 1986] M. Fukugita and T. Yanagida. *Baryogenesis Without Grand Unification.* Phys.Lett., vol. B174, page 45, 1986. (Cited on pages 99 and 121.)

[Fukuyama 2005] Takeshi Fukuyama, Amon Ilakovac, Tatsuru Kikuchi, Stjepan Meljanac and Nobuchika Okada. *SO(10) group theory for the unified model building.* J.Math.Phys., vol. 46, page 033505, 2005. We comment on results of hep-ph/0402122 and hep-ph/0405074. (Cited on page 138.)

[Galli 2009] Silvia Galli, Fabio Iocco, Gianfranco Bertone and Alessandro Melchiorri. *CMB constraints on Dark Matter models with large annihilation cross-section.* Phys. Rev., vol. D80, page 023505, 2009. (Cited on page 35.)

[Gasser 1991] J. Gasser, H. Leutwyler and M.E. Sainio. *Sigma term update.* Phys.Lett., vol. B253, pages 252–259, 1991. (Cited on page 61.)

[Gelmini 2006a] Graciela Gelmini and Carlos E. Yaguna. *Constraints on minimal SUSY models with warm dark matter neutralinos.* Phys. Lett., vol. B643, pages 241–245, 2006. (Cited on page 48.)

[Gelmini 2006b] Graciela B. Gelmini and Paolo Gondolo. *Neutralino with the right cold dark matter abundance in (almost) any supersymmetric model.* Phys. Rev., vol. D74, page 023510, 2006. (Cited on pages 15 and 16.)

[Gelmini 2007] Graciela B. Gelmini, Paolo Gondolo, Adrian Soldatenko and C. E. Yaguna. *Direct detection of neutralino dark mattter in non- standard cosmologies.* Phys. Rev., vol. D76, page 015010, 2007. (Cited on page 15.)

[Gelmini 2008] Graciela B. Gelmini and Paolo Gondolo. *Ultra-cold WIMPs: relics of non-standard pre-BBN cosmologies.* JCAP, vol. 0810, page 002, 2008. (Cited on page 54.)

[Giardino 2012a] Pier Paolo Giardino, Kristjan Kannike, Martti Raidal and Alessandro Strumia. *Is the resonance at 125 GeV the Higgs boson?* 2012. (Cited on page 70.)

[Giardino 2012b] Pier Paolo Giardino, Kristjan Kannike, Martti Raidal and Alessandro Strumia. *Reconstructing Higgs boson properties from the LHC and Tevatron data.* JHEP, vol. 1206, page 117, 2012. (Cited on page 76.)

[Giudice 1997] G.F. Giudice and R. Rattazzi. *R-parity violation and unification.* Phys.Lett., vol. B406, pages 321–327, 1997. (Cited on page 141.)

[Giudice 1999] G.F. Giudice and R. Rattazzi. *Theories with gauge mediated super-symmetry breaking.* Phys.Rept., vol. 322, pages 419–499, 1999. (Cited on pages 96 and 103.)

[Giudice 2001] Gian Francesco Giudice, Edward W. Kolb and Antonio Riotto. *Largest temperature of the radiation era and its cosmological implications.* Phys. Rev., vol. D64, page 023508, 2001. (Cited on pages 13, 15, 16, 30 and 36.)

[Giudice 2004] G. F. Giudice and A. Romanino. *Split supersymmetry.* Nucl. Phys., vol. B699, pages 65–89, 2004. (Cited on pages 29 and 39.)

[Goerdt 2007] Tobias Goerdt, Oleg Y. Gnedin, Ben Moore, Jurg Diemand and Joachim Stadel. *The survival and disruption of CDM micro-haloes: Implications for direct and indirect detection experiments.* Mon.Not.Roy.Astron.Soc., vol. 375, pages 191–198, 2007. (Cited on page 17.)

[Gondolo 1991] Paolo Gondolo and Graciela Gelmini. *Cosmic abundances of stable particles: Improved analysis.* Nucl.Phys., vol. B360, pages 145–179, 1991. (Cited on page 9.)

[Gondolo 2004] P. Gondolo *et al. DarkSUSY: Computing supersymmetric dark matter properties numerically.* JCAP, vol. 0407, page 008, 2004. (Cited on pages 29 and 40.)

[Gondolo 2012] Paolo Gondolo, Junji Hisano and Kenji Kadota. *The Effect of quark interactions on dark matter kinetic decoupling and the mass of the smallest dark halos.* 2012. (Cited on page 129.)

[Grasso 2009] D. Grasso *et al. On possible interpretations of the high energy electron-positron spectrum measured by the Fermi Large Area Telescope.* Astropart. Phys., vol. 32, pages 140–151, 2009. (Cited on page 35.)

[Green 2004] Anne M. Green, Stefan Hofmann and Dominik J. Schwarz. *The power spectrum of SUSY - CDM on sub-galactic scales.* Mon.Not.Roy.Astron.Soc., vol. 353, page L23, 2004. (Cited on page 17.)

[Green 2005] Anne M. Green, Stefan Hofmann and Dominik J. Schwarz. *The First wimpy halos.* JCAP, vol. 0508, page 003, 2005. (Cited on page 17.)

[Green 2007] Anne M. Green and Simon P. Goodwin. *On mini-halo encounters with stars.* Mon.Not.Roy.Astron.Soc., vol. 375, pages 1111–1120, 2007. (Cited on page 17.)

[Griest 1991] Kim Griest and David Seckel. *Three exceptions in the calculation of relic abundances.* Phys. Rev., vol. D43, pages 3191–3203, 1991. (Cited on pages 8 and 9.)

[Haber 1995] Howard E. Haber. *Challenges for nonminimal Higgs searches at future colliders.* 1995. (Cited on page 70.)

[Hall 1984] Lawrence J. Hall and Mahiko Suzuki. *Explicit R-Parity Breaking in Supersymmetric Models.* Nucl.Phys., vol. B231, page 419, 1984. (Cited on page 110.)

[Hall 2012] Lawrence J. Hall, David Pinner and Joshua T. Ruderman. *A Natural SUSY Higgs Near 126 GeV.* JHEP, vol. 1204, page 131, 2012. (Cited on page 72.)

[Hasenkamp 2010] Jasper Hasenkamp and Joern Kersten. *Leptogenesis, Gravitino Dark Matter and Entropy Production.* Phys. Rev., vol. D82, page 115029, 2010. (Cited on page 107.)

[He 2012] Bin He, Tong Li and Qaisar Shafi. *Impact of LHC Searches on NLSP Top Squark and Gluino Mass.* JHEP, vol. 1205, page 148, 2012. (Cited on page 91.)

[Heinze 2011] Martin Heinze and Michal Malinsky. *Flavour structure of supersymmetric SO(10) GUTs with extended matter sector.* Phys.Rev., vol. D83, page 035018, 2011. (Cited on pages 138 and 139.)

[Hirsch 2000] M. Hirsch, M.A. Diaz, W. Porod, J.C. Romao and J.W.F. Valle. *Neutrino masses and mixings from supersymmetry with bilinear R parity violation: A Theory for solar and atmospheric neutrino oscillations.* Phys.Rev., vol. D62, page 113008, 2000. (Cited on pages 111, 119 and 120.)

[Hisano 2001] Junji Hisano, Kazunori Kohri and Mihoko M. Nojiri. *Neutralino warm dark matter.* Phys. Lett., vol. B505, pages 169–176, 2001. (Cited on pages 27, 48 and 49.)

[Hofmann 2001] Stefan Hofmann, Dominik J. Schwarz and Horst Stoecker. *Damping scales of neutralino cold dark matter.* Phys.Rev., vol. D64, page 083507, 2001. (Cited on page 17.)

[Hryczuk 2011] Andrzej Hryczuk, Roberto Iengo and Piero Ullio. *Relic densities including Sommerfeld enhancements in the MSSM.* JHEP, vol. 03, page 069, 2011. (Cited on page 26.)

[Hu 2000] Wayne Hu, Rennan Barkana and Andrei Gruzinov. *Cold and fuzzy dark matter.* Phys. Rev. Lett., vol. 85, pages 1158–1161, 2000. (Cited on page 1.)

[Iocco 2010] Fabio Iocco. *Self-annihilating dark matter and the CMB: reionizing the Universe and constraining cross sections.* AIP Conf. Proc., vol. 1241, pages 379–387, 2010. (Cited on page 35.)

[Ishiwata 2008] Koji Ishiwata, Shigeki Matsumoto and Takeo Moroi. *High Energy Cosmic Rays from the Decay of Gravitino Dark Matter.* Phys. Rev., vol. D78, page 063505, 2008. (Cited on page 122.)

[Jeannerot 1999] R. Jeannerot, X. Zhang and Robert H. Brandenberger. *Non-thermal production of neutralino cold dark matter from cosmic string decays.* JHEP, vol. 9912, page 003, 1999. (Cited on page 12.)

[Jedamzik 2006] Karsten Jedamzik. *Big bang nucleosynthesis constraints on hadronically and electromagnetically decaying relic neutral particles.* Phys. Rev., vol. D74, page 103509, 2006. (Cited on page 107.)

[Jungman 1996] Gerard Jungman, Marc Kamionkowski and Kim Griest. *Supersymmetric dark matter.* Phys.Rept., vol. 267, pages 195–373, 1996. (Cited on pages 58 and 60.)

[Kaplan 2006] Jared Kaplan. *Dark matter generation and split supersymmetry.* JHEP, vol. 0610, page 065, 2006. (Cited on page 43.)

[Kawasaki 2000] M. Kawasaki, Kazunori Kohri and Naoshi Sugiyama. *MeV-scale reheating temperature and thermalization of neutrino background.* Phys. Rev., vol. D62, page 023506, 2000. (Cited on page 13.)

[Knecht 1999] Marc Knecht. *Working group summary: pi N sigma term.* PiN Newslett., vol. 15, pages 108–113, 1999. (Cited on page 61.)

[Kohri 2004] Kazunori Kohri, Masahiro Yamaguchi and Jun'ichi Yokoyama. *Production and dilution of gravitinos by modulus decay.* Phys. Rev., vol. D70, page 043522, 2004. (Cited on page 37.)

[Komatsu 1986] H. Komatsu. *Z0 DECAY INTO NEUTRALINOS AND THE HIGGS FERMION MASS m(H).* Phys.Lett., vol. B177, page 201, 1986. (Cited on page 70.)

[Komatsu 2011] E. Komatsu et al. *Seven-Year Wilkinson Microwave Anisotropy Probe (WMAP) Observations: Cosmological Interpretation.* Astrophys. J. Suppl., vol. 192, page 18, 2011. (Cited on pages 1, 34 and 35.)

[Kors 2005] Boris Kors and Pran Nath. *Hierarchically split supersymmetry with Fayet-Iliopoulos D-terms in string theory.* Nucl. Phys., vol. B711, pages 112–132, 2005. (Cited on page 39.)

[Kuijken 1990] Konrad Kuijken and Gerard Gilmore. *The Galactic disk surface mass density and the galactic force K(z) = 1.1-kpc.* Astrophys.J.Lett., 1990. (Cited on page 60.)

[Lin 2001] W.B. Lin, D.H. Huang, X. Zhang and Robert H. Brandenberger. *Non-thermal production of WIMPs and the subgalactic structure of the universe.* Phys.Rev.Lett., vol. 86, page 954, 2001. (Cited on page 48.)

[Loeb 2005] Abraham Loeb and Matias Zaldarriaga. *The Small-scale power spectrum of cold dark matter*. Phys.Rev., vol. D71, page 103520, 2005. (Cited on page 17.)

[Lunghi 2007] E. Lunghi and J. Matias. *Huge right-handed current effects in $B \to K * (K\pi)l^+l^-$ in supersymmetry*. JHEP, vol. 0704, page 058, 2007. (Cited on page 75.)

[Lyth 1996] David H. Lyth and Ewan D. Stewart. *Thermal inflation and the moduli problem*. Phys. Rev., vol. D53, pages 1784–1798, 1996. (Cited on pages 38 and 109.)

[Mahmoudi 2008] F. Mahmoudi. *SuperIso: A Program for calculating the isospin asymmetry of $B \to K * \gamma$ in the MSSM*. Comput.Phys.Commun., vol. 178, pages 745–754, 2008. (Cited on page 65.)

[Mahmoudi 2009] F. Mahmoudi. *SuperIso v2.3: A Program for calculating flavor physics observables in Supersymmetry*. Comput.Phys.Commun., vol. 180, pages 1579–1613, 2009. (Cited on page 65.)

[Malinsky 2008] Michal Malinsky. *Quark and lepton masses and mixing in SO(10) with a GUT-scale vector matter*. Phys.Rev., vol. D77, page 055016, 2008. (Cited on pages 138 and 139.)

[Martin 1992] Stephen P. Martin. *Some simple criteria for gauged R-parity*. Phys.Rev., vol. D46, pages 2769–2772, 1992. (Cited on page 114.)

[Martin 1997] Stephen P. Martin. *A Supersymmetry Primer*. 1997. (Cited on pages 19, 22, 100 and 135.)

[Monaco] Maurizio Monaco, Maurizio Pierini, Andrea Romanino and Martin Spinrath. (in preparation). (Cited on page 102.)

[Monaco 2011] Maurizio Monaco, Marco Nardecchia, Andrea Romanino and Robert Ziegler. *Extended Tree-Level Gauge Mediation*. 2011. (Cited on pages 99, 101 and 102.)

[Moreau 2002] G. Moreau and M. Chemtob. *R-parity violation and the cosmological gravitino problem*. Phys.Rev., vol. D65, page 024033, 2002. (Cited on page 119.)

[Moroi 1995] T. Moroi, Masahiro Yamaguchi and T. Yanagida. *On the solution to the Polonyi problem with 0 (10-TeV) gravitino mass in supergravity*. Phys. Lett., vol. B342, pages 105–110, 1995. (Cited on page 37.)

[Moroi 1996] Takeo Moroi. *The Muon anomalous magnetic dipole moment in the minimal supersymmetric standard model*. Phys.Rev., vol. D53, pages 6565–6575, 1996. (Cited on page 75.)

[Moroi 2000] Takeo Moroi and Lisa Randall. *Wino cold dark matter from anomaly-mediated SUSY breaking.* Nucl. Phys., vol. B570, pages 455–472, 2000. (Cited on pages 2, 15 and 37.)

[Nakamura 2006] Shuntaro Nakamura and Masahiro Yamaguchi. *Gravitino production from heavy moduli decay and cosmological moduli problem revived.* Phys. Lett., vol. B638, pages 389–395, 2006. (Cited on pages 37 and 42.)

[Nardecchia 2009] Marco Nardecchia, Andrea Romanino and Robert Ziegler. *Tree Level Gauge Mediation.* JHEP, vol. 0911, page 112, 2009. (Cited on pages 99, 101, 103, 104 and 114.)

[Nardecchia 2010] Marco Nardecchia, Andrea Romanino and Robert Ziegler. *General Aspects of Tree Level Gauge Mediation.* JHEP, vol. 1003, page 024, 2010. (Cited on pages 99, 100, 103 and 138.)

[Olechowski 2009] Marek Olechowski, Stefan Pokorski, Krzysztof Turzynski and James D. Wells. *Reheating Temperature and Gauge Mediation Models of Supersymmetry Breaking.* JHEP, vol. 0912, page 026, 2009. (Cited on page 97.)

[Olive 1989] Keith A. Olive and Mark Srednicki. *New Limits on Parameters of the Supersymmetric Standard Model from Cosmology.* Phys.Lett., vol. B230, page 78, 1989. (Cited on page 25.)

[Pallis 2004] C. Pallis. *Massive particle decay and cold dark matter abundance.* Astropart.Phys., vol. 21, pages 689–702, 2004. (Cited on page 15.)

[Papucci 2011] Michele Papucci, Joshua T. Ruderman and Andreas Weiler. *Natural SUSY Endures.* 2011. (Cited on page 20.)

[Pavan 2002] M.M. Pavan, I.I. Strakovsky, R.L. Workman and R.A. Arndt. *The Pion nucleon Sigma term is definitely large: Results from a G.W.U. analysis of pi nucleon scattering data.* PiN Newslett., vol. 16, pages 110–115, 2002. (Cited on page 61.)

[Percival 2010] Will J. Percival *et al.* *Baryon Acoustic Oscillations in the Sloan Digital Sky Survey Data Release 7 Galaxy Sample.* Mon.Not.Roy.Astron.Soc., vol. 401, pages 2148–2168, 2010. (Cited on page 1.)

[Pierce 1997] Damien M. Pierce, Jonathan A. Bagger, Konstantin T. Matchev and Ren-jie Zhang. *Precision corrections in the minimal supersymmetric standard model.* Nucl. Phys., vol. B491, pages 3–67, 1997. (Cited on page 44.)

[Pospelov 2008] Maxim Pospelov, Josef Pradler and Frank Daniel Steffen. *Constraints on Supersymmetric Models from Catalytic Primordial Nucleosynthesis of Beryllium.* JCAP, vol. 0811, page 020, 2008. (Cited on page 99.)

[Pradler 2007] Josef Pradler and Frank Daniel Steffen. *Thermal gravitino production and collider tests of leptogenesis*. Phys.Rev., vol. D75, page 023509, 2007. (Cited on page 97.)

[Pradler 2008] Josef Pradler and Frank Daniel Steffen. *Implications of Catalyzed BBN in the CMSSM with Gravitino Dark Matter*. Phys.Lett., vol. B666, pages 181–184, 2008. (Cited on page 99.)

[Profumo 2003] Stefano Profumo and Piero Ullio. *SUSY dark matter and quintessence*. JCAP, vol. 0311, page 006, 2003. (Cited on page 42.)

[Profumo 2006] Stefano Profumo, Kris Sigurdson and Marc Kamionkowski. *What mass are the smallest protohalos?* Phys. Rev. Lett., vol. 97, page 031301, 2006. (Cited on pages 3 and 27.)

[Randall 1999] Lisa Randall and Raman Sundrum. *Out of this world supersymmetry breaking*. Nucl.Phys., vol. B557, pages 79–118, 1999. (Cited on page 44.)

[Reno 1988] M. H. Reno and D. Seckel. *Primordial Nucleosynthesis: The Effects of Injecting Hadrons*. Phys. Rev., vol. D37, page 3441, 1988. (Cited on page 49.)

[Restrepo 2011] Diego Restrepo, Marco Taoso, J.W.F. Valle and Oscar Zapata. *Gravitino dark matter and neutrino masses with bilinear R-parity violation*. 2011. (Cited on page 120.)

[Riess 2009] Adam G. Riess, Lucas Macri, Stefano Casertano, Megan Sosey, Hubert Lampeit*et al*. *A Redetermination of the Hubble Constant with the Hubble Space Telescope from a Differential Distance Ladder*. Astrophys.J., vol. 699, pages 539–563, 2009. (Cited on page 1.)

[Rosiek 1995] Janusz Rosiek. *Complete set of Feynman rules for the MSSM: Erratum*. 1995. (Cited on page 58.)

[Roszkowski 2010] Leszek Roszkowski, Roberto Ruiz de Austri and Roberto Trotta. *Efficient reconstruction of CMSSM parameters from LHC data: A Case study*. Phys.Rev., vol. D82, page 055003, 2010. (Cited on page 4.)

[Rubino-Martin 2006] J.A. Rubino-Martin, J. Chluba and R.A. Sunyaev. *Lines in the Cosmic Microwave Background Spectrum from the Epoch of Cosmological Hydrogen Recombination*. Mon.Not.Roy.Astron.Soc., vol. 371, pages 1939–1952, 2006. (Cited on page 17.)

[Rychkov 2007] Vyacheslav S. Rychkov and Alessandro Strumia. *Thermal production of gravitinos*. Phys.Rev., vol. D75, page 075011, 2007. (Cited on pages 5 and 97.)

[Sainio 2002] M.E. Sainio. *Pion nucleon sigma term: A Review*. PiN Newslett., vol. 16, pages 138–143, 2002. (Cited on page 61.)

[Salati 2003] Pierre Salati. *Quintessence and the Relic Density of Neutralinos*. Phys. Lett., vol. B571, pages 121–131, 2003. (Cited on page 42.)

[Shifman 1978] Mikhail A. Shifman, A.I. Vainshtein and Valentin I. Zakharov. *Remarks on Higgs Boson Interactions with Nucleons*. Phys.Lett., vol. B78, page 443, 1978. (Cited on page 61.)

[Sjostrand 2006] Torbjorn Sjostrand, Stephen Mrenna and Peter Z. Skands. *PYTHIA 6.4 Physics and Manual*. JHEP, vol. 05, page 026, 2006. (Cited on page 48.)

[Smirnov 1996a] Alexei Yu. Smirnov and Francesco Vissani. *Large R-parity violating couplings and grand unification*. Nucl.Phys., vol. B460, pages 37–56, 1996. (Cited on pages 116, 122 and 141.)

[Smirnov 1996b] Alexei Yu. Smirnov and Francesco Vissani. *Upper bound on all products of R-parity violating couplings lambda-prime and lambda-prime-prime from proton decay*. Phys.Lett., vol. B380, pages 317–323, 1996. (Cited on pages 21 and 113.)

[Smith 1990] P.F. Smith and J.D. Lewin. *Dark Matter Detection*. Phys.Rept., vol. 187, page 203, 1990. (Cited on page 58.)

[Springel 2008] Volker Springel, Jie Wang, Mark Vogelsberger, Aaron Ludlow, Adrian Jenkins*et al*. *The Aquarius Project: the subhalos of galactic halos*. Mon.Not.Roy.Astron.Soc., vol. 391, pages 1685–1711, 2008. (Cited on page 60.)

[Strege 2012] Charlotte Strege, Roberto Trotta, Gianfranco Bertone, Annika H.G. Peter and Pat Scott. *Fundamental statistical limitations of future dark matter direct detection experiments*. 2012. (Cited on pages 82, 83 and 85.)

[Strumia 2011] Alessandro Strumia. *The Fine-tuning price of the early LHC*. JHEP, vol. 1104, page 073, 2011. (Cited on page 20.)

[Takayama 2000] Fumihiro Takayama and Masahiro Yamaguchi. *Gravitino dark matter without R-parity*. Phys.Lett., vol. B485, pages 388–392, 2000. (Cited on pages 99 and 118.)

[Trotta 2008a] Roberto Trotta. *Bayes in the sky: Bayesian inference and model selection in cosmology*. Contemp.Phys., vol. 49, pages 71–104, 2008. (Cited on pages 79, 80 and 81.)

[Trotta 2008b] Roberto Trotta, Farhan Feroz, Mike P. Hobson, Leszek Roszkowski and Roberto Ruiz de Austri. *The Impact of priors and observables on parameter inferences in the Constrained MSSM*. JHEP, vol. 0812, page 024, 2008. (Cited on pages 81 and 82.)

[Vainshtein 1980] A.I. Vainshtein, Valentin I. Zakharov and Mikhail A. Shifman. *Higgs Particles*. Sov.Phys.Usp., vol. 23, pages 429–449, 1980. (Cited on page 61.)

[Vertongen 2011] Gilles Vertongen and Christoph Weniger. *Hunting Dark Matter Gamma-Ray Lines with the Fermi LAT*. JCAP, vol. 1105, page 027, 2011. (Cited on pages 119 and 122.)

[Volkov 1973] D.V. Volkov and V.A. Soroka. *Higgs Effect for Goldstone Particles with Spin 1/2*. JETP Lett., vol. 18, pages 312–314, 1973. (Cited on page 96.)

[Weniger 2012] Christoph Weniger. *A Tentative Gamma-Ray Line from Dark Matter Annihilation at the Fermi Large Area Telescope*. JCAP, vol. 1208, page 007, 2012. (Cited on page 3.)